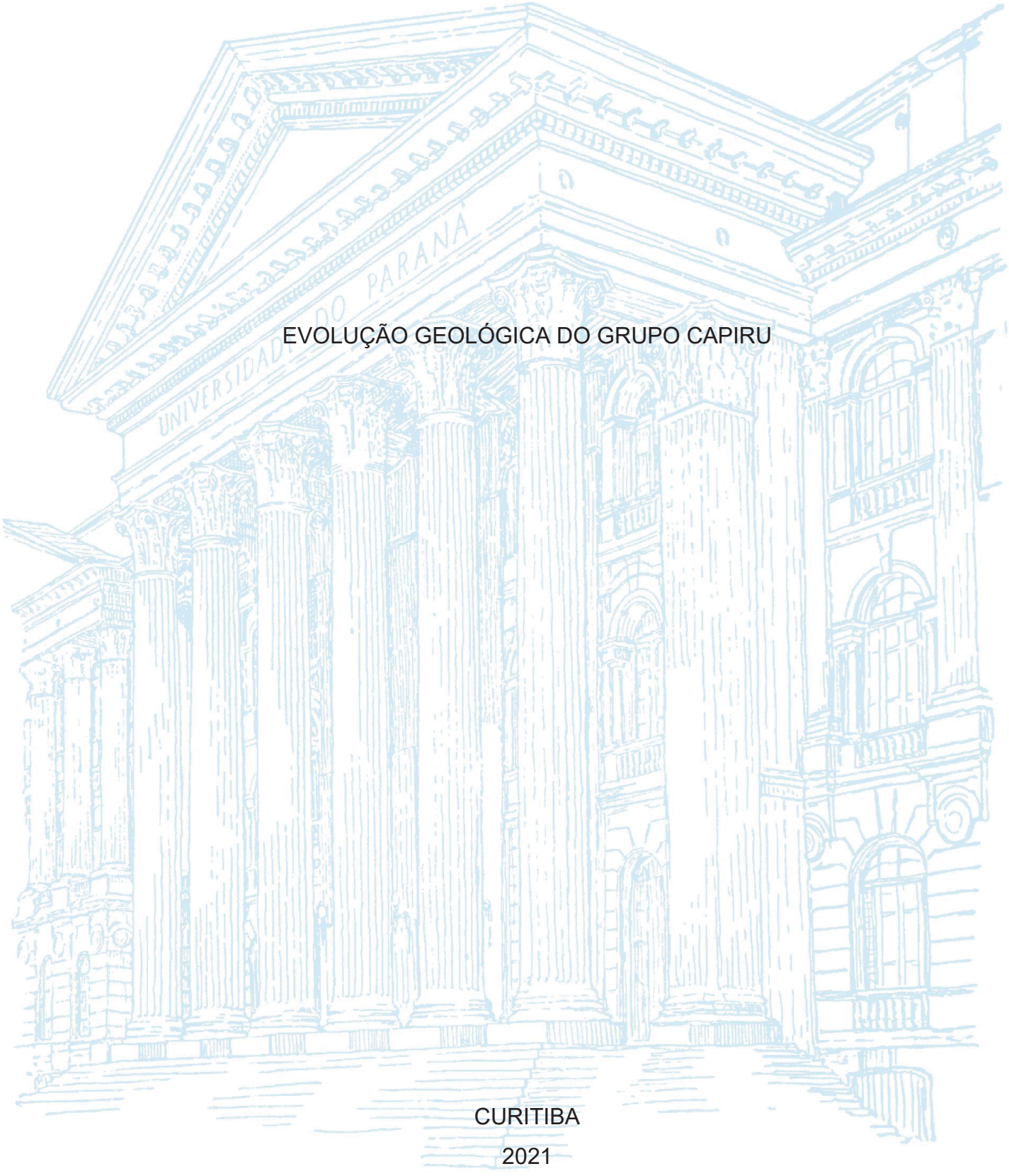
UNIVERSIDADE FEDERAL DO PARANÁ

LARISSA DA ROCHA SANTOS



EVOLUÇÃO GEOLÓGICA DO GRUPO CAPIRU

CURITIBA

2021

LARISSA DA ROCHA SANTOS

EVOLUÇÃO GEOLÓGICA DO GRUPO CAPIRU

Tese apresentada ao curso de Pós-Graduação em Geologia, Setor de Ciências da Terra, Universidade Federal do Paraná, como requisito parcial à obtenção do título de Doutor em Geologia.

Orientador: Prof. Dr. Leonardo Fadel Cury
Co-orientadora: Profa. Dra. Anelize Manuela Bahniuk Rumbelsperger

CURITIBA

2021

Catalogação na Fonte: Sistema de Bibliotecas, UFPR
Biblioteca de Ciência e Tecnologia

S237e Santos, Larissa da Rocha

Evolução geológica do grupo Capiru [recurso eletrônico] / Larissa da Rocha Santos, 2021.

Tese (Doutorado) - Universidade Federal do Paraná, Setor de Ciências da Terra, Programa de Pós-Graduação em Geologia.

Orientador: Prof. Dr. Leonardo Fadel Cury
Coorientadora: Profª. Drª. Anelize Manuela Bahniuk Rumbelsperger

1. Geologia. 2. Geoquímica. I. Cury, Leonardo Fadel. II. Rumbelsperger, Anelize Manuela Bahniuk. III. Universidade Federal do Paraná. IV. Título.

CDD 551.7

Bibliotecária: Vilma Machado CRB-9/1563

TERMO DE APROVAÇÃO

Os membros da Banca Examinadora designada pelo Colegiado do Programa de Pós-Graduação GEOLOGIA da Universidade Federal do Paraná foram convocados para realizar a arguição da tese de Doutorado de **LARISSA DA ROCHA SANTOS** intitulada: **ESTRATIGRAFIA E PROVENIÊNCIA DO GRUPO CAPIRU**, sob orientação do Prof. Dr. LEONARDO FADEL CURY, que após terem inquirido a aluna e realizada a avaliação do trabalho, são de parecer pela sua APROVAÇÃO no rito de defesa.

A outorga do título de doutora está sujeita à homologação pelo colegiado, ao atendimento de todas as indicações e correções solicitadas pela banca e ao pleno atendimento das demandas regimentais do Programa de Pós-Graduação.

CURITIBA, 12 de Novembro de 2021.

Assinatura Eletrônica
18/11/2021 12:39:18.0
LEONARDO FADEL CURY
Presidente da Banca Examinadora

Assinatura Eletrônica
18/11/2021 12:57:31.0
FERNANDO FARIAS VESELY
Avaliador Interno (UNIVERSIDADE FEDERAL DO PARANÁ)

Assinatura Eletrônica
02/12/2021 13:10:04.0
RENATA DA SILVA SCHMITT
Avaliador Externo (UNIVERSIDADE FEDERAL DO RIO DE JANEIRO)

Assinatura Eletrônica
23/11/2021 15:55:00.0
MIGUEL ANGELO STIPP BASEI
Avaliador Externo (UNIVERSIDADE DE SÃO PAULO)

Assinatura Eletrônica
01/12/2021 14:52:38.0
MONICA DA COSTA PEREIRA LAVALLE HEILBRON
Avaliador Externo (UNIVERSIDADE DO ESTADO DO RIO DE JANEIRO)

Documento assinado eletronicamente de acordo com o disposto na legislação federal Decreto 8539 de 08 de outubro de 2015.
Gerado e autenticado pelo SIGA-UFPR, com a seguinte identificação única: 128423
Para autenticar este documento/assinatura, acesse https://www.prppg.ufpr.br/siga/visitante/autenticacaoassinaturas.jsp e insira o codigo 128423

Ministério da Educação
UNIVERSIDADE FEDERAL DO PARANÁ
Setor de Ciências da Terra
Programa de Pós-Graduação em Geologia

D E C L A R A Ç Ã O

Declaramos para os devidos fins que **LARISSA DA ROCHA SANTOS** realizou sua defesa de tese intitulada "**ESTRATIGRAFIA E PROVENIÊNCIA DO GRUPO CAPIRU**" em 12 de novembro de 2021, no Programa de Pós-Graduação em Geologia da Universidade Federal do Paraná, área Geologia Exploratória, nível Doutorado, e que por sugestão da banca examinadora, o título foi alterado para "**EVOLUÇÃO GEOLÓGICA DO GRUPO CAPIRU***".*

Curitiba, 05 de janeiro de 2022.

Carlos C. F. Guedes

Carlos Conforti Ferreira Guedes
Coordenador do Programa
Pós-Graduação em Geologia

Aos meus pais Cássia e Alvacir.

AGRADECIMENTOS

Aos meus pais Cássia e Alvacir, responsáveis por me trazerem até aqui.

À minha irmã Ilara, pela eterna parceria.

Ao meu orientador e amigo, Prof. Leonardo F. Cury, pela oportunidade e confiança durante todos esses anos.

À co-orientadora e amiga, Profa. Anelize Rumbelsperger, pelo apoio e pelas muitas risadas!

Aos meus professores do Dpto. de Geologia da UFPR, por serem responsáveis por toda a minha formação.

Ao iLamir e a todos os colegas de trabalho e estudantes que por ali passaram! Por toda ajuda e pelos momentos de descontração! Eu ri muito nesse lugar e com essas pessoas!

Às minhas primas, Ju e Joyce, que ajudaram e ajudam a segurar todas as barras da nossa mini família curitibana.

Aos amigos, muitos deles que conheci por consequência da geologia aqui na UFPR – aqui fiz os melhores amigos que alguém poderia ter! Além de amizades que atravessam cidades, estados, países e continentes!

Aos colegas da Pós-Graduação em Geologia da UFPR, fica aqui o meu agradecimento e o registro da minha admiração por vocês!

Aos Professores e amigos da USP, que tive o prazer de conhecer e trabalhar durante esses anos!

E por fim, a Universidade Federal do Paraná – Curitiba, Brasil! Da qual me orgulho profundamente! Foi um grande privilégio fazer parte dessa história!

... Meu coração está com pressa
Quando a esperança está dispersa
Só a verdade me liberta
Chega de maldade e ilusão...
(M. Bonfá, D. Villa-Lobos, R. Russo)

RESUMO

O Grupo Capiru é uma unidade metassedimentar Neoproterozóica que aflora na região de Curitiba, Faixa Ribeira Sul, Sul do Brasil. As sucessões do Grupo Capiru foram deformadas durante o ciclo Brasiliano - Pan-Africano, que culminou na amalgamação do Gondwana Oeste. O Grupo Capiru foi estudado por meio de mapeamento geológico, seções medidas, análises químicas e geocronologia U-Pb em zircão detrítico. As interpretações originais e o novo mapa geológico foram compilados e integrados com os dados dos levantamentos geológicos anteriores dos serviços geológicos estaduais (MINEROPAR) e federais (CPRM). Esta compilação representa a síntese mais atualizada da geologia do Grupo Capiru, e o mapa geológico apresentado fornece a base para o reconhecimento e individualização de unidades litoestratigráficas distintas.

Seis formações foram identificadas, da mais antiga para a mais nova, denominadas de: Santana (plataforma marinha siliciclástica proximal a distal), Juruqui (deltaico proximal a distal), Rio Branco (plataforma carbonática), Morro Azul (lagunar a marinho raso), Morro Grande (proximal a distal deltáico / marinho) e Bocaina (estuarino a marinho raso), representativas de dois estágios principais de uma bacia: i) um estágio de margem continental passiva, com quiescência tectônica crescente seguida por uma regressão marinha, e ii) um estágio sinorogênico na margem norte da microplaca Curitiba.

Composições químicas e mineralógicas enriquecidas em Fe e Al para as rochas do Grupo Capiru sugerem forte denudação continental durante o estágio de margem continental passiva, com baixas taxas de aporte sedimentar, fontes de relevo com gradientes relativamente baixos, altamente intemperizadas e estáveis desde o Mesoproterozóico. Durante a deposição da Formação Bocaina, a composição arcoseana dos meta-arenitos e *lags* de conglomerados líticos sugerem rejuvenescimento da fonte durante o estágio sinorogênico.

As interpretações paleoambientais indicam mudanças climáticas durante a deposição do Grupo Capiru, sob influência indireta de glaciações (*Phantom Glacial*) relacionada às discordâncias regionais. Semelhanças sedimentológicas e estratigráficas são encontradas entre sucessões de margens passivas do Grupo Capiru e as unidades depositadas nas margens do cráton Rio de La Plata e Sul do bloco Paranapanema. Os novos dados de proveniência do Grupo Capiru estabelecem *links* entre outros registros de bacias neoproterozóicas da região (grupos Lajeado e Itaiacoca).

Através da proveniência e evolução geocronológica dos grupos Lajeado, Itaiacoca e Capiru, sugere-se que os fragmentos pós-Rodinia da região compartilharam uma evolução desde o Paleoproterozóico (com embasamentos conectados) ao Neoproterozóico (com processos extensionais e surgimento de bacias Neoproterozóicas), com eventos importantes a ca. 1.250 Ma (idade do último evento metamórfico reconhecido nesses blocos) e registros de um evento extensional ca. 900 Ma (idade da extensão Toniana), provavelmente responsável pela separação da microplaca Curitiba e instalação de sua margem continental passiva.

Palavras-chave: Tectonoestratigrafia, margens continentais pré-cambrianas, *Phantom Glacial*, Faixa Ribeira Meridional, Terreno Curitiba, Bloco Paranapanema.

ABSTRACT

The Capiru Group is a Neoproterozoic metasedimentary unit that crops out in the Curitiba terrane, Southern Ribeira Belt, South of Brazil. The Capiru Group successions are deformed within the Brasiliano - Pan African Ribeira Belt, which culminated in the amalgamation of Western Gondwana. The Capiru Group was studied by field mapping, measured sections, bulk-rock chemical compositions and detrial zircon U-Pb geochronology. Original interpretations and the new geological map were compiled and integrated with the past field data of the state (MINEROPAR) and national (CPRM) geological surveys. This compilation represents the most updated synthesis of the Capiru Group, and the geological map presented here provides the basis for recognition and individualization of distinct lithostratigraphic units.

Six formations were identified, termed from oldest to youngest as: Santana (proximal to distal marine shelf), Juruqui (proximal to distal deltaic), Rio Branco (carbonate platform), Morro Azul (lagoonal to shallow marine), Morro Grande (proximal to distal deltaic/ marine) and Bocaina formations (estuarine to shallow-marine), representing two main basin stages: i) a passive continental margin stage, with increasing tectonic quiescence followed by a marine regression, and ii) a syn-orogenic stage at the Curitiba microplate margin.

Chemical and mineralogical Fe- and Al-rich compositions suggest continental denudation during the passive continental margin stage, with low sediment input rates from a relatively low-gradient relief, highly weathered continental source, and stability since Mesoproterozoic time. During deposition of the Bocaina Formation, the arkosic composition of sandstones and lithic conglomerate lags suggest source rejuvenation during the syn-orogenic stage, prior to the collisional thrusting that led to the Western Gondwana assembly.

The paleoenvironmental interpretations indicate climatic changes during the Capiru Group deposition, with far-field or Phantom Glacial influence related to the regional discordances. Sedimentological and stratigraphic similarities were found among Capiru Group passive margin successions and units deposited on the Río de Plata and Southern Paranapanema block margins. The new provenance data of the Capiru Group establish links among other Neoproterozoic basin-records of the region (Lajeado and Itaiacoca groups).

Through the provenance and geochronological evolution of Lajeado, Itaiacoca and Capiru, we suggest that these post-Rodinia fragments shared a linked evolution from Paleoproterozoic (with connected basements) to Neoproterozoic times (with extension and Neoproterozoic basins onsetting), with important events at ~1,250 Ma (age of the last metamorphic event recognized in these blocks), and the ~ 900 Ma event (age of Tonian extension), likely responsible for the Curitiba microplate detachment and onset of its passive continental margin.

Keywords: Tectonostratigraphy, Precambrian continental margins, Phantom Glacial, Southern Ribeira Belt, Curitiba terrane, Paranapanema block.

LISTA DE FIGURAS

Capítulo 1

Figura 1. Contexto geológico do Grupo Capiru 22
Figura 2. A) Localização da área de estudo no contexto do Primeiro Planalto Paranaense. B) Mapa geológico simplificado dos terrenos Apiaí e Curitiba com localização da área de estudo. 24
Figura 3. Mapa geológico simplificado dos terrenos Apiaí e Curitiba 25

Capítulo 2

Figura 4. Localização das faixas móveis Neoproterozóicas e crátons na América do Sul e África (Gondwana Ocidental). 29
Figura 5. Conjuntos litológicos e modelo estratigráfico proposto para a Formação Capiru. Modificado de Fiori e Gaspar (1993).....31

Capítulo 4

Artigo 1

Figure 1. A) Tectonic map of Southern Ribeira Belt; B) Main crustal blocks in South America and Africa; C) Geological context of Capiru Group.....43
Figure 2. A) Geological map of the former Capiru 'Formation'. B) Lithological assemblages and depositional setting interpretation proposed in Fiori (1992) and Fiori and Gaspar (1993). 47
Figure 3. Geological map of the Capiru Group and location of type- and composite sections. 51
Figure 4. Type-sections of the Capiru Group formations.....54
Figure 5. Main field aspects of the Santana Formation 55
Figure 6. Main field aspects of the Juruqui Formation. 58
Figure 7. Main field aspects of the Rio Branco Formation.....59
Figure 8. Main field aspects of the Morro Azul Formation 62
Figure 9. Morro Grande Formation field aspects 63
Figure 10. Main field aspects of the Bocaina Formation.....65
Figure 11. Geochemical classifications of the Capiru Group rocks 76
Figure 12. Summary of the main tectonothermal events in the Curitiba terrane.....81

Figure 13. Model of depositional environment evolution for the Capiru Group 82
Figure 14. Representative basinal correlation of the Capiru Group formations 84
Figure 15. Location of the correlative Neoproterozoic basins in Eastern South America and Western Africa 87

Artigo 2

Figura 1. A) Aerial image of Curitiba and surrounding regions; B) Geological context of the Capiru Group 96
Figura 2. Geomorphologic aspects of the mapped area.....97
Figura 3. Structural cross-sections showing the main structural features of the Capiru Group.. 102
Figura 4. Geophysical maps.....104

Artigo 3

Figure 1. Paleogeographic setting of Western Gondwana (at ca. 500 Ma) 110
Figure 2. Regional geological and tectonic framework of the Southern Ribeira Belt (after Basei et al. 2008) 115
Figure 3. Late Meso- to Neoproterozoic passive margin strata in the Southern Ribeira belt.....117
Figure 4. Representative stratigraphic columns and proposal of correlation through time among the passive – to - active margin records 120
Figure 5. Photographs of the sampled outcrops for this study.....122
Figure 6. Photographs of sampled outcrops for this study 124
Figure 7. Cathodoluminescence imaging of the main detrital zircon populations of the Capiru Group 125
Figure 8. Cathodoluminescence imaging of the main detrital zircon populations of the AL-75 sample (Lajeado Group, Betari Formation) 126
Figure 9. Detrital zircon probability density plots and pie diagrams.....127
Figure 10. A) Concordia diagram of the Apiaí gabbro; B) reconstruction of southwestern Gondwana after Gaucher et al. (2009, 2021) 133

Figure 11. Distribution of ages in Curitiba microplate and Paranapanema block based on detrital zircon ages found in the provenance spectra of Capiru and Lajeado groups, and described in the literature 140
Figure 12. Capiru margin evolution model through the provenance interpretation .. 142
Figure 13. Suggested location of the Capiru margin as a prolongation of the Curitiba microplate – Nico Pérez – Angola craton margin 148

LISTA DE TABELAS

Capítulo 4

Artigo 1

Tabela 1. Mineralogical composition of the main units of the Capiru Group 69
Tabela 2. Whole-rock major element compositions (XRF) of the metasandstones and metamudstones of the Capiru Group 72
Tabela 3. Whole-rock major element compositions (XRF) of the metadolostones and metamarls of the Capiru Group 74
Tabela 4. Summary of the type section features and localities for Formations of the Capiru Group.....77
Tabela 5. Neoproterozoic successions in South America and Africa and possible correlations based on published ages.....85

Artigo 2

Tabela 1. Main geological events recognized in the mapped area.....103

Artigo 3

Table 1. U-Pb zircon geochronological data from the Capiru and Lajeado groups in the Southern Ribeira Belt used in this study 121
Table 2. Selection of published ages of the basement blocks of the region 148
Table 3. Summary of the units used on the model. 151

Lista de abreviaturas

CL	- catodoluminescência
COT	- carbono orgânico total
DRX	- difratometria de raios-X
FRX	- fluorescência de raios-X
MDA	- maximum depositional age
U-Pb	- urânio/ chumbo

SUMÁRIO

1 INTRODUÇÃO 20
1.1 ESTRUTURA DA TESE 21
1.2 LOCALIZAÇÃO DA ÁREA DE ESTUDO 23
1.3 JUSTIFICATIVA 23
1.4 HIPÓTESE 25
1.5 OBJETIVOS 26
2 GEOLOGIA REGIONAL 27
2.1 CONTEXTO GEOLÓGICO DO GRUPO CAPIRU 29
2.2 CONTEXTO TECTONO-ESTRUTURAL 30
2.3 ESTRATIGRAFIA DA FORMAÇÃO CAPIRU 30
2.4 ESTRUTURAS SEDIMENTARES E AMBIENTES DE DEPOSIÇÃO 32
3 MATERIAIS E MÉTODOS 33
3.1 LEVANTAMENTOS DE CAMPO 33
3.1.1 Estudo faciológico 33
3.1.2 Mapeamento e integração geológica 33
3.2 GEOQUÍMICA DE ROCHA TOTAL 34
3.2.1 Fluorescência de raios-X 34
3.2.2 Difratometria de raios-X 35
3.2.3 Carbono Orgânico Total (COT) 35
3.3 MÉTODOS GEOFÍSICOS 35
3.3.1 Aeromagnetometria 35
3.3.2 Aerogamaespectometria 36
3.4 U-PB EM ZIRCÃO DETRÍTICO POR LA-ICP-MS 36
4 RESULTADOS 38

4.1 ARTIGO 1: THE CAPIRU GROUP: FROM PASSIVE MARGIN TO SYN-OROGENIC UNITS, IMPLICATIONS FOR THE EVOLUTION OF THE NORTHERN MARGIN OF THE CURITIBA MICROPLATE, WESTERN GONDWANA 38
4.1.1 INTRODUCTION 39
4.1.2 BACKGROUND 41
4.1.2.1 Regional Tectonics 41
4.1.2.2 Curitiba Terrane 44

4.1.2.3 Previous tectonostratigraphic divisions of the Curitiba Terrane 44
4.1.2.4 Previous stratigraphic divisions of the Capiru Group 45
4.1.2.5 Depositional age of the Capiru Group 47
4.1.3 METHODS 48
4.1.3.1 Field Mapping and Stratigraphic Analysis 48
4.1.3.2 Bulk-rock composition of metasedimentary rocks 48
4.1.3.3 Mineralogical analysis 49
4.1.3.4 Chemical index of alteration (CIA) 49
4.1.4 RESULTS AND INTERPRETATIONS 52
4.1.4.1 Revised stratigraphic divisions of the Capiru Group 52
4.1.5 UNCONFORMITIES 65
4.1.5.1 Santana - Juruqui and basement contact 65
4.1.5.2 Rio Branco and Santana - Juruqui contact 66
4.1.5.3 Morro Azul unconformity 66
4.1.5.4 Morro Grande unconformity 67
4.1.5.5 Bocaina unconformity 67
4.1.6 GEOCHEMISTRY AND SEDIMENTARY PROTOLITHS OF THE METASEDIMENTARY ROCKS 67
4.1.6.1 The ferruginous-rich lower Capiru Group interval 68
4.1.6.2 Rio Branco interval 70
4.1.6.3 Morro Azul Formation 75
4.1.6.4 Morro Grande interval 75
4.1.6.5 Bocaina Formation 75
4.1.7 DISCUSSION 77
4.1.7.1 Capiru basin evolution 77
4.1.7.2 Maturity of parent sediments and source composition 81
4.1.7.3 Capiru basin configuration 83
4.1.7.4 Similar successions in Western Gondwana 84
4.1.7.5 Paleogeographic correlations 88
4.1.8 CONCLUSIONS 90
4.1.9 ACKNOWLEDGMENTS 91

4.2 ARTIGO 2: THE GEOLOGY OF THE CAPIRU GROUP, CURITIBA TERRANE, SOUTHERN RIBEIRA BELT (BRAZIL) 92
ABSTRACT **92**
4.2.1 INTRODUCTION 93
4.2.1.1 Sources of information 94
4.2.1.2 Maps before 1980 94
4.2.1.3 1980's maps 97
4.2.1.4 1990's works 97
4.2.1.5 Integration of previous works and digital datasets 98
4.2.2 METHODS 98
4.2.3 GEOLOGY 99
4.2.3.1 Lithostratigraphic units 99
4.2.3.2 Structure 100
4.2.4 Aerogeophysical features 103
4.2.5 Conclusions 104
4.2.6 Acknowledgements 105
4.2.7 Software 105
4.2.8 Data availability statement 105
4.2.9 Funding 106

4.3 ARTIGO 3: TRACING THE CONTINENTAL MARGINS OF THE SOUTHERN RIBEIRA BELT, BRAZIL: PROVENANCE AND LINKS AMONG THE POST-RODINIA FRAGMENTS 107
4.3.1 INTRODUCTION 108
4.3.2 BACKGROUND 111
4.3.2.1 Paleogeographic Setting 111
4.3.2.2 Regional Geological Setting 112
4.3.2.3 Late Meso- to Neoproterozoic strata in Southern Ribeira belt 116
4.3.3 METHODS 120
4.3.3.1 Sampling Strategy 120
4.3.3.2 U-Pb Geochronology of DETRITAL ZIRCON 123
4.3.4 RESULTS 126
4.3.4.1 Capiru Group Samples 126

4.3.4.2 Lajeado Group Samples 131
4.3.5 INTERPRETATIONS 133
4.3.5.1 Maximum Depositional Ages 133
4.3.5.2 Provenance Analysis 134
4.3.5.3 Summary of Provenance Analysis 138
4.3.6 DISCUSSION 140
4.3.6.1 The Capiru margin evolution through the provenance data 140
4.3.6.2 Regional tectonic model and timing of the continental margins 142
4.3.6.3 Basement links among the Rodinian fragments 146
4.3.7 CONCLUSIONS 153
ACKNOWLEDGMENTS 154
DISCLOSURE STATEMENT 154

5 CONSIDERAÇÕES FINAIS 155
REFERÊNCIAS 159

ANEXO 1 – MAPA GEOLÓGICO DO GRUPO CAPIRU
ANEXO 2 – FORMALIZAÇÃO DAS UNIDADES SEGUNDO O CÓDIGO ESTRATIGRÁFICO
ANEXO 3 – DADOS ISOTÓPICOS

1 INTRODUÇÃO

A evolução crustal na porção sul-sudeste brasileira está relacionada com o ciclo orogênico Brasiliano-Pan Africano, responsável pela justaposição de diferentes blocos continentais que culminaram com a formação do Gondwana Oeste (Fig. 1a) no início do Cambriano (Brito Neves e Cordani 1991, Campos Neto e Figueiredo 1995, Brito Neves et al. 1999, Schimitt et al. 2004, Basei et al. 2008, Heilbron et al. 2008, 2020, Gaucher et al. 2009a, Frimmel et al. 2011). Estes diferentes blocos que compõem o Sistema Orogênico Ribeira (Fig. 1b) mostram um quadro complexo, caracterizado por registros tectonoestratigráficos do Paleoproterozóico até o Cambriano (Heilbron et al. 2008, Schimitt et al. 2004, Passarelli et al. 2018).

A porção sul do Sistema Orogênico Ribeira, ou Faixa Ribeira Sul, é constituída por quatro compartimentos tectônicos distintos (Fig. 1c), denominados de terrenos Apiaí, Curitiba, Luís Alves e Paranaguá (Siga Jr 1995, Campanha e Sadowski 1999, Kaulfuss 2001, Campanha et al. 2008, Heilbron et al. 2008, 2020, Basei et al. 2008, Siga Jr et al. 2009, Cury 2009, Siga Jr. 2011a, 2011b and 2011c).

As assinaturas isotópicas e os dados geocronológicos representam hoje, as principais ferramentas para o estudo da evolução geológica desses blocos Pré-Cambrianos, possibilitando vínculos e comparações, na tentativa de criar modelos paleogeográficos e correlações entre as unidades que compõem um orógeno.

Com o advento dos estudos de proveniência várias das unidades da Faixa Ribeira Sul foram revisitadas com relação a suas áreas-fonte potenciais, tipos de bacia (Campanha et al. 2016, 2019, Ricardo et al. 2020) e seus equivalentes crono-correlatos, agregando assim, informações para interpretações sobre a evolução das margens dos blocos continentais da região.

Alguns trabalhos sugerem diferentes origens para o embasamento desses blocos. Alguns correlacionam os blocos a Leste (Curitiba, Luís Alves e Paranaguá) com os crátons Kalahari e Congo, no lado africano do sistema (Gaucher et al. 2011, Cury 2009). Outros sugerem algumas afinidades com o cráton São Francisco para porções do bloco Paranapanema (Terreno Apiaí), (Henrique-Pinto et al. 2015). Também, alguns sugerem que esses blocos estavam relacionados ao grande cráton Río de la Plata (Santos et al. 2017).

O Grupo Capiru é uma das unidades supracrustais do Terreno Curitiba (Siga Jr 1995, Basei et al. 1992, Basei et al. 2008), um compartimento tectônico composto

por ortognaisses e migmatitos do Complexo Atuba, granitóides deformados do Complexo Setuva, e as coberturas metassedimentares do Grupo Capiru e do Complexo Turvo-Cajati (Fig. 1c). Dado que os estratos metassedimentares do Grupo Capiru se sobrepõem diretamente ao embasamento do Terreno Curitiba (Basei et al. 2008), estes podem fornecer informações a respeito da evolução geológica do terreno e suas interações com os blocos adjacentes.

Neste trabalho são apresentados: i) um novo mapa geológico do Grupo Capiru (**Anexo I**), com dados inéditos e integrações com levantamentos geológicos anteriores; ii) uma nova proposta estratigráfica para o Grupo Capiru, seus modelos deposicionais e aspectos geoquímicos contextualizados com os modelos paleoclimáticos do Neoproterozóico, e por fim, iii) um estudo de proveniência para o Grupo Capiru, com comparações e correlações estratigráficas com unidades similares da faixa Ribeira Sul, além de propostas para a interação entre as margens continentais, correlações entre os embasamentos e prováveis *links* entre os ciclos continentais registrados nos blocos da região.

1.1 ESTRUTURA DA TESE

Esta tese está estruturada em cinco capítulos. Este primeiro capítulo introdutório tem foco na estrutura e localização da área de estudo (**Capítulo 1**). Além de apresentar a justificativa e os principais objetivos do trabalho.

No **Capítulo 2** é apresentado o contexto geológico da região estudada, além da fundamentação teórica sobre os principais aspectos levantados no Grupo Capiru para sua correlação com o contexto do Neoproterozóico.

O **Capítulo 3** apresenta os métodos detalhados utilizados na pesquisa.

O **Capítulo 4** apresenta os resultados do trabalho na forma de três artigos científicos: o primeiro discute uma proposta estratigráfica e paleogeográfica, relacionando os principais aspectos sedimentares e geoquímicos das formações do Grupo Capiru, e sua relação com a tectônica Pós-Rodinia e Pan-Africana/ Brasiliana (Seção 4.1), publicado no Journal of South American Earth Sciences (*https://doi.org/10.1016/j.jsames.2021.103555*).

O segundo artigo, publicado no Journal of Maps (https://doi.org/10.1080/17445647.2021.1982036), é voltado para cartografia geológica e trabalhos de integração geológica, com o objetivo de se estabelecer o trabalho base para os estudos futuros (Seção 4.2).

O terceiro artigo (a ser submetido) será voltado para correlações estratigráficas e paleogeográficas com base em um estudo de proveniência realizado no Grupo Capiru (Seção 4.3).

Por fim, o **Capítulo 5** trata das considerações finais e um sumário das principais conclusões dessa tese, além das referências bibliográficas compiladas.

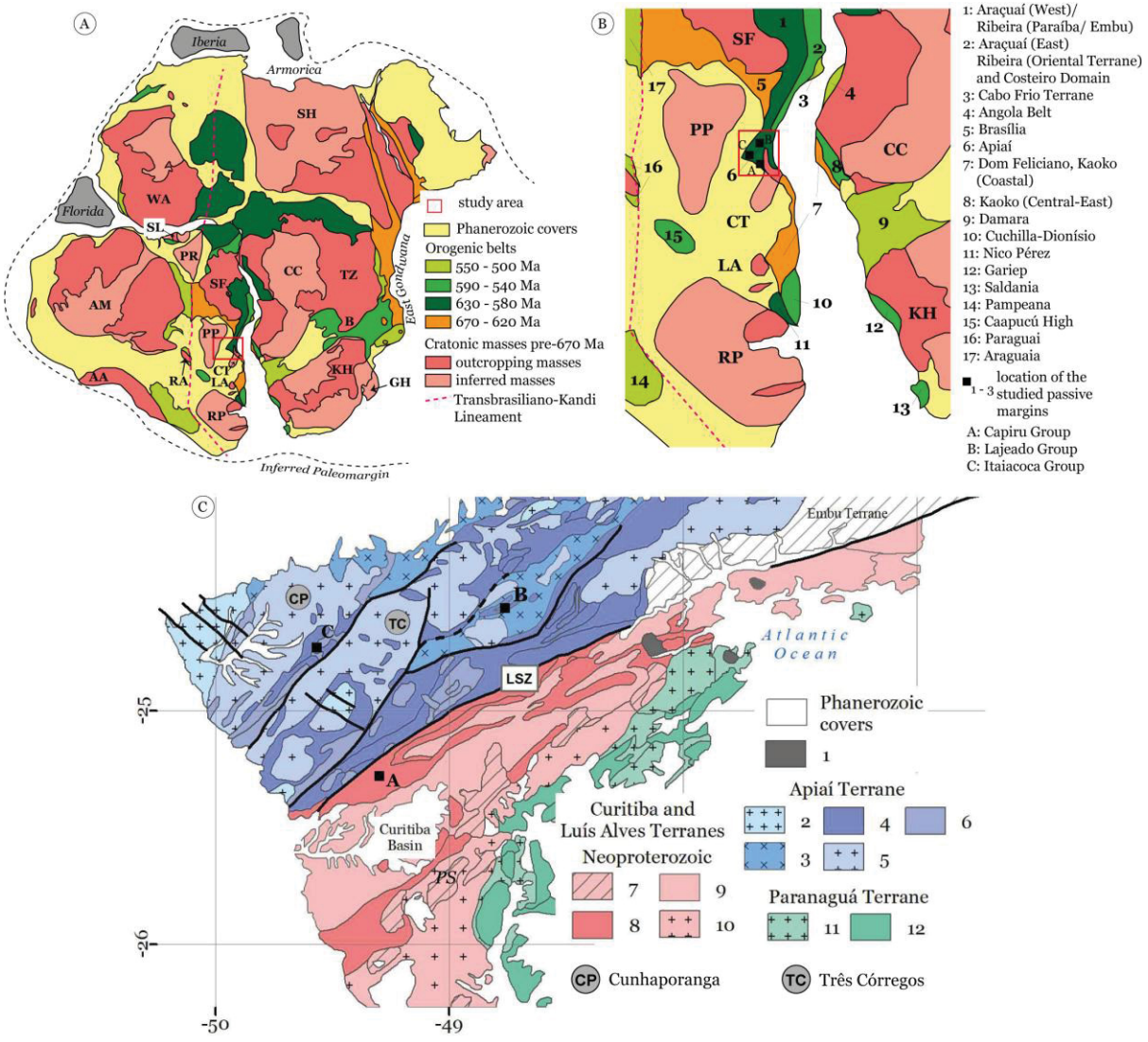


Figura 1. Contexto geológico do Grupo Capiru. A) Contexto paleogeográfico do Gondwana Oeste (ca. 500 Ma) com crátons (continentes pré-Gondwana) suturados por faixas móveis Brasilianas (B) (modificado de Schmitt et al. 2018). AA: Arequipa/ Antofalla, AM: Amazonia, B: Bangweulu Block, CC: Congo, CT: Curitiba, GH: Grunehogna, KH: Kalahari, LA: Luís Alves, PP: Paranapanema, PR: Parnaíba, RA: Río Apa, RP: Río de La Plata, SH: Sahara, SF: São Francisco, SL: São Luís, TZ: Tanzania, WA: West Africa. C) Contexto tectônico regional do Cinturão Ribeira Sul (modificado de Basei et al. 2008): 1: complexos alcalinos, (2-6) TERRENO APIAÍ - 2: Bacias molássicas de Castro e

Camarinha, 3: Granitos, 4: Sucessões Neoproterozóicas, 5: Granitos Neoproterozóicos (CP: Cunhaporanga e TC: Três Córregos); 6: Unidades Estaterianas, (7-10) TERRENOS CURITIBA E LUÍS ALVES - 7: Bacias extensionais e granitos, 8: Sucessões Neoproterozóicas (incluindo o Grupo Capiru e Complexo Turvo-Cajati), 9: Orto-gnaisses Riacianos retrabalhados, migmatitos (Complexo Atuba) e gnaisses Riacianos, 10: Orto-gnaisses e granulitos; (11-12) TERRENO PARANAGUÁ - 11: granitos Neoproterozóicos, 12: Sucessões Meso- e Neoproterozóicas, LSZ: Zona de Cisalhamento Lancinha, SAS: Antiforme do Setuva, PS: Sutura Piên.

1.2 LOCALIZAÇÃO DA ÁREA DE ESTUDO

A área de estudo está localizada na porção leste do estado do Paraná, no âmbito do Primeiro Planalto Paranaense, e engloba as rochas do Grupo Capiru, Complexo Setuva e Complexo Atuba (Fig. 2). A área está situada a norte do município de Curitiba, abrangindo os municípios de Campo Magro, Camplo Largo, Almirante Tamandaré, Colombo, Rio Branco do Sul e Bocaiúva do Sul (Fig. 2a).

A principal via de acesso, partindo-se de Curitiba, se dá através da BR-476 (Estrada da Ribeira). Acessos alternativos podem ser efetuados pela PR-090, PR-417 (ou Rodovia da Uva) e pela PR-092, ou Rodovia dos Minérios (Fig. 2a).

1.3 JUSTIFICATIVA

Estudos recentes nas unidades que compõem o Cinturão Ribeira Sul têm promovido significativos avanços quando a idade de formação das rochas, contextos deposicionais, paleoambientais, idades de sedimentação e suas possíveis fontes, a fim de promover correlações com as sucessões do oeste africano e dentro do âmbito do Gondwana Oeste. As técnicas isotópicas associadas a estudos estratigráficos e mapeamentos de detalhe permitem a reconstrução necessária para proposta de novos modelos evolutivos e paleogeográficos e refinamento de modelos existentes.

A Faixa Ribeira Sul preserva parte da evolução do ciclo continental Brasiliano, onde o Grupo Capiru (Fig. 3) apresenta grande potencial para estudos de reconstrução. Os litotipos do Grupo Capiru são rochas supracrustais localizadas na porção norte do Terreno Curitiba (Fig. 3), compostas essencialmente por rochas metassedimentares que recobrem as unidades do embasamento (Núcleo Setuva e

Complexo Atuba), onde são reconhecidos alvos geológicos para reconstruções estratigráficas, estudos geoquímicos e geocronológicos.

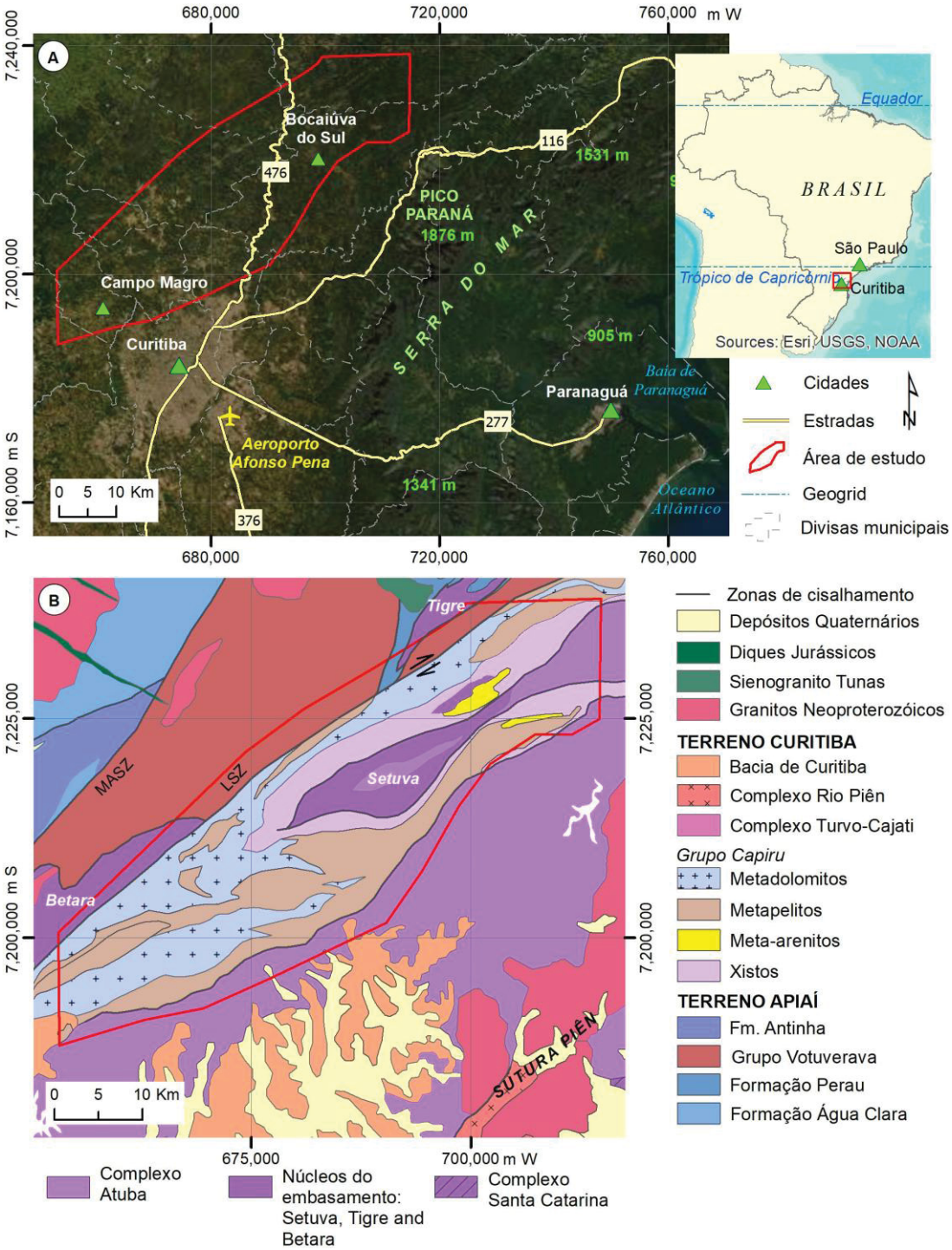


Figura 2. A) Localização da área de estudo no contexto do Primeiro Planalto Paranaense, leste do estado do Paraná, Sul do Brasil, com as principais vias de acesso. B) Mapa geológico simplificado dos terrenos Apiaí e Curitiba com localização da área de estudo.

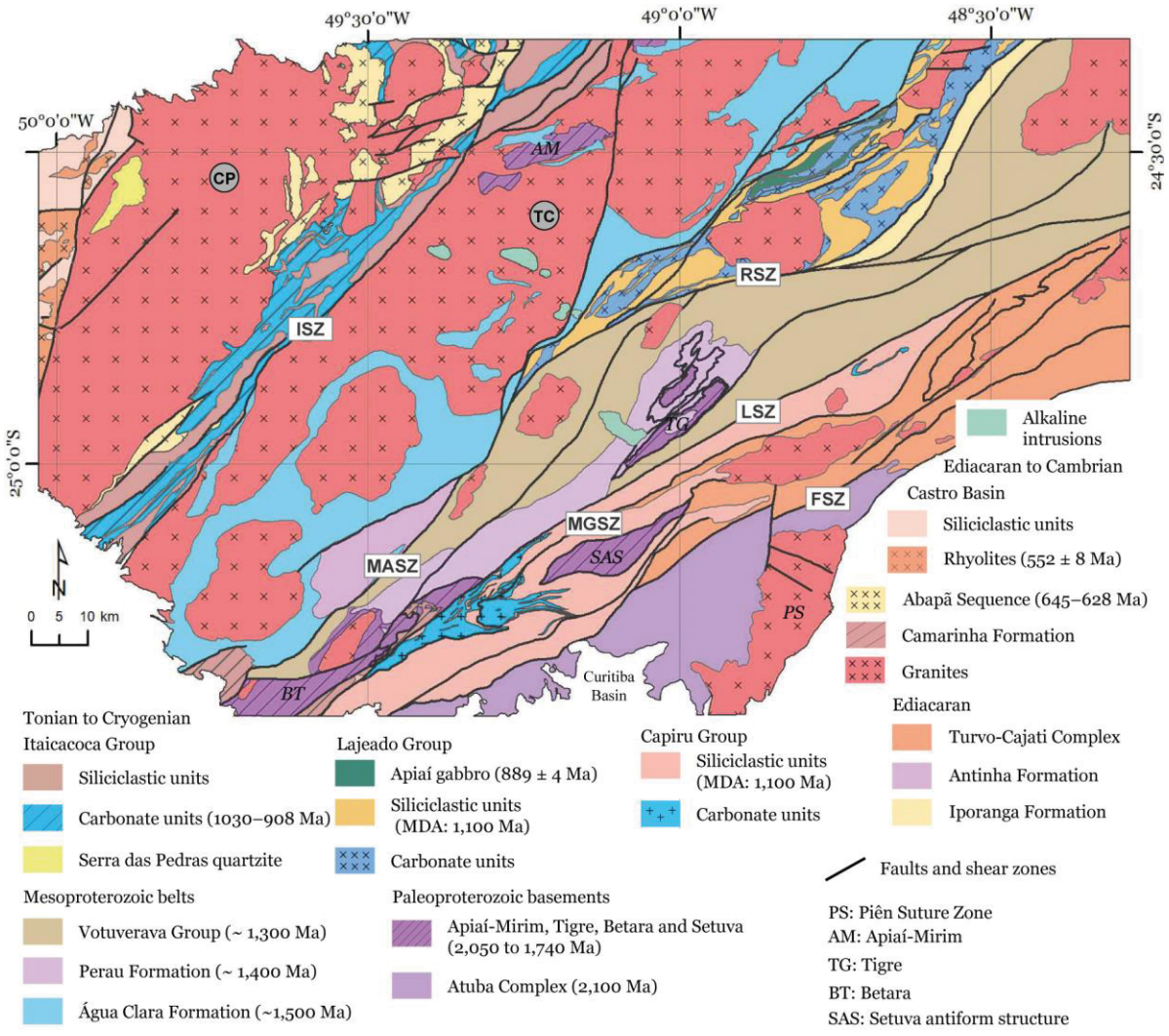


Figura 3. Mapa geológico simplificado dos terrenos Apiaí (a norte da Zona de Cisalhamento Lancinha - LSZ) e Curitiba (a sul). As idades utilizadas foram compiladas de Kaulfuss 2001, Sato et al. 2003, 2009, Weber et al. 2003, Siga Jr. et al. 2002, 2009, 2011, Campanha et al. 2015, 2016, Forero-Ortega et al. 2020, Ricardo et al. 2020. Suítes graníticas - CP: Cunhaporanga, TC: Três Córregos, Núcleos do embasamento - AM: Apiaí-Mirim, TG: Tigre, BT: Betara, SAS: Setuva. Zonas de Cisalhamento - ISZ: Itapirapuã, MASZ: Morro Agudo, RSZ: Ribeira, MGSZ: Morro Grande, LSZ: Lancinha, FSZ: Faxinal.

1.4 HIPÓTESE

Muitas são as questões que permanecem abertas quanto à origem, derivação e evolução dos blocos continentais da Faixa Ribeira Sul. Neste contexto, os registros das bacias que bordejaram esses fragmentos podem ser utilizados como ferramentas para interpretações paleogeográficas.

Na área de estudo o Terreno Curitiba representa um fragmento continental pré-existente de origem desconhecida no contexto da amalgamação do Gondwana

Oeste. A hipótese é de que o Grupo Capiru teria sido depositado num contexto de margem continental passiva na margem norte da microplaca Curitiba, conectado a um oceano Brasiliano durante o Mesoproterozóico Superior – Neoproterozóico Inferior. Dessa forma, os registros sedimentares, ambientes de deposição e ambiente deformador, aliados aos dados de provieniência, podem responder parte da história geológica desse fragmento continental.

1.5 OBJETIVOS

O objetivo principal desta pesquisa é a caracterização do contexto paleogeográfico e classificação do ambiente tectônico do Grupo Capiru. Para isso, foram necessários:

i) Descrever e classificar fácies sedimentares preservadas, suas associações e ambientes deposicionais;
ii) Determinar a composição das rochas, reconhecendo suas paragêneses metamórficas e seus contextos deformacionais;
iii) Compreender os aspectos estruturais, identificando as principais estruturas tectônicas;

Estes estudos foram necessários para:

a) Discutir o ambiente tectônico das sucessões sedimentares do Grupo Capiru para proposta de um novo modelo estratigráfico.
b) Identificar as principais assinaturas geoquímicas nessas formações e seus significados paleoambientais;
c) Compreender a relação genética entre as formações do Grupo Capiru, determinar suas idades máximas de deposição e possíveis áreas fontes.

2 GEOLOGIA REGIONAL

O Grupo Capiru, previamente classificado como Formação Capiru, definida por Bigarella e Salamuni (1956), está inserido dentro do contexto do Sistema Orogênico Ribeira, um grande sistema orogênico do Neoproterozóico (Fig. 4), relacionado à amalgamação do Gondwana Oeste (Heilbron et al. 2008).

O Cinturão Ribeira é definido como um sistema orogênico de direção NE-SW que resultou da colisão entre o paleocontinente São Francisco-Congo com a parte sudoeste do Cráton de Angola (Heilbron et al. 2008). Outras microplacas também foram envolvidas nessa acresção (Campos Neto 2000, Trouw et al. 2000, Heilbron et al. 2000), e a convergência se deu através de episódios orogênicos com desenvolvimento principal durante o Neoproterozóico-Cambriano e com os últimos estágios no início do Ordoviciano (Heilbron et al. 2008, Schmitt et al. 2004).

A porção sul do Sistema Orogênico Ribeira, ou Faixa Ribeira Sul, ocorre nos estados de São Paulo, Paraná e Santa Catarina, e é constituída por quatro compartimentos tectônicos denominados de terrenos Apiaí, Curitiba, Luís Alves e Paranaguá (Fig. 1c; Siga Jr 1995, Campanha e Sadowski 1999, Kaulfuss 2001, Campanha et al. 2008, Heilbron et al. 2008, 2020, Basei et al. 2008, Siga Jr et al. 2009, Cury 2009, Siga Jr. 2011a, 2011b and 2011c).

O Terreno Apiaí (Fig. 1c) é formado por rochas paleoproterozóicas representadas por sienogranitos anorogênicos e rochas metabásicas de c. 1,75 Ga (Kaulfuss 2001, Cury et al. 2002, Siga et al. 2005). Uma característica marcante do Terreno Apiaí é a ampla ocorrência de sucessões mesoproterozóicas (c. 1600–1500, 1500–1400, 1030–908 Ma), ricas em rochas carbonáticas, com unidades siliciclásticas e metavulcânicas (*e.g.* Betara, Água Clara, Perau, Votuverava, Itaiacoca e Lajeado).

Várias sucessões neoproterozóicas também ocorrem no Terreno Apiaí (*e.g.* Sequência Abapã, Iporanga, Grupo São Roque), e estão representadas por unidades (meta) siliciclásticas-vulcânicas e (meta) carbonáticas-vulcânicas. Os dados geocronológicos disponíveis sugerem deposição em torno de c. 645-628, 620-605 e 600 Ma, parcialmente correlatas com a geração de batólitos cálcio-alcalinos relacionados ao arco de c. 620-600 Ma, sugerindo ambientes de *back-arc* ou *intra-arc* para essas sequências (Hackspacher et al. 2000).

As principais deformações, magmatismo e metamorfismo no Terreno Apiaí ocorreram entre 620 e 600 Ma. As zonas de cisalhamento que separam os domínios tectônicos do terreno Apiaí estão relacionadas a uma tectônica tardia datada em c. 590–575 Ma (Campanha et al. 2005).

O Terreno Curitiba (Fig. 1c) é delimitado ao norte pela Zona de Cisalhamento Lancinha, considerada o contato entre os terrenos Apiaí e Curitiba. Ao Sul as Zonas de Cisalhamento Piên-Mandirituba e Icapara o separam das unidades tectônicas Luís Alves e Paranaguá, respectivamente. Este bloco é formado principalmente por ortognaisses paleoproterozóicos do Complexo Atuba, migmatizados durante o Ediacarano (Siga Jr. et al. 1995, Sato et al. 2003, 2009), alguns núcleos de rochas granulíticas de ca. 2,1 Ga (Siga et al. 1995, Basei et al. 2000, 2003), granitóides deformados do Núcleo Setuva, unidades supracrustais mesoproterozóicas (Esteniano) e Neoproterozóicas (Ediacarano), representadas pelo Grupo Capiru e Complexo Turvo-Cajati, respectivamente (Siga Jr. et al. 2012; Campanha et al. 2016, Leandro 2016) e intrusões graníticas Ediacaranas (Siga Jr. 1995).

As rochas do embasamento e supracrustais foram afetadas pelo episódio metamórfico neoproterozóico de c. 600 Ma. Os terrenos Curitiba e Luís Alves são conectados pela zona de sutura Piên, de tendência NE (Fig. 1c), caracterizada por rochas relacionadas ao arco de c. 610 Ma, consideradas uma evidência de subducção para noroeste (Basei et al. 2000).

O Terreno Luís Alves (Fig. 1c) é considerado um bloco cratônico formado principalmente por ortognaisses arqueanos a paleoproterozóicos, migmatitos e granitos com afinidades TTG (Hartmann et al. 2000; Basei et al. 2009). Este bloco é o embasamento para o arco magmático de Piên (Harara 2001), parte dos granitos Tipo-A da Suite Serra do Mar (Vlach et al. 2011, Vilalva et al. 2019), e para as bacias extensionais pós-colisionais ediacaranas (Basei et al. 1998; Quiroz-Valle et al. 2019).

Por fim, o Terreno Paranaguá (Fig. 1c), estende-se a NE-SW, consistente com a tendência regional do Cinturão Ribeira, limitado por zonas de cisalhamento que o separam do Terreno Luís Alves. Ao norte, o contato com o Terreno Curitiba ocorre por zonas de cisalhamento de baixo ângulo (Siga Jr. 1995, Cury 2009). O Terreno Paranaguá é formado principalmente por suítes graníticas ediacaranas

intrudindo os *inliers* do embasamento paleoproterozóico e rochas metassedimentares mesoproterozóicas (Cury 2009).

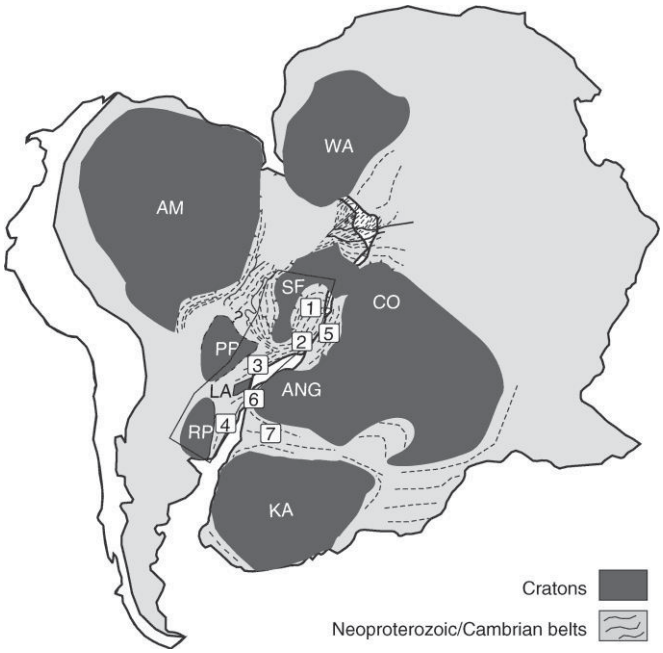


Figura 4. Localização das faixas móveis Neoproterozóicas e crátons na América do Sul e África (Gondwana Ocidental). Fonte: Heilbron et al. 2008. Faixas móveis Neoproterozóicas: 1: Araçuaí, 2: Ribeira Central, 3: Ribeira Sul, 4: Dom Feliciano, 5: Oeste-Congo, 6: Kaoko, 7: Damara. Grandes blocos cratônicos: AM: Amazonia, SF: São Francisco, LA: Luís Alves, RP: Rio de La Plata, WA: Oeste-Africa, CO: Congo, ANG: Angola, KA: Kalahari.

2.1 CONTEXTO GEOLÓGICO DO GRUPO CAPIRU

O Grupo Capiru é uma das unidades supracrustais do Terreno Curitiba (Siga Jr 1995, Basei et al. 1992, Basei et al. 2008), um compartimento tectônico composto por ortogneisses e migmatitos do Complexo Atuba, granitóides deformados do Complexo Setuva, e as coberturas metassedimentares do Grupo Capiru e do Complexo Turvo-Cajati (Fig. 3).

O Grupo Capiru é composto por unidades litológicas de baixo a médio grau metamórfico, delimitadas por falhas de cavalgamento e transcorrências, e inclui metapelitos, metapsamitos e metadolomitos, que afloram segundo uma faixa alongada de direção NE-SW, confinada entre o Complexo Atuba e a Zona de Cisalhamento da Lancinha (Fiori 1992, Fiori e Gaspar 1993, Siga Jr et al. 2007, Leandro 2016, Santos et al. 2018).

O Grupo Capiru faz contato com as rochas do Terreno Apiaí em sua porção norte, através da Zona de Cisalhamento da Lancinha (ZCL). Os contatos com os Complexos Setuva e Turvo-Cajati são dados por importantes falhas de cavalgamento (Faleiros et al. 2011, 2016), enquanto que em seu limite sul está em contato com os gneisses e migmatitos do Complexo Atuba (Fig. 3).

2.2 CONTEXTO TECTONO-ESTRUTURAL

A deformação no Grupo Capiru exibe padrões complexos. O Grupo Capiru parece ser representativo de um *thrust-and-fold belt* que foi relativamente transportado sobre o embasamento como um corpo relativamente coerente, e seu padrão estrutural pós-colocação foi afetado por vários eventos tectônicos mais jovens (Tabela 1, Seção 4.2).

São reconhecidos pelo menos dois estágios tectono-metamórficos no Grupo Capiru: o primeiro relacionado com a tectônica colisional e outro associado a uma tectônica transcorrente (Fiori 1992, Faleiros et al. 2011, Leandro 2016, Santos 2017, Santos et al. 2018). A tectônica de cavalgamentos é posterior a uma fase regional de metamorfismo, desenvolvido sob condições de fácies subxisto verde a xisto verde, podendo chegar a condições de fácies anfibolito em porções localizadas (Santos et al. 2018).

A tectônica de cavalgamentos é responsável por posicionar unidades distintas lado a lado (Fiori 1992). A deformação relacionada a este evento possui caráter heterogêneo, e com isso, algumas sequências litológicas mantiveram sua sucessão estratigráfica preservada (Leandro 2016).

A tectônica transcorrente deforma os registros tectônicos previamente formados com grandes sistemas de dobras e zonas de cisalhamento (Faleiros et al. 2011), com geração de paragêneses metamórficas restritas às zonas miloníticas, com deformação mais intensa próxima às principais falhas transcorrentes regionais (Leandro 2016, Santos et al. 2018).

2.3 ESTRATIGRAFIA DA FORMAÇÃO CAPIRU

As rochas do Grupo Capiru foram previamente subdividas em três “Conjuntos Litológicos” distintos, segundo a definição proposta por Fiori (1992),

denominados de conjuntos Juruqui, Rio Branco e Morro Grande (Fig. 5). Essa divisão considera as associações litológicas dessas unidades, estruturas sedimentares, características estruturais presentes, aspectos morfológicos e, principalmente, os limites dos conjuntos, que estão representados por importantes falhas de cavalgamento.

Segundo o modelo estratigráfico proposto por Fiori (1992) e Fiori e Gaspar (1993), na base da formação ocorrem os metassedimentos do Conjunto Juruqui, caracterizado pela intercalação de filitos avermelhados com quartzitos.

O Conjunto Rio Branco, que representa a porção intermediária da formação, engloba mármores dolomíticos com intercalações de filitos rítmicos e quartzitos, e está posicionado tectonicamente sobre o Conjunto Juruqui (Fiori 1992).

No topo da formação ocorre o Conjunto Morro Grande, caracterizado pela presença de meta-arenitos e filitos rítmicos carbonosos, intercalados a quartzitos e níveis de mármores dolomíticos. Este conjunto está posicionado sobre o Conjunto Rio Branco (Fiori 1992).

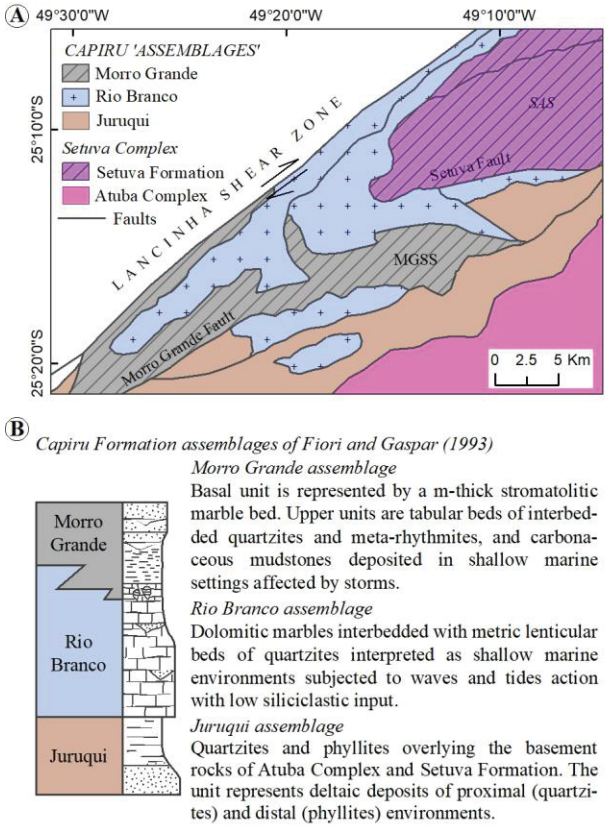


Figura 5. Conjuntos litológicos e modelo estratigráfico proposto para a Formação Capiru. Modificado de Fiori e Gaspar (1993).

2.4 ESTRUTURAS SEDIMENTARES E AMBIENTES DE DEPOSIÇÃO

Um dos aspectos mais marcantes do Grupo Capiru diz respeito à presença de zonas intensamente deformadas, contrastando com zonas apresentando registro sedimentar preservado, como observado por Biagrella e Salamuni (1956, 1958), Fiori (1992), Fiori e Gaspar (1993), Juschacks (2006), Bahniuk (2007), Silva (2010), Leandro (2016).

As principais estruturas sedimentares identificadas são as estratificações plano-paralelas, estratificações cruzadas, marcas onduladas assimétricas, gradações normais e inversas, gretas de contração, *tidal bundles* e *hummockys* nas sequências terrígenas, além de brechas intraformacionais, estruturas pisolíticas-oolíticas e estruturas estromatolíticas nos metadolomitos (Bigarella e Salamuni 1956, 1958, Fiori 1992, Fiori e Gaspar 1993, Yamato 1999, Juschacks 2006, Silva 2010, Leandro 2016).

Inicialmente as sucessões sedimentares foram interpretadas como ambientes plataformais variando de rasos a profundos (Fiori 1992). Posteriormente as sequências siliciclásticas foram reinterpretadas associando o Conjunto Juruqui a depósitos de leque deltáico e o Conjunto Morro Grande como depósitos de uma plataforma marinha rasa (Fiori e Gaspar 1993).

Leandro (2016) interpreta para as sequências siliciclásticas do Conjunto Morro Grande, um ambiente de deposição estuarino, com influência de correntes de maré. Já nas sequências carbonáticas, os sedimentos estariam associados a plataformas carbonáticas rasas, em zonas de supramaré a inframaré (Juschacks, 2006, Bahniuk 2007, Silva 2010).

3 MATERIAIS E MÉTODOS

Para a realização desta pesquisa foram utilizados os seguintes métodos:

3.1 LEVANTAMENTOS DE CAMPO

Durante os levantamentos de campo foram construídas seções geológicas estruturais de semidetalhe, em escala 1:25.000, buscando a descrição dos principais litotipos e suas composições, estruturas tectônicas, fácies sedimentares e suas associações. Foram efetuados, no total, 78 dias de campo, divididos em várias etapas.

Após o levantamento das seções de semidetalhe, localidades específicas foram escolhidas para o levantamento e detalhamento de seções-tipo. Informações sobre as seções-tipo de cada formação constam no **Anexo 2**.

3.1.1 ESTUDO FACIOLÓGICO

Para o estudo estratigráfico foram descritas e individualizadas as fácies sedimentares, suas associações e interpretações ambientais, com o objetivo de construir modelos deposicionais nos locais com estratigrafia preservada. Os resultados dos modelos deposicionais interpretados podem ser consultados na Seção 4.1 – Resultados do artigo 1.

3.1.2 MAPEAMENTO E INTEGRAÇÃO GEOLÓGICA

As práticas de mapeamento geológico padrão foram aplicadas nas exposições do Grupo Capiru, com o objetivo de identificar as principais descontinuidades estruturais ou estratigráficas. O mapa geológico principal é apresentado no **Anexo 1**.

Um mapeamento geológico detalhado foi realizado durante 2016 a 2020. As interpretações originais e o novo mapa geológico foram recentemente compilados e integrados com os dados de campo anteriores dos levantamentos geológicos

estaduais (MINEROPAR) e nacionais (CPRM), e com pesquisas não publicadas e recentes estudos publicados.

A Seção 4.2 – Resultados do Artigo 2 apresenta a compilação com a síntese mais atualizada da geologia do Grupo Capiru. As bases geológicas em *mpk e suas atualizações estão disponibilizadas em https://data.mendeley.com/datasets/mywdxyfkwr/1.

3.2 GEOQUÍMICA DE ROCHA TOTAL

Após a identificação das principais unidades litoestratigráficas foram coletadas amostras para identificação da composição química e mineralógica dos litotipos estudados. Os resultados das análises químicas e mineralógicas por fluorescência e difratometria de raios-X, respectivamente, são apresentados na Seção 4.1.6 – Artigo 1.

3.2.1 FLUORESCÊNCIA DE RAIOS-X

Amostras representativas das rochas descritas foram selecionadas para análises de rocha total com o objetivo de estabelecer assinaturas geoquímicas para cada uma das unidades mapeadas.

As amostras foram trituradas em britador de mandíbulas e moinho de discos. As amostras pulverizadas foram analisadas por fluorescência de raios-X para quantificação dos principais óxidos em um espectrômetro Panalytical AXIOS MAX do Instituto LAMIR - Universidade Federal do Paraná, utilizando pastilhas fundidas (0,9 g de amostra + 0,1 g de tetraborato de lítio).

A calibração é realizada rotineiramente usando padrões internacionais, e correções para sobreposição espectral foram aplicadas. Os limites de detecção são 0,01 por cento em peso de óxido. A perda por ignição (*LOI*) foi determinada por aquecimento de amostras a 1000° C por 2 horas, utilizando 2 g da amostra em pó.

3.2.2 DIFRATOMETRIA DE RAIOS-X

As fases minerais foram identificadas por meio de difração de raios X (DRX) para determinar a composição mineralógica das rochas estudadas. Varreduras de amostras em pó de rocha total foram efetuadas com um difratômetro Empyrean PanAlytical, equipado com um ânodo de Cu (Kα1 = 1.5406 Å), 40kV, 40mA.

A faixa de varredura 2θ foi o intervalo padrão 3,0 - 70 °, com um *size/step* de 0,016º2θ e um tempo de contagem de 10,16s por *step*, seguindo os procedimentos do Instituto LAMIR. As fases minerais foram determinadas com o software HighScore Plus® para análise qualitativa, usando o banco de dados 2002-PDF2-ICDD para interpretação de fases com base em padrões de difratogramas.

3.2.3 CARBONO ORGÂNICO TOTAL (COT)

O teor de carbono orgânico total (COT) dos metapelitos foi obtido pelo método de combustão a seco, utilizando um analisador infravermelho C, H e N, LECO Truspec CHN no Laboratório de Solos – do Setor de Agrárias da UFPR. O procedimento utilizou uma alíquota de 0,25 g de amostra em pó. Não houve necessidade de seguir a etapa de remoção do carbono inorgânico, uma vez que nenhum teor de carbono inorgânico foi identificado.

3.3 MÉTODOS GEOFÍSICOS

3.3.1 AEROMAGNETOMETRIA

Domínios magnéticos e estruturas potenciais foram interpretados a partir de dados aeromagnéticos. Tais estruturas foram verificadas e comparadas com dados de campo.

A fonte de dados utilizada foi o levantamento aerogeofísico magnetométrico e gamaespectrométrico do Serviço Geológico do Brasil (CPRM 2010). Com linhas

de vôo espaçadas 500 m na direção N-S. As grades geofísicas têm células de 250 x 250 m, que foram interpoladas com o algoritmo bidirecional e usando o azimute preferencial N135 (Geosoft 2001).

Devido à notável assinatura magnética do enxame de diques máficos mesozoicos da província magmática do Paraná, a localização precisa das principais estruturas de embasamento orientadas NE-SW pode ser escondida por anomalias magnéticas NW-SE. Portanto, a anomalia magnética NW foi filtrada com cosseno direcional (Geosoft 2001), a fim de mitigar a tendência NW-SE e aumentar os padrões magnéticos das unidades do embasamento.

3.3.2 AEROGAMAESPECTOMETRIA

A partir dos dados gamaespectrométricos foram confeccionados mapas de contorno dos radioelementos (^{40} K, ^{232} Th e ^{238} U) e de contagem total. Os mapas gerados foram utilizados para a delimitação dos corpos rochosos e de contatos geológicos.

3.4 U-PB EM ZIRCÃO DETRÍTICO POR LA-ICP-MS

O método U-Pb em zircão tem como uma das principais aplicações a determinação de idades de cristalização em rochas metamórficas e granitóides. Idades obtidas nas diferentes populações de grãos detríticos individuais de arenitos e pelitos informam sobre a geocronologia dos distintos eventos formadores de rocha da área-fonte, permitindo discriminar a proveniência sedimentar com maior precisão.

Apoiados em estudos estratigráficos, estruturais e geoquímicos, as idades dos sedimentos são comparadas com as idades das possíveis áreas fontes selecionadas. Quando as idades são apoiadas em informações estratigráficas, estruturais e geoquímicas, o significado geológico destas pode ser utilizado em reconstruções paleogeográficas globais.

A técnica analítica por LA-ICP-MS (*Laser Ablation – Inductively Coupled Plasma - Mass Spectrometry*), é uma técnica de alta resolução, que possibilita

analisar grãos individuais de zircão, suas estruturas internas (com registros isotópicos de núcleo e borda), em quantidades estatisticamente representativas.

Oito amostras do Grupo Capiru (Tabela 1, Seção 4.3) foram separadas a partir de ~ 5-7 kg de rocha seguindo os protocolos de separação mineral usados na Universidade de São Paulo, usando as técnicas-padrão isodinâmica, gravimétrica e magnética.

Após a separação, os grãos detríticos de zircão foram escolhidos manualmente, montados em discos de resina epóxi juntamente e imagens de elétrons retroespalhados (*back scattering*) foram coletadas.

Além disso, imagens de catodoluminescência (CL) foram coletadas usando um microscópio eletrônico de varredura para orientar a seleção das posições dos pontos de *laser*. Para cada amostra 100 grãos de zircão foram analisados em analisador Photon-machine® G2 - 193 nm - Excimer Laser Ablation System a laser acoplado ao MC-ICP-MS Thermo® Neptune do CPGeo da Universidade de São Paulo . Um *spot* de 30 µm foi usado com uma profundidade de 30-50 µm. As razões de isótopos foram monitoradas e corrigidas para desvio e fracionamento U-Pb com repedtidas análises dos materiais de referência: zircão GJ-1 (Jackson et al. 2001), brancos, padrão NIST-613 sintético e desconhecidos. Os dados obtidos foram reduzidos e corrigidos seguindo os procedimentos de Siqueira et al. (2014), e os resultados foram relatados usando o *software* Isoplot 4.0 (Ludwig 2012) e AgeCalcML 1.42 (Sundell et al. 2021).

As amostras adicionais (do Grupo Lajeado e do gabbro de Apiaí, ver Seção 4.3) foram separadas a partir de ~ 5 e ~ 15 kg de rocha, respectivamente, seguindo os procedimentos de separação mineral usados na Universidade de Ouro Preto. Essas duas amostras foram analisadas por meio do analisador Photon-machine® G2 - 193 nm - Excimer Laser Ablation System a laser acoplado ao MC-ICP-MS Thermo® Neptune da Universidade de Ouro Preto. Um *spot* de 20 µm foi usado com uma profundidade de 5-10 µm. Detalhes dos procedimentos podem ser consultados em Lana et al. (2017).

Os resultados do U-Pb foram relatados usando o software isoplot 4.0 (Ludwig 2012) e AgeCalcML 1.42 (Sundell et al. 2021). Apenas idades de zircão U – Pb com discordância igual ou <10% de ambos os conjuntos de dados foram consideradas para este trabalho. Todos os dados isotópicos coletados de U – Pb de zircão constam no **Anexo 2** desde volume.

4 RESULTADOS

4.1 ARTIGO 1: THE CAPIRU GROUP: FROM PASSIVE MARGIN TO SYN-OROGENIC UNITS, IMPLICATIONS FOR THE EVOLUTION OF THE NORTHERN MARGIN OF THE CURITIBA MICROPLATE, WESTERN GONDWANA

https://doi.org/10.1016/j.jsames.2021.103555

Larissa da Rocha Santos[1,2]; Renato Leandro[2]; Guilherme Fedalto[1,2]; André Spisila[3]; Anelize Bahniuk[1,2]; Oswaldo Siga Jr.[4]; Leonardo Fadel Cury[1,2].

1: Department of Geology, Federal University of Paraná, Brazil
2: LAMIR Institute - Laboratory of Mineral and Rocks, Brazil
3: Geological Survey of Brazil (CPRM) – Paraná, Brazil
4: University of São Paulo, Brazil

Highlights

- The Capiru Group shows two distinct evolutionary stages of a basin developed on the northern Curitiba microplate margin.
- Definition and regional correlation of six formations from the Capiru Group allow uniformization of stratigraphic nomenclature.
- We propose paleo-latitudinal correlation with the Phantom Glacial units of the Paranapanema and Rio de la Plata cratons.

ABSTRACT: The Capiru Group (Neoproterozoic) is a 4 km-thick succession deposited on the northern margin of the Curitiba microplate, Southern Ribeira Belt, Brazil. The Capiru Group successions are deformed within the Brasiliano - Pan African Ribeira Belt, which culminated in the amalgamation of Western Gondwana. Even though the rocks are metamorphosed and deformed, preserved sedimentary structures and outcrop exposures allowed the interpretation of depositional environments and stratigraphic analysis. The Capiru Group metasedimentary rocks

were studied by field mapping, measured sections and bulk-rock chemical compositions. Six formations were identified, termed from oldest to youngest as: Santana (proximal to distal marine shelf), Juruqui (proximal to distal deltaic), Rio Branco (carbonate platform), Morro Azul (lagoonal to shallow marine), Morro Grande (proximal to distal deltaic/ marine) and Bocaina formations (estuarine to shallow-marine). Two main basin stages were identified: a passive continental margin stage, with increasing tectonic quiescence followed by a marine regression, and a syn-orogenic stage at the Curitiba microplate margin.

Chemical and mineralogical Fe- and Al-rich compositions suggest continental denudation during the passive continental margin stage, with low sediment input rates from a relatively low-gradient relief, highly weathered continental source, and stability since Mesoproterozoic time. Sedimentological and stratigraphic similarities were found among Capiru Group passive margin successions and units deposited on the Río de Plata and Southern Paranapanema margins.

The paleoenvironmental interpretations, such as greenhouse conditions and high weathering rates alternated with depositional gaps, indicate climatic changes during the Capiru Group deposition, with far-field or Phantom Glacial influence related to the regional discordances. These features are important for the paleogeographic reconstructions that must consider a tropical or equatorial position ~ 650 - 635 Ma for the Curitiba microplate.

During deposition of the Bocaina Formation, the arkosic composition of sandstones and lithic conglomerate lags suggest source rejuvenation during the syn-orogenic stage, prior to the collisional thrusting that led to the Western Gondwana assembly.

Keywords: Tectonostratigraphy, Precambrian continental margins, Phantom Glacial, Southern Ribeira Belt, Curitiba terrane.

4.1.1 INTRODUCTION

Break-up of the Rodinia supercontinent resulted in the development of numerous rift and passive margin successions that were later rearranged within the

Gondwana framework. Many remnants of this break-up history are partially preserved in South American (Brito Neves et al. 1999, Cordani et al. 2003, Tupinambá et al. 2007, Fuck et al. 2008, Passarelli et al. 2019) and African counterparts (Meert and Powell 2001, Evans and Mitchell 2011, Li et al. 2008, 2013). One of these passive continental margin successions is referred to as the metasedimentary Capiru Group in southern Brazil, formerly known as the Capiru Formation (Fig. 1; Fiori and Gaspar 1993, Passarelli et al. 2018).

Previous work on these metasedimentary rocks revealed a polyphasic history with multiple deformation phases, all of which post-date deposition of the succession (Fiori 1992, Faleiros et al. 2016, Santos et al. 2018). Consequently, the Capiru Group experienced deformation and metamorphism after deposition, where its original features were folded and sheared along eastern coast of Brazil.

The available tectonic models in the region suggest a basin onset and depositional history starting after dismembering of the Rodinia Supercontinent (Sato et al. 2003, Mantovani and Brito Neves 2005, Fuck et al. 2008) followed by the closure of the Brasiliano oceans (Brito Neves et al. 2014), which was responsible for collisional thrusting in the region (Faleiros et al. 2011, 2016) that evolved to an indentation tectonic phase (Passarelli et al. 2011).

Despite good exposure of the Capiru Group rocks, depositional settings and paleogeography that predate deformation remain poorly understood. Unlike studies in Phanerozoic strata, interpretation of Precambrian depositional systems can be challenging due to the absence of diagnostic trace and body fossils. However, some key-criteria are used for recognition of ancient passive continental margins, which include the geographic distribution surrounding cratons or microcontinents, successions that are underlain by continental basement which may or may not have a pre-sedimentary cover, association with rift basins and basement that together are overlain by immediately younger, seaward-thickening and deepening prisms (Bradley 2008).

To date, there has been little systematic sedimentological and stratigraphic analysis of the Capiru Group rocks. Prior to this work, only some specific segments of the succession were studied in detail. However, these studies mainly focused on stromatolites and other biogenic structures in carbonate rocks (*e.g.* Guimarães et al. 2002, Juschaks 2006, Bahniuk 2007, Silva 2010).

In this study, we present a detailed and systematic outcrop study, a revised geological map, representative cross sections, a new comprehensive stratigraphic column, and bulk-rock geochemical data. We integrate these data to define six formations within the Capiru Group. The main outcomes of this work are: (1) refining the stratigraphy and defining the group status for these successions, (2) establishing an intrabasinal correlation that allows a uniform stratigraphic nomenclature to be applied throughout the region, and (3) discussing the basin geometry and its relationships to the surrounding cratonic blocks, aiming to provide paleogeographic constraints for the pre-collisional Western Gondwana.

4.1.2 BACKGROUND

4.1.2.1 Regional Tectonics

The Precambrian tectonic history of southeastern South America contains a record of the assembly of Western Gondwana during the Neoproterozoic Brasiliano – Pan-African orogenic cycle (Brito Neves et al. 1999, Campos Neto 2000, Heilbron et al. 2000, 2008, Faleiros et al. 2011). The Brasiliano orogen strikes subparallel to the coastline of southeastern Brazil (Fig. 1a) and its counterparts are presently located in the Kaoko and West Congo Belts of western Africa (Almeida et al. 1976, Heibron et al. 2008, Basei et al. 2005, 2018, Frimmel et al. 2013). The Brasiliano orogen comprises a complex arrangement of large cratonic masses, intermediate, and small crustal segments (Fuck et al. 2008).

The southeastern sector of the Brasiliano orogen in South America is referred to as the Ribeira Belt, which is comprised of fault-bounded terranes of different origins including reworked Archean to Paleoproterozoic basement blocks, Mesoproterozoic and Neoproterozoic (meta) passive margin strata, volcanic rocks, granitoids interpreted as arc complexes, and post-collisional granites (Basei et al. 1992, Campos Neto and Figueiredo 1995, Campanha and Sadowski 1999, Campos Neto 2000, Heilbron et al. 2004, 2008). The evolution of these micro- and continental plates during the Brasiliano – Pan-African convergence is difficult to establish, since its modern distribution is controlled by late, orogen-parallel, crustal-scale transcurrent shear systems related to the oblique collision between the large

continental masses of the Paranapanema, São Francisco, Luís Alves, and Congo cratons (Campanha and Brito Neves 2004, Heilbron et al. 2008, Faleiros et al. 2011, Passarelli et al. 2018).

The Southern Ribeira Belt in southern Brazil (Fig. 1c) includes the Apiaí and Paranaguá terranes, the Curitiba microplate, and the Luís Alves craton (Basei et al. 1992, 2009, Siga Jr et al. 2011a, 2011b). The Apiaí terrane consists of Meso to Neoproterozoic (meta) volcanics and sedimentary successions, originally deposited on the eastern margin of the Paranapanema paleocontinent (Basei et al. 1992, Passarelli et al. 2018). During the Neoproterozoic, as an active margin, this Ribeira Belt segment was intensely affected by calc-alkaline magmatism represented by granitic batholiths that constitute the roots of the Três Córregos, Cunhaporanga and Agudos Grandes magmatic arcs (Janasi et al. 2001, Prazeres Filho et al. 2003, Leite et al. 2007, Cury et al. 2008). The main metamorphism and deformation also occurred at this time (Basei et al. 1992, Siga Jr et al. 2009, Faleiros et al. 2016).

Basei et al. (1992) suggested a NW-subduction model between the Curitiba microplate (lower plate) and the Apiaí terrane (upper plate), resulting in a suture zone referred to as the Lancinha Shear Zone (Fig. 1). This suture zone was later affected by shearing, which resulted in the dextral shear zone between the Curitiba microplate and the Apiaí terrane (Fiori 1992, Castro and Ferreira 2015, Faleiros et al. 2016, Passarelli et al. 2018).

The contact between the Neo-Archean Luís Alves craton and the Paleoproterozoic Curitiba microplate is marked by the occurrence of Ediacaran granitoids and the Piên ultramafic complex (Basei et al. 2000, 2008). This rock association is considered to be the suture zone, and records the inversion and northwestward subduction between these two terranes (Basei et al. 2000, Harara 2001). The Luís Alves (lower plate) and Curitiba Microplate (upper plate) docked at ca. 590 Ma, as marked by the emplacement of syn-collisional I-type granitoids followed by the emplacement of Palermo, Agudos do Sul and Rio Negro A-type post-collisional granites (Harara 2001).

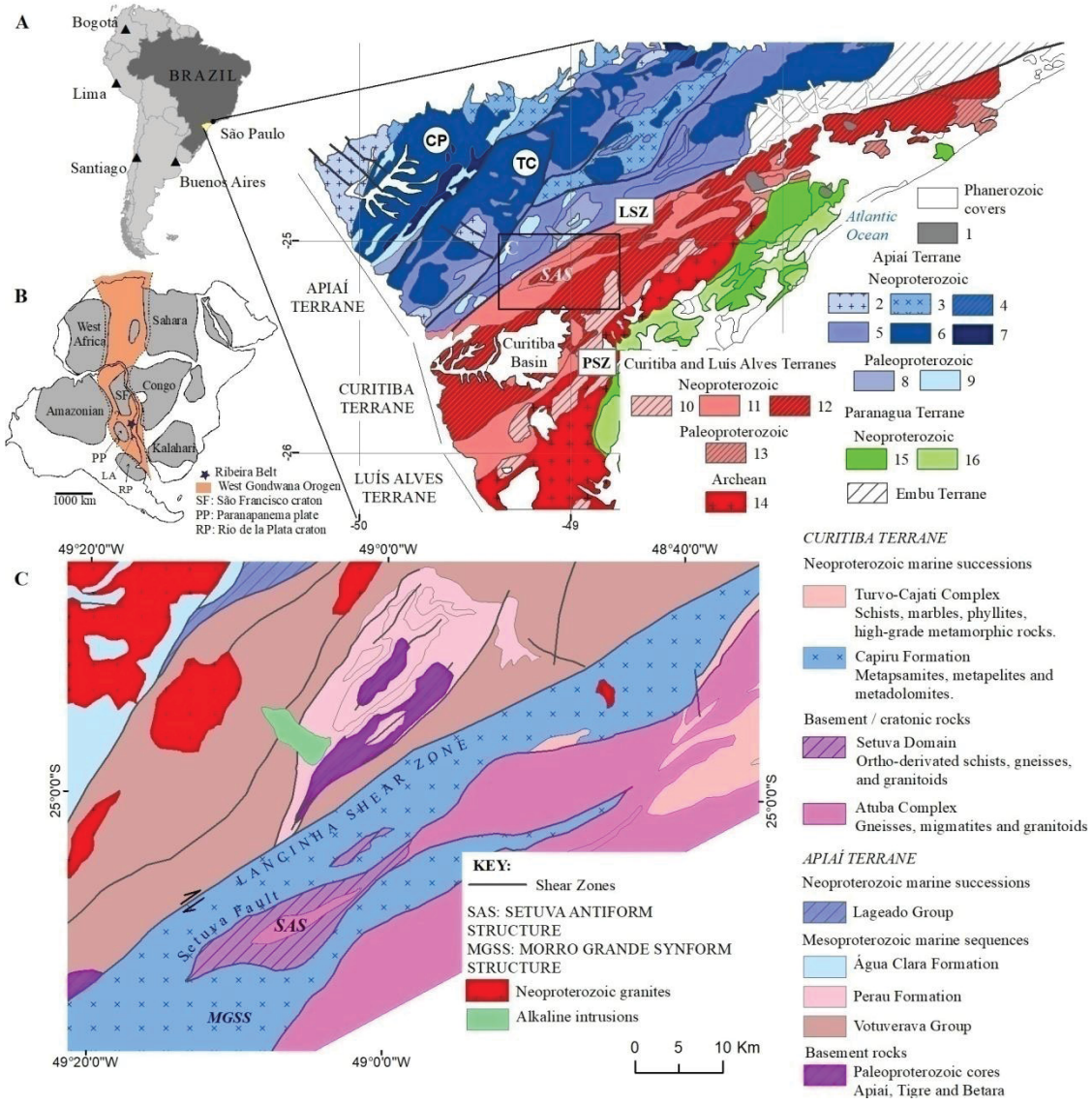


Figure 1. A) Tectonic map of Southern Ribeira Belt (after Basei et al. 2008): 1: Alkaline complexes, (2-9) APIAÍ TERRANE - 2: Molasse basins of Castro Group and Camarinha Formation, 3: Type-A granites, 4: Itu Suite, 5: Upper Neoproterozoic successions, 6: Neoproterozoic granites (CP: Cunhaporanga and TC: Três Córregos Complexes); 7: Lower Neoproterozoic succession, 8: Statherian formations, 9: Statherian orthogneisses, (10-14) CURITIBA AND LUÍS ALVES TERRANE - 10: Extensional basins and granites, 11: Neoproterozoic successions (including Capiru Group and Turvo-Cajati Complex), 12: Reworked Rhyacian orthogneisses and migmatites (Atuba Complex), 13: Rhyacian gneisses, 14: Orthogneisses and granulites; (15-18) PARANAGUÁ TERRANE - 15: Neoproterozoic granites, 16: Meso- to Neoproterozoic successions, LSZ: Lancinha Shear Zone, SAS: Setuva Antiform Structure, PSZ: Piên Suture Zone; B) Main crustal blocks in South America and Africa, including location of the Western Gondwana Orogen (after Gray et al. 2007, Brito Neves et al. 2014, Oriolo et al. 2017); C) Geological context of Capiru Group (after Fiori et al. 1985).

Lastly, the Paranaguá Terrane represents an exotic segment in the coastal region, formed by a variety of granitoids and supracrustal Mesoproterozoic remnants (Cury 2009, Patias et al. 2020). The docking of this tectonic unit took place after the Luís Alves and Curitiba Microplate collision, at ca. 600-550 Ma (Basei et al. 1992).

4.1.2.2 Curitiba Terrane

The Curitiba terrane is interpreted to be a microcontinent located between the Luís Alves and the Paranapanema cratonic masses (Basei et al. 2008, Passarelli et al. 2018, Passarelli et al 2019), which was stable during most of the Mesoproterozoic (Siga Jr et al. 1995, Sato et al. 2003).

The most striking structural feature in the studied area is known as the Setuva Antiform Structure (Fig. 1c), which was recognized as the core of a km-scale antiformal structure by early works (Bigarella and Salamuni 1956, Fiori 1992, Yamato 1999). More recently, this structure was interpreted as a large E-W trending anticlinorium stack that exposes a granitic basement core and the Capiru Group along its rims (Fig. 1c; Fiori et al. 2003, Siga Jr et al. 2016). The axial plane of the structure trends ~N60-70E, dipping 20° to SW (Fiori 1992). The main foliation is generally a crenulation cleavage (S2), which is better developed in the northern flank of the structure. A previous deformation phase (D1) is supported by the presence of a sub-parallel slaty cleavage (S1), poorly defined in the northern flank, due to the transposition by S2 surface (Faleiros et al. 2016). Fiori (1992) recognized folded-thrust faults along this structure (Fig. 1c) and identified the Setuva thrust as the main detachment horizon of the Capiru Group in relation to the Setuva core.

4.1.2.3 Previous tectonostratigraphic divisions of the Curitiba Terrane

Rocks of the Curitiba terrane were described as the Atuba Complex (Rhyacian, 2,100-2,050 Ma), the metasedimentary supracrustal covers referred to as the Setuva and Capiru Formations (Meso-Neoproterozoic?) and the metasedimentary Turvo-Cajati Complex (Ediacaran, 635-541 Ma); (Fig. 1c; Siga Jr et al. 1995, Passarelli et al. 2018 and references therein).

The basement of the Curitiba terrane is referred to as the Atuba Complex, which consists of banded biotite-amphibole gneisses, amphibolites and a variety of granitoids (Siga Jr et al. 1995), cropping out in the core of the Setuva Antiform as an elliptical, NE-trending, sheared, fault-bounded body (Fig. 1c), and to the south as a NE-trending belt. These rocks underwent medium- to high-grade metamorphism followed by an extensive migmatization during the Neoproterozoic (Siga Jr et al.

1995, Sato et al. 2003). The subsurface features of the Atuba Complex show a crustal thinning from NW to SE, and the main transcurrent shear zones define the major boundaries of distinct crustal thicknesses within the Atuba Complex and adjacent crustal blocks (Castro and Ferreira 2015).

The Setuva Formation consisted of the low- to medium grade schists, quartz-schists, and quartzites that surround the core of the Setuva structure (Fig. 1c). However, there is no consensus regarding the stratigraphic position for all the intervals within the formation, and some studies point out that portions of the unit may be part of the Capiru Group (*e.g.*, Yamato 1999).

The Capiru Group includes metapsamites, metapelites, metadolomites, phyllites and quartzites cropping out in NE-trend belts surrounding the Setuva structure, between the Atuba Complex and the Lancinha Shear Zone (Fig. 1). The metamorphic grade and deformation patterns are highly variable, and rocks have generally attained the greenschist grade (Fiori 1992, Yamato 1999, Santos et al. 2018).

The Turvo-Cajati Complex is represented by schists, calc-schists, dolomitic marbles, quartzites, calc-silicate rocks, paragneisses, migmatites and para-amphibolites of greenschist, amphibolite and granulite metamorphic conditions (Faleiros 2008, Faleiros et al. 2011, 2016, Ricardo et al. 2020). The detrital zircon U–Pb ages indicate late Cryogenian-Ediacaran arc-related and Rhyacian sources to the Tuvo Cajti Complex, suggesting a segmented basin developed in an accretionary wedge, and a back-arc basin formed on the Curitiba microplate margin during the Ediacaran (Ricardo et al. 2020).

4.1.2.4 Previous stratigraphic divisions of the Capiru Group

The metasedimentary Capiru Group is the primary focus of this study and covers part of the Curitiba terrane in the southern Ribeira Belt, Brazil. The former ‘Capiru Formation’ has been subdivided into three lithologic assemblages: Juruqui, Rio Branco, and Morro Grande (Fiori and Gaspar 1993). These lithologic assemblages do not hold genetic correlations, and their definition was based on lithologic packages of similar composition bounded by faults (Fig. 2a). No type-sections were designated by previous workers, although those authors (Fiori 1992,

Campanha and Sadowski 1999) suggested that detailed studies should be carried out in each of these informal assemblages.

In this previous subdivision, the lowermost and oldest beds of the Capiru Formation are known as the Juruqui lithological assemblage, cropping out as a narrow NE-strip bordering the basement rocks. The Juruqui assemblage (Fig. 2b) is composed of reddish iron-rich phyllites and slates, and quartzite beds. This unit was likely deposited in a deltaic setting and the grain size variations might represent delta lobes and prodelta environments (Fiori and Gaspar, 1993). The middle unit comprises all the undifferentiated carbonate rocks within the Capiru Formation, and it has been referred to as the Rio Branco assemblage (Fig. 2b). This unit contains clastic and massive-recrystallized dolomitic marbles in addition to subordinate meta-sandstones. The interpreted sedimentary environment is a shallow marine carbonate-dominated coast (Guimarães et al. 2002, Silva 2010). The upper unit or Morro Grande assemblage (Fig. 2b) also contains undifferentiated units, including a lower stromatolitic bed, which is overlain by rhythmic units with meta-sandstones, siltstones, and organic-rich mudstones. The previous interpreted depositional setting is a shallow-marine platform (Leandro 2016).

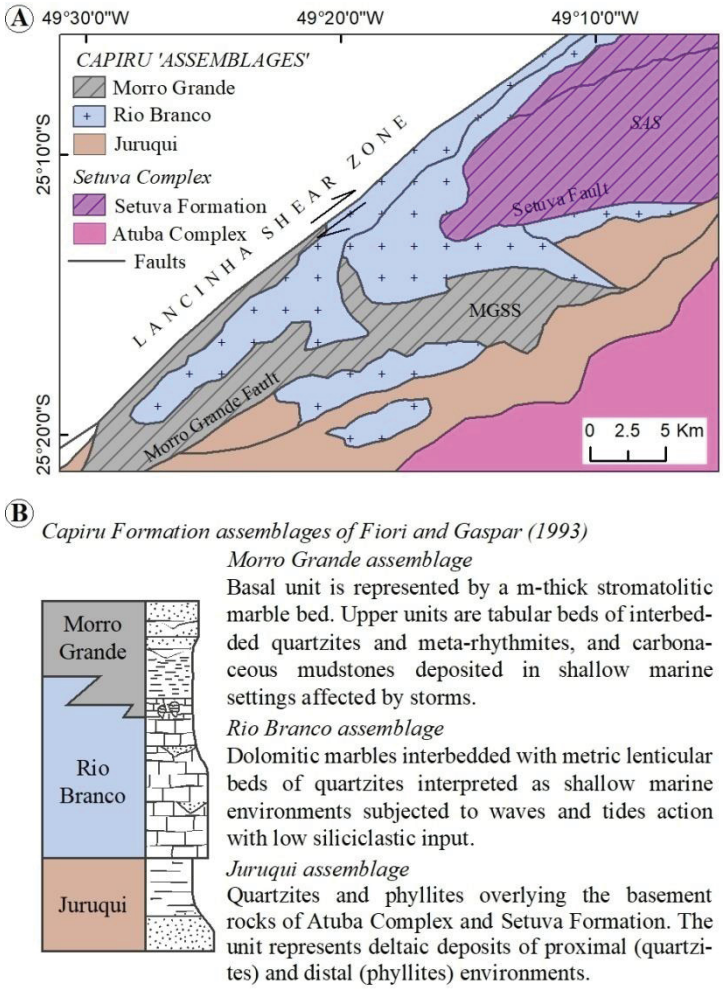


Figure 2. A) Geological map of the former Capiru 'Formation' showing the main lithological assemblages (Juruqui, Rio Branco and Morro Grande), structures and localities after Fiori and Gaspar (1993). B) Lithological assemblages and depositional setting interpretation proposed in Fiori (1992) and Fiori and Gaspar (1993).

4.1.2.5 Depositional age of the Capiru Group

The depositional age of the Capiru Group has not been well-constrained because it lacks fossils. Geochronological constraints are rare, and most ages have been determined using indirect lithostratigraphic and chemostratigraphic correlations to similar units and regional geologic events (*e.g.* Faleiros 2008, Faleiros et al. 2011, Ricardo et al. 2020). Currently, the only absolute radiometric constraints are SHRIMP U–Pb detrital zircon ages providing a unimodal distribution of ~2.2 Ga in the Rio Branco unit (Basei et al. 2008), and LA-ICP-MS U–Pb detrital zircon in Morro Grande unit that has yielded rare 1.4-1.0 Ga ages in addition to the Paleoproterozoic ages, suggesting the succession may be as young as Neoproterozoic (Siga Jr et al.

2012, Cury et al. 2017). Based on these data, the depositional age for the base of the Capiru Group strata remains unconstrained and the Morro Grande unit may be younger than 1.0 Ga. All the Capiru Group strata are older than 555 ± 4 Ma, based on $^{40}Ar/^{39}Ar$ biotite metamorphism ages obtained in Turvo Cajati Complex (Faleiros et al. 2011).

4.1.3 METHODS

4.1.3.1 Field Mapping and Stratigraphic Analysis

Geologic field mapping was conducted to identify major structural and stratigraphic features (Fig. 3) aiming to assess potential correlation among the Capiru Group strata. A total of 25 cross-sections were measured and described in detail along an approximately northeast-southwest structural transect. Representative measured type-sections were chosen based on the structural and the stratigraphic work, and drawn in a 1:50,000-scale (Fig. 4). The measured sections consist mostly of composite sections that were correlated using key-beds and avoiding highly deformed strata. The 1:250,000 geologic map of the Capiru Group is given in Figure 3.

4.1.3.2 Bulk-rock composition of metasedimentary rocks

Representative samples of described rocks were selected for bulk-rock analyses with the aim of establishing geochemical signatures for each of the mappable units. After crushing the samples using a jaw crusher and disc mill, bulk-rock compositions were analyzed by X-ray fluorescence to quantify the major oxides on a Panalytical AXIOS MAX spectrometer at the LAMIR Institute – Federal University of Paraná, using fused beads (0.9 g of sample + 0.1 g of lithium tetraborate) scannings. Calibration is routinely carried out using international standards, and corrections for spectral overlap were applied. The limits of detection are 0.01 weight percent of oxide. The loss on ignition (LOI) was determined by heating samples at 1000° C for 2 hours, using 2 g of the powdered sample.

The bulk organic carbon content (BOC) of metapelites was obtained by the dry combustion method, using an infrared C, H and N analyzer, LECO Truspec CHN at the Soils Laboratory - UFPR. The procedure used an aliquot of 0.25 g of powdered sample. There was no need to follow the step of inorganic carbon removal, since no inorganic carbon content was identified.

4.1.3.3 Mineralogical analysis

Mineral phases were identified by means of x-ray diffraction (XRD) in order to determine the mineralogical composition of the studied rocks. Scans of bulk-rock powdered samples were conducted with an Empyrean PANalytical diffractometer, equipped with a Cu anode (Kα1= 1,5406 Å), 40kV, 40mA. The 2θ scanning range was the standard 3.0 – 70° interval, using a step size of 0.016º2θ, and a count time of 10.16s per step, following the procedures of the LAMIR Institute.The mineral phases were determined with the HighScore Plus® software for qualitative analysis, using the 2002-PDF2-ICDD database for phase interpretation based on difratogram standards.

4.1.3.4 Chemical index of alteration (CIA)

The major-element geochemistry and mineralogy of siliciclastic sediments are strongly affected by chemical weathering that leaches soluble elements such as Ca, Na, and K relatively to Al (Nesbitt and Young 1982, Mclennan 1993, Fedo et al. 1997). The chemical index of alteration (CIA) of sediments is interpreted to record the intensity of chemical weathering and climate conditions during deposition. Generally, low CIA values indicate nearly absence of chemical alteration, suggesting cold-arid climatic condition, whereas high CIA values suggest periods of intense weathering under greenhouse conditions (Nesbitt and Young 1982).

The CIA is calculated as:

$$CIA = [Al_2O_3/ (Al_2O_3 + CaO^* + Na_2O + K_2O)] \times 100$$

where the elemental abundances are expressed as molar proportions, and CaO* represents the CaO contained only in the silicate fraction.

The CIA of a sediment increases as the extent of chemical weathering increases, from values of approximately 50 for "unweathered" feldspar-rich rocks to values near 100 for highly weathered, kaolinite-gibbsite-rich sediments. CIA values for "average" shales, dominated by illite, range from 70 to 75 (Young and Nesbitt 1998).

All analyzed rocks underwent variable degrees of metamorphism, in which pervasive K-metasomatism (resulting in the production of illite) and metamorphism (resulting in the production of K-mica) have affected the bulk composition of the studied samples. The K-metasomatism and metamorphism converted most original clays (*e.g.* kaolinite) into illite/muscovite. The effects of K-metasomatism can be removed by correcting the K_2O values (Fedo et al. 1995, Panahi et al. 2000). The K_2O addition was calculated according to:

$K_2O_{corr} = [m \times A + m \times (C^* + N)]/(1 - m)$ (Equation 1), following the procedures described in Panahi et al. (2000).

where, $m = K/(A + (C^* + N) + K)$ for the parent sample (protolith),

A, $(C^* + N)$ and K are molar values of Al_2O_3, $(CaO^* + Na_2O)$ and K_2O, respectively, and CaO^* indicates that CaO has been corrected for presence of apatite and calcite.

The “prealteration” K_2O value can be calculated by using Equation 1. Using K_2O_{corr}, the corrected CIA (CIA_{corr}) can be recalculated as it follows:

$CIA_{corr} = \text{molar } [(Al_2O_3)/(Al_2O_3 + CaO^* + Na_2O + K2O_{corr})] \times 100$

For a comparison, both CIA corrected values (CIA_{corr}) and uncorrected values are presented.

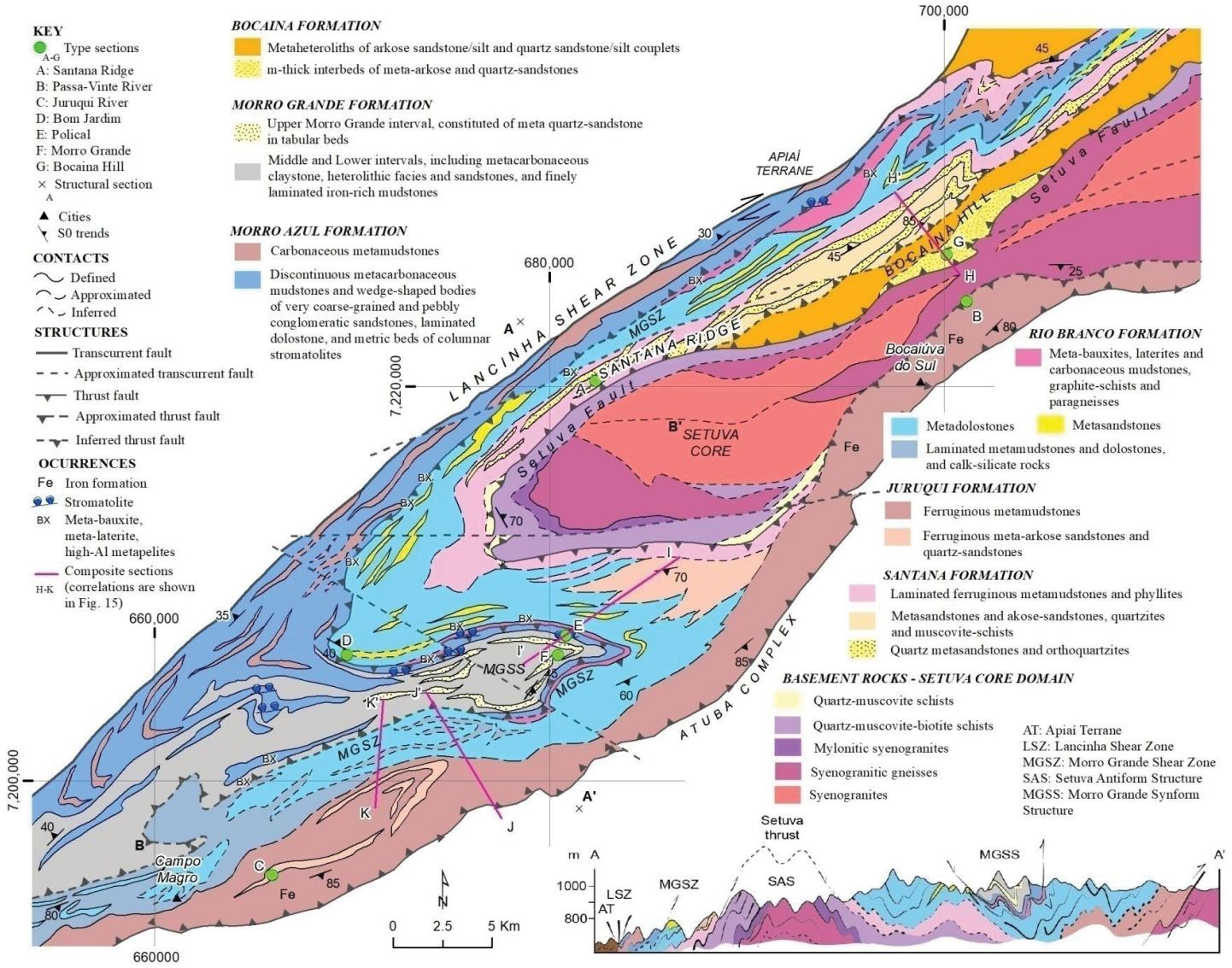


Figure 3. Geological map of the Capiru Group and location of type- and composite sections. Type-sections are detailed in Figure 4. Composite sections were used for basinal correlations (Figure 14).

4.1.4 RESULTS AND INTERPRETATIONS

4.1.4.1 Revised stratigraphic divisions of the Capiru Group

Previous works on Capiru Group strata (Bigarella and Salamuni 1956, Fiori 1992, Fiori and Gaspar 1993) established three informal stratigraphic units (*i.e.* Juruqui, Rio Branco, and Morro Grande lithological assemblages, Fig. 2) that were not formally defined. We here adopt and formalize six formations (Fig. 3 and 4). These formal units are presented on the new geological map (Fig. 3). The location and information of each type-section is shown in Table 4. The interpretations presented here are based on geological mapping, key sedimentary structures, stratigraphic sections and mineralogical compositions. To facilitate descriptions, the prefix ‘meta’ was omitted below. The information regarding the formal definition of each unit can be consulted in the Supplementary Material. The stratigraphic surfaces and their spatial distribution are formally presented under Section 4.1.5.

Santana Formation

The Santana Formation (Fig. 3 and 4) includes the quartzite, phyllite, and schist strata of the Santana Ridge (Fig. 5a), northern Setuva Antiform structure flank, comprising 12% of the Capiru Group succession. The representative type-section can be consulted in figure 4. The basal parautochthonous contact with the Setuva Domain schists is sharp, and bounded either by thrust (Setuva thrust) or the late-tectonic brittle faults. Here, we restrict the ‘Setuva Domain’ to the ortho-derived schists and mylonitic granitoids, consisting of the basement for Capiru Group metasedimentary stack (Fig. 3).

The Santana Formation includes a lower 400 m succession of medium- to fine-grained tabular quartz-sandstone beds (Fig. 5b), 1 to 3 m-thick, and laterally continuous for up to 20 m. The quartz grains are sub-rounded to rounded, and feldspar grains are limited to the basal strata. White-mica is common toward the upper interval. The sandstone Santana lithofacies display, from base to top: horizontal lamination/ low-angle cross-stratification (Fig. 5c), symmetrical ripple cross-lamination, and wavy bedding. Swaley and hummocky cross-stratification

commonly occur in the upper parts of succession. This facies association is succeeded by the Santana ferruginous mudstone beds (Fig. 4). The upper Santana interval consists of a 350 m succession of laminated mudstones (Fig. 5d), and the primary sedimentary features are overprinted by metamorphic foliations. When preserved, the mudstone beds are laterally persistent and flat. The composition is mainly constituted by quartz, white mica, chlorite and large amounts of magnetite (~15%).

Interpretation: The succession of low-angle cross-stratified, wavy ripple cross-laminated, and swaley and hummocky cross-bedded sandstones are characteristic of wave-dominated coastal settings (upper to lower shoreface) subject to storm events. We interpreted these deposits as remnants of inner shelf settings. The extensive, meter-scale, tabular sets of sandstone with low-angle cross stratification were interpreted as upper shoreface deposits, whereas the hummocky and swaley cross-bedded sandstones as deposited above storm wave base, by a combinations of high aggradation rates and low unidirectional current speeds, although swaley cross-stratification are reflective of deposition in shallower settings compared to hummocky (Dumas and Arnott 2006). The sheet-like mudstone is interpreted as a product of settling in the offshore settings below and near the storm wave base. The vertical succession displays a transgressive stacking pattern where offshore mudstones overlie shoreface sandstones.

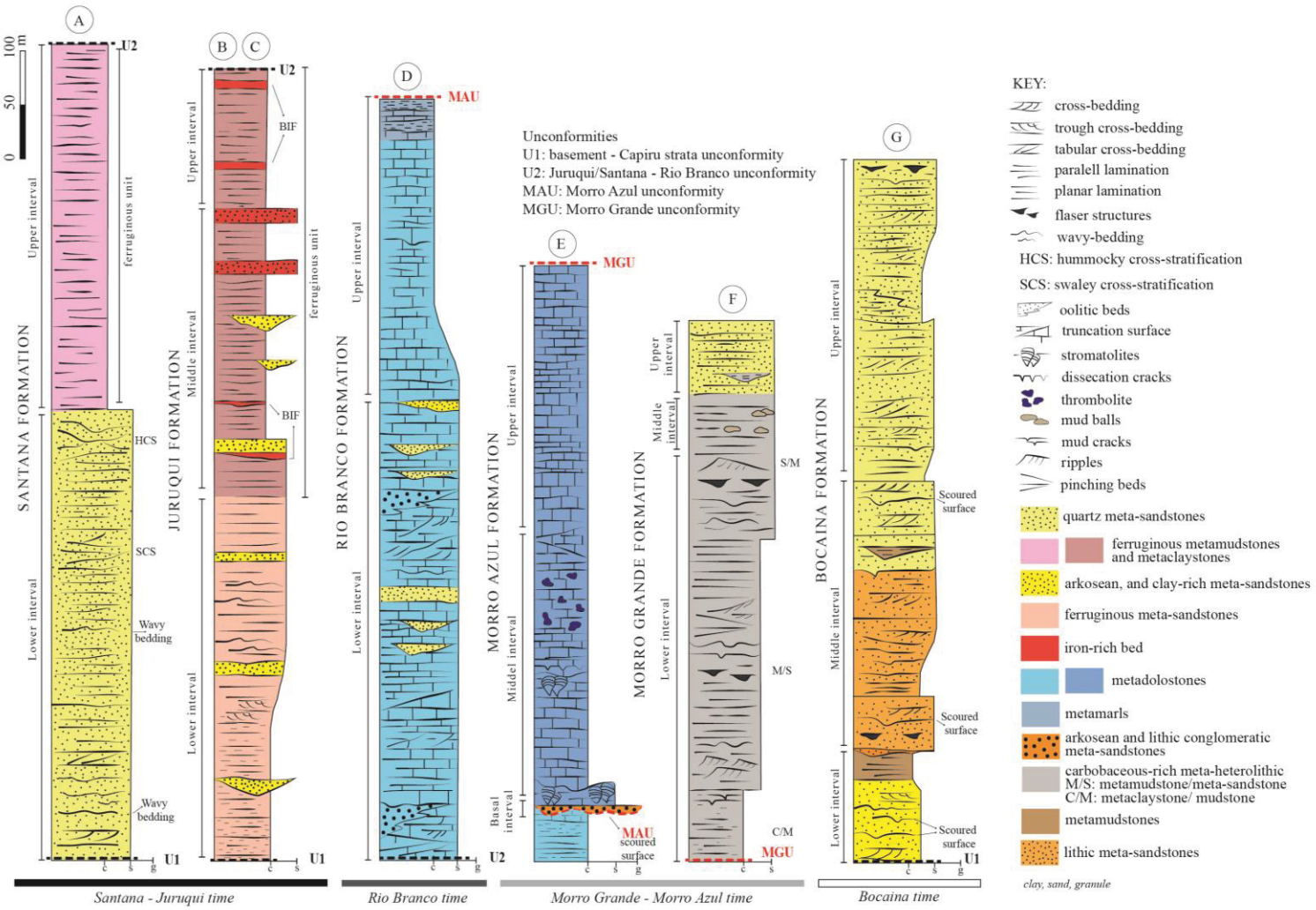


Figure 4. Type-sections of the Capiru Group formations. Locations are indicated on the geological map. Details of the stratigraphic formalization of the units can be consulted in the Supplementary Material.

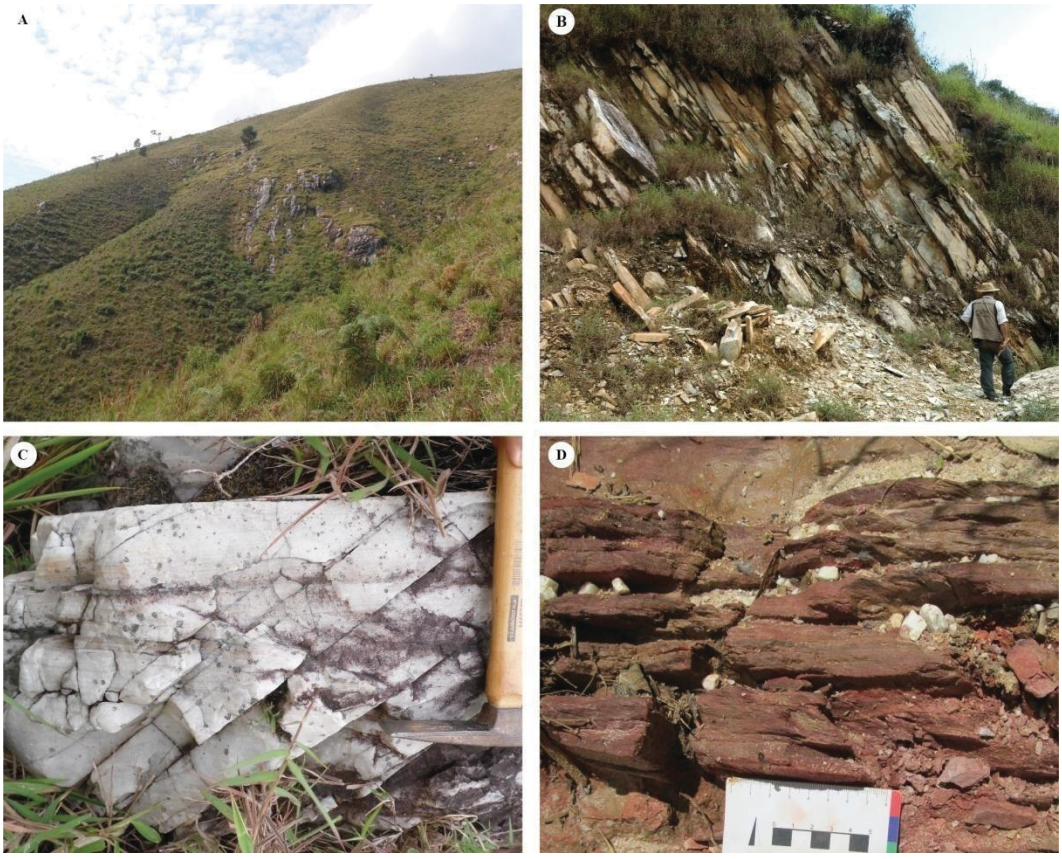


Figure 5. Main field aspects of the Santana Formation. A) Quartzite beds of the Santana Ridge, B) outcrop view of the sandstone beds, showing preserved bed geometries, lower interval, C) low-angle planar-cross stratification and planar stratification, D) ferruginous planar laminated mudstones of the upper interval.

Juruqui Formation

The Juruqui Formation (Fig. 4), holding the original definition of Fiori and Gaspar (1993), includes the quartzites and ferruginous phyllite and schist strata of the southern Setuva Antiform structure flank, comprising 23% of the Capiru Group succession (Fig. 4). The basal contact with the Setuva ortho-derived schists is sharp and bounded by thrust faults.

The lower Juruqui Formation interval (325 m) is mainly constituted by tabular beds of coarse- to medium-grained arkose sandstones (Fig. 6a) with lenses of conglomeratic feldspathic and quartz sandstones (Fig. 6b). These coarse-grained sandstones are poorly sorted, and frequently trough cross-stratified (Fig. 6c). The immature coarse-grained deposits finally pass into moderately well-sorted, medium-grained sandstones with asymmetric wave ripples on the bed tops (Fig. 6d). The middle interval (~ 250 m) consists of m- fining-upward cycles of laminated

medium grained-sandstones to ferruginous mudstones in dm-scale beds (Fig. 6e), and the main sedimentary structures are the planar lamination, and normally graded sandstone beds. Toward the top, the occurrence of dm-scale ferriferous laminated beds interbedded with variable amounts of clastic Fe-coated quartz sand grains becomes common. Lastly, the upper interval (~125 m-thick) consists of ferruginous muddy siltstones interbedded with finely laminated mudstones (Fig. 6f). Continuous flat beds of interbedded chert and hematite layers, up to 0.5-m-thick, are also common.

Interpretation: We interpret the Juruqui lower interval as the edge of a delta environment, corroborating the model of Fiori and Gaspar (1993). The trough cross-bedded, coarser arkoses of the lower member may represent delta-plain deposits. The occurrence of incised channels points out to current activity. The middle interval interlaminated sandstone–mudstone strata represent more distal parts of the delta edge. The thickness, consistent lithology, and fine grain-size of the upper deposits suggest deposition in a dominantly calm setting, with Fe and Si precipitation in a relatively deep water column.

Rio Branco Formation

The Rio Branco deposits overlie the siliciclastic rocks of the Santana and Juruqui formations and one important unconformity marks the boundary between the Juruqui and Rio Branco formations (Fig. 4). The Rio Branco Formation is predominantly constituted by dolomitic marbles (Fig. 7a) and quartzitic lenticular beds, displaying an intense degree of recrystallization, comprising 27% of the Capiru Group.

The Rio Branco Formation lower interval (~ 400 m) is mainly constituted by cm- to m-scale ooid grainstone (Fig. 7b) and intraclast grainstone beds, with carbonate sand-sized grains, showing horizontal lamination (Fig. 7c), symmetric ripples, planar (Fig. 7d), and hummocky cross-stratification upsection.

Ooids are rounded and polymodal, with diameter sizes varying from 0.1 up to 1 mm (mean size = 0.25 mm). The oolitic beds may be single to amalgamated sets, containing planar lamination at the bottom, and symmetrical ripples and cross-stratification at the top. The m-thick beds of intraclast grainstone display massive to incipient laminated structure. The intraclasts are also polymodal in size, rounded,

ranging from 0.5 to 3 mm, with an average size of 0.8 mm. Subordinately, 0.5 to 1 m wedge-shaped sets with cross-stratification are seen. Lenticular m-shaped bodies of well-sorted massive to incipient planar laminated quartz-sandstones, locally normal-graded, form bed sets up to 50 cm and are associated with the grainstone cross-beds. Hummocky cross-bedded grainstones occur upsection, and are generally dm-thick. The upper Rio Branco interval (~ 300 m) is mainly composed of finely laminated dolograinstone or packstone - shale couplets and wackestone - siltstone in m-thick tabular and laterally continuous beds interbedded with cm-massive to nodular mudstone (Fig. 7e). The dolograinstone/packstone–shale facies makes up 1 to 5 m-thick intervals that contain a carbonate-rich lower and a shale-rich upper part. The uppermost part of the Rio Branco Formation comprises a ~ 50-m-thick succession of cm-thick stacked beds of muddy dolostone interbedded with dolostone shale and siltstone, which becomes increasingly shale-rich toward the top (Fig. 7f).

Interpretation: The Rio Branco Formation basal interval represents clastic carbonate deposits. The ooid and intraclast grainstones may represent shoal and even beach settings. The large and laterally persistent planar cross-stratification is interpreted as a product of shallow water deposition, above fair weather-base. Hummocky cross-stratified grainstones are classic storm deposits, probably formed by down-dip transport of shallower water grains and subsequent reworking under conditions of oscillatory shear (Dott and Bourgeois 1982, Haines 1988). Symmetric ripple cross-laminated grainstones reflect deposition under less intense oscillatory currents, probably associated with fair-weather waves (de Raaf et al. 1977).

The quartz-sandstones are interpreted as sand from a siliciclastic proximal source, incorporated in the carbonate system due to variations in the depositional energy. These quartz-rich sandstones fill the topographic depressions between shoal crests, and some of the beds are later cemented with dolomite. The sandstone beds increase in the frequency and thickness upsection, suggestive of increasing clastic input.

The upper interval of finely laminated mudstones is interpreted to represent distal deposits formed by settling (Grotzinger and Al-Rawahi 2014). The interbedding of massive and nodular mudstone beds are interpreted as remobilized muds, transported off the platform (Grotzinger and Al-Rawahi 2014). The uppermost interval is interpreted as a gentle transition between the carbonate platform and the basinal setting. The basinal facies represents uniform sedimentation over a large

area. The vertical patterns are consistent with marl and laminated dolostones overlaying the shallow carbonate-clastic facies.

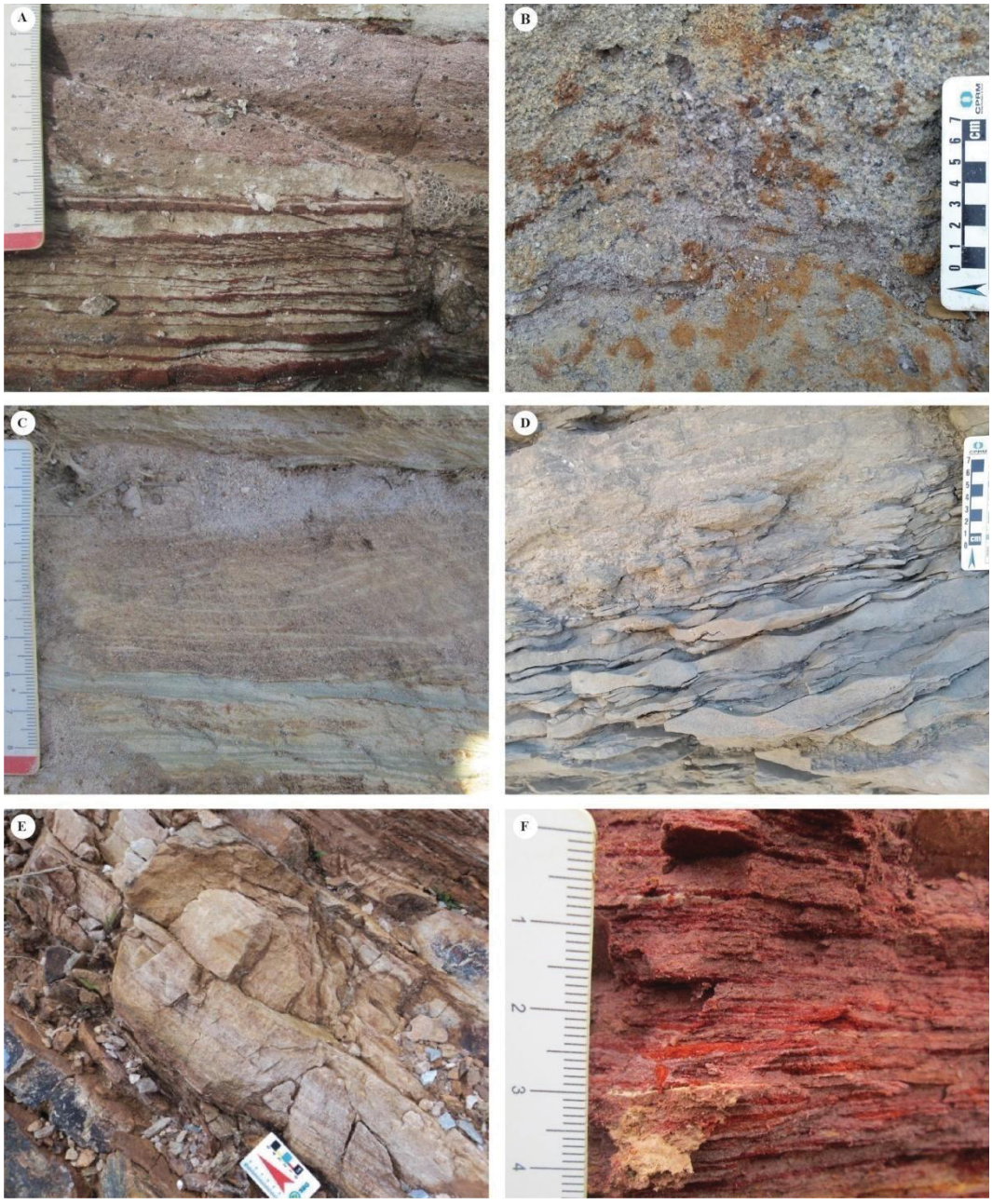


Figure 6. Main field aspects of the Juruqui Formation. A) Tabular coarse-grained arkosic sandstone beds with planar stratification of the lower interval, B) arkosic conglomeratic sandstones lenses, C) trough cross-stratified coarse-grained sandstones, D) asymmetric wave ripples on the bed tops of the lower interval, E) fining-upward cycles of medium grained-sandstones to ferruginous mudstones with planar lamination and normal-graded beds of the middle interval, F) ferruginous muddy siltstones interbedded with finely laminated mudstones and hematite layers of the upper interval.



Figure 7. Main field aspects of the Rio Branco Formation. A) Outcrop view of the Rio Branco marbles, B) ooid grainstone dolostones of the lower interval, C) grainstone beds with horizontal lamination, D) grainstone beds with planar cross-stratification, E) laminated dolograinstone/ packstone-shale and wackestone-siltstone interbedded with massive to nodular mudstone beds, F) muddy dolostone interbedded with dolostone shale, and siltstone.

Morro Azul Formation

The contact between the Rio Branco and the Morro Azul formations is given by a major disconformity (Fig. 8a). The presence of subaerial exposure features such as channel-incision, and occurrence of para-conglomerate beds (Fig. 8b) above

the carbonate units of the Rio Branco Formation is a common feature along the Morro Grande Synform structure (Fig. 3).

The Morro Azul Formation represents 19% of the Capiru Group and it is constituted by a basal and discontinuous, up to 30 m-thick, interval of laminated carbonaceous mudstones (Fig. 8c), in addition to wedge-shaped bodies of very coarse-grained and pebbly conglomeratic sandstones (Fig. 8d). The middle and most representative interval of the Morro Azul Formation is composed of a 250 m-thick bed of intensely laminated dolostone and m-scale beds of columnar stromatolites, often bifurcated, scattered in isolated m-bioherms (Fig. 8e). Structures such as desiccation cracks, teepees, intraformational breccias and laminated mudstones with fenestral porosity (Fig. 8f) are seen upsection. The upper interval (~ 250 m thick) is constituted of mm- to cm-laminated dolostone defined by alternation of darker/lighter couplets, arranged in m-thick beds (up to 5 m), with striking fenestral porosity filled with euhedral crystals of dolomite, and clotted-like structures. Subordinately, discontinuous m-thick lenses of carbon-rich mudstones with planar lamination occur interbedded with the laminated dolostones.

Interpretation: Morro Azul Formation dolostones (previously described as part of the Rio Branco Formation, *e.g.* Guimarães et al. 2002, Juschaks 2006, Bahniuk 2007, Silva 2010) were interpreted to have formed in shallow water settings. The mud-cracks, teepees and brecciated microbial laminites suggest sporadic subaerial exposure. The conformation of isolated stromatolitic colonies and laminites filling between-spaces, with no reworking features or intraclasts, suggest calm sheltered environments, such as lagoons or protected embayments. The substrate claystone and pebbly sandstone lenses of the basal interval probably played an important role in the growth of the microbialite colonies, developing ‘pool-like’ sheltered environments, and this paleotopography might have played an important role in the distribution of the stromatolitic colonies. Even if the original contacts are seldom seen and the substrate of the stromatolitic bioherms is not observed, the conglomerate and pebbly sandstone bed commonly occurs near the colonies.

Morro Grande Formation

The Morro Grande Formation consists of 12% of the Capiru Group. The contact with the underlying Morro Azul Formation is sharp.

The Morro Grande lower interval consists of a ~ 400 m coarsening-upward succession of carbonaceous claystone, heterolithic facies and sandstones (Fig. 9a). The laminated, organic carbon-rich claystone (> 1 wt% TOC, Santos et al. 2018) occurs in mm to cm irregular layers interbedded with mudstone (C/M heterolith) or fine-grained sandstone layers (C/S). The sandstone facies show horizontal lamination, ripple cross-lamination and rare cross-stratification in concave-up base sets with conglomeratic sandstone lags (Fig. 9b). The middle interval is a ~ 50 m-thick bed of finely laminated iron-rich mudstones, showing cm-scale, scattered and rounded clay clasts (Fig. 9c). Clasts are elongated and sand-coated, constituted of the same material from the substrate (Fig. 9d).

The fine-grained tabular quartz-sandstone beds constitute the upper Morro Grande interval (~ 50 m) and uppermost Capiru Group unit in the Morro Grande Synform region (Fig. 3). The contact with the middle intervals is sharp. The sandstones are constituted of sub-rounded to rounded grains, planar laminated and tabular continuous for more than 25 m (Fig. 9e).

Interpretation: Most lithofacies in this succession are mud-rich and typified by heterolithic sediments characterized by alternating grain-size changes between claystone or mudstone and fine-grained sandstone. The facies of the basal and middle intervals were interpreted as a estuary or an embayment shallow setting. The upper interval is representative of a shallow marine setting, with well preserved hummocky cross stratification and massive sandstone fills in wide but shallow channels. Tabular sheet quartzites of the upper interval suggest deposition as sand sheets near the mouth of the estuary.

Some sedimentary structures were interpreted as soft-sediment deformation structures (Fig. 9f), based on their shapes and contact relations. A variety of compactional and soft-sediment deformation features is common on intertidal flats. Variable water contents and density contrasts of interbedded sediments, in addition to sudden rapid depositional events produce differential compaction and soft-sediment deformation features (Shanmugam 2017). Failure of these materials is common, and sediment might move as a slurry, debris flow and slump, leaving small-scale slump scars and slump folds in their wake. Preliminary interpretations of these structures suggest the possibility of a seismic trigger on the formation of the soft-sediment deformation structures, although we do not exclude the genesis due to overload after the action of storm-waves on a shallow depositional environment.

The organic-rich mudstones indicate ubiquitous microbial participation on the margins, since the accumulation of carbonaceous material requires abundant microorganisms in surface water which they sink into, and the right depositional and burial conditions to the organic matter accumulation (Arthur and Sageman 1994). The organic-rich shales are usually deposited in the oxygen-poor depositional settings within embayments, lagoons, deep lakes or nutrient-rich basins, and on continental shelf depths below wave base (Zou et al. 2019). Coupled with our environment interpretation, we assumed a marine embayment setting for deposition of the carbon-rich mudstones.

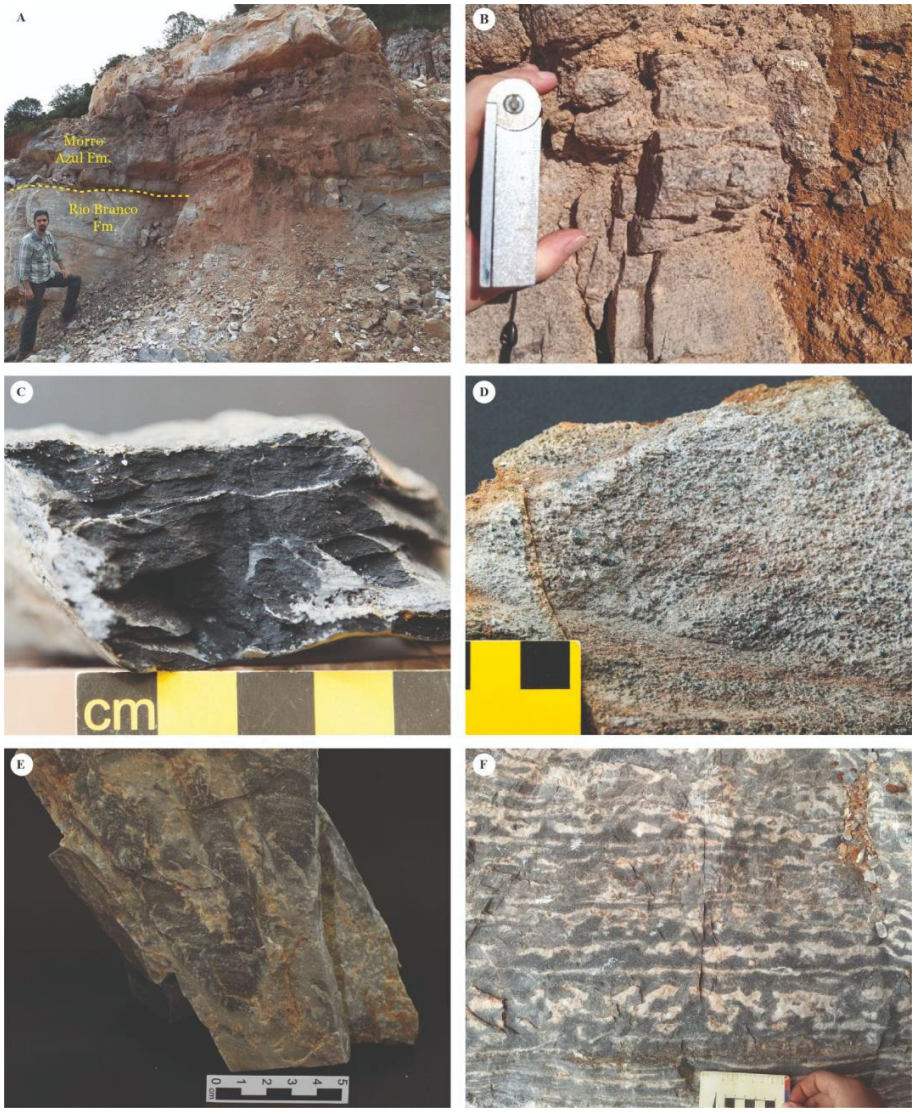


Figure 8. Main field aspects of the Morro Azul Formation. A) Morro Azul disconformity in outcrops of the lower interval, B) Conglomeratic sandstone channels of the lower interval, C) Carbonaceous-rich mudstones, D) Conglomeratic sandstones, E) Columnar bifurcated stromatolites of the middle interval, F) Mudstones with fenestral porosity.

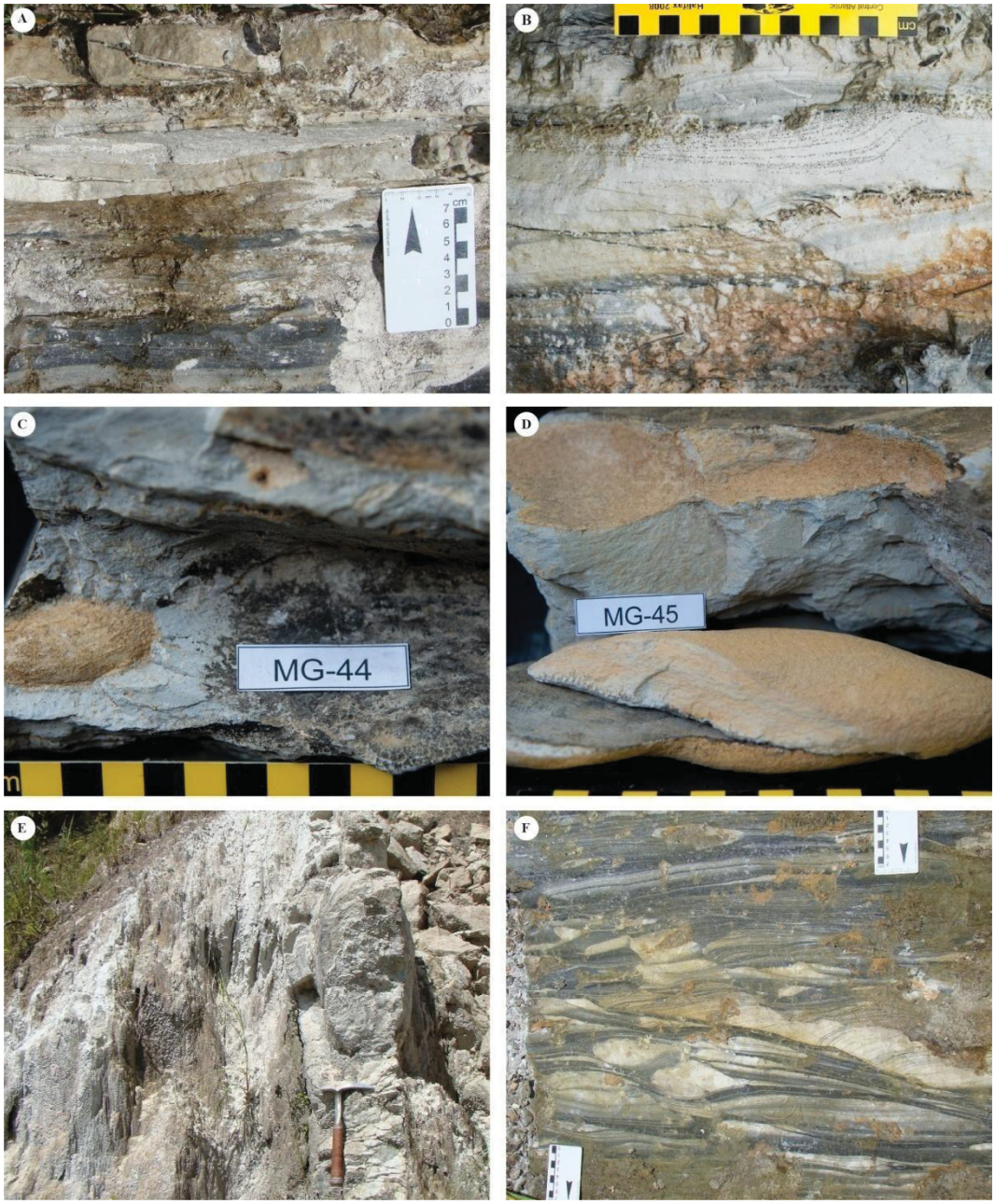


Figure 9. Morro Grande Formation field aspects. A) Coarsening-upward beds of carbonaceous claystone, heterolithic facies and sandstones of the lower interval, B) cross-stratification in concave-up base sets with conglomeratic sandstone lags, C) iron-rich mudstones with scattered clay rounded clasts of the middle interval, D) elongated sand-coated clay-rich clasts, E) tabular quartz-sandstone beds of the upper interval, F) soft-sediment deformation structures of the Morro Grande Formation.

Bocaina Formation

The Bocaina Formation includes the quartzite and schist strata at Bocaina Hill (Fig. 10a), northern flank of the Setuva Antiform Structure, comprising ~7% of the Capiru Group succession. The boundaries of the Bocaina Formation are

characterized by highly foliated sandstones (Fig. 10b). The parautochthonous southern boundary is sharp, passing abruptly from schist bodies into highly foliated sandstones. The northern contact is given by the Bocaina thrust zone (Fig. 3), where muscovite schists grade southward to preserved lenticular m-scale sandstone bodies.

Most of the Bocaina Formation section lacks discernable facies trends, but a general fining-upward succession is present. The lower interval of the Bocaina Formation (~100 m thick) overlies and is in thrust contact with the crystalline basement gneisses of the Setuva Domain (Fig. 3). It is difficult to apply conventional classifications for unmetamorphosed sandstones, especially due to the effects of recrystallization and mica formation, in addition to the development of metamorphic foliations. The lower interval comprises lenticular amalgamated stacks of dm-thick, yellow, angular to rounded, poorly to moderate sorted, coarse-to medium-grained quartz to feldspathic sandstones (Fig. 10c), showing scoured surfaces and trough cross-stratification. A ~ 25 m-thick bed of finely laminated sandy siltstone to mudstone overlie this sandstone interval. The middle interval consists of tabular coarse to fine-grained arkosic to quartz-sandstones, in a ~ 250 m-thick, fining-upward succession, where the sandstone facies are organized in 5 to 50 cm tabular beds, with abrupt top and bases, laterally continuous for ~ 80 m. The sandstones are characterized by medium to high grain rounding and sorting. Detrital feldspar grains are euhedral clasts concentrated along bed bases, and are generally weathered, often smeared with iron-oxides (Fig. 10d). Sedimentary structures such as asymmetric ripple cross-lamination, horizontal lamination and planar cross-stratification are often seen within the tabular bodies. Some of these structures are deformed, but overall, they are visible. The upper interval (~300 m) presents basal sharp boundary, and includes heterolithic facies arranged in coarsening-upward cycles, and fine- to medium-grained quartz-sandstone cm- sand sheets. The sand/siltstone couplets (cm- scale) display sharp basal and upper contacts, tabular cross-stratification, truncated current ripples and flaser bedding.

Interpretation: The Bocaina succession is interpreted as representative of an estuarine system. The high K-feldspar content and granite pebbles suggest that the sediments were derived from a granitic proximal source. Poor sorting and high frequency of angular clasts and granules at the basal interval, collectively point to a near source derivation, rapid deposition and low reworking rates. Further upsection,

beginning with the sandstone bodies of the middle interval, the textural maturity increases, from which we interpret increasing energy and reworking.

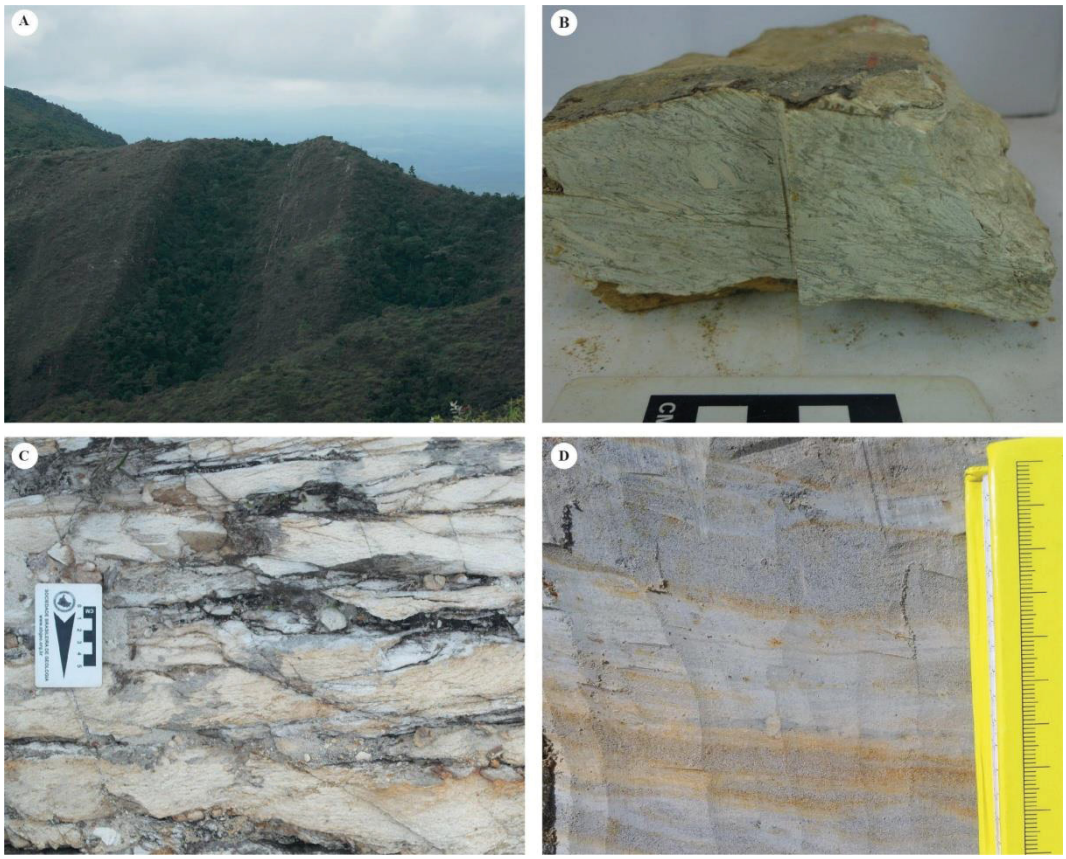


Figure 10. Main field aspects of the Bocaina Formation. A) Quartzite and schist strata of the Bocaina Hill, B) high-foliated sandstones of the Setuva thrust region, C) lenticular stacks coarse-to medium-grained quartz to feldspathic sandstone of the lower interval, D) feldspathic sandstones at the bases of beds in the lower interval.

4.1.5 UNCONFORMITIES

We identify five regional unconformities in the Capiru Grup, four that we can confidently correlate among the measured sections across a lateral distance of more than 10 km, and another potential unconformity.

4.1.5.1 Santana - Juruqui and basement contact

The measured sections indicate that basal strata of the Santana and Juruqui formations rest unconformably on the Mesoproterozoic Atuba Complex basement rocks. This nonconformity (U1, Fig. 4) was initially identified by Bigarella and Salamuni (1956), and later described by Fiori (1992). Some authors have considered the contact between the Santana (formerly part of the Setuva Domain) and Juruqui formations as an angular unconformity, and some deformation aspects were brought up to support the definition of the 'Setuva Formation', interpreted as an older unit formed in a previous tectonic cycle (Bigarella and Salamuni 1958). Other studies have considered the 'Setuva Formation' as a Capiru Formation tectonofacies (Yamato 1999). This topic was addressed during our geological survey, where we have not found evidence of previous (pre - D1) deformation in the Santana Formation. The contact between Santana and Juruqui formations is lateral-transitional and both share the same structural patterns.

4.1.5.2 Rio Branco and Santana - Juruqui contact

The Rio Branco Formation dolomites rest either over the Santana or Juruqui formations (U2, Fig. 4). In the northern sector of Setuva Antiform Structure, the dolostones conformably overlay Santana Formation shelf sandstones, whereas in the Morro Grande Synform region (Fig. 4), the Rio Branco Formation lies conformably over the Juruqui deltaic deposits.

4.1.5.3 Morro Azul unconformity

The contact between the Rio Branco and the Morro Azul formation is is an unconformity that passes laterally to a correlative conformity. The Morro Azul unconformity is the most recognizable stratigraphic surface within the Capiru Group. There are two classifications of this surface, which rely on the fact that the Rio Branco and Morro Azul formations show a potentially conformable contact at the deepest parts of the basin (to SW), whereas in the shallower portions their contact is given by a major disconformity (Fig. 8a). Additional evidence includes a siliceous crust up to 0.5 m-thick occurring on the top of the Rio Branco dolomite, implying long term leaching and weathering, and the occurrence of high-Al and Fe-rich pelites,

which is interpreted as the result of exposure and lateritization of Rio Branco Formation prior to the deposition of the Morro Azul Formation.

4.1.5.4 Morro Grande unconformity

The contact between the Morro Grande Formation and the underlying Morro Azul Formation is given by a depositional shift between the Morro Azul dolomites and the heterolithic units of the Morro Grande Formation. Climatic fluctuations are suggested to explain this depositional shift and the sharp contact.

4.1.5.5 Bocaina unconformity

The Bocaina Formation is considered here as a Capiru Group unit, which only occurs along the northern flank of the Setuva Antiform Structure. Weathered lateritic beds are commonly found at the top of the Setuva Domain rocks, indicative of weathering, which likely took place prior to the deposition of the Bocaina Formation (nonconformity). Based on field observations of 2 sections, we also described a weathered disconformable surface between the Santana and Bocaina formations (disconformity); however this surface is discontinuous due to subsequent deformation.

In one specific section the coarse- to medium-grained trough cross-bedded arkose sandstones of Bocaina Formation are unconformably overlying the typical Santana yellow quartz-sandstones. Hematite and limonite beds were developed on this contact. To explain the occurrence of both contact types (Bocaina-basement and Bocaina-Santana), we interpreted a new sediment pulse, during which the continental-shallow marine Bocaina deposits were shed from the Setuva Domain rocks and Santana shoreface units (Fig. 4).

4.1.6 GEOCHEMISTRY AND SEDIMENTARY PROTOLITHS OF THE METASEDIMENTARY ROCKS

The lithogeochemical results complement the stratigraphic proposal. We use major oxide concentrations (wt %) of SiO_2, $Al2O_3$, Fe_2O_3, K_2O, Ca_2O, Mg_2O, P_2O, TiO_2, SrO and S to illustrate the compositional variations related to the paleoenvironmental conditions, depositional settings and sources. Mineral identification and mineralogical assemblage interpretations by means of XRD are listed in Table 1.

4.1.6.1 The ferruginous-rich lower Capiru Group interval

The iron-rich particularity of the Capiru Group strata has been known since its definition by Bigarella and Salamuni (1956), when the first reference to the iron formation occurrence (BIF) was reported to the south of the Morro Grande synform (Fig. 3). Later, this particular feature was used to constrict the Juruqui Assemblage definition (Fiori and Gaspar 1993) and the lower Morro Grande Formation interval (Santos et al. 2018). The Fe-rich mineral phases include magnetite, hematite, and their weathered products such as goethite (Table 1) disseminated throughout all the Capiru Group, where metamorphic grade and current weathering processes are responsible for the mineral changes.

The Santana ferruginous metapelites show metamorphic magnetite (up to 20%), hematite and goethite as weathering products, whereas the Fe in Juruqui Formation occurs preferentially in hematite disseminated in the pseudomatrix, whereas the magnetite is a subordinate phase (Table 1).

The Juruqui iron-rich phases occur preferably in metapelites, and some sandstones show ferruginous cements (Santos et al. 2018). The iron formations are brick-red hematite-rich pelites, and hematite-quartz cm- (1 – 5 m) bedding-concordant layers, occurring as irregular bands, interbedded with quartz grains. Beds up to 10 cm of hematitic argillite and siltites show iron content up to 80 wt% measured by means of XRF (Santos et al. 2018).

Chemical classifications using Fe_2O_3 (total)/ K_2O ratios against SiO_2/Al_2O_3 (Herron 1988) show average shale to wacke compositions for the lower Capiru interval mudstones enriched in Fe (Table 2), and lithic to arkose sandstones (Fig. 11a).

Tabela 1. Mineralogical composition of the main units of the Capiru Group identified by means of x-ray diffraction relative to their approximate stratigraphic position (m).

Formation	Interval	Rock	Sample	Mineralogy assemblage (XRD id)	Fe-rich weathering products	Relative Stratigraphic Position (m)
Santana	Lower	Metasandstone	SAN 47	quartz, muscovite, K-feldspar, magnetite, titanite, ± biotite	goethite	150
			SAN Q 06			250
			CP-07			350
	Upper	Metamudstone	SAN 43	muscovite, quartz, magnetite, titanite, chlorite, rutile, ± biotite	goethite	400
			SAN 48			450
			SAN 44			500
			SAN 45			550
			SAN 46			600
			SAN 04			650
Juruqui	Lower	Metasandstone	MQ-016-001*	quartz, muscovite, K-feldspar, titanite	hematite	700
			MQ-016-002*			750
	Middle	Metasandstone	MQ-016-003*	quartz, K-feldspar, muscovite, hematite, chlorite	hematite	800
			MQ-016-004*			825
			MQ-016-005*			850
	Upper	Metamudstone	MQ-59	quartz, muscovite, magnetite, chlorite	hematite	950
			MG-01 B			1000
Rio Branco	Lower	Meta dolostone	CP-04	dolomite, quartz, ankerite, muscovite, rhodocrosite, ± albite		1050
			OOLÍTICO			1050
			7-IX-18			1250
			107-VI-18			1300
			CP-01			1400
			CP-50			1440
	Upper	Meta dolostone	CP-52	dolomite, quartz, ankerite, muscovite, rhodocrosite, ± albite		1460
			CP-36			1480
			VII-16			1500
		Metamarl	CP-03	dolomite, quartz, muscovite, pyrrhotite, apatite		1600
			MQ-62			1650
			MQ-88			1700
			CP-02			1750
Morro Azul	Lower	Metaclaystone	CP-20	quartz, muscovite, magnetite, kaolinite, titanite, rutile, ± kyanite, ± chloritoid, ± graphite	goethite, limonite, hematite	1775
			CP-21			1800
			PONTO 41			1825
			ML-01			1830
			MG-31*			1835
			MP-16-01*			1840
			CP-37			1845
			CP-38			1850
Morro Azul	Lower	Meta dolostone	POLICAL	dolomite, quartz		1880
			ST-05			1900
			ST-06			1920
			ESTEIRAS VI-18			1925
	Middle	Meta dolostone	120-VI-18	dolomite, quartz, muscovite		1980
			121-VI-18			1990

Formation	Interval	Rock	Sample	Mineralogy assemblage (XRD id)	Fe-rich weathering products	Relative Stratigraphic Position (m)
			122-VI-18			2000
	Upper	Meta dolostone	9-IX-18	dolomite, quartz, muscovite, ± chlorite		2100
			6-IX-18			2200
			MG-01 A			2300
			5-IX-18			2400
Morro Grande	Lower	Metamusdstone	MG48	quartz, muscovite, magnetite, kaolinite, chlorite (or vermiculite), titanite, ± albite, ± graphite	hematite, goethite	2450
			MG44			2550
			MG45			2650
			MG46			2750
			MG47			2850
	Middle	Metamusdstone	MG43	quartz, muscovite, kaolinite, magnetite, ± graphite	hematite	2950
	Upper	Metasandstone	MG-015-006*	quartz, muscovite, kaolinite, magnetite, tourmaline, ± apatite, ± graphite, Mn-hydroxides, spangolite	hematite, goethite	3200
			MG-016-018*			3300
			MG-016-023*			3400
Bocaina	Lower	Metasandstone	MP-016-002	quartz, muscovite, K-feldspar, titanite, ± biotite	goethite	3500
			MP-016-004			3600
			MP-016-005			3700
	Upper	Metamudstone	MP-015-033	quartz, muscovite, K-feldspar, magnetite, ± biotite	goethite	3800
			MP-016-035			3900
			MP-016-036			4000

4.1.6.2 Rio Branco interval

The dolomite component is ubiquitous (Table 1) and the chemical composition is considered to be homogeneous throughout the Rio Branco Formation. The SiO_2 contents are low, usually < 2.5% (Fig 11b, Table 3). Increases in K_2O, and Al_2O_3 (wt %) are common in the uppermost interval of the Rio Branco Formation, related to the marl unit (Table 3). Another important occurence to be addressed consists of phosphate minerals (Table 2). The phosphates were documented in an internal report of the Paraná State Geological Survey - MINEROPAR (Cava 1985a, b, c and d, Cava and Falcade 1986), where the authors identified P_2O_5 contents ranging from 2 up to 8.5 (wt %) by means of XRF analysis. Based on their unit description and sample location, we considered these occurrences as belonging to the uppermost Rio Branco Formation interval. Apatite was also identified (XRD id) in the metamarls of the Upper Rio Branco Formation.

A cm to m-thick bed of a lateritic crust occurs between the Rio Branco and Morro Azul formations, filling the karstic paleotopography of the Rio Branco dolostone (Fig. 8a). This paleocrust consists of bauxite, laterite, and breccias indicating long-term exposure and erosion. In the northern sector of the Capiru Group this paleocrust is intensely metamorphosed and it is recognized by the presence of kyanite, forming the high-alumina phyllites, and schists to paragneisses along the Morro Grande Shear Zone (Fig. 3). In the southern sector the weathered crust is not developed, and the contact is given by a paraconformity.

Tabela 2. Whole-rock major element compositions (XRF) of the metasandstones and metamudstones of the Capiru Group (wt%). Fe_2O_3T: Total iron; L.O.I.: Loss on ignition, CIA: chemical index of alteration, CIA_{corr}: corrected chemical index of alteration.

Formation	Interval	Rock	SAMPLE	SiO_2	Al_2O_3	Fe_2O_3	CaO	MgO	K_2O	Na_2O	TiO_2	MnO	P_2O_5	L.O.I.	Total	N (%)	C (%)	Fe2O3T/ K2O	SiO2/ AlO3	CIA	CIAcorr	Relative Stratigrap. Position (m)
Santana	Lower	Meta sandstone	SAN 47	66.49	15.16	7.46	0.05	1.81	4.07	0.62	0.81	0.03	0.09	3.44	100.04	na	na	1.83	4.39	na	na	150.00
			SAN Q 06	79.74	8.35	4.62	0.05	1.67	3.06	0.03	0.7	0.01	0.04	2.05	100.33	na	na	1.51	9.55	na	na	250.00
			CP-07	61.13	19.4	4.84	0.02	2.29	7.27	0.04	0.69	0.01	0.03	4.81	100.53	na	na	0.67	3.15	na	na	350.00
	Upper	Meta mudstone	SAN 43	52.03	25.19	7.83	0.01	1.17	6.27	0.18	1.19	0.06	0.07	6.01	100.01	na	na	1.25	2.07	77.97	81.59	400.00
			SAN 48	59.75	19.55	6.94	0.14	1.33	4.98	0.18	0.97	0.02	0.09	5.54	99.48	na	na	1.39	3.06	76.65	80.25	450.00
			SAN 44	59.22	18.95	9.69	0.02	1.54	5.5	0.16	0.96	0.05	0.05	3.89	100.03	na	na	1.76	3.13	75.15	79.60	500.00
			SAN 45	55.7	19.37	11.53	0.02	1.67	5.53	0.12	0.99	0.03	0.08	4.63	99.67	na	na	2.08	2.88	75.65	80.05	550.00
			SAN 46	55.35	19.46	11.94	0.04	1.76	5.54	0.15	0.99	0.03	0.08	4.64	99.97	na	na	2.16	2.84	75.45	79.79	600.00
			SAN 04	54.55	22.78	8.38	0.28	2.34	4.46	0.64	0.85	0.07	0.21	5.3	99.85	na	na	1.88	2.39	78.06	80.27	650.00
Juruqui	Lower	Meta sandstone	MQ-016-001*	86.3	5.25	3.35	0.03	0.44	1.78	0.07	0.23	0.01	0.03	2.08	99.57	na	na	1.88	16.44	na	na	700.00
			MQ-016-002*	75.56	11.73	3.25	0.02	1.04	3.97	0.07	0.61	0.03	0.04	3.21	99.53	na	na	0.82	6.44	na	na	750.00
	Middle	Meta sandstone	MQ-016-003*	88.11	5.32	1.98	0.03	0.49	1.93	0.07	0.32	0.03	0.03	1.27	99.58	na	na	1.03	16.56	na	na	800.00
			MQ-016-004*	84.81	7.17	2.02	0.04	0.68	2.63	0.08	0.37	0.01	0.04	1.68	99.53	na	na	0.77	11.83	na	na	825.00
			MQ-016-005*	88.57	5.91	1.28	0.02	0.33	1.4	0.06	0.3	< 0.01	0.02	1.8	99.69	na	na	0.91	14.99	na	na	850.00
	Upper	Meta mudstone	MQ-59	63.15	7.22	11.95	0.2	5.07	0.06	0.01	0.28	0.19	0.05	11.73	99.90	na	na	199.17	8.75	94.18	94.19	950.00
			MG-01 B	58.9	16.85	11.67	0.03	1.73	6.42	0.06	0.94	0.01	0.04	3.09	99.75	na	na	1.82	3.50	70.30	76.78	1000.00
Morro Azul	Lower	Meta claystone	CP-07	61.13	19.40	4.84	0.02	2.29	7.27	0.04	0.69	0.01	0.03	4.81	100.53	0.033	0.810	0.67	3.15	70.83	77.23	1750.00
			CP-20	51.93	28.99	2.22	0.03	1.00	8.09	0.39	1.78	< 0,01	0.08	5.40	99.94	0.053	0.788	0.27	1.79	75.37	79.51	1775.00
			CP-21	51.18	32.88	2.55	0.09	0.30	5.33	0.42	0.77	< 0,01	0.07	6.78	100.36	0.041	1.295	0.48	1.56	83.20	85.02	1800.00
			PONTO 41	51.63	32.82	2.34	0.08	0.30	5.39	0.41	0.77	< 0,01	0.08	6.46	100.28	0.067	1.185	0.43	1.57	83.11	84.98	1825.00
			ML-01	55.51	21.51	6.72	0.04	2.52	7.54	0.05	0.75	0.01	0.10	5.25	100.00	0.091	0.514	0.89	2.58	72.07	77.92	1830.00
			MG-31*	46.00	31.00	3.67	0.02	1.50	10.26	0.19	1.87	< 0.01	0.04	5.08	99.63	0.029	0.565	0.36	1.48	72.97	78.35	1835.00
			MP-16-01*	43.33	31.97	5.69	0.01	0.80	8.42	0.42	2.06	< 0,01	0.10	7.06	99.85	0.079	1.700	0.68	1.36	76.45	80.29	1840.00
			CP-37	42.12	31.03	5.12	0.01	0.70	9.01	0.42	2.70	< 0,01	0.10	8.02	99.23	0.120	1.700	0.57	1.36	74.74	79.13	1845.00

Formation	Interval	Rock	SAMPLE	SiO_2	Al_2O_3	Fe_2O_3	CaO	MgO	K_2O	Na_2O	TiO_2	MnO	P_2O_5	L.O.I.	Total	N (%)	C (%)	Fe2O3T/ K2O	SiO2/ AlO3	CIA	CIAcorr	Relative Stratigrap. Position (m)
			CP-38	41.70	30.95	4.10	0.15	0.96	9.55	0.65	2.24	< 0,01	0.10	8.55	98.95	0.190	2.950	0.43	1.35	72.56	77.11	1850.00
Morro Grande	Lower	Meta musdstone	MG48	59.75	19.55	6.94	0.14	1.33	4.98	0.18	0.97	0.02	0.09	5.54	99.48	0.085	0.450	1.39	3.06	76.65	80.25	2450.00
			MG44	59.22	18.95	9.69	0.02	1.54	5.5	0.16	0.96	0.05	0.05	3.89	100.03	0.356	0.220	1.76	3.13	75.15	79.60	2550.00
			MG45	55.7	19.37	11.53	0.02	1.67	5.53	0.12	0.99	0.03	0.08	4.63	99.67	0.052	0.123	2.08	2.88	75.65	80.05	2650.00
			MG46	55.35	19.46	11.94	0.04	1.76	5.54	0.15	0.99	0.03	0.08	4.64	99.97	0.185	1.200	2.16	2.84	75.45	79.79	2750.00
			MG47	66.49	15.16	7.46	0.05	1.81	4.07	0.62	0.81	0.03	0.09	3.44	100.04	0.115	1.270	1.83	4.39	73.28	76.78	2850.00
	Middle	Meta musdstone	MG43	52.03	25.19	7.83	0.01	1.17	6.27	0.18	1.19	0.06	0.07	6.01	100.01	0.225	2.040	1.25	2.07	77.97	81.59	2950.00
	Upper	Meta sandstone	MG-015-006*	82.24	10.68	0.99	0.02	0.51	2.71	0.04	0.42	0	0.01	2.36	99.98	na	na	0.37	7.70	na	na	3200.00
			MG-016-018*	89.22	6.55	1.33	0.02	< 0.01	0.08	< 0.01	0.32	< 0.01	0.01	2.89	100.42	na	na	16.63	13.62	na	na	3300.00
			MG-016-023*	80.64	3.66	13.09	0.02	< 0.01	0.01	< 0.01	0.08	< 0.01	0.01	2.66	100.17	na	na	1309.00	22.03	na	na	3400.00
Bocaina	Lower	Meta sandstone	MP-016-002	89.27	6.55	1.06	0.02	0.08	1.84	0.02	0.16	< 0.01	0.02	1.14	100.16	na	na	0.58	13.63	na	na	3500.00
			MP-016-004	77.46	9.55	7	0.02	0.17	1.63	0.08	0.71	0.1	0.11	3.07	99.90	na	na	4.29	8.11	na	na	3600.00
			MP-016-005	64.68	16.59	7.85	0.06	0.8	2.73	0.06	1.16	0.25	0.12	5.48	99.77	na	na	2.88	3.90	na	na	3700.00
	Upper	Meta mudstone	MP-015-033	55.05	24.94	4.56	0.03	1.46	5.58	0	1.22	0	0.09	6.961	99.89	na	na	0.82	2.21	79.90	83.02	3800.00
			MP-016-035	59.79	20.56	4.8	0.03	1.62	7.23	0.05	1.26	0.03	0.06	4.246	99.68	na	na	0.66	2.91	72.16	78.08	3900.00
			MP-016-036	57.83	23.27	3.38	0.02	1.5	6.65	0.03	1.39	0.01	0.11	5.453	99.64	na	na	0.51	2.49	76.12	80.61	4000.00
			PAAS**	62.80	18.90	7.22	1.30	2.20	3.70	1.20	1.00	0.11	0.16	6.00	na	na	na	1.95	3.32	na	na	

* Santos et al. (2018),

** Taylor and Mclennan (1985),

na: no analysis

Tabela 3. Whole-rock major element compositions (XRF) of the metadolostones and metamarls of the Capiru Group (wt%). L.O.I.: loss on ignition.

Formation	Interval	Rock	SAMPLE	CaO	MgO	SiO_2	Al_2O_3	Fe_2O_3	Na_2O	K_2O	SrO	TiO_2	MnO	P_2O_5	L.O.I.	TOTAL	CaO/ MgO	Relative Stratigraphic Position (m)
Rio Branco	Lower	Meta dolostone	CP-04	29.75	21.31	2.3	0.68	0.21	< 0.01	0.23	0.01	0.03	0.02	0.01	45.34	99.89	1.40	1050
			OOLÍTICO	30.85	22.09	0.23	0.01	0.06	< 0.01	< 0.01	< 0.01	< 0.01	< 0.01	0.03	46.30	99.59	1.40	1050
			7-IX-18	31.06	21.78	0.54	0.14	0.16	< 0.01	0.04	0.01	0.01	0.01	0.01	45.64	99.40	1.43	1250
			107-VI-18	31.03	22.04	0.49	0.06	0.09	< 0.01	0.02	0.03	< 0.01	0.01	0.01	45.71	99.50	1.41	1300
			CP-01	29.48	20.95	2.85	0.78	0.34	< 0.01	0.55	0.01	0.03	0.01	0.02	44.69	99.74	1.41	1400
			CP-50	29.99	20.79	1.66	0.54	1.02	< 0.01	0.29	0.01	0.03	0.03	0.01	45.28	99.67	1.44	1440
	Upper	Meta dolostone	CP-52	30.33	21.67	1.11	0.16	0.36	< 0.01	0.05	0.02	0.01	0.05	< 0.01	46.13	99.90	1.40	1460
			CP-36	30.82	21.69	1.01	0.28	0.19	< 0.01	0.03	0.01	0.01	0.01	0.02	45.71	99.79	1.42	1480
			VII-16	30.81	21.76	0.83	0.12	0.18	< 0.01	0.04	< 0.01	0.01	0.01	0.04	45.75	99.55	1.42	1500
		Metamarl	CP-03	5.12	9.9	49.68	12.38	7.11	0.04	3.58	na	1.65	0.05	1.48	9.09	100.07	0.52	1600
			MQ-62	5.07	23.57	53.69	2.97	1.11	0.04	0.11	na	0.18	0.09	0.13	13.46	100.42	0.22	1650
			MQ-88	1.78	25.19	47.87	5.09	5.07	< 0.01	0.03	na	0.56	0.14	0.07	14.56	100.35	0.07	1700
			CP-02	17.34	12.37	42.98	0.04	0.12	< 0.01	0.01	0.01	< 0.01	0.01	< 0.01	26.93	99.82	1.40	1750
Morro Azul	Lower	Meta dolostone	POLICAL	29.95	21.22	3.49	0.14	0.11	< 0.01	0.08	0.01	0.01	0.01	0.01	44.41	99.43	1.41	1880
			ST-05	26.02	18.56	8.98	0.11	0.07	< 0.01	0.06	0.01	0.01	0.01	0.01	45.78	99.62	1.40	1900
			ST-06	27.81	19.6	7.25	0.02	0.05	< 0.01	0.25	0.01	0.01	0.01	0.01	45.21	100.23	1.42	1920
			ESTEIRAS VI-18	27.64	19.44	11.12	0.05	0.18	< 0.01	0.01	0.01	< 0.01	0.01	0.01	40.81	99.20	1.42	1925
	Middle	Meta dolostone	120-VI-18	26.98	19.02	12.04	0.17	0.03	< 0.01	0.37	0.02	0.01	0.01	0.01	42.12	100.78	1.42	1980
			121-VI-18	26.85	19.52	13.56	0.04	0.03	< 0.01	0.08	0.01	0.01	0.02	0.01	40.21	100.34	1.38	1990
			122-VI-18	26.78	18.94	13.73	0.27	0.1	< 0.01	0.12	0.02	0.01	0.01	0.01	39.55	99.54	1.41	2000
	Upper	Meta dolostone	9-IX-18	29.95	21.56	3.98	0.06	0.01	< 0.01	0.30	0.01	0.01	0.01	0.01	44.30	100.20	1.39	2100
			6-IX-18	29.26	20.95	2.66	0.40	0.23	< 0.01	0.11	0.01	0.01	0.01	0.01	46.12	99.77	1.40	2200
			MG-01 A	30.00	21.14	2.24	0.61	0.45	< 0.01	0.22	0.01	0.04	0.02	0.01	45.40	100.14	1.42	2300
			5-IX-18	30.29	21.72	2.66	0.09	0.09	< 0.01	0.01	0.05	< 0.01	0.01	< 0.01	44.46	99.38	1.39	2400

4.1.6.3 Morro Azul Formation

The Morro Azul pelites show high Al contents (Fig. 11a, Table 2) and organic carbon is also present, varying from 0.5 up to 2.95 wt% in the studied samples (Table 2).

The Morro Azul carbonates show the dolomite as the main component (Fig. 11b, Table 3). Compared to the Rio Branco carbonates, the iron and phosphorus contribution is minimal, and the oxides related to siliciclastic input are common, making the SiO_2 contents higher in the lower and middle intervals (Fig. 11b).

4.1.6.4 Morro Grande interval

The Morro Grande Formation consists mainly of average-shale composition mudstones, similar to the Santana - Juruqui interval (Fig. 11a), with carbonaceous material contents that can reach 2.04 % in the studied samples (Table 2). The iron contents are also a striking feature, and rare pyrite occurrences were described. The main carbonaceous-rich beds are immediately overlying the Morro Azul dolostones, with decreasing C (wt%) content upsection. No iron formations were described in this unit, and the main iron-rich phase is the disseminated metamorphic magnetite (Table 1).

4.1.6.5 Bocaina Formation

The Bocaina mudstones show slightly lesser iron contents compared to the previous ones (Fig. 11, Table 2) with a slight increase of TiO_2. The Bocaina sandstones show arkosic compositions and anomalous Fe-sands due to the subsequent cementing.

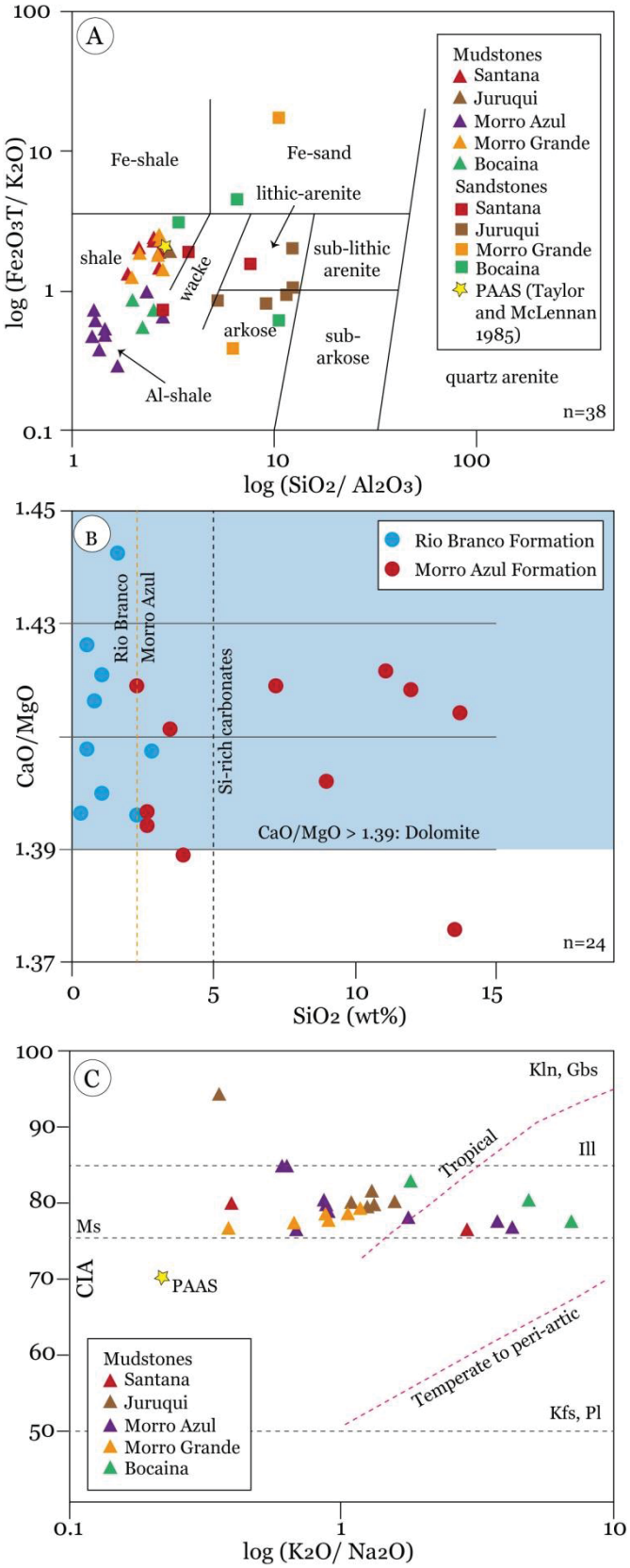


Figure 11. Geochemical classifications of the Capiru Group rocks. A) Chemical classification of the sedimentary protoliths using Fe_2O_3T/K_2O *vs* SiO_2/Al_2O_3 oxide ratios; PAAS: Post-Archean Australian shale (Taylor and McLennan 1985). Increases in K_2O due to metamorphism might lower the Fe_2O_3T/K_2O ratios. Fields are adapted from Herron (1988). Anomalous values of Fe_2O_3T/K_2O (>100 $_{log}$) were excluded and considered as BIFs (Table 2); B) chemical classification of carbonates based

on the CaO/MgO *vs* SiO_2. CaO/MgO ratios > 1.39 are considered to represent pure dolomite composition (blue sahded polygon); C) silicate weathering proxies. CIA - Chemical Index of Alteration (Nesbitt and Young 1982, Fedo et al. 1995); Samples are dispersed between weathered rocks or minerals fields, and compositions are dominated by Al-rich, Na-poor phases (potential clay end-members: Ill -illite/smectite to Kln—kaolinite, Gbs–gibbsite). Pink dashed lines delineate the approximate limits of extreme climatic controls: average suspended fine-grained sediments in recent tropical rivers at top (Orinoco, Amazon, Parana, Congo, Niger) and temperate to periarctic rivers at bottom (St. Lawrence, Mackenzie), data from McLennan (1993). The plagioclase series delimitates CIA = 50 and K_2O/Na_2O ~ 0).

Tabela 4. Summary of the type section features and localities for Formations of the Capiru Group.

Formation	% of Capiru Group (area)	Thickness (m)	Key features	Geochemical properties	Interpreted depositional system	Northing (UTM WGS84)	Easting (UTM WGS84)
Bocaina Formation	7	650	Fining upward, basal conglomeratic sandstone, feldspathic sandstone, heterolithics.	Slightly TiO2 increasing.	Estuarine to shallow marine system	700115	7226670
Morro Grande Formation	12	500	Coarsening upward, carbon-rich, iron-rich mudstone, heterolithics, soft sediment deformation.	>1% TOC.	Shallow marine, estuarine tidal flats	68005	7207139
Morro Azul Formation	19	550	Basal unconformity, lag deposits, stromatolites, mudcracks.	Dolostone, siliciclastic input.	Calm shallow water, lagoons, protected embayments.	680851	7207379
Rio Branco Formation	27	700	Clastic carbonates, ooids, grainstones, hummocky cross-strat.	Dolostone with phosphate contents.	Shallow marine, SW-deepening upsection.	669754	7206394
Juruqui Formation	23	700	Arkosic at base, coarsening upward intervals, iron-rich mudstones at the top.	Iron formations up to 80% of iron oxides.	Deltaic to marine.	701139 665959	7224306 7195224
Santana Formation	12	750	Ortho-quartzites, hummocry cross-strat, and swaley cross-strat.	~15% Magnetite, chlorite.	Marine, near-storm wave base.	682344	7220276

4.1.7 DISCUSSION

4.1.7.1 Capiru basin evolution

Capiru 'margin' early stages: Santana-Juruqui time

The lower Capiru Group interval crops out in NE-SW trending belts, dipping preferably to SE. Although the Brasiliano thrust faults caused a slight allochthony between the Santana-Juruqui interval and the basement, we interpreted that these rocks were unconformably deposited on the Rhyacian Atuba Complex rocks (2.1 Ga U-Pb in zircon, Sato et al. 2003), and the Setuva Domain (2.05 – 2.0 Ga, U-Pb in zircon, Siga Jr et al. 2007). In this depostional context, the Setuva Domain was likely a topographic high since the Capiru strata deposition times. The geochronological studies in the Atuba Complex and Setuva Domain suggested that relevant Mesoproterozoic activity is lacking (Sato et al. 2003, Siga Jr. et al. 2007), and that these basement blocks were likely stable since the Stenian, with tectonic reworking during Neoproterozoic time (Sato et al. 2003, Siga Jr et al. 2007). Considering the youngest zircon grains of 1.1 Ga in the Morro Grande Formation (Siga Jr et al. 2012, Leandro 2016), the deposition of the Capiru Group may have started after the Rodinian Curitiba Plate phase (Fig. 12). In South America, scarce and controversial evidence of the Rodinia rifting episodes are diachronically recorded between 845 and 810 Ma, and ~750 Ma (Fuck et al. 2008, Li et al. 2008, Gaucher et al. 2011, Campanha et al. 2016). Evidence of oceanic crust development is recorded at ca. 840 Ma in the Ribeira Belt (Heilbron and Machado 2003, Pedrosa–Soares et al. 1998). Additionally, preserved rift-related siliciclastic and bimodal volcanic rocks within the Brasiliano schist belts of Rio de la Plata/Paranapanema and Congo/Kalahari cratonic margins suggest a continental rifting phase between 900 and 780 Ma (Pedrosa–Soares et al. 1998, Basei et al. 2009, 2018, Campanha et al. 2016).

The maximum depositional ages of 1.1 Ga, in addition to the widespread iron content in the Santana-Juruqui interval, point to a Mesoproterozoic source-derivation, with sediment sinking after Stenian time. In this context, the Santana-Juruqui interval is interpreted as continental margin deposits after the Rodinia break-up phase (Fig. 13). The environmental interpretations and the main features of the iron formations (detrital component rather than silica precipitates), suggest that the iron might have been derived from denudation of continental margin sources, and not directly precipitated into deep anoxic oceans. As we also did not observe glacial-derived lithofacies in the Capiru Group, we suggest it is unlikely that the iron source was derived from any glacial meltwater. However, we link this succession with sinking into

anoxic and ferruginous Neoproterozoic marine basins (Canfield et al. 2008, Halverson et al. 2011, Cox et al.2016). The paleogeographic distribution of Neoproterozoic iron formations (NIFs) is consistent with anoxic and ferruginous conditions occurring in basins within Rodinia or in rift-basins developed on its margins, and the available geochemical data for these occurrences imply that NIF record is a mixture of hydrothermal and detrital components (Cox et al. 2016).

Rio Branco carbonate platform time

The Rio Branco time corresponds to a switch from siliciclastic to carbonate sedimentation, recording tectonically quiescent times and passive margin development. Considering the distribution of Rio Branco Formation, we interpreted a general transgressive pattern followed by a relatively rapid regressive time (Fig. 13). The sea level fall caused shoaling of the carbonate platform and development of a sabkha landward, with siliciclastic sediments being occasionally transported into the basin. The occurrence of interbedded sandstone attests the siliciclastic influx and marks the end of this long-lived, highly stable carbonate platform, followed by the development of a karst plain over the shallower portions of this shelf margin (Fig. 13).

After Rio Branco time, the widely distributed Morro Azul disconformity is interpreted as a consequence of sea-level fall on the northern margin of Curitiba microplate, giving rise to the weathering and laterite development that mark the end of the Rio Branco time. No dating constraints allow us to determine the duration of this sedimentation gap (Fig. 13).

Morro Azul and Morro Grande time

Our results suggest that this succession was deposited in a marine embayment system (Fig. 13). At the bottom of this succession, the lateritic crust above the Rio Branco Formation is eroded by channels filled with lithic conglomeratic sandstone almost entirely derived from granitic sources, implying a new sediment pulse on the northern Curitiba microplate margin with erosion of the Setuva Domain rocks. The nature of the waterbody at Morro Azul carbonate interval time is not clear, since there is no sedimentological evidence favoring neither a lagoon nor a marine embayment. However, previous works have suggested tidal influence and water

table variations based on the stromatolitic features that point to a shallow tide-influenced marine environment (Guimarães et al. 2002, Juschaks 2006, Silva 2010).

Deposition of the siliciclastic rhythmites of the Morro Grande Formation above the Morro Azul Formation marks a major shift of the sedimentation patterns, but the depositional setting remained the same. Our observations demonstrate that both formations developed at shallow environments where short-term exposure was common due to relative sea-level changes. The Morro Grande time is marked by intense input of clay, especially Al-rich types, and iron, indicating leaching of the continental source and subsequent transport, where the Al-clays and dissolved Fe are mainly derived from the lateritic crusts developed atop the basement and the Rio Branco Formation.

Bocaina time - last sediment pulse prior to the thrust collision?

The stratigraphic position of the Bocaina unit has been controversial, especially due to the difficulties imposed by the intense deformation. However, we interpreted the Bocaina unit as a continental-to-shallow marine unit unconformably overlying the Setuva Domain and the previous passive margin successions (Fig. 14). Although there is no time constraint regarding the depositional gap between the passive margin succession and the Bocaina Formation, we interpret a new sediment pulse related to a younger evolutionary stage, given that the Bocaina formation overlies at least two different units (basement units and Santana Formation). Considering the time-span between the basin onset and its first deformation phase, we interpreted that the Bocaina sediment pulse might be related to syn-orogenic activity on the Curitiba microplate margin (Fig. 12).

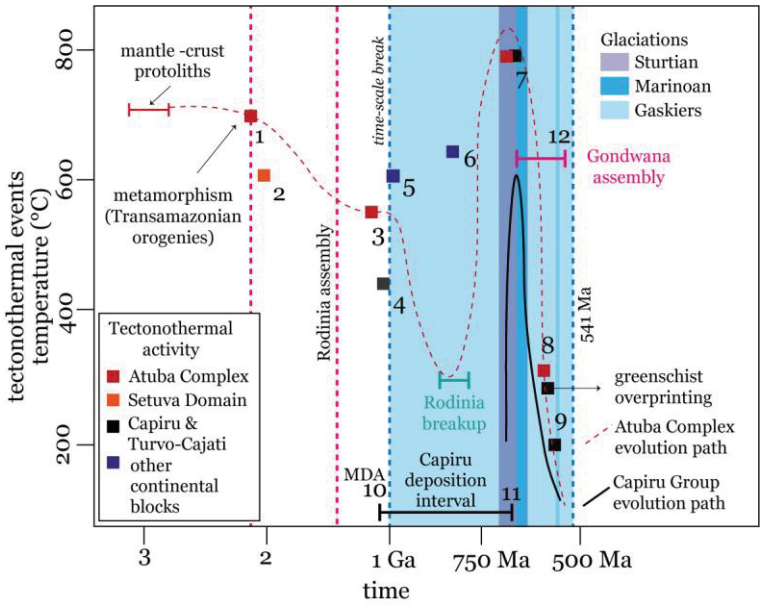


Figure 12. Summary of the main tectonothermal events in the Curitiba terrane. 1: Atuba Complex 2.1 Ga metamorphic event related to the Transamazonian orogenies (Sato et al. 2003, Basei et al. 2008, Santos et al. 2017); 2: crystallization ages of the Setuva Domain rocks (2.05 – 2.0 Ma, Siga Jr et al. 2007); 3: Mesoproterozoic activity in the Atuba Complex (Sato et al. 2003, 2009); 4: maximum depositional age of the Capiru Group (1.1 Ga, Cury et al. 2017); 5: mafic igneous activity (MORB-like) in Itaiacoca Group (~ 900 Ma, Siga Jr et al. 2009), Paranapanema continent; 6: Apiaí gabbro, Apiaí terrane (877 ± 8 Ma, Campanha et al. 2016); 7: metamorphism in deep collision between Atuba and Turvo-Cajati complexes (Faleiros et al. 2016, Ricardo et al. 2020); 8: cooling of Atuba Complex (Faleiros et al. 2016); 9: greenschist overprinting and cooling in Turvo-Cajati Complex (Faleiros et al. 2011 2016); 10 and 11: interpreted deposition interval (from passive margin [10] to syn-orogenic units [11], respectively) for the Capiru Group based on the Neoproterozoic tectonic context. The age of the Piedra Amarilla surface (Poiré et al. 2018), and the correlative Morro Azul disconformity is around 650 - 635 Ma (chrono-correlated with the Marinoan glaciation); 12: Western Gondwana Assembly (Oriolo et al. 2017, Bruno et al. 2018, Heilbron et al. 2020 and references therein)

4.1.7.2 Maturity of parent sediments and source composition

Information regarding the maturity of the metasediment protoliths is limited to chemical composition due to subsequent metamorphism. The chemical index of alteration (CIA, Nesbitt and Young 1982) was designed to reflect weathering of feldspars as a proxy for silicate weathering, through the molar ratios of Al over Na, K, Ca. The index is not altered by diagenesis if mineral reactions occur in a closed system (e.g., the illitization of smectites by decomposition of K-feldspar, Pearson and Small 1988); however, K-uptake from pore- or sea-water into sands with subsequent illitization of Al-phases (K-metasomatism, Fedo et al. 1995) cannot be excluded.

Considering the correction of CIA values for K-metasomatism (Table 2), and excluding calksilicate-bearing samples, the calculated CIAcorr is considered to be

homogeneous throughout the whole Capiru Group, with values between 76 to 94, typical of high weathering ratios (>75), with an average CIA of 80 (Fig. 11c).

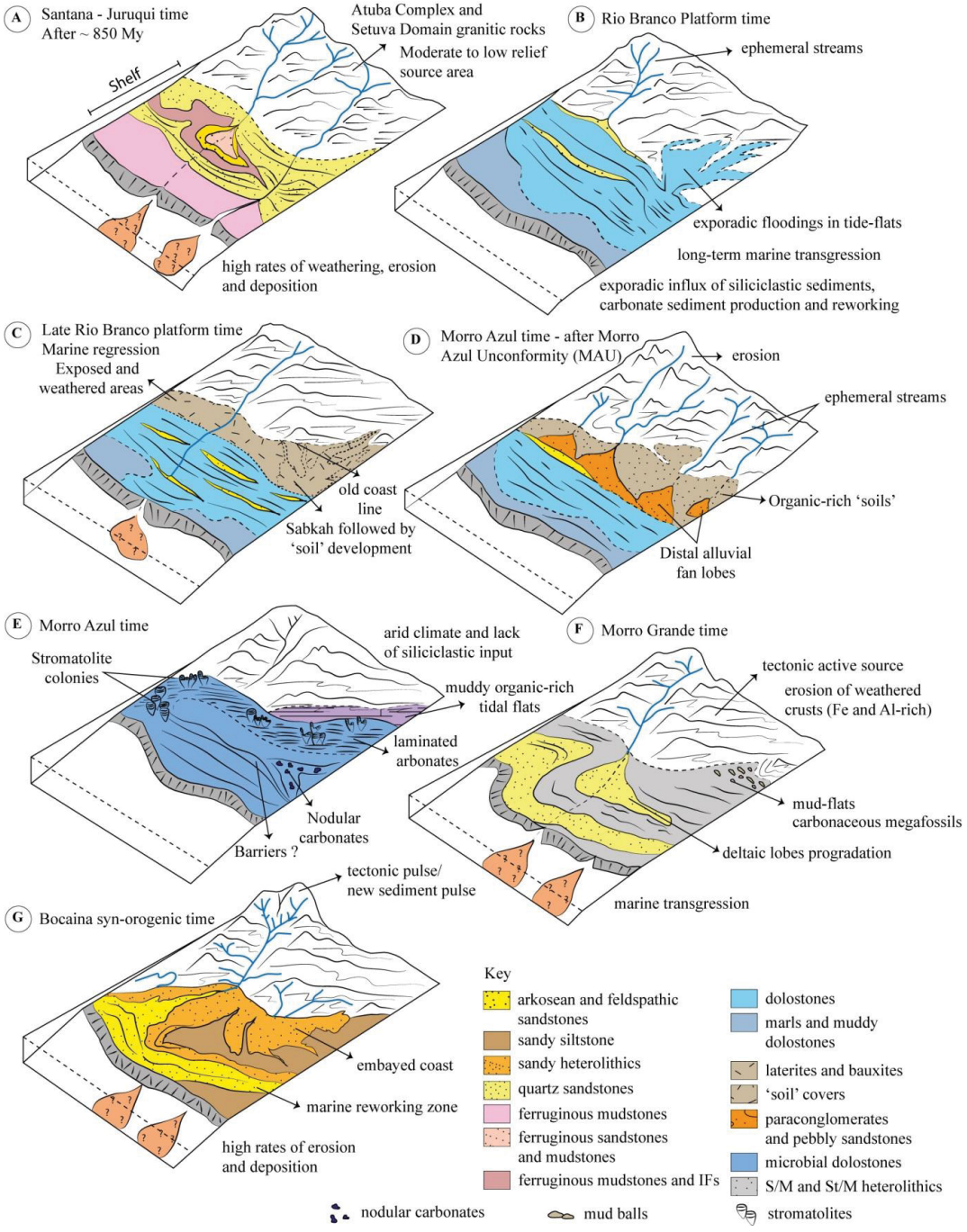


Figure 13. Model of depositional environment evolution for the Capiru Group displaying the successions and their main sedimentary environments deposited on the northern Curitiba microplate shelf. A) Deposition of the Santana - Juruqui interval after ~850 Ma, with leaching and erosion of Atuba Complex and Setuva Domain rocks during wet environmental conditions, B) Carbonate platform development during Rio Branco time, with marine transgression trends that were likely formed under arid conditions, C) marine regression during arid and dry environmental conditions, forming sabkhas landward, D) climatic changes during a depositional break followed by wet and warm environmental conditions, E) development of the Morro Azul carbonates during a low sea level and arid conditions, F) new sediment pulse originates the Morro Grande Formation, with leaching and erosion of the continental margin, and deposition in a shallow marine environment, G) Bocaina new sediment pulse and deposition prior to the Paranapanema and Curitiba plates collision.

4.1.7.3 Capiru basin configuration

The Capiru Group has been described as a passive margin succession, although the age and number of the precursor rift events are uncertain (Fiori and Gaspar 1993, Leandro 2016). A typical passive margin deposit is km-scale thick and consists of clinoforms with oceanward thickening and lateral transition, or alternation of deep and shallow-marine sediments (Pettijohn et al. 2012). The Capiru Group includes marine rocks of deltaic to shelf origin of the Santana-Juruqui interval, the Rio Branco platform and the Morro Azul - Morro Grande times, with evidence for more open marine conditions toward southwest (Fig. 14). Total thickness of these strata increases gradually southward (Fig. 3) to a maximum thickness of about 4 km. In contrast, the unconformably overlying Bocaina Formation contains relatively immature sandstones mainly derived from the continental block, thus representing a subsequent stage of the basin.

Based on lateral facies transitions from proximal to distal, a general sediment transport trend from north to south is interpreted for all the units (Fig. 14). Also, similar rock composition (Fig. 11) indicates that the paleomargin reference was consistent among all the units, and basin orientation remained the same from passive margin to Bocaina time. The high amount of clay fraction sediments and rare conglomerate beds throughout the passive-margin succession suggest low sediment input rates and a relatively low-gradient relief source-area. During the Bocaina time, the arkosic composition of sandstone and conglomerate lags suggest changes in accommodation and sedimentation patterns that might be linked to the development of a syn-orogenic unit.

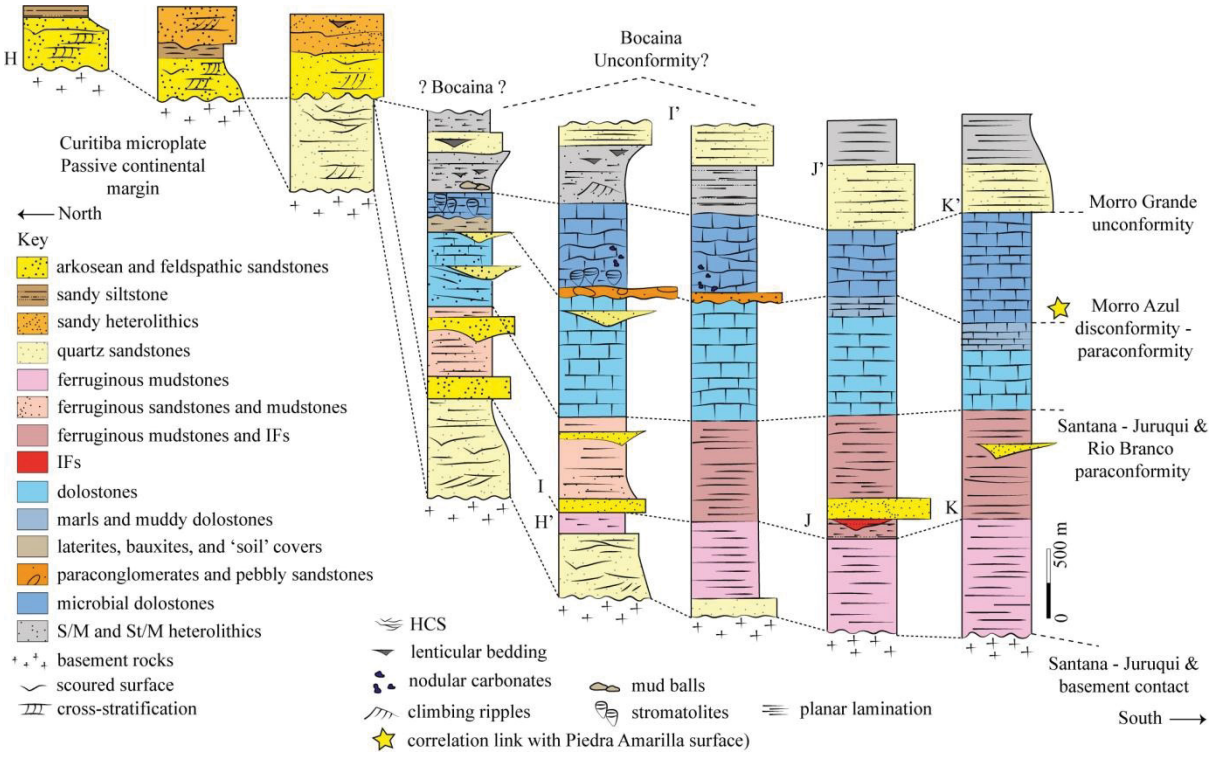


Figure 14. Representative basinal correlation of the Capiru Group formations across a NE-SW composite section. The thickness of these strata increases southward to a maximum thickness of about 4 km. Lateral facies transitions from proximal to distal imply a general sediment transport trend from north to south for all the units with a consistent paleomargin reference and basin orientation. H to K axes positions (of sections) are indicated on the map. Correlations among sections were made using key-beds.

4.1.7.4 Similar successions in Western Gondwana

Although the depositional age of the Capiru Group has not been well-documented using absolute age dating techniques, it contains stramatolites, which are a common occurrence among Neoproterozoic carbonate units in South America and correlative units in Africa (Fig. 15). For the purposes of correlation and relative age-dating, previous and new descriptions of the Capiru Group stramatolites were compared with Neoproterozoic carbonate units from South America in addition to potential correlative units on the African side (Fig. 15; Table 5). This comparison suggests that the Capiru stromatolites should be included in discussions regarding the Neoproterozoic carbonate basins of Western Gondwana.

Many of these units (Table 5) were interpreted within the context of the Neoproterozoic extreme climatic variations, exemplified through the association of glacial deposits, warm climate carbonate platforms, and iron formations (NIFs) occurrences, used as trademark features of the Neoproterozoic record (Hoffman et al. 2017, Knoll 2000, Grotzinger and Knoll 1999, Evans 2003, Halverson 2006, Cox

et al. 2013). The identification of Neoproterozoic glaciogenic deposits and cap carbonates, as well the attempt of lithostratigraphic correlations were made for most of those cited units (Table 5), but this correlation remains uncertain to the Capiru Group, since glacial deposits or putative cap carbonates have not been documented in the unit.

Tabela 5. Neoproterozoic successions in South America and Africa and possible correlations based on published ages. Other units and correlations based on radiogenic $^{87}Sr/^{86}Sr$ ratios, and carbon isotope trends across South America are available in Sial et al. 2016 and references therein. MDA: maximum depositional ages, BIF: banded iron formation.

Unit	Location	Depositional setting	Age
		Units on the Amazon craton	
(1) Mirassol do Oeste Formation (and its succession to the Araras Group carbonates).	Paraguay belt, southeastern margin of the Amazon Craton.	Carbonate platform, passive margin (Font et al. 2006).	Late Cryogenian The youngest zircon was dated at 706 ± 9 Ma (in the underlying Puga Formation), The MDA of the diamictites (and associated BIFs), together with Sr and carbon isotope data of the cap carbonate in Mirassol do Oeste Formation, indicate deposition after 700 Ma (Babinski et al. 2013). *Cloudina* and other metazoans contemporaneous with the Ediacaran fauna occur in the upper carbonates (Gaucher et al. 2003).
		Units on the Apa cratonic block	
(2) Bocaina and Tamengo Formation (Corumbá Group)	Southern portion of Paraguay Belt, Brazil.	Shallow marine to Storm-dominated carbonate ramp (Boggiani 2003, 2010, Fontaneta 2012, Oliveira et al. 2019).	Late Ediacaran U-Pb (LA-ICP-MS) in zircon of an ash bed, in the upper Tamengo Formation interval, yielded 543 ± 3 Ma and ~ 542 Ma ages (Babinski et al. 2008 and Parry et al. 2017, respectively). Phosphatic beds were identified in Bocaina Formation (Boggiani 1997). *Cloudina* fossils were described in Tamengo Formation (Boggiani et al. 2010, Oliveira et al. 2019). Correlative with the upper interval of Araras Group (on Amazon craton) and Itapucumí Group (Paraguay).
(3) Itapucumi Group	Northeastern Paraguay, east Paraguay River margin.	Shallow intertidal to supratidal setting on a rimmed carbonate ramp (Warren et al. 2011).	Late Ediacaran *Cloudina* fossils (Warren et al. 2011), correlative with Corumbá Group carbonates, Río de La Plata carobonate units and Nama Group (Gaucher and Sprechmann 1999, Gaucher et al. 2003, 2005a, Boggiani et al. 2010).
		Units on the São Francisco-Congo craton	
(4) Salitre Formation (Una Group, Irecê Basin)	Central Bahia State, NE Brazil. São Francisco craton.	Shallow carbonate restricted platform, close to the coastline with detrital input (Redivo et al. 2019), High-energy carbonate platform (Sanders and Groetzinger 2021).	Cryogenian U-Pb (SHRIMP) in zircon from tuphaceous siltite, where the youngest single grain is 670 Ma, constraining the MDA (Santana, 2016). Glacial deposits and diamictites with ferruginous matrix in the underlying Bebedouro Formation. Phosphatic stromatolites and sulfide deposits (Caird et al. 2017).

Unit	Location	Depositional setting	Age
			Correlative with Sete Lagoas Formation (Sanders and Groetzinger 2021).
(5) Sete Lagoas Formation	Left margin of the São Francisco river, São Francisco craton, Brazil.	Carbonate platform (Vieira et al. 2016, Okubo et al. 2018, Okubo 2019), High-energy carbonate platform (Sanders and Groetzinger 2021).	Cryogenian Pb–Pb isochron (depositional age) of 740 ± 22 Ma (Babinski et al. 2007). *Cloudina* fossils (Sanchez 2014). Correlative with the Salitre Formation.
(6) Schisto - Calcaire Group	West Congo Belt, Democratic Republic of Congo.	Platform and carbonate ramp (Alvarez 1995, Delpomdor 2007).	Late Ediacaran Sr isotope ratios suggest deposition between ca. 575 to 550 Ma (Poidevin 2007, Frimmel et al. 2009, 2011, Delpomdor and Préat 2013).
(7) Rasthof Formation	Otavi Group, Damara Belt, Northern Namibia.	Microbial-dominated syn-rift sequence (Pruss et al. 2010, Nascimento et al. 2017).	Cryogenian In northern Namibia the Rasthof Formation overlies diamictite and conglomerate of the Chuos Formation of presumed Sturtian age. The age of the Rasthof Formation is constrained below by 746 ± 2 Ma (U-Pb TIMS zircon age) volcanic rocks of the Naauwpoort Formation (Hoffman et al. 1996) and above by a 635.6 ± 0.5 Ma (U-Pb TIMS zircon age) rhyolite in the Ghaub Formation (Hoffmann et al. 2004).
		Units on the Paranapanema craton	
(8) Itaiacoca Formation	Apiaí terrane, Southern Ribeira Belt, Brazil.	Passive margin (Reis Neto 1994), active margin (Siga Jr et al. 2003), back-arc/arc basin (Forero-Ortega et al. 2018).	Two major lithotectonic units with ages in the ranges: Meso/Neoproterozoic transition of 1030–908 Ma (metabasic rocks interbedded with stromatolite-bearing metalimestone), and 645–628 Ma (metatuff rocks interbedded with siliciclastic rocks)- U-Pb (SHRIMP) in zircon from meta-volcanic beds of 628 ± 18 Ma and 636 ± 30 Ma (conventional multigrain analyses), (Siga Jr et al. 2003, 2009).
(9) Lajeado Group	Apiaí terrane, Southern Ribeira Belt, Brazil.	Platform and carbonate ramp settings (Pires 1989, 2017, Campanha et al. 2016,Paula-Santos et al. 2021).	Stenian – Tonian (Meso/Neoproterozoic transition). MDA given by the youngest detrital zircon of 1,400 and 1,200 Ma, minimum age is constrained by the Apiaí Gabbro intrusion at 877 ± 8 Ma (Campanha et al. 2016).
		Units on the Kalahari craton	
(10) Nama Group	Nama foreland basin, Southern Namibia.	Microbial- dominated, isolated carbonate platform (Adams et al. 2004).	Late Ediacaran U–Pb zircon age of 548.8 ± 1 Ma (Grotzinger et al. 1995) and relative age based on distribution of Ediacaran *Cloudina* and *Namacalathus* fossils (Grotzinger et al. 2000, Watters and Grotzinger 2001), as well as carbon isotope stratigraphy (Grotzinger et al. 1995, Saylor et al. 1998).
		Units on the Rio de La Plata craton	

Unit	Location	Depositional setting	Age
(11) Polanco Formation, Arroyo del Soldado Group	Nico Perez terrane, Uruguay Correlative to the Corumbá and Nama Groups.	Pericontinental, storm-dominated carbonate ramps (Einsele 2000), Marine stable continental shelf (Gaucher et al. 2003).	Late Ediacaran to Early Cambrian Maximum U-Pb SHRIMP zircon age of 633 ± 12 Ma for the Puntas del Santa Lucía pluton (Hartmann et al. 2002), which is overlain through an erosional unconformity by the Arroyo del Soldado Group. The basal rhythmites of Polanco Formation correspond to an age of 580 Ma, based on Sr isotope ratios (Kawashita et al. 1999). Biostratigraphic data point to an upper Ediacaran age for the lower Arroyo del Soldado Group and a Cambrian age for the top of the unit (Cerro Victoria Formation). *Cloudina* fossils (Germs 1972).
(12) Marco de los Reyes Formation	Nico Pérez Terrane, Uruguay.	Deep shelf deposits (Chiglino et al. 2010)	Ediacaran depositional age based on high-resolution Sr isotope ratios and C isotope chemostratigraphy (Chiglino et al. 2010). BIF-limestone assemblage (Chiglino 2008).
(13) Sierras Bayas Group	Tandília System, Buenos Aires Province, Argentina. Formerly referred to as 'La Tinta' Group, correlated with Nama Group (Dalla Salda 1982).	Carbonate platform	Late Ediacaran The Loma Negra Formation fits in global δ13C and 87Sr/86Sr trends suggesting an age range of ~ 580 – 590 Ma. Isotopic signatures of Loma Negra Formation and the presence of a unique shelly fauna stablish a direct connection with carbonate intervals in Uruguay (Polanco Formation) and Brazil (Corumbá Group), (Gómez Peral et al. 2007). *Cloudina* in Loma Negra Formation (Gaucher et al. 2005a) is consistent with this estimate and suggests a MDA ~ 550 Ma (Condon et al. 2005).

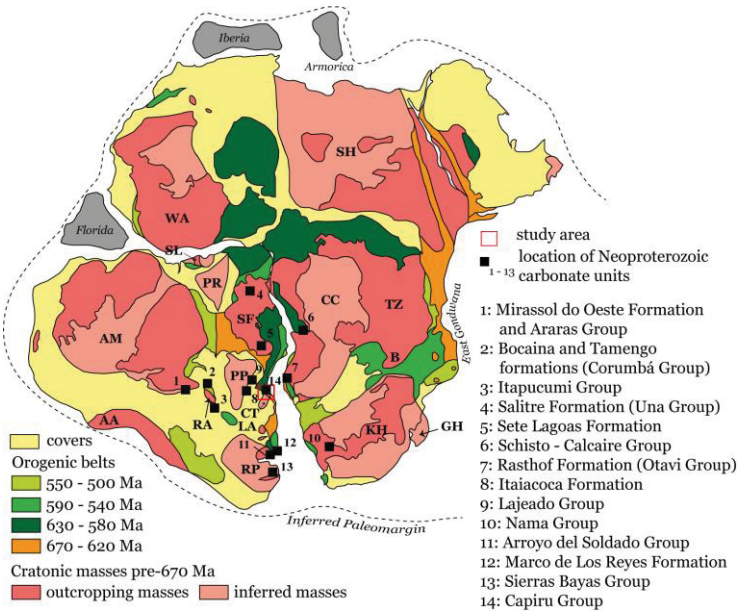


Figure 15. Location of the correlative Neoproterozoic basins in Eastern South America and Western Africa. The Western Gondwana setting (at ca. 500 Ma) with cratons (pre-Gondwana continents) sutured by Gondwana mobile belts are adapted from Schmitt et al. (2018). AA: Arequipa/ Antofalla, AM: Amazonia, B: Bangweulu Block, CC: Congo, CT: Curitiba, GH: Grunehogna, KH: Kalahari, LA: Luís Alves, PP: Paranapanema, PR: Parnaíba, RA: Río Apa, RP: Río de la Plata, SH: Sahara, SF: São Francisco, SL: São Luís, TZ: Tanzania, WA: West Africa.

4.1.7.5 Paleogeographic correlations

The Neoproterozoic successions are recorded in many areas of South America and their Africa counterparts (Table 5), and have been interpreted within the context of the Snowball Earth (Hoffman et al. 1998, Hoffman and Schrag 2002), the Slushball Earth *(e.g.* McMechan 2000, Condon et al. 2002, Kellerhals and Matter 2003), and more recently, the Phantom Glacial (Poiré et al 2005, Cozzi et al. 2004, Gómez-Peral et al. 2021) models and their paleoenvironmental proxies.

Even though we interpreted a Neoproterozoic depositional age for the Capiru Group, glaciogenic sediments and cap carbonates were not identified.

This Neoproterozoic depositional context coupled with the absence of those distinct features, such as glaciogenic deposits and cap carbonates, have also been described for similar South American units, for example, the Sierras Bayas Group in the Rio de la Plata Craton (Argentina) and its correlatives in Uruguay, Paraguay, and Brazil (*e.g.* Arroyo del Soldado Group, Itapucumí Group and Corumbá Group, respectively). In those studies, the authors have suggested that icebergs have never reached equatorial positions (Poiré et al. 2018, Gómez-Peral et al 2011, 2014, 2018, 2021), but the strong polar glaciations led to sea level fall, as recorded by karstic surface development above carbonate platforms in the tropical and equatorial latitudes (Poiré and Spaletti 2005, Gómez-Peral et al. 2014, 2017, 2021).

The Sierras Bayas Group (Villa Mónica, Colombo, Cerro Largo, Olavarría and Loma Negra formations) and the overlying La Providencia Group (Avellaneda, Alicia and Cerro Negro formations) are composed of carbonate and siliciclastic successions separated by regional unconformities (Poiré 1987, Iñiguez et al. 1989, Poiré and Spalletti 2005, Gaucher et al. 2005b, Gaucher et al. 2008, Poiré and Gaucher 2009, Arrouy et al. 2015). Two major stratigraphic discontinuities are recorded in the Sierras Bayas Group: a lower surface at the contact between the Villa Mónica and Cerro Largo formations, named as the Piedra Amarilla Surface, and an upper one above the Loma Negra Formation, known as the Barker Surface. Both are interpreted as the result of glacially-driven sea-level falls during the Marinoan and Gaskiers glaciations, respectively (Poiré 2008, Praekelt et al. 2008, Gómez Peral et al. 2011, Germs and Gaucher 2012, Poiré et al. 2018), and have been correlated

with other Neoproterozoic surfaces in SW Gondwana in Uruguay, Brazil, South Africa and Namibia (Poiré et al. 2008, Gaucher and Poiré 2009, Gaucher et al. 2009).

We consider the Capiru Group units as chrono- and paleo- latitudinal correlative units with these shelf successions of the Río de La Plata craton, together with the Lajeado and Itaiacoca Group (Southern Paranapanema craton), owing to the fact that they share the same features of sedimentation in a non-glacial or Phantom glacial environment (Cozzi et al. 2004, Poiré 2004).

Although no glacial deposits were recorded either on the Curitiba or Río de La Plata margins, syn-glacial sea level falls are represented by unconformities, and we interpreted that Morro Azul disconformity (Fig. 14) might have been correlate with the Piedra Amarilla surface, considered to be a response of seawater falling in a distant position related to the ice cover, under a lesser extreme climate context (Gómez Peral et al. 2011, 2021, Poiré et al. 2018). Furthermore, the presence of the laterite beds and high-Al pelites (Fig. 11) after Rio Branco time are indicative of weathering processes that occur under wet and warm climates, at least during this time-interval (Fig. 13).

The Bocaina unconformity would have a more local meaning, and might be correlated with the collision processes between the Paranapanema (active) and Curitiba (passive) plate margins, where the metamorphic peak would have occurred at ca. 589 ± 12 Ma (Faleiros et al. 2016). Regarding the Baker surface identified atop of the Loma Negra Formation (Sierras Bayas Group), it is unlikely that we can correlate this surface with a similar one within Capiru Group, as its approximate age is ~ 580 Ma (age of Gaskiers glaciation, Knoll 2000, Gaucher and Poiré 2009), while the Curitiba microplate and its Neoproterozoic supracrustal covers were in a broad post collisional regime after the Brasiliano orogeny. In this sense, other units might be more suitable for correlation with this time-period, such as the Cambrian Camarinha Formation, which holds an important glacial-influenced record (Moro and Brito Neves 2009).

Given the sedimentological similarities among Capiru Group and the units deposited on the Río de Plata craton and Southern Paranapanema margin, future paleogeographic models must consider a similar paleogeography for the Curitiba microplate at a tropical or equatorial position ~ 650 - 635 Ma (age of Marinoan glaciation, Knoll 2000, Gaucher and Poiré 2009).

4.1.8 CONCLUSIONS

The Capiru Group consists of a pile of metasedimentary rocks deposited in distinct evolutionary stages of a basin that developed on the northern margin of the Curitiba microplate (Fig. 14 and 15).The strata the Curitiba microplate provide an important record of passive continental margin sedimentation that may represent a link between the Neoproterozoic basins of the South American and African continents.

In this study, we present six formations for the Capiru Group relative to the three that were previously defined (*e.g.,* Fiori and Gaspar 1993). The six formations, in stratigraphic order, are as follows: Santana, Juruqui, Rio Branco, Morro Azul, Morro Grande, and Bocaina formations. For each formation, we performed bulk-rock geochemical analyses to compliment our sedimentological interpretations. In general, the geochemistry suggests that the Capiru Group was deposited in a tropical environment, which received sediment from highly weathered Fe-rich continental sources. Although glacial deposits have not been documented in the Capiru Group, similar to findings of other workers (*e.g.,* Poiré et al. 2018), these Neoproterozoic strata may have also been influenced by far-field effects of glaciation based on the presence of regional unconformities.

The sequential history within the context of Rodinia dismembering to Gondwana assembly is: (1) in the earliest Santana-Juruqui time, a west-east trending seaway bordered by low gradient coastal plains received siliciclastic iron-rich sediments, (2) during Rio Branco time, a carbonate platform and shelf margin expanded under a transgressive trend, with phosphate contribution in the deepest parts of the basin; (3) at the end of Rio Branco time, sea level falling probably driven by a global glaciation caused shoaling of the carbonate platform and development of sabkhas landward, 4) after Rio Branco time a karst plain was formed, developing the Morro Azul disconformity. Processes of weathering and laterite formation took place during this interval, both in basement and basinal sectors, forming the iron-rich and bauxite beds, together with the Al-rich pelites of the Morro Azul Formation; (5) deposition in shallow marine environments in a sheltered embayment returned during Morro Azul upper interval, followed by deposition of Morro Grande Formation; (6) deposition of Bocaina Formation was a response of a tectonically-driven new

sedimentation pulse, and erosion of the Setuva Domain rocks, (7) collisional thrust and nappe emplacement followed by escape tectonics deformed the sedimentary pile, during the collisional processes between Curitiba and Paranapanema plates, involved in the Western Gondwana assembly.

This evolution and the sedimentological similarities among Capiru Group and the units deposited on the Río de Plata craton and Southern Paranapanema margin are important for the paleogeographic reconstructions that must consider a similar paleogeographic position to the Curitiba microplate at a tropical or equatorial position ~ 650 - 635 Ma.

4.1.9 ACKNOWLEDGMENTS

This work was supported by the Microbial Project (a partnership between PETROBRAS and Federal University of Paraná) and Diagenesis Project (a partnership between SHELL Brazil and Federal University of Paraná). We thank Dr. J. Rosenblume and Professors A.B. França, F. Vesely, and F. Varejão that gave suggestions and endorsed fruitful discussions about the Capiru Group units, their structural geology features, and sedimentary aspects.

4.2 Artigo 2: THE GEOLOGY OF THE CAPIRU GROUP, CURITIBA TERRANE, SOUTHERN RIBEIRA BELT (BRAZIL)

https://doi.org/10.1080/17445647.2021.1982036

Larissa da Rocha Santos[1,2]; André Luis Spisila[3]; Daniel Patias Guimarães[4]; Luizemara Szameitat[1,5]; Alessandra de Barros e Silva Bongiolo[1,5]; Leonardo Fadel Cury[1,2].

1: Department of Geology, Federal University of Paraná, Brazil
2: LAMIR Institute - Laboratory of Mineral and Rocks, Brazil
3: Geological Survey of Brazil (CPRM) – Paraná, Brazil
4: School of Earth and Environmental Sciences, University of Queensland, Australia
5: LPGA - Laboratory of Research in Applied Geophysics, Federal University of Paraná, Brazil.

ABSTRACT

The Capiru Group is a Neoproterozoic metasedimentary unit that crops out in the Curitiba terrane, Southern Ribeira Belt, South of Brazil. A detailed geological mapping of this unit was performed during 2016 to 2020. Original interpretations and the new geological map were recently compiled and integrated with the past field data of the state (MINEROPAR) and national (CPRM) geological surveys, and to unpublished and recent published studies. This compilation represents the most updated synthesis of the Capiru Group, and the geological map presented here (Main Map) provides the basis for recognition and individualization of distinct lithostratigraphic units. The lithostratigraphic units reflect depositional/tectonic events, which involved: a) passive continental margin sedimentary evolution on the Curitiba microplate, b) compressional episodes during the Brasiliano - Pan African Orogeny (Late Neoproterozoic), being responsible for two main deformation phases: i) a thrust phase followed by ii) a strike-slip lateral scape system, c) extensional processes that followed the collisional stage (Cambrian), and finally, the d) extensional tectonics related to the Gondwana breakup during the Lower Cretaceous, that culminated to the Proto-Atlantic Ocean opening.

4.2.1 INTRODUCTION

The Capiru Group is a Neoproterozoic metasedimentary unit located in eastern Paraná State, Brazil, within the Precambrian shield - a rugged E-W plateau shaped on igneous and metamorphic rocks (Fig. 1a). The Capiru Group was affected by collisional and extensional tectonics, related to the Gondwana assembly and its subsequent breakup (Heilbron et al. 2004, Fuck et al. 2008, Brito Neves et al. 2014, Faleiros et al. 2016, Florisbal et al. 2014, Rossetti et al. 2018, Owen-Smith et al. 2017). The 4 km-thick stack is bounded to the north by the Lancinha Shear Zone and to the south by the Atuba Complex basement rocks (Fig. 1b). To the east, the Serra do Mar Ridge defines the geomorphologic boundary between the Precambrian plateau and the Atlantic Ocean coast areas (Fig. 2), whereas to the west, the Capiru Group is considered as a portion of the Precambrian basement that underlies the Paraná basin (Ordovician-Cretaceous).

The research interest for the Capiru Group units dates from the 1960s, with a relative increase during the 1990s, based on interest in limestone units. During the subsequent years, the exploitation of carbonate rocks, and the groundwater hosted in karstic and fractured aquifers, resulted in a series of mapping surveys and academic research in the region. Since 1978, the (unfortunately) extinct Geologic Survey of Paraná (MINEROPAR) completed a series of projects, some of which included geologic maps with variable scales and purposes. Those maps were extensively studied in order to integrate the data in this new map. During the 1990s, Fiori (1992) published a structural map of the region, which is considered the first synthesis of modern knowledge about tectonics of the Capiru Group. Due to constant advances in geochronological techniques, some of those units were revisited and tectonic models were re-evaluated; as a result, major edits were made regarding prior geologic cartography in this contribution.

The map presented here (Main Map, Anexo I) is at 1:150,000 scale and was based on our mapping survey (2016 – 2020, 1:5,000 to 1:25,000) and the 1:250,000 map by Fiori et al. (1985). It also takes into account and includes the results of Geological Survey of Brazil mapping projects, which were carried out over the last 25 years in Paraná State, as well as other maps and information published by other

authors in a series of academic works developed in the Graduate Program of Geology at the Federal University of Paraná and University of São Paulo (in Portuguese: Fiori 1991, Siga Jr 1995, Yamato 1999, Guimarães 2002, Bahniuk 2006, Juschaks 2007, Silva 2010, Leandro 2016, Filpi 2021). One of the major sources of geological data used in this work, if not the main, was the detailed 1:10,000 dataset provided by the mapping courses held in the Geology Department, at the Federal University of Paraná, especially those carried out since 2014, which have digital sources of information.

The aims of our mapping work and integration were to define a stratigraphic nomenclature, and to resolve some of the problems related to regional correlation. The “lithologic assemblages” of Fiori (1991) were elevated to formation status and three newly defined units — the Santana, Morro Azul, and Bocaina formations were included within the Capiru Group. The "Setuva Formation" definition was replaced by the term "Setuva Complex", which is used now to refer only to the granitic rocks that constitute the basement beneath the metasedimentary cover. In certain cases, the boundaries between previously recognized formations have been redefined. This explanatory text supplements the new map (Main Map, Anexo I) and provides background information to assist in its interpretation. This text also describes the historical antecedents of the map, and the sources from which the map was compiled, with the aim of discussing the general topics related to it.

4.2.1.1 Sources of information

Source data for previous geologic maps comprising the Capiru Group are plentiful, so we have chosen to present a narrative account. This section describes the circumstances under which the maps were prepared and comments on their more interesting features, rather than providing a list of details, which readers can find in the published sources.

4.2.1.2 Maps before 1980

Concerning the pioneer works regarding the geologic mapping of the Paraná state, we acknowledge the works carried out by Oliveira (1918), Oliveira (1927), Oliveira and Leonardos (1943), and the classic published article of Maack (1947), written as a text to accompany sketches made to the revision of the Geological Map of South America. Fortunately, these early works are currently available online in the

files of the Brazilian Archives of Biology and Technology. Historical details and footage of one interesting treatise about the first geological commissions in south-west Brazil, are listed in the Pinto and Janasi (2015) work, published in *Terrae Ditatica*, a Journal of the Campinas State University.

The following years were very fruitful for the geology of Paraná State. During this time, the works of Bigarella (1948) and the classic series of Preliminary Studies of the Açungui Group, by Bigarella and Salamuni, (1956, 1958) were documented. Our recent research found copies of these works in the Science and Technology Library, at the Federal University of Paraná. The 1958 can be easily found because it is indexed online in the *Boletim Paulista de Geografia*. The very first systematic geologic survey of Paraná was carried out by the Paraná Geologic Commission, which was established in 1964.

In 1974, the Federal Department of Mineral Production (extinct DNPM, currently ANM – Bureau of Mines of Brazil), within the scope of the 1:1,000,000 Geologic Map of Brazil, presented new maps covering the Paraná territory. In 1977, the East Project (a partnership between the DNPM and the Geologic Survey of Brazil - CPRM), developed new geological maps for the eastern portion of the state, in 1:100,000 scale.

Some of the maps of the Geologic Survey of Paraná were extensively studied in order to integrate the data in this new map. The technical reports related to these projects are now available at the Water and Land Institute of Paraná (IAT) website, many of them in digital forms.

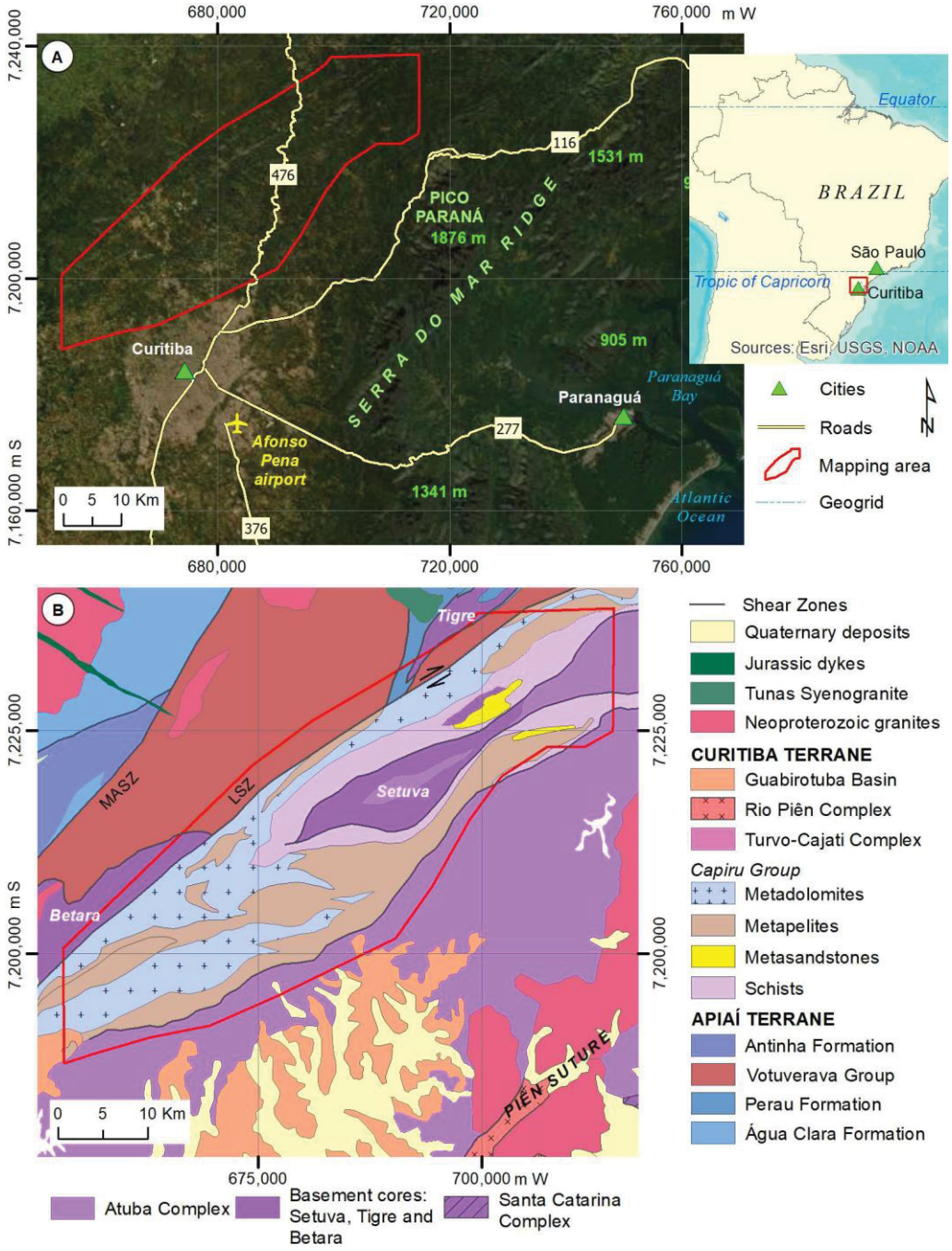


Figure 1. A) Aerial image of Curitiba and surrounding regions. Red polygon depicts the location of the mapped area, b) Geological context of the Capiru Group within the Curitiba Terrane, after Fiori (1985). MASZ: Morro Agudo Shear Zone, LSZ: Lancinha Shear Zone.

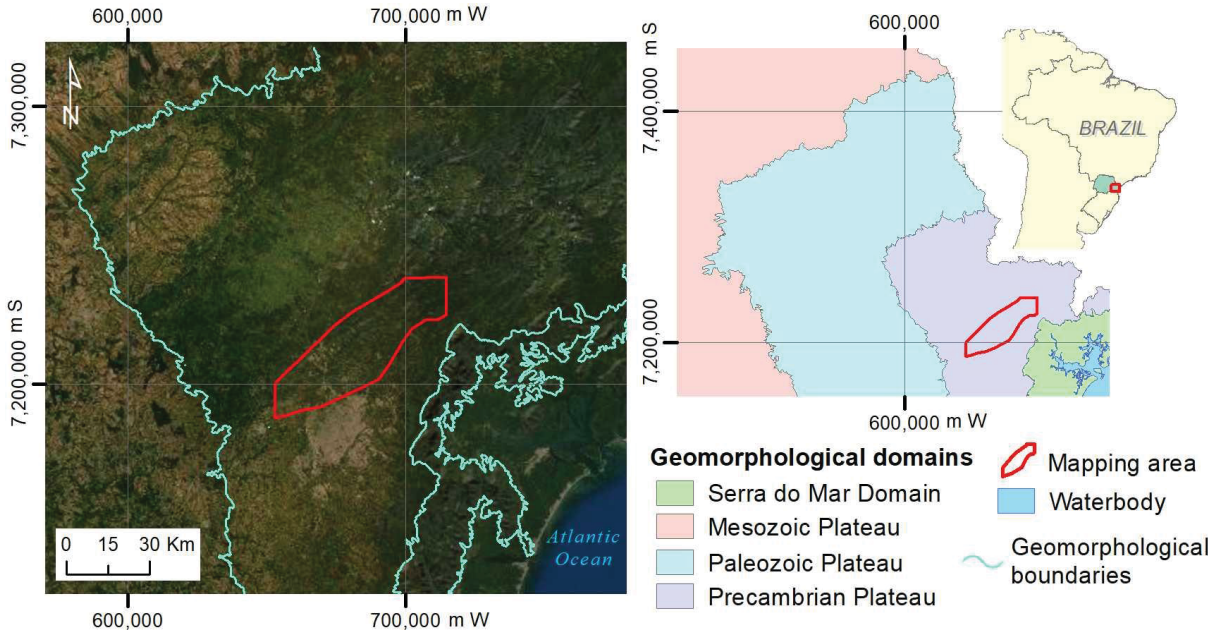


Figure 2. Geomorphologic aspects of the mapped area. The study area is included within the Precambrian plateau of Paraná state, Southern Brazil.

4.2.1.3 1980's maps

In the 1980's, many projects in partnership with the Federal University of Paraná led to a series of maps and academic works including the Southern Ribeira Belt units. For this study, we consulted projects that describe the 'Capiru Formation' as their primary focus; those projects are highlighted herein. The Phosphorite project (*Projeto Fosforita*) was a series of internal reports that contain a systematic outcrop study and geological maps of research targets, from which many outcrops in the southwestern portion of the Capiru Group were revisited for this study (Cava and Falcade 1896). In addition, two geologic maps made under the project entitled Geologic integrated studies of the Paraná Precambrian units (*Estudos geológicos integrados do Pré-Cambriano Paranaense*) were used as a base for the new survey presented herein. Although this project led to compilation of a series of maps and reports, the two of particular importance for this study were the Geologic map from the integrated studies of the Paraná Precambrian shield (Fiori 1985) and the Geological Map of Paraná State, in 1:650,000 scale (Mineropar 1989).

4.2.1.4 1990's works

Several academic works were completed during the 1990's; these included numerous descriptions of the 'Capiru Formation' in addition to interpretations

regarding the history of the Curitiba Terrane (Siga Jr 1995). These works, which are extensively cited, are those of Fiori (1991), Fiori (1992), Fiori and Gaspar (1993), Siga Jr. (1995), Yamato (1999), and the papers of Basei et al. (1992, 2008), included within the project: Geochronological Map of the Precambrian terrains of Paraná and Santa Catarina States; most of which were published in peer-reviewed journals—which has allowed for further dissemination of more recent regional tectonic models.

4.2.1.5 Integration of previous works and digital datasets

Our work started with a review of the digital integration made by the Geologic Survey of Paraná in 2001. Their compilation includes several of their projects, of variable scales, and is presented as the Curitiba Geological Chart (1:250,000). In addition to this database, the geologic units of the Precambrian shield of Paraná have been surveyed every year since 1975, during the annual mapping courses taught by the Geology Department, Federal University of Paraná. This has resulted in detailed 1:10,000 scale geologic maps, which include the following geologic features: mapped rock types, structural and tectonic aspects, and environmental features. The University's survey mosaic is systematic, constantly updated, and the portions of the mosaic that cover the Capiru Group were integrated as a regional map for this project.

In addition to that, the increasing demand for water production around the urban areas of the Paraná Precambrian shield (Fig. 2) led to integration of the carbonate units of the Capiru Karstic Aquifer into the public supply system of the region. This demand for groundwater exploitation resulted in smaller, new surveys conducted by the Water Supply Company of Paraná (SANEPAR) in partnerships with the IAT and the Federal University of Paraná. Some academic works regarding the hydrogeological aspects have been conducted in the Capiru Group water-producer units (Filpi 2021, Rigoti *in prep*), with projects in development at the Laboratory of Hydrogeological Research (*Laboratório de Pesquisas Hidrogeológicas* – LPH, Federal University of Paraná).

4.2.2 METHODS

Standard geologic field mapping practices were applied in the available exposures of the Capiru Group, aiming to identify major structural or stratigraphic

discontinuities. The Main Map (Anexo I) has been compiled using both published and unpublished data. It is noteworthy that the geological features of the Ribeira Orogenic System are hindered by generally poor outcrop exposure and intense weathering processes that have produced thick regolith and soils covering the underlying bedrock.

Further evaluation of target map areas and the location of some geological contacts were taken from the airborne magnetometric and gammaspectrometric survey by the Geologic Survey of Brazil (CPRM 2010); flight lines were about 500 m self-spaced in N-S direction. The final geophysical grids were 250 x 250 m cell-sized, which were interpolated with the bi-directional algorithm and using the N135 preferential azimuth (Geosoft 2001).

Due to the remarkable magnetic signature of the Ponta Grossa Arch (PGA) dyke swarm, the precise location of major NE-SW oriented basement structures can be hidden by several NW-SE narrow magnetic anomalies. Therefore, the magnetic anomaly was filtered with directional cosine (Geosoft 2001), in order to mitigate the NW-SE tendency and to enhance magnetic patterns from the basement units. This procedure consists of mitigating N135 oriented magnetic anomalies which represents the PGA anomalous axis (Alves 2006, Shukowsky et al. 2006).

4.2.3 GEOLOGY

4.2.3.1 Lithostratigraphic units

The Main Map (Anexo I) provides an overview of the geology of the Capiru Group, where the rocks crop out in a fold belt about 24,000 km^2. These rocks record some of the most important global geological events that occurred during the Neoproterozoic Era (1,000 - 541 Ma). They are as follows: the evolution of a passive margin after the Rodinia continent breakup (Neoproterozoic), the closure of the Brasiliano oceans (Neoproterozoic - Cambrian) during the Brasiliano - Pan African orogeny (Brito Neves et al. 2014), and the events that culminated in the Gondwana assembly (Heilbron et al. 2004, Fuck et al. 2008, Brito Neves et al. 2014, Faleiros et al. 2016). Gondwana assembly was followed by subsidence that led to infilling of the Paraná intracratonic basin (Ordovician - Cretaceous), the breakup of Gondwana, and

the opening of South Atlantic Ocean (Jurassic – Cretaceous), (Florisbal et al. 2014, Rossetti et al. 2018, Owen-Smith et al. 2017).

The map presented in this study includes the following:

(1) The Capiru Group basement, composed of medium-grade metamorphic rocks of the Setuva Complex, including banded gneisses and deformed granitoids, which crop out as the core of the Setuva Antiform Structure.

(2) The Capiru Group, which includes from bottom to top six different formations: Santana, Juruqui, Rio Branco, Morro Azul, Morro Grande and Bocaina, following the stratigraphic proposal of Santos et al. (2021). Those units represent distinct stages of a passive continental margin to syn-orogenic evolution, deposited on the continental shelf of the Curitiba microplate. Nevertheless, the depositional age of the Capiru Group has not been well constrained. Detrital zircon dating (SHRIMP U–Pb) provided a unimodal distribution of ~2.2 Ga aged grains from quartizes of the Rio Branco Formation (Basei et al. 2008), whereas LA-ICP-MS U–Pb of the Morro Grande Formation has yielded only rare 1.4-1.0 Ga ages in addition to the same ~2.2 Ga Paleoproterozoic ages. However, based on other constraints—such as elevated levels of iron, stromatolite occurrences, and Neoproterozoic aged grains in the overlying Turvo-Cajati Formation—the succession may be as young as Neoproterozoic (Siga Jr et al. 2012, Cury et al. 2017).

(3) The Serra Geral dykes (Lower Cretaceous, ~132 Ma, Renne et al. 1996) are correlative to the basalts of the Paraná-Etendeka Igneous Province, which is interpreted to represent a large volume of subaerial lavas, dike swarms, and other intrusive igneous rocks that mainly record tholeiitic affinities. These volcanic rocks are distributed over central South America (Brazil, Argentina, Uruguay, and Paraguay) and a small part of southwestern Africa (Namibia and Angola). In Brazil, they are stratigraphically referred to as Serra Geral Formation.

The Paraná-Etendeka Igneous Province represents a major magmatic event of the Lower Cretaceous and precedes the dismembering of Southern Gondwana and opening of the South Atlantic Ocean (Rossetti et al. 2018).

4.2.3.2 Structure

The deformation patterns in the area have been a controversial topic since the earliest works in the region (Fiori 1992). In the last 30 years, structural models were proposed to explain the distribution of Capiru Group units, and new concepts

and ideas were included into the previous ones (Leandro 2016, Faleiros et al. 2016, Santos et al. 2018). Our model takes into account different levels of contributions from: i) the Fiori (1992) model, which recognized the Setuva and Morro Grande thrusts as the main D1 phase structures; ii) the Pinheiro Jr et al. (1998) integration and mapping (Mineral Provinces - Açungui and Setuva region) that represented some of the interference patterns between the collisional thrusts and the late-stage of transpressive tectonics; iii) the Yamato (1999) mapping of the Bocaiúva do Sul region, which interpreted the protoliths to metamorphic products in distinct structural contexts that provided a description of the main metamorphic surfaces in the region; iv) lastly, the Faleiros et al. (2016) tectonic model (carried out in the adjacent Turvo-Cajati Complex rocks), which presented a dynamic tectonic model of the region based on metamorphic data, $^{40}Ar/^{39}Ar$ dating, and chemical dating of monazite, in addition to detailed description of the deformation phases.

Two main ductile deformation phases were recognized through our field observations: the D1 phase is supported by sub-parallel slaty cleavage (S1), poorly defined in the northern flank of the Setuva Antiform Structure, due to overprinting by S2 surface (Faleiros et al. 2016). Tight to isoclinal folds are rare and restricted to the vicinity of F1 thrusts. Also, zones of high strain and locally higher metamorphic grade or mylonitization are restricted along the D1 thrusts-planes (Santos et al. 2018). Fiori (1992) recognized the folded-thrust F1 Setuva and Morro Grande faults along the Setuva Antiform Structure, and identified the Setuva thrust as the main detachment horizon of the Capiru Group in relation to the Setuva core domain.

The D2 phase is represented by a series of oblique-slip faults, where the Lancinha Shear Zone is the main fault of the system, its secondary structures (as the N70E system represented on the Main Map – Anexo I), in addition to a series of closed asymmetric mesofolds.

The Setuva Antiform Structure (See Main Map – Anexo I) is the most striking feature in the mapped region (Fig. 3), which is described by early workers as a large E-W trending anticlinorium stack that exposes a granitic basement core (Siga Jr et al. 2007) and the Capiru Group along its rims (Fiori 1992, Campanha and Sadowski 1999, Fiori et al. 2003, Siga Jr et al. 2007). The axial plane of the structure trends ~N60-70E, dipping 20° to SW (Fiori 1992). The main metamorphic foliation in the region is generally a crenulation cleavage (S2), which is better developed in the northern flank of the structure.

After the escape-tectonics stage during Neoproterozoic - Cambrian, the region went through long phases of extensional tectonics, with NW-SE faulting that led to the emplacement of tholeitic dolerite dykes related to the Ponta Grossa Arch (the dyke swarm source). The Ponta Grossa Arch is related to the rifting process that led to the Atlantic Ocean opening, which was responsible for reactivating a series of basement structures, restructuring older basins and creating new ones (Raposo et al. 1991, Strugale et al. 2007, Ruiz et al. 2009, Almeida et al. 2013). This rifting has been linked to the activity of a mantle plume (Tristão da Cunha) that was under the South American platform during Mesozoic time (Morgan 1981, O'Connor and Duncan 1990, Castro et al. 2007).

The extensional events related to the Continental Rift of Southern Brazil (Riccomini 1989, Riccomini and Assumpção 1999, Riccomini et al. 2004) during the Cenozoic, led to the opening of a series of small and N-S aligned basins, including the Curitiba basin (Fig. 1b).

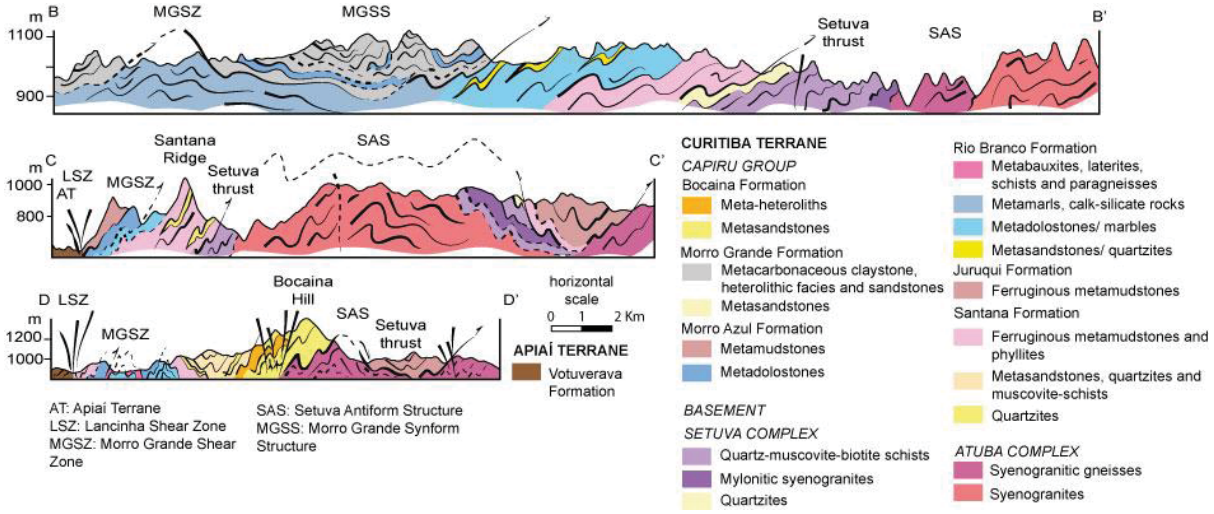


Figure 3. Structural cross-sections showing the main structural features of the Capiru Group. Vertical exaggeration of 2X. Section A is shown on the Main Map (Anexo I). Location of sections B, C and D are on the Main Map (Anexo I).

Table 1 summarizes the geologic events responsible for the main structures represented on the Main Map (Anexo I), and their available ages.

Tabela 1. Main geological events recognized in the mapped area and their related structures.

Event	Related structures	Age
Pre-Brasiliano structures		
Unknown	Ductile shear zone in Setuva Domain granitoids.	Unknown
Brasiliano – Pan African orogeny related structures		
Thrust-collision	Setuva and Morro Grande shear zones and subsidiary F1 thrust faults, F1-recumbent folding and S1 slaty cleavage. Mylonitic zones at lower crustal levels, main regional metamorphism (M1) and metamorphic peak.	~590 Ma (Faleiros et al. 2016).
Strike-slip ductile faulting	Lancinha Shear Zone and related faults, transpressive zones and F2-folding as Setuva Antiform Structure and Morro Grande Synform pair, S2 crenulation cleavage, and mylonitic zones. M2 metamorphic stage followed by greenschist overprinting.	~580 Ma (Faleiros et al. 2016).
Strike-slip ductile to brittle faults	Lancinha reactivations and N70E brittle faults, splays, and flower-structures.	Unknown
Gondwana breakup		
NW faulting and dyke swarm emplacement	Serra Geral dykes after extensional tectonics and NW brittle structures.	~132 Ma in the dykes of Ponta Grossa Arch (Renne et al. 1996). 134-114 Ma to the complete rifting (Zalan and Oliveira 2005).
Cenozoic Rift System of Southeastern Brazil		
NE brittle faulting	Reactivation of basement discontinuities and Curitiba basin onset.	89-65 Ma to the Cenozoic Rift development (Zalan and Oliveira 2005).

4.2.4 AEROGEOPHYSICAL FEATURES

Magnetic domains and potential structures were interpreted from aeromagnetic data (Figs. 4a). Despite good correlation between filtered magnetic data and mapped geological units, the available magnetic data have up to 500 km of

line space, and therefore not enough spatial resolution to supplement local features from small-scale geological mapping. However, deep magnetic sources strongly responsible the medium-scale structures, whereas the gammaspectrometric anomalies were preferred for tracing near-surface geological contacts (Fig. 4b).

We used the ternary RGB composite image (R=K, G=eTh, B=eU, Fig. 4c), in order to represent the total radiometric effect of each geological unit in the map. In this technique, K is represented in percentage and Th and U were converted to their equivalents for comparison to the K values (Ferreira et al. 2014). The radiometric maps presented in this study have shown good correlation with geological contacts between mudstones (K-rich) and carbonate units (Fig. 4b), which led us to constrain lateral extension of these units. Examples of Capiru units with distinct geophysical signature are syenogranites of the Setuva core (intermediate magnetic anomalies and Th and Th-K enrichment); and ferrouginous metasediments of the Juruqui unit (high-K and highly magnetic anomalies). A distinct geophysical signature (bright yellowish colors on ternary map) occurs in the Apiaí Terrane domain, northwestern of Lancinha Shear Zone.

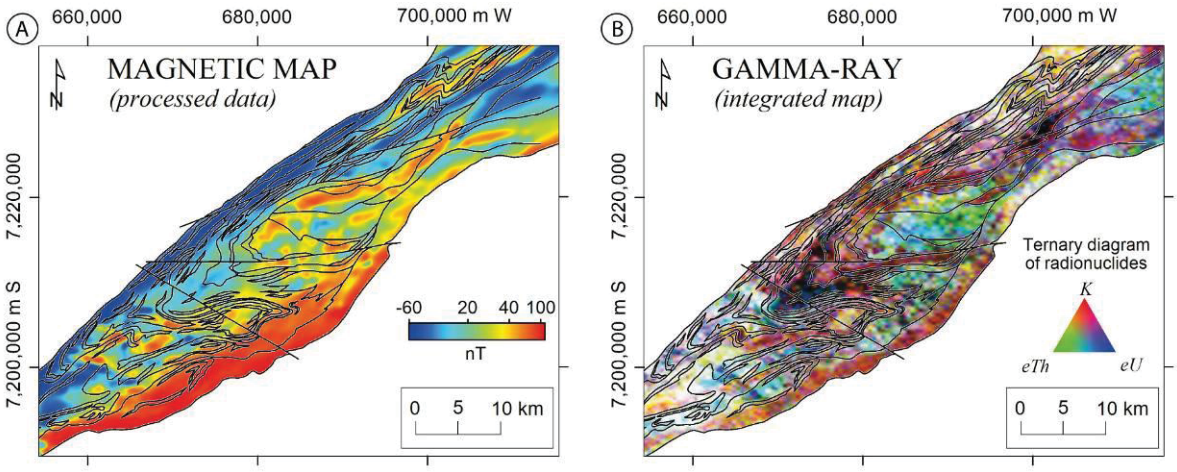


Figure 4. Geophysical maps. A) Magnetic map: processed magnetic data, in order to mitigate magnetic elongations from the Ponta Grossa Dyke Swarm (see text). B) Gamma-ray: ternary image of gammaspectrometric data, summarizing the spatial distribution of radionuclides (composite RGB image, with R=K, G=eTh, B=eU).

4.2.5 CONCLUSIONS

Presented herein is a new edition of the Geological map of the Capiru Group at 1:150,000 scale. This contribution is the most up-to-date regional map, which

integrates all the available published and unpublished data for these rocks. In addition, it incorporates multiple techniques to improve the knowledgebase of this unit. The map includes all the recent geological information delivered by the mapping project of the Capiru Project, Fiori (1985) and earlier maps, in addition to the Survey databases. In this new map six total lithostratigraphic units—in addition to the basement—were described and the main types of contacts and structural accuracy were revaluated. Throughout decades of study, significant progress in geological knowledge was made, which has provided the basis for new research targets in the area.

4.2.6 ACKNOWLEDGEMENTS

Many people offered their help during this work: MScs. G. Fedalto, R. Leandro, Dr. J. Rosenblume and Professors B.Trzaskos, A.B. França, F. Vesely, F. Varejão and E. Salamuni, gave suggestions and endorsed fruitful discussions about the Capiru Group units, their structural features, and sedimentary aspects. We thank Professor F. Ferreira for helping with the geophysical data. We thank Professors O. Siga Jr, O. Harara, and M.A. Basei for furthering the tectonic discussions. We also thank Professor A.P. Fiori, and the geologists and technicians of the Geologic Survey of Paraná (MINEROPAR) and the Geologic Survey of Brazil (CPRM), for documenting and describing with such quality many of the outcrops that were revisited in this work.

4.2.7 SOFTWARE

All geologic data was first processed to compile a geodatabase using Esri ArcGIS. Geophysical data was processed using Oasis Montaj™ software. Outlined structures were imported to the Adobe Illustrator for layout design and key editing.

4.2.8 DATA AVAILABILITY STATEMENT

The GIS data that support the findings of this study are openly available in Mendeley data repository at doi: 10.17632/mywdxyfkwr.1.

4.2.9 FUNDING

This work was supported by the Capiru Project under Grant number 481429/2013; (CNPq, Brazil), Microbial Project (a partnership between Federal University of Paraná and PETROBRAS), and Diagenesis Project (a partnership between Federal University of Paraná and SHELL Brazil).

4.3 Artigo 3: TRACING THE CONTINENTAL MARGINS OF THE SOUTHERN RIBEIRA BELT, BRAZIL: PROVENANCE AND LINKS AMONG THE POST-RODINIA FRAGMENTS

Larissa da Rocha Santos [1], Leonardo Fadel Cury [1], Justin Rosenblume [1], Marcela Trindade Mendes [2], Guilherme Fedalto [1], Angela Pacheco Lopes [3], Renato Leandro [1], Oswaldo Siga Jr. [2], Miguel Basei [2]

1: Lamir Institute, Federal University of Paraná, Curitiba, Brazil
2: University of São Paulo, São Paulo, Brazil
3: Geological Survey of Brazil, São Paulo office, Brazil

Highlights:

- Provenance signatures of the Curitiba microplate are recorded in the Capiru Group;
- Three basin-stages are recognized through the Capiru Group provenance;
- Basement similarities among Curitiba - Paranapanema - Nico Pérez - Angola craton;
- Curitiba-Angola-Nico Pérez recorded a Mesoproterozoic connection.

ABSTRACT

Reconstruction of ancient continental margins encompassed in continent-continent collisional settings is a complex task. The continental blocks generally record a multiphase evolution, with interaction of tectonic settings, plate polarities, basins and depositional architecture.

The Ribeira Belt (Southeast-Southern Brazil) resulted from the juxtaposition of several crustal blocks affected by collisions during the Brasiliano/Pan-African Orogeny (800 - 490 Ma), leading to the amalgamation of Western Gondwana. The Western Gondwana encompassed a series of pre-Brasiliano blocks that underwent variable rates of tectonic reworking, many of which including fragments derived from Rodinia.

Some of the metasedimentary strata of the Southern Ribeira belt are representative of this Late Meso- to Neoproterozoic cycle of basins, which bordered the pre-Brasiliano continental fragments, such as the Capiru Group. Given that metasedimentary strata of the Capiru Group directly overlie the basement of Curitiba microplate—and may have been shed directly from this block - they provide a hint for these Precambrian continental cycles.

In this work we show new provenance data of the Capiru Group and compare them to the other chrono-correlative continental margins of the region (Lajeado and lower Itaiacoca groups). Through the evolution of Capiru, Lajeado, and Itaiacoca groups, we suggest that the post-Rodinia continental margins of the Southern Ribeira belt show similar Paleoproterozoic contributions (2,000 – 2,185 Ma) and slightly different Mesoproterozoic populations suggesting distinct paleogeography contexts. The Mesoproterozoic “exotic” populations (1,508 – 1,110 Ma) in the Capiru Group imply a Curitiba-Angola-Nico Pérez connection, as one of the post-Rodinia crustal-segment of the region. The Capiru Group was deposited on the Northern margin of the Curitiba-Angola-Nico Pérez block, recording passive to active margin-stages. On the other hand, the Lajeado and Itaiacoca groups recorded these stages from the Paranapanema block Southern margin perspective.

Keywords: Rodinia, Western Gondwana, Capiru Group, Lajeado Group, Itaiacoca Group, Neoproterozoic basin-cycle.

4.3.1 INTRODUCTION

Rodinia supercontinent assembled through worldwide orogenic events between 1,300 Ma and 900 Ma, lasting for about 150 million years after its complete assembly (Li et al. 2008). Like its assembly, its break-up occurred diachronously, where widespread continental rifting occurred between ca. 825 Ma and 740 Ma, with episodic plume events at ca. 825 Ma, ca. 780 Ma and ca. 750 Ma (Li et al. 2008). Evidence of rifting, break-up and drifting in the several descendant blocks of Rodinia in South America is scarce and controversial, being the diachronous nature in

different blocks one of the few consensuses in the literature (Brito Neves and Cordani 1991, Almeida et al. 2000, Meert and Torsvik 2003, Fuck et al. 2008).

The Ribeira belt (Almeida 1967, Almeida et al. 1973) is a NE-trending orogenic belt subparallel to the southern Brazilian coast (Fig. 1), and its structural framework has resulted from the juxtaposition of several crustal blocks affected by subductions followed by collisions during the Neoproterozoic Brasiliano/Pan-African Orogeny (800 - 500 Ma; Brito Neves et al 1999, Basei et al. 2009, Brito Neves et al. 2014, Heilbron et al. 2020). The assembly of these continental blocks (Fig. 1) led to the formation of Western Gondwana (Brito Neves et al. 1999, Basei et al. 2000, 2008, Campos Neto et al. 2011), a supercontinent that encompassed a series of pre-Brasiliano blocks, including descendant fragments from Rodinia (Brito Neves et al. 1999, Fuck et al. 2008).

In the context of pre-Brasiliano blocks involved in this accretion, the Southern segment of the Ribeira Belt evolved from the interaction between the Paranapanema block (Fig. 1), now fully covered by the Paleozoic sediments of the Paraná Basin (Basei et al. 2009, Mantovani and Brito Neves 2009), and the trondhjemite-tonalite-granodiorite terranes constituting the basements of the Curitiba and Luís Alves microplate(s?); (Siga Jr. et al. 1995, Basei et al. 1992, Hartmann et al. 2000, Sato et al. 2003, Basei et al. 2008, 2009, Passarelli et al. 2011, 2018, Fig. 1). Further east, the Paranaguá terrane represents an accreted arc of calk-alkaline granitoids (Cury 2009, Patias et al. 2019; Fig 1) docked during the late stages of this collisional evolution (Patias et al. 2020).

Some portions of the belt have been paleogeographically reconstructed by means of platform/shelves deposits and their correlative slope zones (Bigarella and Salamuni 1956, 1967, Fairchild 1977, Reis Neto 1994, Campanha et al. 2016, Guimarães et al. 2002, Sallun Filho and Fairchild 2005), in addition to the oceanic crust remnants (Campanha and Sadowski 1999, Harara 2001, Basei et al. 2009, Siga Jr. et al 2012, Siga Jr. et al. 2014, Campanha et al. 2015, 2019).

Together with the provenance studies, several units of the Southern Ribeira belt were described in terms of their potential source areas (Campanha et al. 2016, 2019, Ricardo et al. 2020) and their chrono-correlative equivalents, thus adding information to further interpretation on the evolution of these plate margins.

The metasedimentary strata of the Capiru Group directly overlie the basement of the Southern Ribeira belt (Basei et al. 2008, Santos et al. 2021a) and

they might help to tight the evolutive links, especially in this area on the eastern edge of the present South American continental margin.

In this work we show: i) new provenance data of the Capiru Group, aiming to understand the depositional setting and basin infill during the Brasiliano oceans onset; ii) Although the primary focus of this study is the Capiru Group, a few additional samples were collected from the Lajeado Group for the purposes of comparison; and iii) discussing the Late Meso- to Neoproterozoic passive continental margin records from the integration of new and existing geochronologic data of the supracrustal sequences of the region. Through the provenance study, we aim to establish the paleogeographic links between these successions and the post-Rodinia continental margins of the region.

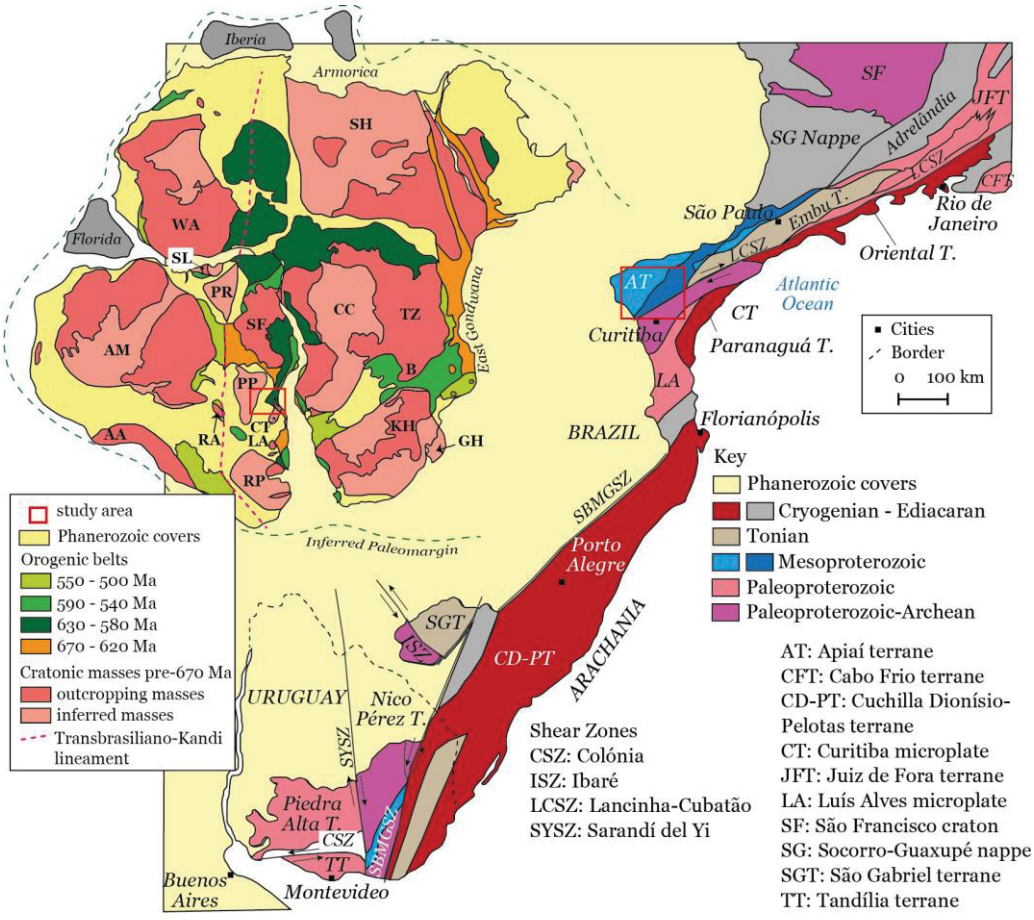


Figure 1. Paleogeographic setting of Western Gondwana (at ca. 500 Ma) with cratons (pre-Brasiliano continents) sutured by Gondwana mobile belts (adapted from Schmitt et al. 2018). AA: Arequipa/ Antofalla, AM: Amazonia, B: Bangweulu Block, CC: Congo, CT: Curitiba, GH: Grunehogna, KH: Kalahari, LA: Luís Alves, PP: Paranapanema, PR: Parnaíba, RA: Río Apa, RP: Río de la Plata, SH: Sahara, SF: São Francisco, SL: São Luís, TZ: Tanzania, WA: West Africa, and regional tectonic framework of the South American Eastern terranes and cratonic blocks (Passarelli et al. 2011, after Gaucher et al. 2021).

4.3.2 BACKGROUND

4.3.2.1 Paleogeographic Setting

The main cratonic blocks of Southern South America are represented by the Río de la Plata craton, Nico Pérez terrane, Curitiba and Luís Alves microplates, and the Paranapanema block (Fig. 1). The majority of these crustal blocks are total or partially covered by Phanerozoic basins, and their main exposures happen to be near to the Atlantic margin of the South American continent.

These blocks are dominated by autochthonous Rhyacian (2,300 - 2,050 Ma) units (*e.g.* Cordani and Teixeira 2007, Dalla Salda et al. 2006, Rapela et al. 2007, Santos et al. 2017, Hartmann et al. 2002a, 2002b, Siga Jr. et al. 1995, Sato et al. 2003) encompassing Archean (3,850 - 2,500 Ma) inheritances (*e.g.* Santos et al. 2000, Hartmann et al. 2000b, Cingolani 2011, Sato et al. 2003), Statherian (1,800 - 1,600 Ma), (Mallmann et al. 2007, Bossi and Cingolani 2009, Gaucher et al. 2011, Siga Jr et al. 2011a), and Mesoproterozoic (Oyhantçabal et al. 2005, 2011, Gaucher et al. 2011, Campanha et al. 2015, 2016) belts/rocks. It is likely possible that some of these larger crustal units (such as Río de La Plata craton) were amalgamated to the African cratons (McCourt et al. 2013, Van Schijndel et al. 2014) in the pre-Brasiliano times (Santos et al. 2008, Santos et al. 2017, Gaucher et al. 2011, Oriolo et al. 2016, 2019), and later separated from Africa (Sinclair and Rehoboth Mesoproterozoic 'Kibaran' belts, De Waele et al. 2003) during Rodinia fragmentation (ca. 820–800 Ma, Pisarevsky et al. 2003 or ca. 825–740 Ma, Li et al. 2008 or ca. 900 Ma, Siga Jr et al. 2009, Campanha et al. 2016).

Subsequent collisions between the South American and African cratonic blocks occurred during the late Brasiliano–Pan-African orogenic cycle (850–550 Ma, Brito Neves et al. 1999, Kröner and Stern 2004), followed by a Mesozoic rift-drifting during the Western Gondwana fragmentation (Rapalini and Vilas 1991a and 1991b, Dalziel et al. 2000, Lovecchio et al. 2020). During the Gondwana rifting, remnants of the Neoproterozoic mountain belt were left behind on the South American and African continents, making these blocks of South American margin with complex

geological history, therefore, to have several competing interpretations regarding their sizes, borders, extension and extent of geological events (Rapela et al. 2007, 2011, Casquet et al. 2012, Fuck et al. 2008, Bossi and Cingolani 2009, Ramos et al. 2010, Gaucher et al. 2011, Oyhantçabal et al. 2011, Dragone et al. 2017, Passarelli et al. 2018).

4.3.2.2 Regional Geological Setting

The study area is located entirely within the South American side of the Brasiliano–Pan-African mountain belt in São Paulo and Paraná State, Southeast-Southern Brazil. In this region, the Southern Ribeira Belt contains rocks of the Precambrian shield (Fig. 2). These terranes docked during the Neoproterozoic Brasiliano–Pan-African Orogeny and were later intruded by syn- to post-collisional Neoproterozoic granitoids (Basei et al. 2008, Heilbron et al. 2008, Faleiros et al. 2016, Bruno et al. 2018, and Heilbron et al. 2020). In this sector of the Ribeira Belt, there are four terranes (from SE to NW) referred to as the Paranaguá, Luís Alves, Curitiba, and Apiaí terranes (Fig. 2a). These four terranes generally comprise Pre-Brasiliano tectonic units, such as reworked Archean to Paleoproterozoic basement blocks, Mesoproterozoic and Neoproterozoic (meta-) passive margin strata, volcanics, and granitoids interpreted as arc complexes, later affected by post-collisional granites and structures that were responsible for the emplacement of post-orogenic basins (Basei et al. 1992, Campos Neto and Figueiredo 1995, Campanha and Sadowski 1999, Campos Neto 2000, Heilbron et al. 2004, 2008).

The Paranaguá terrane extends in the NE-SW direction (Fig. 2a) along the south-southern Brazilian coast (Basei et al. 1992, Siga Jr. et al. 1995). It is limited by sinistral strike-slip shear zones to the south, in contact with the Luís Alves microplate (Patias et al. 2019). To the north, the terrane is in thrust contact with the Curitiba microplate (Cury 2009). The Paranaguá terrane is primarily constituted of Ediacaran granitic suites (ca. 640-580 Ma) that have intruded basement inliers of Paleoproterozoic migmatitic-orthogneisses and Mesoproterozoic metasedimentary rocks of the São Francisco do Sul Complex and Rio das Cobras Formation, respectively (Cury 2009). The Paranaguá terrane is interpreted to contain an arc complex accreted on the southern margin of the Luís Alves microplate (Cury 2009,

Bruno et al. 2018). Three main granitic suites have been documented within these rocks (Morro Inglês, Canavieiras-Estrela, and Rio do Poço), where each one of them displays geochemical features consistent with the evolution from a magmatic arc passing through anorogenic to post-collisional granites (Cury 2009). These granites have been previously correlated to the Kaoko Belt on the African side of the Brasiliano orogen (Cury 2009, Bruno et al. 2018).

The Luís Alves microplate (Fig. 2a, Hartmann et al. 1979, 2000c, Basei et al. 1992, 1998b, Siga Jr. et a. 1995, Harara 2001, Basei et al. 2009) represents the oldest crustal fragment of the region, consisting of a Paleoproterozoic NW-trending migmatitic-gneissic ortho-derived basement with Archean inheritance (Hartmann et al. 1979, 2000c, Basei et al. 1998b). The Luís Alves microplate is bounded by the Piên Mafic-Ultramafic Suite to the North (Machiavelli et al. 2011), interpreted as the remnants of an ophiolitic complex between Luís Alves and Curitiba microplates that might represent evidence of a suture zone and a record of a northwestward subduction (Fig. 2a, Basei et al. 1992, Siga Jr. et al. 1993, Machiavelli et al. 2011, Basei et al. 2000, Harara 2001). The basement of the Luís Alves terrane is unconformably overlain by Neoproterozoic strata and volcanics that record the late-tectonic and transitional stages after the Brasiliano orogen stabilization. The volcano-sedimentary basins of Campo Alegre, Corupá and Guaratubinha, are considered to be as syn-to post-collisional late-tectonic basins, bounded by normal and strike-slip faults (Basei et al. 1998a, Basei et al. 2009, Barão et al. 2017, Zanella et al. 2020, Lino et al. 2021). In contrast, the Itajaí Basin may have been deposited in a peripheral foreland setting related to the Dom Feliciano Belt, at the southern border of the Luís Alves microplate (Basei et al. 1998a, Rostirolla et al. 1999, Basei et al. 2011).

The Curitiba microplate (Fig. 2b, Basei et al. 1992) is located between Luís Alves and Paranapanema cratonic fragments. The basement of this terrane—referred to as the Atuba and Setuva Complexes (Siga Jr et al. 1995, 2007)—is mainly constituted of banded and migmatitic gneisses (biotite-amphibole gneissic mesosome and tonalitic-granodioritic leucosome), banded granitic-gneisses, foliated leucogranites, lepidoblastic biotite gneisses and amphibolites, mafic-ultramafic rocks and magnesian schists (Siga Jr. et al. 1995, 2007, Sato et al. 2003). This gneissic banding shows a main NE-trending foliation, suggesting deformation controlled by ductile shearing, with anatexis and migmatization during the Neoproterozoic (Siga Jr.

et al. 1995). The Atuba Complex has been correlated to the Registro Domain (further North; Passarelli et al. 2004, 2007), constituted mainly by granite-gneisses-migmatites and paragneisses.

The Neoproterozoic metasedimentary cover of the northern margin of the Curitiba microplate is represented by the Capiru Group and portions of the Turvo-Cajati Complex (Fig. 2b; Faleiros et al. 2011a, Passarelli et al. 2018, Santos et al. 2021a, Ricardo et al. 2020). The Capiru Group was likely deposited in a shallow, continental shelf setting along the passive continental margin of the Curitiba microplate (Santos et al. 2021a). In contrast, segments of the Turvo-Cajati Complex may represent the assembly of two distinct basins: i) an accretionary wedge, which developed on the active margin of the Curitiba microplate, where ultra-high-pressure metamorphism has been documented within the Turvo-Cajati assemblage (Ricardo et al. 2020), and ii) a back-arc basin, which may have formed over the Curitiba microplate based on a high geothermal gradient documented within the Atuba Complex basement (Ricardo et al. 2020).

The Apiaí terrane consists of Meso- to Neoproterozoic (meta) volcanics and sedimentary successions originally deposited on the eastern and southern margins of the Paranapanema paleocontinent (Basei et al. 1992, Passarelli et al. 2018). In its southern segment, the Rhyacian Paleoproterozoic tonalitic gneisses (~ 2.1 Ga), and deformed Statherian A-type granites (~1.75 Ga, Cury et al. 2002) constitute the basement inliers of the Apiaí, Tigre, and Betara basement-cores. During the Neoproterozoic, as an active margin, this segment was intensely affected by calk-alkaline magmatism represented by granitic batholiths that constitute the roots of the Três Córregos, Cunhaporanga and Agudos Grandes magmatic arcs (Fig. 2b; Janasi et al. 2001, Prazeres Filho et al. 2003, Leite et al. 2007, Cury et al. 2008).

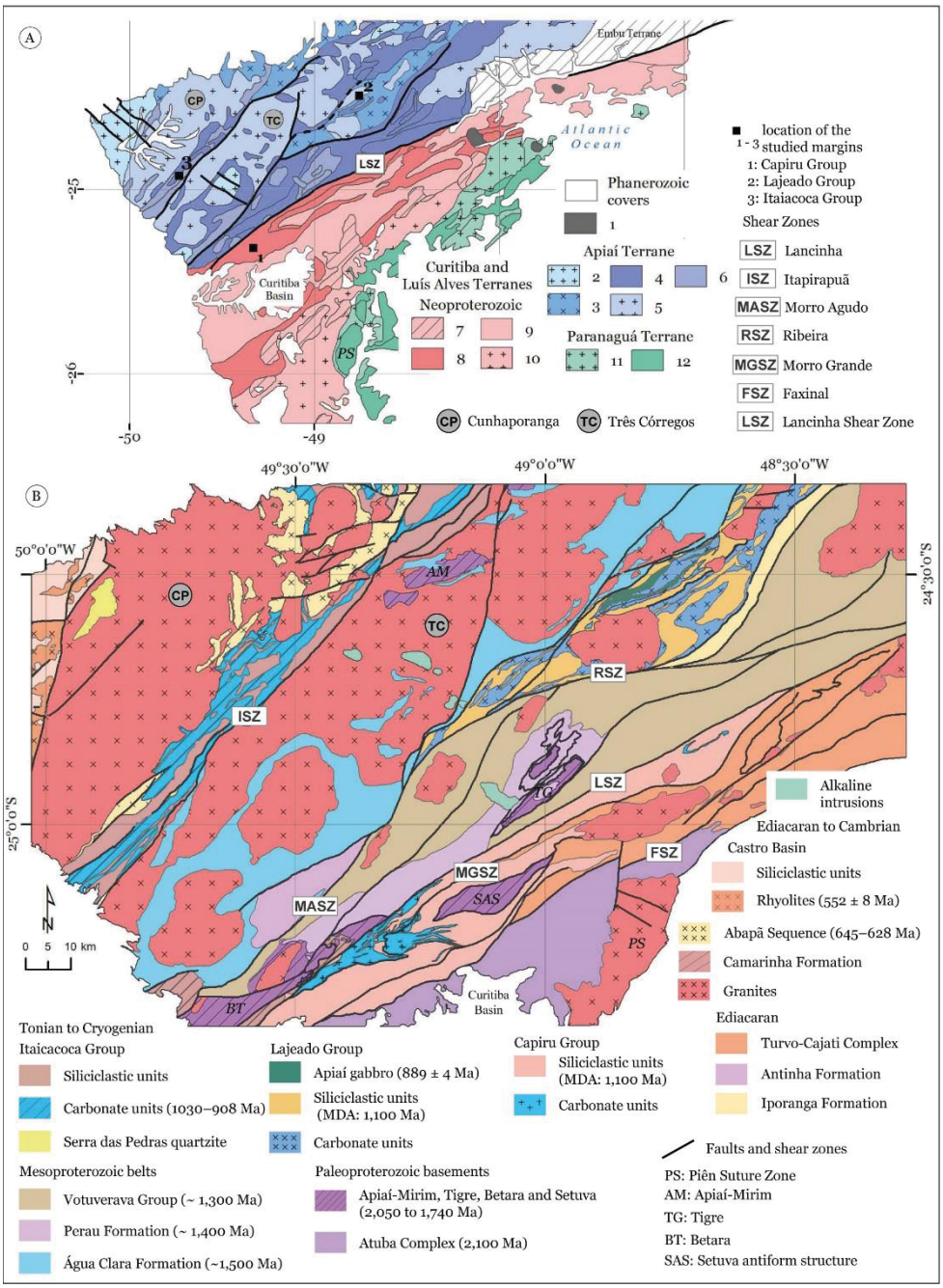


Figure 2. A) Regional geological and tectonic framework of the Southern Ribeira Belt (after Basei et al. 2008), and location of the Neoproterozoic Capiru, Lajeado and Itaiacoca margins: 1: Alkaline complexes, (2-6) APIAÍ TERRANE - 2: Molasse basins of Castro Group and Camarinha Formation, 3: Granites, 4: Neoproterozoic successions, 5: Neoproterozoic granites (CP: Cunhaporanga and TC: Três Córregos Complexes); 6: Statherian units, (7-10) CURITIBA AND LUÍS ALVES TERRANE - 7: Extensional basins and granites, 8: Neoproterozoic successions (including Capiru Group and Turvo-Cajati Complex), 9: Reworked Rhyacian orthogneisses, migmatites (Atuba Complex) and Rhyacian gneisses, 10: Orthogneisses and granulites; (11-12) PARANAGUÁ TERRANE - 11: Neoproterozoic granites, 12: Meso- to Neoproterozoic successions, LSZ: Lancinha Shear Zone, SAS: Setuva Antiform Structure, PSZ: Piên Suture Zone; B) Simplified geology of Curitiba and Apiaí terranes.

4.3.2.3 Late Meso- to Neoproterozoic strata in Southern Ribeira belt

The passive continental margin records are substantial in the Southern Ribeira belt (Fig. 3) spanning from Meso- to Late Neoproterozoic (Reis Neto 1994, Sallun Filho and Fairchild 2004, Campanha et al. 2016). On the Apiaí terrane, the passive margin strata of that age are represented by the Lajeado and lower Itaiacoca groups (Campanha et al. 2016, Siga Jr et al. 2009). In contrast, on the Curitiba terrane, the Capiru Group passive margin strata may be as young as Neoproterozoic (late Cryogenian ca. 715-630) based on iron-rich Juruqui Formation and in the presence of stromatolite-rich beds of the Morro Azul Formation (Fairchild 1982, Guimarães et al. 2002, Sallun Filho and Fairchild 2004, Passarelli et al. 2018, Santos et al. 2021a).

In a broader tectonic context, these units are all considered to be related to the break-up of Rodinia (Fuck et al. 2008, Brito Neves et al. 2014, Campanha et al. 2016), and despite being present on different basement blocks (such Capiru, on Curitiba microplate) and/or different positions of a block (Lajeado and Itaiacoca, Paranapanema block), these three units share stratigraphic similarities (Fig. 4). For example, some authors have considered the Itaiacoca and Capiru carbonate platform successions chrono-correlated margins based on the stromatolite content of both units (Reis Neto 1994, Guimarães et al. 2002, Sallun Filho and Fairchild 2004). The Itaiacoca Group represents deposits of shallow waters, whereas the Lajeado Group displays a gradual E-deepening based on normally-graded beds interpreted as turbidites (Campanha et al. 2016). However, both units are considered to have formed on the passive margin stage of the Paranapanema block (Campanha and Sadowski 1999, Campos Neto 2000; Fig. 4).

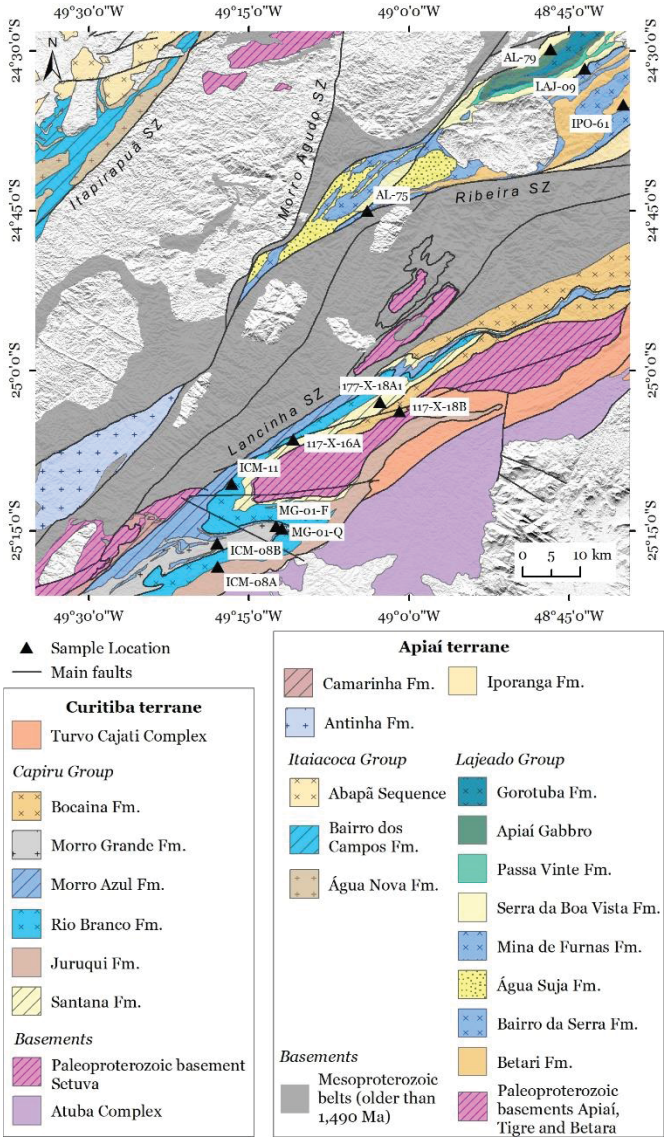


Figure 3. Late Meso- to Neoproterozoic passive margin strata in the Southern Ribeira belt. Formations are presented in stratigraphic order for both continental fragments (Curitiba microplate and Paranapanema block). Location of the studied samples are included on the map, and the samples details can be consulted on Table 1.

Itaiacoca Group – Southern Paranapanema block

The Itaiacoca Group (Fig. 3) consists of Tonian to Ediacaran successions of metasedimentary and metavolcanic rocks divided in two major lithologic associations: the lower interval is interpreted as a (Tonian) shallow carbonate platform composed of dolomitic metalimestones, metamarls, and carbonate phyllites (Fairchild 1977, 1982, Sallun Filho and Fairchild 2004, Siga Jr. et al. 2009, Forero-Ortega 2018) interbedded with metabasic rocks. These metabasic sills show subalkaline/ tholeiitic basalt compositions suggesting genesis in an extensional environment (Reis Neto

1994) around Late Mesoproterozoic/ Early Neoproterozoic time (1,000–870 Ma) based on U–Pb dates from magmatic zircon (Siga Jr. et al. 2009).

A tuff bed described in Bairro dos Campos Formation (upper Itaiacoca interval) yielded an age of 613.5 ± 9.6 Ma (Forero-Ortega 2018), constraining an Ediacaran age for the growth of a stromatolitic interval, implying an additional carbonate pulse during Ediacaran.

This upper interval (referred to as the Abapã Sequence, Fig. 3) is mainly composed of clastic deposits (meta-arkoses, metavolcanics, metaconglomerates, and metapelites) with Neoproterozoic maximum depositional ages (645–628 Ma, U–Pb in zircon of metavolcanic rocks; Siga Jr. et al. 2009).

The Abapã Sequence is thought to be part of the volcanic arc complex related to the Três Córregos and Cunhaporanga batholiths that range from ca. 650–600 Ma in age (Prazeres Filho et al. 2003, Cury et al. 2002, Siga Jr et al. 2003, Siga Jr et al. 2009). A basic intrusive unit termed as Fazenda Velha metabasic suite (Forero-Ortega 2018) has yielded ages of 571 ± 25 Ma (U–Pb SHRIMP from magmatic zircon), suggesting a younger basic magmatism in the Itaiacoca Group, interpreted as a back-arc stage during Late Ediacaran time.

Lajeado Group – Eastern Paranapanema block

The Lajeado Group (Fig. 3) is a ca. 5-km thick stack interpreted as a record of a Stenian-Tonian (ca. 1,200 - 850 Ma) passive margin (Campanha et al. 2016), comprising seven overlapping siliciclastic and carbonate formations (Faleiros et al. 2012, Campanha et al. 2016), from oldest to youngest (Fig. 4) termed as: the terrigenous Betari Formation (turbidite transgressive succession), Bairro da Serra (carbonates of a distal platform), phyllites of Água Suja Formation (distal shelf with storm influence), carbonates of Mina de Furnas Formation (distal marine), siliciclastics of Serra da Boa vista Formation (shallow marine), Passa Vinte Formation (shallow marine, locally exhibiting algal mats), and the Gorutuba Formation (distal rhythmites). The fault-bounded contact between the underlying Passa-Vinte limestone (shallow marine) and the Gorutuba distal rhythmites suggests allochthony (Campanha 1991).

The upper portion of the Lajeado Group (Gorutuba Formation) is intruded by—and interbedded with—the Apiaí Gabbro (Campanha et al. 1985), which is a lopolith-like intrusion (Campanha and Sadowski 1999, Campanha et al. 2016) of

similar metabasic composition to other intrusions in the region, such as the Itaiacoca lower interval and the Carumbé dyke-swarm (Tonian); (Maniesi 1997, Maniesi and Oliveira 2000, 2002, Oliveira et al. 2002, 2012).

The Apiaí Gabbro is composed of gabbro, diabase or microgabbro with augite + hypersthene + (andesine-labradorite) plagioclase, and minor magnetite and ilmenite, with equigranular ophitic to subophitic textures (Campanha et al. 2016). These rocks display ~50% SiO_2 content and positive εNd values, and have been classified as subalkaline tholeiitic basalts with MORB affinity (Frascá et al. 1997, Oliveira et al. 2002, 2012).

Previous U-Pb detrital zircon dating from metasedimentary rocks of the Betari and Serra da Boa Vista formations (Fig. 4) documented maximum depositional ages of ca. 1,400 and 1,200 Ma, respectively (Campanha et al. 2016). Previous U-Pb dating of magmatic zircon from a portion of the Apiaí Gabbro that underlies the Gorutuba Formation has yielded an age of 877 ± 8 Ma, which provided a minimum depositional age for the Lajeado Group (Campanha et al. 2016).

Capiru Group – Northern Curitiba microplate

The Capiru Group (Fig. 3), (Tonian to Ediacaran) is a ca. 4 km-thick stack deposited on the northern margin of the Curitiba microplate (Santos et al. 2021a). Six formations have been described within the group (Fig. 4). From oldest to youngest they are as follows: Santana (proximal to distal marine shelf), Juruqui (proximal to distal deltaic), Rio Branco (carbonate platform), Morro Azul (lagoonal to shallow marine), Morro Grande (proximal to distal deltaic/ shallow marine), and Bocaina formations (estuarine to shallow marine). Two main basin stages have been interpreted at the Curitiba microplate margin (Santos et al. 2021a): (1) a passive continental margin stage (Santana - Juruqui times), with increasing tectonic quiescence (Rio Branco), followed by a marine regression (Morro Azul time) and (2) a synorogenic stage (beginning with Morro Grande to Bocaina time). During the syn-orogenic stage, the arkose composition of sandstones and lithic conglomerate lags suggest source rejuvenation and accommodation changes, prior to the assembly of Western Gondwana (Santos et al. 2021a).

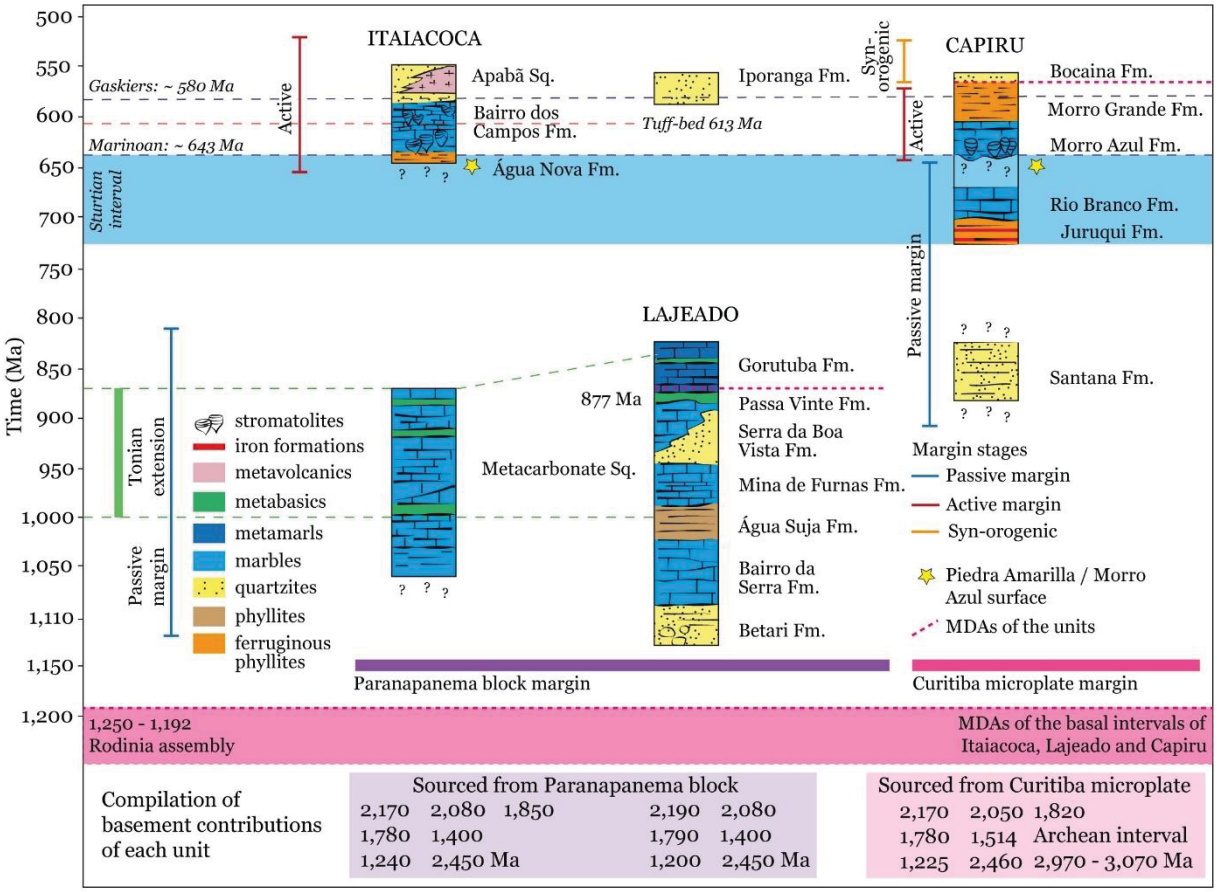


Figure 4. Representative stratigraphic columns and proposal of correlation through time among the passive – to - active margin records (Late Meso- to Neoproterozoic cycle of basins) in Southern Ribeira belt. Ages and ambience interpretation are compiled from: Itaiacoca - Fairchild (1977, 1982), Theodorovicz et al. (1986), Reis Neto (1994), Sallun Filho and Fairchild (2004), Siga Jr. et al. (2003, 2009), Forero-Ortega (2018), Forero-Ortega et al. (2020); Lajeado: Campanha (1985), Campanha (1991), Frascá et al. (1997), Campanha and Sadowski (1999), Faleiros et al. (2012), Campanha et al. (2016), Maniesi and Oliveira (2000, 2002), Oliveira et al. (2002, 2012), Lopes et al. (2017); Capiru: Fiori (1992), Fiori and Gaspar (1993), Guimarães et al. (2002), Leandro (2016), Santos et al. (2018), Santos et al. (2021a and 2021b). End of the passive margin stage on the Paranapanema block-side is stipulated between 645 - 628 Ma (age of crystallization of arc-related zircon). Synorogenic stage on the Curitiba microplate starts at ca. 565 ± 7 Ma (age for the MDA of Bocaina Formation - see Section 5.1 for explanation).

4.3.3 METHODS

4.3.3.1 Sampling Strategy

Sampled localities were selected based on previous stratigraphic work and mapped outcrops of the Capiru and Lajeado groups from a broad geographic area in the Eastern Paraná State, Brazil (Fig. 3, Table 1, Santos et al. 2021a, Campanha et al. 1985, 1986, Faleiros et al. 2012, Campanha et al. 2016). In total, ten samples

were collected and analyzed for U-Pb zircon geochronology; nine are detrital and one is magmatic. Eight of the samples were collected from outcrops of the Capiru Group. The Morro Azul Formation (Fig. 4), which is dominantly carbonate, was not sampled; the samples were collected from clastic intervals (Figures 5 and 6) within each of the other five recently revised map units (Fig. 3, Santos et al. 2021a). In addition, one sample was collected from the Betari Formation—the lowermost unit of the Lajeado Group (Campanha et al. 2016) for the purpose of comparison with U-Pb detrital zircon data from the Capiru Group strata. Lastly, one sample was also collected from the Apiaí Gabbro—a laccolith-like intrusion on the Apiaí terrane which crosscuts and overlies the Lajeado Group strata (Campanha et al. 2016). Given that the Apiaí Gabbro has a MORB geochemical signature (Campanha et al. 2016) the purpose of this sample was to improve timing constraints for extensional tectonism in the region.

Table 1. U-Pb zircon geochronological data from the Capiru and Lajeado groups in the Southern Ribeira Belt used in this study. Samples IPO 61 and LAJ 09 are from Campanha et al. (2016).

Formation	Sample	Sample description	YSG	YPP	WMA	Latitude	Longitude
Capiru Group							
Bocaina	117-X-18B (n=76)	Lower interval of formation, feldspathic quartzite	565 ± 7	564	--	700,174	7,226,660
Morro Grande	ICM-08B (n=79)	Upper interval, orthoquartzite	1,226 ± 8	1,245	--	6,711,52	7,204,129
Morro Grande	MG-01-F (n=54)	Middle interval, phyllite	1,110 ± 11	1,108	--	680,501	7,206,959
Morro Grande	MG-01-Q (n=78)	Lower interval, arkose	1,473 ± 74	1,481	1493 ± 25 MSWD = 0.42 (n=5)	681,408	7,206,570
Rio Branco	ICM-11 (n=71)	Upper portion of formation, orthoquartzite	1,740 ± 28	1,727	--	673,580	7,214,392
Juruqui	ICM-08A (n=86)	Lower interval, subarkose	1,741 ± 43	1,744	1752±18 MSWD = 0.22 (n=4)	671,231	7,200,099
Santana	177-X-18A1 (n=75)	Upper interval, orthoquartzite	1,742 ± 31	1,732	--	697,137	7,228,281
Santana	117-X-16A (n=62)	Lower interval, meta-arkose	1,922 ± 40	1,925	2136 ± 21 MSWD = 20 (n=49)	683,423	7,221,949
Lajeado Group							

Apiaí Gabbro	AL-79 (n=17)	Uppermost unit of Group, mafic intrusive	--	--	888.6 ± 5.6 MSWD=1.4 (n=17)	725,006	7,288,948
Serra da Boa Vista (Campanha et al. 2016)	LAJ 09 (n=65)	meta- sandstone	1,192 ± 20	1,199	--	730,409	7,285,470
Betari (Campanha et al. 2016)	IP 61 (n=17)	Basal unit of Group, meta-conglomerate	1,390 ± 38	1,386	--	736,369	7,279,132
Betari	AL-75 (n=75)	Basal unit of Group, feldspathic quartzite	1,724 ± 30	1,718	--	730,409	7,285,470

Note. Maximum depositional age estimates are shown for each sample in mega annum (Ma). Coordinates are listed as WGS 84, UTM 22 S. YSG = youngest single grain; YPP = youngest graphical peak; MSWD = mean square weighted deviation; n = total number of individual grain analyses; WMA = weighted mean average. For detrital samples, WMA was calculated using a 2σ overlap in ages when possible. For the Apiaí Gabbro, WMA was calculated using a 1σ overlap in ages.

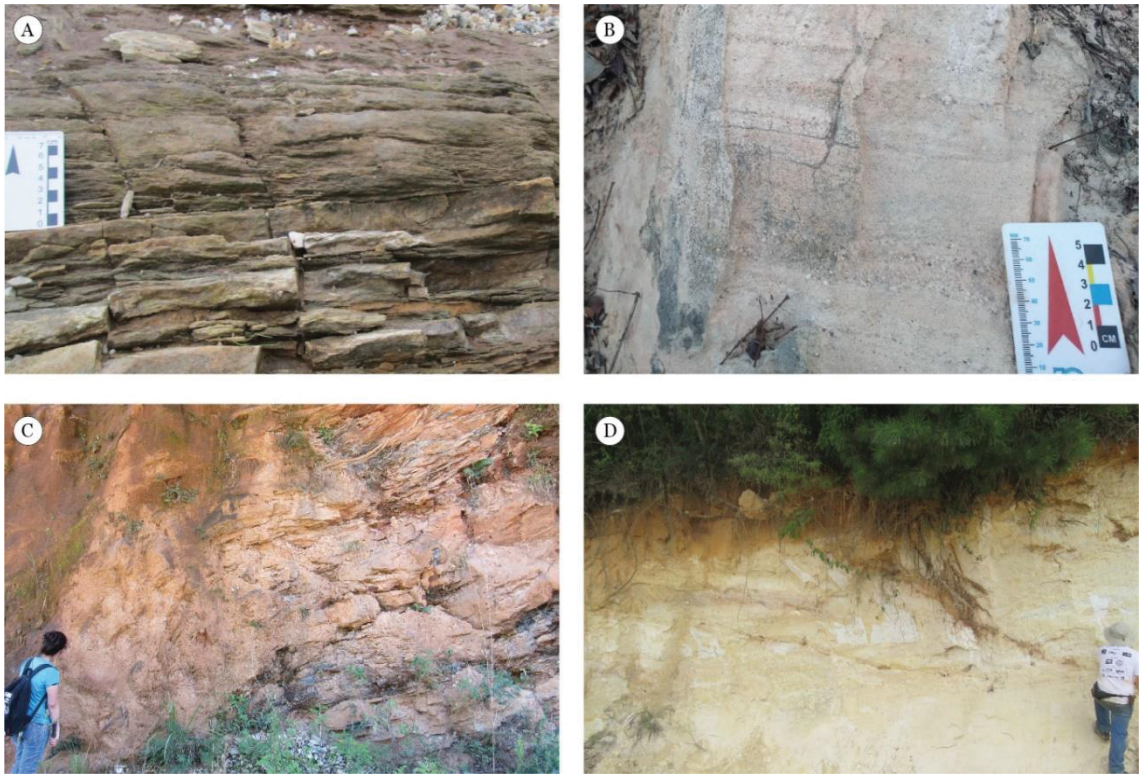


Figure 5. Photographs of the sampled outcrops for this study. A) Meta-arkose of the Santana Fm. lower interval (sample 117-X-16A); B) orthoquartzites of the upper interval of Santana Fm. (177-X-18A1); C) metasubarkose of Juruqui Fm. (ICM-08A); D) orthoquartzites beds of Rio Branco Fm (ICM-11).

4.3.3.2 U-Pb Geochronology of detrital zircon

Eight samples of the Capiru Group were separated from ~5-7 kg of rock following the mineral separation protocols used at the University of São Paulo - using the standard isodynamic, gravimetric and magnetic techniques. After separation, the detrital zircon grains were handpicked, mounted in epoxy resin disks, and backscattered electron images were acquired. In addition, cathodoluminescence (CL) images (Figures 7 and 8) were collected using a scanning electron microscope to guide the selection of laser spot positions.

For each sample, the zircon grains (n= 100) were analyzed on a Photon-machine® analyzer G2 – 193 nm – Excimer Laser Ablation System laser coupled with the MC-ICP-MS Thermo® Neptune at CPGeo at the University of São Paulo. A 30 µm spot size was used with a depth of 30-50 µm. The isotope ratios were monitored and corrected for drift and within-run U-Pb fractionation by repeated analyses of the GJ-1 zircon reference material (Jackson et al. 2001), blanks, synthetic NIST-613 standard, and unknowns. The obtained data were reduced and corrected following the procedures of Siqueira et al. (2014), and the results are reported herein using Isoplot 4.0 software (Ludwig 2012) and AgeCalcML 1.42 (Sundell et al. 2021).

The Lajeado Group and Apiaí Gabbro samples were separated from ~ 5 and ~15 kg of rock, respectively, following the mineral separation procedures used at the University of Ouro Preto. These two samples were analyzed using the Photon-machine® analyzer G2 – 193 nm – Excimer Laser Ablation System laser coupled with the MC-ICP-MS Thermo® Neptune at the University of Ouro Preto. A 20 µm spot size was used with a depth of 5-10 µm. Details of the procedures can be consulted in Lana et al. (2017). The U-Pb results are reported using Isoplot 4.0 software (Ludwig 2012) and AgeCalcML 1.42 (Sundell et al. 2021).

Only U–Pb zircon ages with discordance equal to or <5% from both datasets were considered for this work. All the zircon U–Pb isotopic data collected for this study are tabulated in the Supplementary Material.



Figure 6. Photographs of sampled outcrops for this study. A) Arkose meta-sandstones of the lower interval of Morro Grande Fm. (sample MG-01-Q); B) phyllites of the middle Morro Grande Fm. (MG-01-F); C) orthoquartzites of the upper Morro Grande interval (ICM-08B); D) feldspathic quartzites of the lower Bocaina Fm. (117-X-18B); E) feldspathic quartzite of the Betari Fm., Lajeado Group (AL-75); F) Apiaí Gabbro (AL-79).

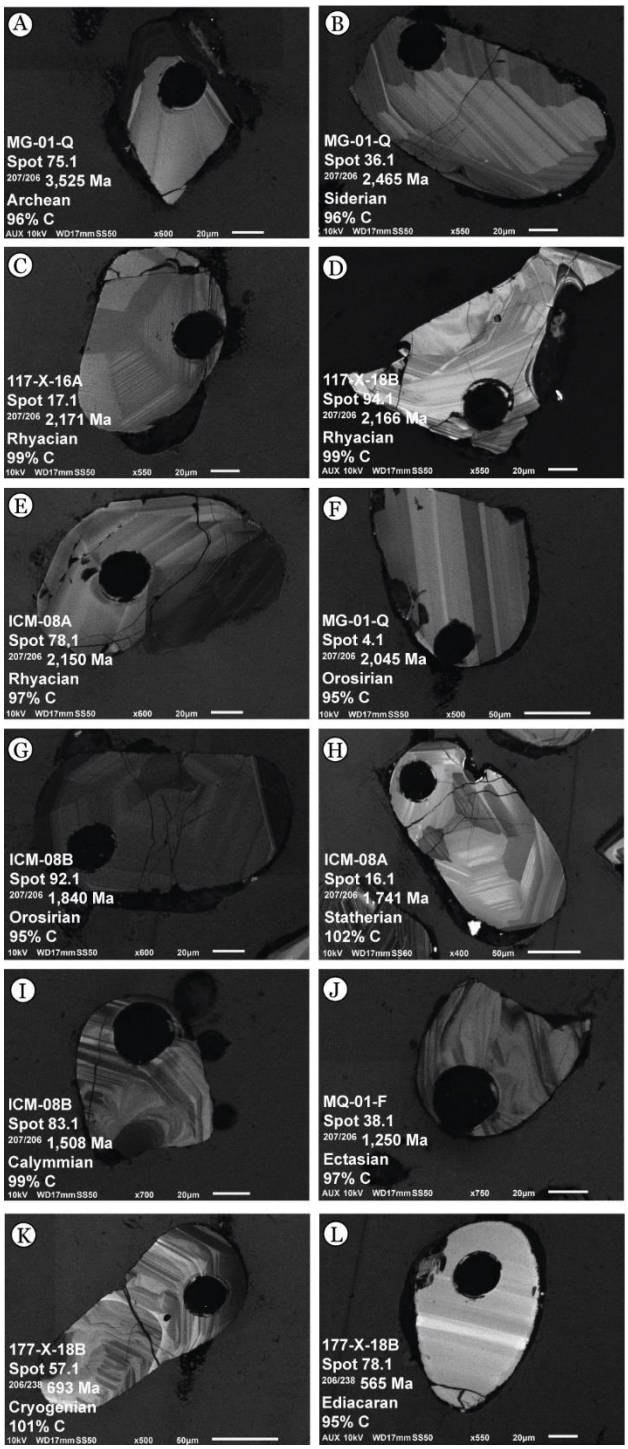


Figure 7. Cathodoluminescence imaging of the main detrital zircon populations of the Capiru Group. A: oldest zircon, Morro Grande Fm. lower interval; B: Siderian population (~2,460 Ma), Morro Grande Fm. lower interval; C-E: Rhyacian contributions at 2,170 Ma (Santana Fm.), 2,160 Ma (Bocaina Fm.), and 2,150 Ma (Juruqui Fm), respectively. F: Orosirian contribution ~2,050 Ma, Morro Grande Fm. lower interval; G: Orosirian population ~1,840 Ma, Morro Grande Fm. upper interval; H: Statherian population ~1,740 Ma (Juruqui Fm.); I: Calymmian grains at 1,508 Ma, Morro Grande Fm. upper interval; J: Ectasian grains (mostly rims) ~1,250 Ma (Morro Grande Fm. middle interval); K and L: Neoproterozoic grains of the Bocaina Fm - Cryogenian (693 Ma) and Ediacaran (565 Ma) single concordant grains.

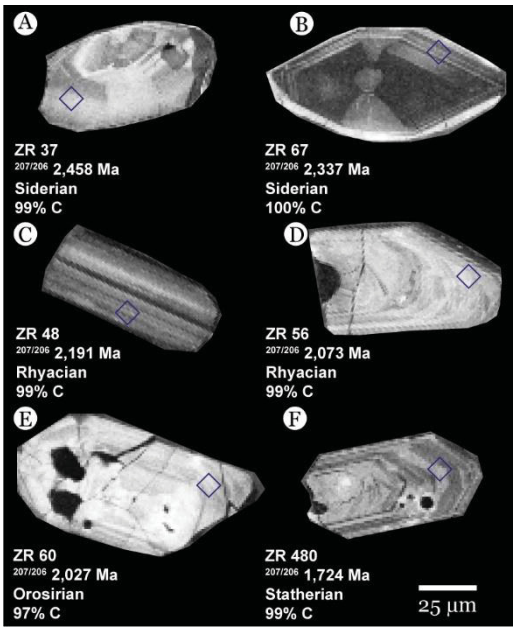


Figure 8. Cathodoluminescence imaging of the main detrital zircon populations of the AL-75 sample (Lajeado Group, Betari Formation). A: oldest population n>3, Siderian; B: Siderian population (~2,330 Ma); C and D: Rhyacian contributions (main populations at 2,185 and ~2,073 Ma, respectively); E: Orosirian contribution (2,000 – 2,030 Ma); F: Statherian grains of ~1,720 Ma.

4.3.4 RESULTS

4.3.4.1 Capiru Group Samples

We present U-Pb detrital zircon data from eight new samples collected from the Capiru Group. A combination of visual analysis of the detrital zircon age data and identification of statistically significant populations using AgePick (Gehrels 2010) was used (Fig. 9). The samples contain a strong unimodal peak at ca. 2,150-2,175 Ma throughout the entire succession. One of the eight samples - the lower interval of the Morro Grande Formation - contains a prominent age peak at ca. 2,080 Ma (Fig. 9a). However, it is noteworthy that this sample also contains abundant ages between the 2,150-2,175 Ma interval. Subtle variations are noticed in the minor populations, with special attention to Juruqui Formation spectra, where the main peak occurs at 2,150 Ma.

For all eight of the Capiru Group samples, the CL images (Fig. 7) show mainly sub-rounded and rounded zircon grains, and subordinate sub-angular grains (Fig. 7d). The grains range from ~50 to 350 µm in length, and are predominant brown in color. Oscillatory zoning is present in most of the grains, but some show sectored

zoning (Fig. 7). In the following sections, individual descriptions of the new U-Pb age data from the Capiru Group are provided in stratigraphic order (Fig. 4) with the aim of describing subtle differences among the detrital age spectra.

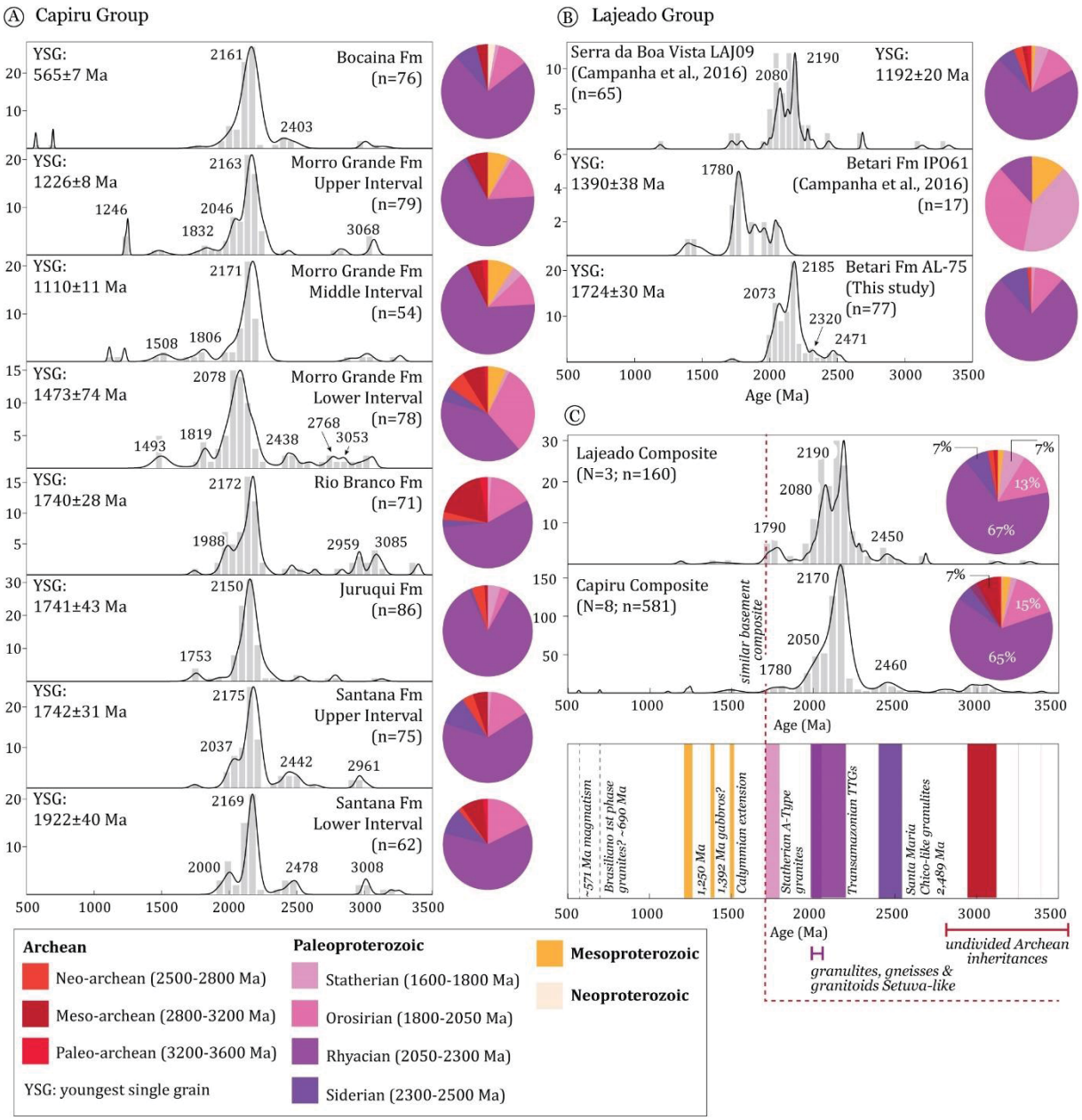


Figure 9. Detrital zircon probability density plots and pie diagrams of A) Capiru Group samples; B) Lajeado Group samples; C) type-signatures of Lajeado and Capiru groups based on detrital zircon analysis and interpretation of the main zircon-forming events from the literature. The ages and references are compiled in Table 2.

Santana Formation

The Santana Formation (Fig. 3) includes quartzite, phyllite, and schist strata overlying the Setuva Domain ortho-derived schists through an angular unconformity, interpreted as the remnants of internal shelf settings (Santos et al. 2021a).

Two samples from the Santana Formation were analyzed; one each from the lower and upper intervals of the formation (Fig. 3 and 4). A sample of meta-arkose was collected from the lower interval (Fig. 5a), from which 62 concordant analyses were obtained (Fig. 9a). The probability density plot for this sample displays a major peak at 2,169 Ma (Rhyacian), and subordinate peaks at 2,000 (Orosirian), 2,478 (Siderian), and 3,008 Ma (Meso-Archean). The two oldest ages are 3,257 ± 25 to 3,193 ± 23 Ma grains (Paleo to Meso-Archean). The youngest single grain of this sample yielded an age of 1,922 ± 40 Ma (Orosirian).

A sample of orthoquartzite (Fig. 5b) from the upper interval of the Santana Formation (Fig. 4) yielded 75 concordant analyses (Fig. 9a). The detrital age spectrum of this sample shows one major peak at 2,175 Ma (Rhyacian), which comprises ~70% of the total ages in this sample. Subordinate peaks at 2,037 (Orosirian), 2,442 (Neoarchean to Siderian), and 2,961 Ma (Meso-Archean) also occur within the age spectrum. The oldest zircon crystals are clustered within a graphical peak at 2,961 Ma. The youngest grain yielded a concordant age of 1,742 ± 31 Ma (Statherian).

Juruqui Formation

The Juruqui Formation (Fig. 4) overlies the Santana Formation and includes quartzites and ferruginous phyllite and in basal contact with the Atuba Complex rocks (Fig. 3). The lower Juruqui Formation interval is mainly constituted of tabular beds of subarkose sandstones (Fig. 5c). Toward the top, the occurrence of dm-scale ferriferous laminated beds interbedded with variable amounts of clastic Fe-coated quartz sand grains becomes common. The Juruqui lower interval is interpreted as the edge of a delta environment (Fiori and Gaspar 1993).

A subarkose sample from the top of the Juruqui Formation yielded 86 concordant analyses. The detrital zircon age spectrum (Fig. 9a) for this sample shows one main peak at 2,150 Ma with a younger shoulder at 2,050 Ma (Rhyacian).

This age spectrum also contains a minor peak of four ages at 1,753 Ma (Statherian). These four ages comprise the youngest graphical peak at 1,753 Ma. The youngest single grains yielded an age of 1,741 ± 43 Ma. A notable difference in this sample is that the Rhyacian peak occurs at 2,150 Ma, which is ~20 Ma younger than most other samples (Fig. 9a).

Rio Branco Formation

The Rio Branco deposits overlie the siliciclastic rocks of the Santana and Juruqui formations and the boundary between the Juruqui and Rio Branco formations is marked by an unconformity. The Rio Branco Formation is predominantly constituted by dolomitic marbles and quartzite lenticular beds (Fig. 5d).

The Rio Branco Formation basal interval represents clastic platform carbonate deposits and the quartz-sandstones were interpreted as sand from a siliciclastic proximal source, incorporated in the carbonate system due to variations in the depositional energy (Santos et al. 2021a).

An orthoquartzite sample collected from the upper parts of the Rio Branco Formation yielded 71 concordant U-Pb ages (Fig. 9a). The probability density plot shows one major peak at 2,172 (Rhyacian), followed by three subordinate age peaks at 1,988 (Orosirian), 2,959 and 3,085 Ma (Meso-Archean), (Fig. 9a). The oldest detrital zircon grains are Paleo-Archean with ages of 3,381 ± 21 Ma and 3,402 ± 17 Ma. The youngest grain yielded an age of 1,740 ± 28 Ma (Statherian). Although Paleoarchean ages are a relatively minor component of this detrital age spectrum (Fig. 8), it contains the highest abundance of those ages among all the samples.

Morro Grande Formation

Most of the Morro Grande Formation lithofacies are mud-rich and typified by heterolith sediments characterized by alternating grain-size changes between claystone or mudstone and fine-grained sandstone (Fig. 6a-c; Santos et al. 2021a). The facies of the basal and middle intervals were interpreted as an estuary or an

embayment shallow setting. The upper interval is representative of a shallow marine setting (Santos et al. 2021a).

The Morro Grande lower interval consists of a succession of (meta-) carbonaceous claystone, heteroliths and arkose sandstones (Fig. 6a). The middle interval is constituted of finely laminated iron-rich mudstones (Fig. 6b), and the fine-grained tabular quartz-sandstone beds constitute the upper Morro Grande interval (Fig. 6c). Three detrital zircon samples were collected from the Morro Grande Formation; one from each interval of the formation.

A quartzite sample (Fig. 6a) collected from the lower interval of the Morro Grande Formation yielded 78 concordant analyses and provided a slightly distinct spectrum (Fig. 9a). The probability density plot displays its major peak at 2,078 Ma (Rhyacian), and additional minor peaks at 1,493 (Calymmian), 1,819 (Orosirian), 2,438 (Siderian), with small contributions of Neo and Meso-Archean (Fig. 9a). The oldest grains are one 3,525 ± 18 Ma grain, and the 3,053 Ma (Meso-Archean) cluster (n=3). The youngest analysis from this sample yielded an age of 1,473 ± 74 Ma (Calymmian).

A phyllite sample (Fig. 6b) collected from the middle interval of the Morro Grande Formation yielded 54 concordant analyses (Fig. 9a). This detrital age spectrum shows one major peak at 2,171 Ma (Rhyacian) and minor age groups of 1,508 Ma (Calymmian) and 1,806 Ma (Orosirian to Statherian). The oldest detrital zircon grain yielded a concordant age of 3,261 ± 27 Ma. The two youngest grains yielded ages of 1,110 ± 11 Ma (Stenian) and 1,223 ± 12 Ma (Ectasian).

An orthoquartzite sample (Fig. 6c) from the Upper Interval of the Morro Grande Formation yielded 79 concordant analyses (Fig. 9a). The probability density plot for this sample shows a main peak at 2,163 Ma (Rhyacian), and a secondary peak at 2,046 Ma (Rhyacian to Orosirian). Additional peaks at 1,246 (Ectasian), 1,832 Ma (Orosirian to Statherian), and 3,068 Ma (Meso-Archean) also occur. The oldest grains are contained in the 3,068 (Meso-Archean) cluster (n=4). Four zircon grains yielded ages between 1,251 ± 8 Ma and 1,226 ± 8 Ma, representing the youngest age fraction of this sample. A noteworthy feature of the detrital zircon age spectra from the Morro Grande Formation is the presence of minor ca. 1,100-1,500 Ma grains which were not documented in any of the underlying formations or the overlying Bocaina Formation.

Bocaina Formation

The Bocaina Formation includes highly foliated quartzite and schist strata in addition to a feldspar-rich interval at the base (Santos et al. 2021a). The lower interval of the Bocaina Formation overlies and is in thrust contact with the crystalline basement gneisses of the Setuva Domain (Fig. 3). The Bocaina Formation is interpreted as representative of an estuarine to shallow marine system (Santos et al. 2021a). The high K-feldspar content and granite pebbles suggest that the sediments were derived from a granitic proximal source.

A feldspathic quartzite sample (Fig. 6d) from the lower unit of the Bocaina Formation yielded 76 concordant U-Pb ages (Fig. 9a). The detrital age spectrum of this sample shows one major peak at 2,161 Ma (Rhyacian) and a minor secondary peak at 2,403 Ma (Siderian). The oldest zircon yielded an age of 3,132 ± 53 Ma (Meso-Archean). The youngest zircon grains yielded $^{206}Pb/^{238}U$ concordant ages of 693 ± 6 Ma (Cryogenian) and 565 ± 7 Ma (Ediacaran). Due to the high disparity between the youngest ages of the Bocaina Formation (Fig. 7K and L, and Fig. 9a) in comparison to the aforementioned units, the Th/U ratios were used to distinguish possibly primary igneous zircon grains (ratios >0.1) from metamorphic ones (ratio between 0.01 and 0.1, Williams and Claesson 1987). Both 565 ± 7 Ma and 693 ± 6 Ma Th/U ratios were >0.1, and these grains were classified either as igneous or high-grade metamorphic (*cf.,* Moller et al. 2003, Köksal et al. 2008).

4.3.4.2 Lajeado Group Samples

We present U-Pb zircon data from two new samples collected from the Lajeado Group; one detrital zircon sample from the Betari Formation (Figures 8 and 9b) and one magmatic zircon sample from the Apiaí Gabbro (Fig. 10, Table 1). We integrate these new data with three existing U-Pb detrital zircon samples from the Lajeado Group (Campanha et al. 2016).

Betari Formation

The Betari Formation is constituted of metasandstones and oligomictic metaconglomerates interpreted as alternating A-B turbiditic beds, grading towards the top into thinner metarythmites interpreted as a series of C-D-E turbiditic layers, suggesting a transgressive sequence (Campanha et al. 2016).

One sample of a feldspathic quartzite (Fig. 6e) from the basal interval of the Betari Formation (AL-75) yielded 75 concordant analyses (Fig. 9b). The probability plot shows four main peaks, a major one at 2,185 Ma (Rhyacian), a subordinate one at 2,073 Ma (Rhyacian to Orosirian), and minor ones at 2,320 Ma and 2,471 Ma (Siderian); (Fig. 9b). The oldest analyses are clustered in the 2,471 (Siderian) contributions, and the youngest concordant single zircon grain shows a 1,724 ± 30 Ma age (Statherian); (Fig. 9b).

The sample IP-61 (Fig. 9b) was collected from a metaconglomerate of the basal Betari Formation (Campanha et al. 2016). Nineteen zircon grains were analyzed by SHRIMP, and the PDP analysis showed a main peak at 1,780 Ma (Calymmian), and a subordinate at 2,045 Ma (Orosirian). Additional peaks at 1,891 and 1,960 Ma complete the sample spectra.

Serra da Boa Vista Formation

The Serra da Boa Vista Formation is constituted of m-thick fine-grained sandstone banks locally interbedded with thin layers of metapelites that were interpreted as distal shelf deposits.

A metasandstone sample (LAJ09, n=65) stratigraphically positioned at the Serra da Boa Vista Formation (Campanha et al. 2016), is characterized by a dominant population of ~2,190 Ma Rhyacian ages, and an important contribution at ~ 2,078 Ma (Rhyacian to Orosirian). Small contributions ~ 2,003 (Orosirian), 2,136 and 2,283 Ma (also Rhyacian) make up lesser proportions (Fig. 9b).

Apiaí Gabbro

The studied sample of the Apiaí Gabbro is composed of augite + hypersthene + labradorite microgabbro facies with minor ilmenite, with equigranular ophitic texture. This sampled unit underlies the Gorutuba Formation (Fig. 4). The zircon crystals (n=17 concordant ages) provided a concordant $^{206}Pb/^{238}U$ age of 889 ± 5.6 Ma (2σ, Tonian); (Fig. 10, Table 1), interpreted as the time of the sill emplacement. Th/U ratios are between 0.33 - 0.62, consistent with the Th/U ratios for gabbroic rocks (Kirkland et al. 2015).

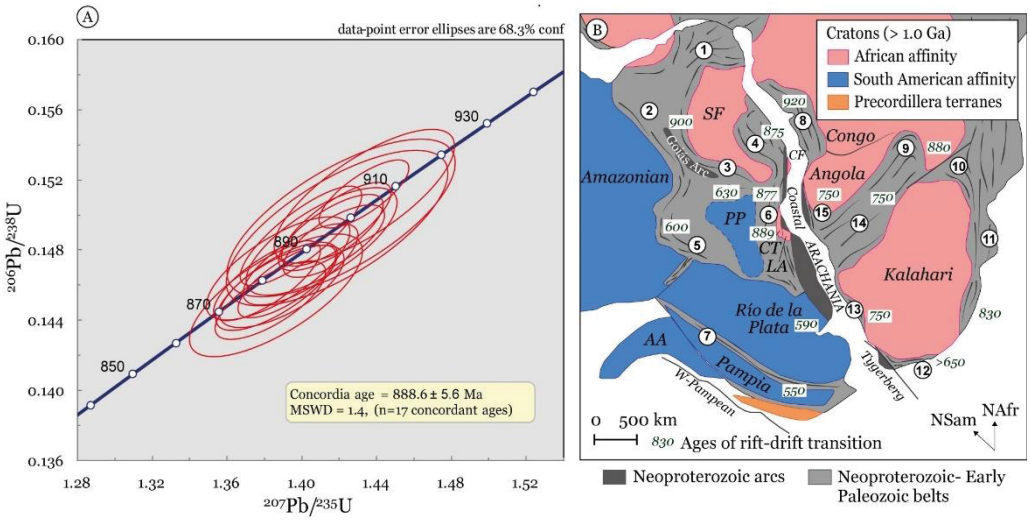


Figure 10. A) Concordia diagram of the Apiaí gabbro (sample AL-79); B) reconstruction of southwestern Gondwana after Gaucher et al. (2009, 2021) displaying the ages of rift-drift transitions in the region, including the gabbros from Itaiacoca and Lajeado groups. Neoproterozoic belts are also indicated: 1: Sergipe, 2: Araguaia, 3: Brasília, 4: Araçuaí, 5: Paraguay, 6: Ribeira, 7: Pampean, 8: W-Congo, 9: Lufilian, 10: Zambezi, 11: Mozambique, 12: Saldania, 13: Gariep, 14: Damara, 15: Kaoko - Paranaguá. SF: São Francisco, AA: Arequipa-Antofalla, PP: Paranapanema, CT: Curitiba, LA: Luís Alves, CB: Cabo Frio.

4.3.5 INTERPRETATIONS

4.3.5.1 Maximum Depositional Ages

The youngest single grain (YSG) and youngest graphical peak (YPP) from all samples are presented in Table 1 (Dickinson and Gehrels 2009). Aside from the samples collected from the Bocaina Formation and the Apiaí Gabbro, we interpret that none of the other samples contain near-depositional age grains. Although most of the detrital samples do not allow for determination of a true depositional age, they

do provide some insight because the Capiru Group samples were systematically collected from each of the five formations containing siliciclastic beds (Fig. 4). In this context, the new MDAs from the Capiru Group strata display a general younging upsection with the exception of the sample from the upper interval of the Morro Grande Formation (Table 1; Fig. 9a). This general younging is consistent with the previously established stratigraphic order and framework (Santos et al. 2021; Fig. 4).

The presence of stromatolitic beds in Morro Azul Formation, iron-rich metasedimentary strata in the Juruqui Formation, and generally elevated iron levels throughout the entire succession (Santos et al. 2021a)—coupled with youngest single grain ages that are younger than ca. 1.8 Ga to the basal Capiru Group Succession — may suggest that most of the Capiru Group strata are Late Mesoproterozoic to Neoproterozoic in age (Cox et al. 2013, 2016).

Based on one concordant age of 565 ± 7 Ma from the Bocaina Formation, we interpret that this age represents the maximum depositional age for the youngest Capiru Group strata. Zircon sources of that age are considered here to be related to the 571 ± 25 Ma volcanism described (Forero-Ortega 2018) in the Itaiacoca ambit.

The maximum depositional ages obtained for the Lajeado Group are 1,390 and 1,192 Ma from the Betari and Serra da Boa Vista formations, respectively (Table 1), younging upsection in accordance with the stratigraphic framework established by Campanha et al. (2016). In addition, the Apiaí gabbro sill in the upper part of the Lajeado Group, with an age of 889 ± 4 Ma gives the minimum age to the Gorutuba Formation (Fig. 4).

4.3.5.2 Provenance Analysis

The potential sources considered for this study are the cratons that represent the basement blocks in eastern South America and Western Africa (Fig. 1) within the context of the Western Gondwana. The origins of the basement blocks in the Ribeira belt currently remain unclear: the Paranapanema block is fully covered by the sediments of the Paraná basin, and therefore, its limits remain object of debate (Brito Neves and Cordani et al. 1984, Cordani et al. 2009, Mantovani and Brito Neves 2005, Julià et al. 2008, and more recently in Affonso et al. 2021). The Curitiba and Luís Alves microplates (Basei et al. 2000, 2008, Passarelli et al. 2018), or even a

single Curitiba – Luís Alves block (Siga Jr. et al. 1995, Santos et al. 2017) make up the picture, and are currently located in a borderline area in which the limits and timing of docking during the Brasiliano may have left fragments that represent the connections with the African side blocks and cratons.

Sources of the detrital zircon for the studied units are mainly Paleoproterozoic with subordinate Mesoproterozoic, minor Archean and very minor Neoproterozoic contributions (Fig. 9c). The analysis from the PDP plots for the Capiru and Lajeado studied samples show similar distribution of the type-signatures between Siderian - Statherian (Fig. 9c), with slightly differences regarding the Mesoproterozoic contributions. Compilation of geochronological data from the basements can be found in Table 2. Based on the identified signatures, the possible source rocks are:

A - The main Rhyacian contribution, identified in all studied samples (2,160 - 2,190 Ma), is recognized in several Paleoproterozoic domains across South American Platform, such as gneisses and granulites of the Atuba Complex (Siga Jr. et al. 1995, Sato et al. 2003, 2009), Santa Catarina Granulitic Complex in Luís Alves microplate (Sato et al. 2008, Basei et al. 2009), portions of the Rio de la Plata craton, represented by tonalite, gneisses and granites of the Tandília belt (Hartmann et al. 2002a, Cingolani 2011), gneisses and granitoids of the Piedra Alta Terrane (Santos et al. 2003, Peel and Preciozzi 2006), and granulites of Nico Pérez Terrane and Taquarembó Block (Santos et al. 2003). All these units are interpreted as products of a major crustal reworking of Archean rocks during the Paleoproterozoic, that affected rocks in Río de La Plata craton, Curitiba and Luís Alves microplates, Nico Pérez terrane and presumably Paranapanema block, during the Transamazonian Cycle (Hartmann et al. 2002b, Santos et al. 2003, 2017). The main source to Capiru Group is most likely the Atuba Complex and we imply a similar basement to the Southern Paranapanema block, due to the similarities between Capiru and Lajeado spectra in terms of Paleoproterozoic contributions (Fig. 9c).

B - We interpreted that the Rhyacian to Orosirian contribution (2,000 - 2,050 Ma) might represent the post-orogenic Transamazonian cycle granitoids. Although the units described under the Transamazonian post-orogenic definition show a distinct peak ~2,050 Ma (Hartmann et al. 2000b, 2008, Cingolani 2011, Santos et al. 2003, 2017), we assume that the basements of Capiru and Lajeado groups were affected by the Transamazonian high-grade metamorphism, and their following

crustal stabilization (Hartmann et al. 2002b, Santos et al. 2003). However, our interpretation does not exclude the possibility of some influence of the Santa María Chico-like metamorphism in Curitiba and Paranapanema basements (Fig. 9c), which describes the presence of granulites and granodioritic gneisses within the 2,080 - 2,000 Ma interval, identified in the age spectra of the Nico Pérez terrane and Taquarembó block (Santos et al. 2003, Hartmann et al. 2008, Gaucher et al. 2008).

Local units that might have sourced the Rhyacian to Orosirian grains are represented in the region by the Setuva basement core in the Curitiba microplate (Fig. 3). In the Capiru Group age spectra, the 2,078 Ma main contribution and the Orosirian - 1,815 - 1,835 Ma range - identified in the Morro Grande Formation (Fig. 9a) are interpreted as reflective of a strong local component given by the Setuva basement-core (Table 2). Based on the presence of ~ 2,073 Ma peaks in the Lajeado Group composite (Fig. 9b), we assume that these ~2,050 Ma Paleoproterozoic granitoids were present in both basements (Fig. 9c).

C- Another ubiquitous signature in the studied samples is the Statherian 1,740 - 1,780 Ma peak (Fig. 9c). This age-interval is considered to be sourced from the deformed alkaline anorogenic (Type-A) granites (Cury et al. 2002), described in basement-cores, especially in the Apiaí terrane ambit (Fig. 2), such as Betara and Tigre (Fig. 3). U-Pb (zircon) dating indicates ages of 1,748 ± 5,4 Ma for the Betara and 1,772 ± 9,5 Ma in the Tigre basement-cores (Cury et al. 2002). These source-candidates of the region were interpreted as result of extensional processes and might represent the break-up ages of the Paleoproterozoic Atlantic Supercontinent (Cury et al. 2002, Siga Jr. et al. 2011b). The Lajeado Group samples show a strong local component from these local Statherian sources (Fig. 9b). Although the Statherian rocks were not recognized in the Curitiba sector, we assumed that these anorogenic granitoids may be one of the basement components due to the presence of sparse ~ 1,740 Ma grains in the Capiru Group spectra (Fig. 9a). From the Statherian period onwards, some differences in terms of provenance are recognized between the spectra of Capiru and Lajeado groups.

D- The Calymmian contribution (1,475 - 1,500 Ma) occurs in Capiru and Lajeado upper units (Fig. 11). However, the Calymmian grains are slightly older in Capiru Group spectrum.

The source candidates previously described for the Lajeado units are the basics rocks identified in the Apiaí terrane domain with dated examples in the

Mesoproterozoic belt (Fig. 3); (Faleiros et al. 2011, Campanha et al. 2015), and Betara Formation (Siga Jr. et al. 2011a).

Another concurrent major Calymmian (~ 1,490 Ma) event is recognized in metagabbros (1,492 ± 4 Ma) and volcanics (~ 1,430 Ma) in the Nico Pérez terrane (Oyhantçabal et al. 2005, Gaucher et al. 2010, Gaucher et al. 2021).

To the African side, in the Angola portion of the Congo Craton (Fig.11), Calymmian ages ~1,505 from dolerite sills and gabbro-noritic dykes are proposed to be part of a Mesoproterozoic magmatic event identify in the Precambrian supercontinent Nuna (Ernst et al. 2013). It is important to mention that the identification of three Mesoproterozoic magmatic events (ca. 1,505 - Calymmian; 1,380 - Ectasian; and 1,110 Ma - Stenian) represent a magmatic 'barcode' for this portion of SW-Congo Craton (Ernst et al. 2013).

The granulite facies Epembe unit (south of the anorthosite Kunene Intrusive Complex) in NW Namibia shows Mesoproterozoic ages between 1,520 and 1,510 Ma for prograde zircon growth (Seth et al. 2003).

No dated rocks of Calymmian age were described in the Curitiba microplate, although we can infer their presence from the scarce contribution identified in the Morro Grande Formation spectrum.

E- The Ectasian sources (1,110 - 1,240 Ma) have no previously known candidates either in Curitiba or in Apiaí sectors. Among all the age intervals, these Ectasian sparse grains are the most enigmatic ones. The Morro Grande Formation shows a distinct peak at ~1,246 Ma, reflecting zircon grains derived from a Ectasian source (Fig. 9 and 11). The Lajeado samples, however, contain grains ~1,190 Ma.

This age-range was previously interpreted as related to the Sunsás Orogeny (Southern Amazonian craton), correlative with the Grenvillian Orogeny (Santos et al. 2003, 2008, Teixeira et al. 2010, Campanha et al. 2015, 2016), however this Mesoproterozoic belt represents a collisional-type orogen located to the West of the studied blocks, and might not represent a potential source for the Capiru Group. This particular grain (~1,190 Ma) in Lajeado Group was previously interpreted as a product of Sunsás-like process (Campanha et al. 2015, 2016).

Gaucher et al. (2004, 2010) proposed that the Amazonian and Río de la Plata cratons were docked as a single landmass in the late Neoproterozoic. Therefore, an extension of the Sunsás belt to the southern blocks is a possibility within the ambit of Paranapanema block.

Considering the Curitiba microplate context, the potential source units representing this age-interval occur within the Angola craton and are: i) intrusions of pyroxenite, gabbro and syenite emplaced into the Epupa Complex and the Kunene Intrusive Complex, preferably along fault zones (Menge 1998, Drüppel et al. 2007). Two intrusions of nepheline–syenite in NW Namibia were dated at 1216 ± 2.4 Ma and 1213 ± 2.5 Ma (U–Pb zircon ages, Littmann et al. 2000) reflecting pre-Pan-African magmatic activity in that region (Seth et al. 2003); an ii) 1,110 ± 2,5 Ma age obtained for a prominent NNW–NNE trending gabbro-noritic dyke swarm in southeastern Angola (Ernst et al. 2013), and, lastly, iii) Namaqua-like metamorphic grains, derived from leucogranites formed during melting from metasedimentary sources in Kaapvaal craton (South Africa). Bial et al. (2015) dated zircon grains between 1,220–1,180 Ma, followed by a second heat pulse at ~1100 Ma. Besides the large geographic distance, the zircon typology and the 1,220 – 1,100 associated ages fit well with those found in Morro Grande formation spectra, and must be considered as a potential type of source for the unit.

4.3.5.3 Summary of Provenance Analysis

We interpret that both Capiru and Lajeado groups share provenance signatures reflective of similar mainly Paleoproterozoic local basements, represented by the association Rhyacian - Rhyacian to Orosirian – Statherian rocks (Fig. 11).

The most conspicuous ages of detrital zircons in the metasedimentary units of the Southern Ribeira belt are Paleoproterozoic, mainly between 2,200 and 2,000 Ma, which match the widespread Transamazonian orogeny (Hartmann et al. 2002b; Santos et al. 2003, Gaucher et al. 2009). Transamazonian ages occur in all analyzed samples comprising their dominant population. Also, the occurrence of the ~ 1,780 Ma contribution attests that these basements share a long and linked evolution through time.

The Lajeado samples show main source areas with ages of ca. 2,190; 2,080; 1,790 and 2,456 Ma, relatively older regarding the Rhyacian - Rhyacian to Orosirian – Statherian peaks, however, similar to the mainly unimodal distribution of ca. 2,170 Ma, in addition to the subordinate ~ 2,050; 1,780; and 2,464 Ma obtained from Capiru Group, with the exception of relatively more Archean contributions (Fig. 11).

An arkose quartzite belonging to the Itaiacoca unit sample (32928; UTM 619250 W/ 7241755 S) was described in Basei et al. (2008). In this sample, two Archean grains were dated at 3,2 and 3,5 Ga, whereas the remaining grains yielded Paleoproterozoic ages between 1,9–2,2 Ga, also reflecting a similar age-spectra consistent with the South American basement signature.

A comparison of the detrital zircon ages with basement data from the literature (Table 2) reveals that the sedimentary protoliths of the Capiru and Lajeado rocks are most likely situated in different domains/fragments derived from a similar Paleoproterozoic basement (Fig. 11).

However, it is also important to note that the contributions of ~1,820 Ma for the Morro Grande Formation, together with the peaks of 1,510; 1,250; and 1,110 Ma represent a distinct age-composite for the upper parts of the Capiru Group. The Juruqui Formation spectrum also shows slightly differences - due to the main peak of 2,150 Ma, and Bocaina - due to the Neoproterozoic contributions (Fig. 9).

The Paranapanema block eastern border was the Lajeado margin area, and might have caught Mesoproterozoic Sunsás-derived zircon grains coming from the Western edge of Paranapanema block (Fig. 12), whereas the Capiru Group was sourced from a different basement composite, represented by the Curitiba microplate, catching scattered sources typically found in Angola craton domain (Fig. 12).

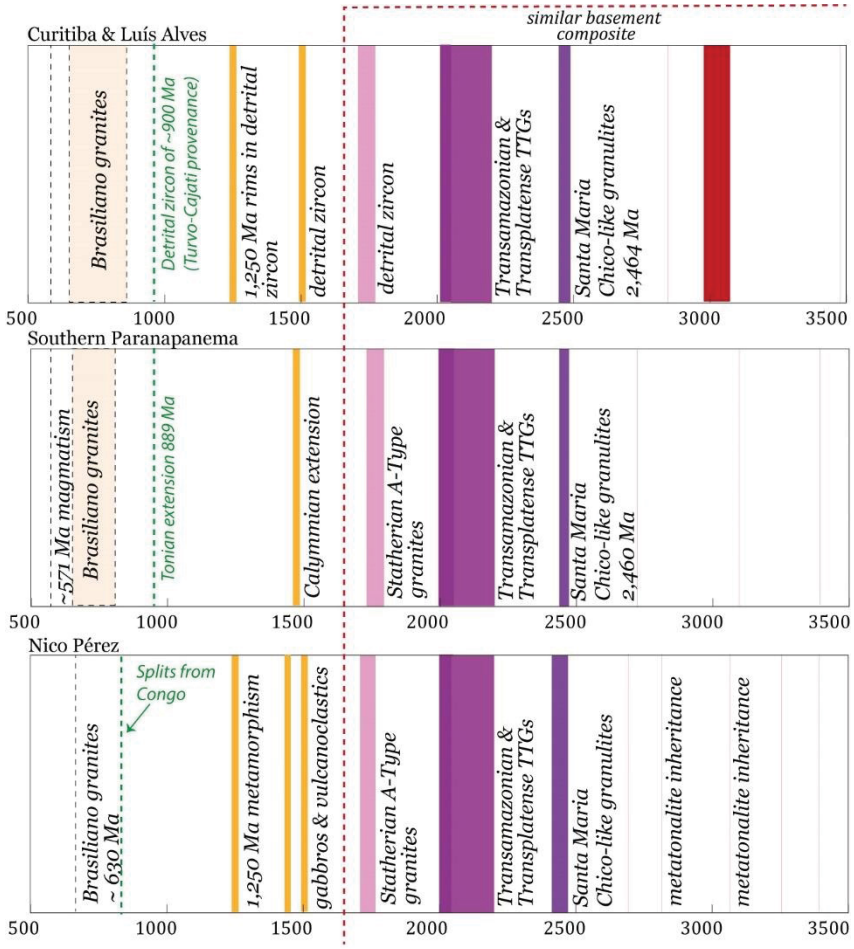


Figure 11. Distribution of ages in Curitiba microplate and Paranapanema block based on detrital zircon ages found in the provenance spectra of Capiru and Lajeado groups, and described in the literature. The Curitiba microplate and Southern Paranapanema block signatures are compared to the Nico Pérez age-spectra due to the similar age-distribution. The interpretation of events forming zircon grains are given in the plot. Ages and interpretations for the forming-events of zircon grains are from: Curitiba and Luís Alves: Hartmann et al. (1979), Basei (1985), Siga Jr. et al. (1995), Hartmann et al. (1999), Harara (2001), Siga Jr. et al. (2002), Sato et al. (2003), Siga Jr et al. (2009); Paranapanema: Cury et al. (2002), Siga Jr. et al. (2011a, 2011b), Faleiros et al. (2011), Campanha et al. (2015, 2016); Río de la Plata and Nico Pérez: Hartmann et al. (2001), Cingolani et al. (2002), Santos et al. (2003), Mallmann et al. (2007), Hartmann et al. (2008), Oyhantçabal et al. (2005, 2009, 2010, 2018, 2021),Gaucher et al. (2010), Oriolo et al. (2016, 2017), Santos et al. (2017), Gaucher et al. (2021).

4.3.6 DISCUSSION

4.3.6.1 The Capiru margin evolution through the provenance data

The Capiru Group successions recorded passive margin to synorogenic phases on the Curitiba microplate with sediment dispersion along a W-E trending

margin (Santos et al. 2021). There are no age-constraints indicative of the sedimentation start, however, some slight differences in the provenance coupled with the stratigraphic model suggest three different stages of evolution (Fig. 12).

The first stage, or Santana – Rio Branco time (Fig. 12a), represents the passive continental margin stage, reflecting the local Paleoproterozoic Atuba-Setuva basement sources.

The Juruqui Formation spectrum might be representative of a different basement domain, essentially composed by the Atuba Complex (strong unimodal distribution at 2,150 Ma). This might represent either a distinct sediment route or paleogeographic position for the delta-derived sediments of Juruqui Formation. In this sense, the stratigraphic position of the Juruqui Formation needs additional studies to define its stage during the Capiru margin evolution (Fig. 12a).

The second stage, or Morro Azul - Morro Grande time (Fig. 12b), also shows provenance contributions bracketed between 1,500 – 1,110 Ma in addition to the main Paleoproterozoic composite, denoting a different source-composite with Mesoproterozoic scattered contributions. The Morro Azul – Morro Grande stage is separated from the other successions of the Capiru Group through the pre-Morro Azul surface (Fig. 4), classified as a major disconformity that probably represents an important gap in the stratigraphic record. This interval is interpreted as a marker for the beginning of the interaction between the Curitiba microplate and the Paranapanema block, where the stratigraphic records on both sides can be compared in terms of major sequences and their boundaries (Fig. 4).

Lastly, the pre-Bocaina unconformity and the renewed tectonics led to the sedimentation of the arkose deposits of Bocaina Formation, denoting the syn-orogenic deposits overlying all the previously deposited successions (Fig. 12c).

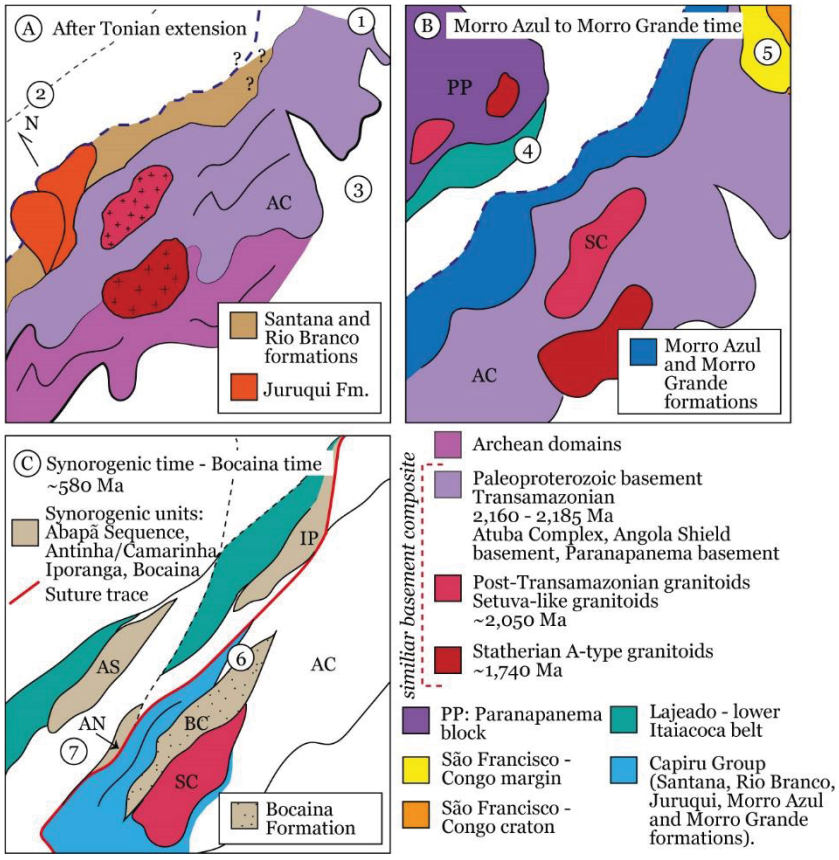


Figure 12. Capiru margin evolution model through the provenance interpretation. A) Stage 1: the passive continental margin stage includes the spectra of Santana and Rio Branco formations. This stage may or may not contain the spectrum of the Juruqui Fm. The hypothesis of a different basement domain/ paleogeography for the deltaic deposits of the Juruqui Fm is brought to explain the 2,150 Ma unimodal distribution, which is slightly shifted from the main 2,170 Ma peak in the other successions (See Fig. 9 for PDPs). B) Stage 2: end of the passive continental margin stage (Morro Azul Fm. carbonate pulse) and probable inversion (Morro Grande time) on the Northern margin of Curitiba microplate. This stage is interpreted as correlative to the Turvo-Cajati-time; C) collision stage and interaction between Paranapanema and Curitiba masses. 1: Transition zone between Angola and Congo masses; 2: oceanic domain; 3: Angolan Shield; 4: Lajeado – lower Itaiacoca belt; 5: São Francisco – Congo craton; 6: Turvo-Cajati Complex and Capiru Group contact zone through thrusts. HT-HP paragenesis are described in this region (Faleiros et al. 2011); 7: Mesoproterozoic belts and Cunhaporanga – Três Córregos granites. AC: Atuba Complex, SC: Setuva Complex, AS: Abapã Sequence, IP: Iporanga Formation, AN: Antinha-Camarinha basins, BC: Bocaina Formation. All the units used on the model are summarized in Table 3.

4.3.6.2 Regional tectonic model and timing of the continental margins

A Neoproterozoic NW-subduction model between the Curitiba microplate (lower plate) and the Apiaí terrane (Paranapanema upper plate) during Neoproterozoic has been suggested (Basei et al. 1992, 2008), resulting in a suture zone in the vicinity of the Lancinha Shear Zone (Fig. 3). This suture zone was later affected by shear progression resulting in the dextral shear zone contact between the

Curitiba microplate and the Paranapanema block (Fiori 1992, Castro and Ferreira 2015, Faleiros et al. 2016, Passarelli et al. 2018). The data presented herein document a long, protracted extensional history prior to this Neoproterozoic suture, with a time- range similar to those that have been documented on other continents during this particular period (*cf.*, Yonkee et al. 2014). The Capiru, Lajeado and Itaiacoca groups record evidence of opening to closure of basins, and are interpreted to be related through time following the model below:

Stage 1 — Stenian – Tonian (1,030 - 890 Ma) extension – one or two extension pulses?

There is a general consensus that a supercontinent formed between ~1,200–1,000 Ma, although its exact configuration remains speculative (Paleopangea: Piper 2000, Rodinia: McMenamin and McMenamin 1990, Hoffman 1999, Li et al. 2008). Subsequently, this supercontinent broke-up into several fragments creating a series of basins during the Neoproterozoic time (ca. 850–550 Ma, Li et al. 2008).

The sequence of opening and closure of oceanic basins prior to Pan-African/Brasiliano orogeny is unlikely to be coeval in the different sectors of Rodinia (Gaucher et al. 2009). Gaucher et al. (2009) proposed that oceanic basins opened and closed sequentially from east to west in southwestern Gondwana, and that the paleogeographic evolution from Rodinia to Gondwana could be described in terms of stepwise rifting of Rodinia and concomitant sequential closure of the previously formed basins.

This evolution, however, is notably related to the peripheral or metacratonic areas between large cratonic blocks (such as São Francisco-Congo or Río de la Plata and Kalahari), in which the Paranapanema and Curitiba blocks remain as fragments of “uncertain affinity” regarding the larger masses (São Francisco-Congo, Rio de la Plata - Kalahari) in different time-periods.

On the Apiaí terrane side (Fig. 1), the Lajeado Group successions recorded open-ocean stages deposited on the eastern margin of the Paranapanema block (Campanha 1991, Campanha et al. 2016). We interpreted rift-related deposition to the conglomerate and arkose sandstones of the Betari Formation (Fig. 4) that record the initial continental extension phase, deposited after 1,390 Ma. The evolving

lithospheric stretching led to the sea development and created accommodation space for the thick basin-to-slope deposits of the Água Suja Formation, which displays limestone banks with hummocky cross-stratification and slump breccias, reflective of a distal shelf often affected by storms (Campanha et al. 2016). The Serra da Boa Vista Formation overlies the carbonate shelf deposits of the basal Lajeado sequence, with an MDA of 1,192 Ma.

The same time span (1,192 Ma to 890 Ma) also encompasses the deposition of the lower Itaiacoca Group successions, corroborating that the extensional processes took place at the E-SE margin of Paranapanema block around that time. Although we have no U-Pb detrital zircon ages from the Itaiacoca Group to estimate MDAs, we consider that the carbonate platform sequence overlying the metabasic rocks has a minimum deposition age related to the Late Meso- Early Neoproterozoic given by the emplacement of basic rocks (1,030 - 908 Ma, U–Pb, zircon of metabasic rocks, Siga Jr et al. 2009).

Stage 2 — Carbonate platform expansion (pre-890 - 870 Ma?) – Is Rio Branco carbonate platform chrono-correlative to this interval?

During this interval extensive carbonate platforms were developed on the E-SE margin of the Paranapanema block, and possibly on the northern margin of the Curitiba microplate as well, as documented by Lajeado carbonate shelf, Itaiacoca basal shallow metacarbonate sequence (Paranapanema margin), and possibly the Rio Branco Formation (Curitiba microplate margin).

This time interval on Curitiba microplate is interpreted to encompass the transgressive and highstands systems of the Rio Branco Formation, recording a long period of high tectonic stability, followed by the development of an extensive disconformity of unknown duration - the pre-Morro Azul unconformity (Santos et al. 2021a).

Stage 3 — Tonian break-up (890 - 870 Ma)

The primary evidence for the break-up stage is gabbroic rocks that have been emplaced in the basal intervals of the Itaiacoca Group and in Lajeado Group at the hyperextension time. The emplacement of the Apiaí Gabbro and other intrusive rocks have been interpreted as tholeiitic MORB-like magmatism related to the break-up of a Mesoproterozoic continent and the “Ribeira Ocean” onset (Reis Neto 1994, Siga Jr. et al. 2009, Campanha et al. 2016). The Apiaí terrane side was recording E-deepening basinal domains around this time (Campanha et al. 2016), implying a margin onset and successions deposited pre- 875 Ma. The Apiaí Gabbro displays similar age to the other intrusive basic rocks in the region (Fig. 10) and may represent the link between Lajeado and Itaiacoca groups.

These basic rocks (mostly sills) of the lower Itaicoca Group occur in the SE portion of the belt, concordantly interbedded with the metacarbonate sequence (Siga Jr et al. 2009); however, they are relatively older (related to the first extension pulse?). The original mineralogy (plagioclase and pyroxene) also indicates subalkaline tholeiitic compositions, suggesting genesis in an extensional environment (Reis Neto 1994, Siga Jr. et al. 2009). No metabasic rocks of that age were described in the Capiru Group. However, detrital zircon grains ~ 900 Ma were described in Turvo-Cajati Complex provenance spectra (Cury 2009).

Stage 4 – Morro Azul – Morro Grande time on the Curitiba microplate margin

The Capiru Group also includes a younger interval during which a new carbonate deposition pulse was produced (Morro Azul Formation, Santos et al. 2021a). After this quiescent interval, renewed tectonics and source rejuvenation led to the deposition of the Morro Grande Formation. This tectonic instability was responsible for the high erosion rates of Setuva core granitoids providing the main 2,040 Ma, also allowing the dispersion of the “exotic” populations spanning from 1,500 – 1,110 Ma into the lower Morro Grande signature (Fig. 9). In addition to that, soft sediment deformation structures were produced in the Capiru rock record during the unstable Morro Grande time (Leandro 2016). No tectonic event is elected to have triggered this new sediment pulse. However, interpretations for the erosion of new basement domains include the hypothesis of the subduction start and its crustal

responses on the lower plate, and the drastic climatic changes during the Neoproterozoic context.

Stage 5 - Contraction and syn-orogenic records (630 - 540 Ma) – Interaction between Paranapanema block and Curitiba microplate during Neoproterozoic

This stage is recorded in Capiru, Lajeado, and Itaiacoca units, however showing distinct evolutions within this contraction context:

A- In the Itaiacoca Group, the period between 645–628 Ma records volcanic activity interpreted as related to the Três Córregos and Cunhaporanga magmatic arcs, meaning tectonic inversion in which the lower Itaiacoca sequence became the substrate for the flysch deposits of the overlying Abapã Sequence (Siga Jr. et al. 2009). Deposition of the Abapã Sequence along the southern border of the Paranapanema block denotes an active margin and convergence between Paranapanema block and Curitiba microplate, where the arc complexes emplacement gives the upper plate polarity for the Paranapanema block (Reis Neto 1994, Siga Jr. et al 2009).

B- After the Morro Grande time on the Curitiba microplate, the pre-Bocaina unconformity followed by the deposition of the Bocaina Formation is recorded in the Capiru Group. The Bocaina Formation is interpreted as product of a syn-collisional phase on the Curitiba microplate (Santos et al. 2021a). The MDA of Bocaina Formation is marked at 565 ± 7 Ma, consistent with the last magmatism pulses that occurred at the Itaiacoca upper interval (~ 571 Ma, Forero-Ortega 2018).

C- Lastly, overlying the Lajeado Groups rocks, a late collisional unit is recorded, termed as Iporanga Formation. The Iporanga maximum depositional age is determined at 580 Ma, given by a felsic volcanic unit immediately underneath the Iporanga Formation (Campanha et al. 2008), also the potential glacial origin for the Iporanga Formation would place it in the late Ediacaran, probably equivalent to the Gaskiers glaciation ~ 580 Ma (Campanha et al. 2008).

4.3.6.3 Basement links among the Rodinian fragments of the Southern Ribeira Belt

The Paleoproterozoic Transamazonian (2,190 - 2,000 Ma) zircon grains were identified in all the analyzed samples (Figs. 9). Both Paranapanema block and Curitiba microplate show a similar Paleoproterozoic evolution attested by their basement composites (See Section 5.2).

Comparisons of the Capiru Group provenance with other blocks of the region have found geochronological similarities with the Nico Pérez terrane ages (Fig. 9, Table 2). Although detrital zircon contributions of the Capiru Group (and Turvo-Cajati Complex) - mainly between 2.0 and 2.2 Ga - are commonly found in local sources (such as the Atuba Complex, Setuva Domain, and other basement cores of the region), some ages found in Morro Grande Formation show exotic patterns, common in the pre-Gondwana African side (Angola craton), ranging between 1,508 – 1,110 Ma.

Through the provenance and geochronological evolution of the Capiru Group, we suggest that connections between Curitiba-Nico Pérez with the Western Angola likely occurred during Mesoproterozoic times, and the Stenian - to - Tonian extension might be responsible for the post-Rodinia configuration of the continental margins of the region.

Similar stratigraphic features between Apiaí and Nico Pérez terrenes, such as the ca. 1,750 Ma anorogenic granites (Mallmann et al. 2007, Sánchez-Bettucci et al. 2004), Calymmian units (Parque UTE and Mina Verdún; 1,480 - 1,430 Ga; Poiré et al. 2005, Chiglino et al. 2010, Gaucher et al. 2011, Poiré 2004) to Ectasian volcano-sedimentary successions (Tapes Complex; MDA of 1360 ± 12 Ma) were also addressed by Gaucher et al. (2021); (Table 2). Other similarities encompass the post-Brasiliano units, such as glacial rocks of Gaskiers age (Las Ventanas Formation; Gaucher et al. 2008), in addition to Ediacaran granitic magmatism (Gaucher et al. 2021).

Based on these stratigraphic and tectonic similarities, from Paleo- to Neoproterozoic, Gaucher et al. (2021) argue in favor of a Nico Pérez derivation for the Apiaí terrane (Paranapanema + covers) as well, suggesting the hypothesis of a NW displacement through the Ibaré Shear Zone ~ 720 Ma (age of São Gabriel orogeny, Philipp et al. 2018). Through the provenance of the Lajeado Group, we can only imply that the Southern portion of the Paranapanema block share a few similarities with the Curitiba - Nico Pérez -Angola in terms of Paleoproterozoic basement. Nevertheless, derivation from Nico Pérez terrane remains as a possibility.

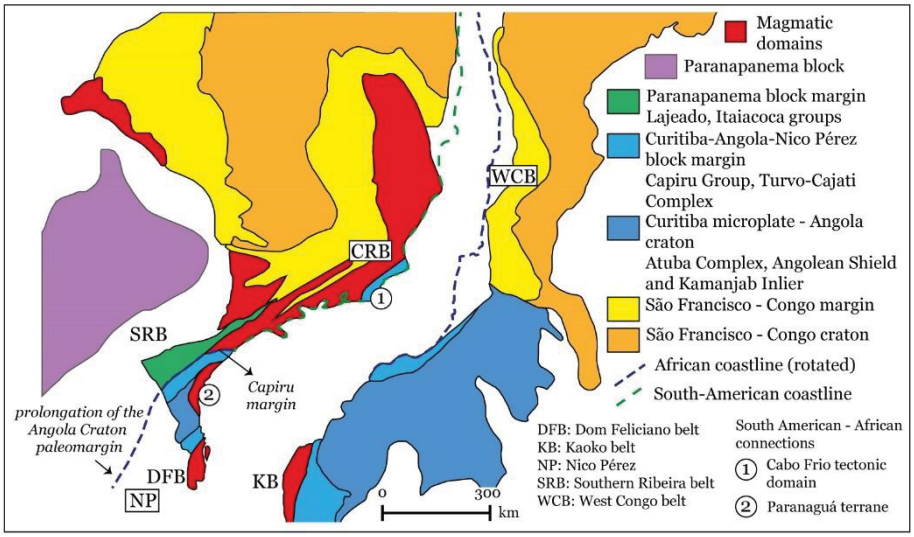


Figure 13. Suggested location of the Capiru margin as a prolongation of the Curitiba microplate – Nico Pérez – Angola craton margin. The reconstruction of South-American and African margins is according to Schmitt et al. (2018), and after Vieira et al. (2022). A prevailing local source composite is inferred both to Paranapanema block and Curitiba microplate, based on the provenance of Lajeado and Capiru groups. Curitiba microplate and Angola craton connections are inferred during Mesoproterozoic, based on provenance of the Morro Grande Formation to explain the "exotic" contributions spanning from 1,508 to 1,110 Ma.

Table 2. Selection of published ages of the basement blocks of the region, including data from Curitiba microplate, Apiaí terrane (Paranapanema block and supracrustal covers), Río de la Plata craton, and the Calymmian to Stenian ages of the African counterparts. The main ages are presented from the perspective of the related geological event. Based on a simplistic analyze of ages, note the similarities among the continental fragments of the region.

Event	Obs	Age (Ma)	Period	References
Curitiba Terrane				
Mantle/ crust differentiation	Addition of mantle-derived material to the crust ($Sm–Nd_{TDM}$)	2,900 – 2,600	Meso to Neoarchean	Sato et al. (2003), Kaulfuss (2001), Siga Jr et al. (1995, 2007), Passarelli et al. (2001, 2011).
Inheritances in granitoids – Setuva Complex	U-Pb (TIMS) e Pb-Pb (EV-TIMS) in granitoids of Setuva Domain	2,464		
Metamorphic event – granulite to amphibolites facies	Atuba Complex gneiss-migmatites - U–Pb zircon and Rb–Sr (WR)	2,200-2,000	Rhyacian	
Inheritances in granitoids – Setuva Complex	U-Pb (TIMS) e Pb-Pb (EV-TIMS) in granitoids of Setuva Domain	~2,150	Rhyacian	Kaulfuss (2001), Siga Jr. et al. (2007).
Granitoids – Setuva Complex	U-Pb (TIMS), deformed granitoids – post-Transamazonian age	2,080 – 2,050	Rhyacian	
Extensional event?	Setuva Complex mafic dykes?	~1,750	Statherian	
Extensional event	Gabbroic dykes of the Registro	1,430	Calymmian	Passarelli et al. (2001,

Event	Obs	Age (Ma)	Period	References
	Complex (Atuba Complex correlate; Passarelli et al., 2004; 2007); U-Pb zircon SHRIMP			2011)
Apiaí Terrane				
Igneous crystallization	Granitic-gneissic cores (Apiaí, Betara and Tigre), U-Pb zircon TIMS	~2,200; ~2,800 (inheritance)	Rhyacian	Summarized in Siga Jr et al. (2011) and references therein
Extensional event	Syenogranites and metabasic rocks within the cores (Apiaí, Betara and Tigre), U-Pb zircon TIMS	1,790 – 1,750	Statherian	
Extensional event	Metavulcanossedimentaty sequences (Água Clara, Votuverava, Perau and Betara), U-Pb zircon (TIMS, SHRIMP)	1,600 – 1,450	Calymmian	
Back-arc basic magmatism	Votuverava Group, U-Pb zircon SHRIMP	1,490	Calymmian	Faleiros et al. (2011), Campanha et al (2015)
Grenvillian-age tectono-metamorphic event?	Votuverava Group, Rb-Sr ages	1,212 – 1,283	Stenian	Batolla et al. (1981), Daitx, (1996), Oliveira et al. (2002), Campanha et al. (2015)
Inheritance in granites – collisional orogeny – Rodinia assembly?	Embu Terrane – U-Pb in zircon LA-ICP-MS	1,100	Stenian	Alves et al. (2013)
Luís Alves Terrane – Granulite Complex				
Mantle/ Crust differentiation	Addition of mantle-derived material to the crust ($Sm–Nd_{TDM}$)	2,800 – 2,700 3,400? (inheritance)	Neoarchean	Hartmann et al. (1979), (2000a, b), Sato et al. (2008), Basei (1985), Basei et al. (1998b, 1999, 2000, 2009), Siga Jr. et al. (1995), Harara (2001)
Magmatism	TTG igneous activity U–Pb zircon SHRIMP, Rb–Sr WR isochrons	2,700	Neoarchean	
Metamorphic event - granulite-facies	Felsic granulite-U-Pb zircon SHRIMP-middle crust	2,680	Neoarchean	
Magmatism	Intrusion of igneous rocks, Rb–Sr WR isochrons	2,600	Neoarchean	
Amphibolite-facies event?	Felsic granulite-U-Pb zircon SHRIMP	2,480	Siderian	
Mantle/crust differentiation	Addition of mantle-derived material to the crust ($Sm–Nd_{TDM}$)	2,480-2,300	Siderian	

Event	Obs	Age (Ma)	Period	References
Granulite-facies regional metamorphism	Development of orthopyroxene in many rocks (U–Pb, Sm–Nd mineral isochrone)	2,350	Siderian	
Magmatism	Deformed granitoids U–Pb zircon SHRIMP	2,250 – 2,150	Rhyacian	
Granulite-facies event	Felsic granulite-U-Pb zircon SHRIMP-middle crust	2,170	Rhyacian	
Amphibolite-facies regional metamorphism	Pb–Pb, Rb–Sr WR isochrons, U–Pb mineral, Sm–Nd mineral isochrons-middle crust	2,100 – 2,000	Rhyacian	
Retrograde metamorphism	U–Pb mineral -upper crust	2,000 – 1,900	Orosirian	
Tectonic stabilization	Regional cooling (K–Ar)	1,800 – 1,700	Statherian	
Pre-Gondwana African counterpart (Mesoproterozoic ages)				
Mafic magmatism - LIP Event	Gabroic dykes, U-Pb zircon TIMS	~1,505	Calymmian	Ernst et al. (2013)
Metamorphism - granulite	Epembe granulites	1,520-1,510	Calymmian	Seth et al. (2003, 2005)
Magmatism	Red Granites: Otechinjau, Ompupa, Matala; Rb–Sr ages	1,400-1,350	Ectasian	Carvalho et al. (1987)
Magmatism	Kunene Complex with felsic rocks; U–Pb zircon	1,385-1,374	Ectasian	Mayer et al. (2004) and Drüppel et al. (2007)
Mafic magmatism	LIP Event	1,380	Ectasian	McCourt et al. (2006)
Back-arc magmatism	Namaqua Metamorphic Complex	1,220 and 1,180	Ectasian	Bial et al. (2015)
Mafic magmatism - LIP Event	Gabroic dykes, U-Pb zircon TIMS	1,110	Stenian	Ernst et al. (2013)
Back-arc magmatism	Namaqua Metamorphic Complex – 2nd heat pulse	1,100	Stenian	Bial et al. (2015)
Río de La Plata craton				
Basement inheritances	La China Complex	3,101 2,721	Meso- to Neoarchean	Hartmann et al. (2001)
Granulites	Santa María Chico-like metamorphism	2,489 2,366	Siderian	Hartmann et al. (2008)
Granulite inheritance	Tandília Belt, Nico Pérez terrane	2,228 2,224	Rhyacian	Hartmann et al. (2001), Cingolani et al. (2002)

Event	Obs	Age (Ma)	Period	References
Metamorphic event – granulite to amphibolites facies	Westernmost Domain, Tandília Belt, Piedra Alta and Nico Pérez terranes and Taquarembó block – Transamazonian/ Transplatense orogenies	2,189 – 2,113	Rhyacian	Cingolani et al. (2002), Rapela et al. (2007), Santos et al. (2003)
Post-Transamazonian/ Transplatense granitoids	Westernmost Domain, Tandília Belt, Piedra Alta and Nico Pérez terranes and Taquarembó block	2,088-2,051	Rhyacian	Cingolani et al. (2002), Rapela et al. (2007), Santos et al. (2003), Peel and Preciozzi (2006)
Taphrogenic mafic dike swarm	Nico Pérez terrane	1,754- 1,735	Statherian	Mallmann et al. (2007), Sánchez Bettuti et al. (2004)
Metagabbros and volcaniclastic rocks	Nico Pérez terrane	1,492 – 1,429	Calymmian	Oyhantçabal et al. (2005), Gaucher et al. (2010, 2021)
Metamorphic event	K-Ar age of the Zapicán thrust	1,253 ± 32 Ma	Ectasian	Bossi and Cingolani (2009)

Table 3. Summary of the units used on the model. [1]: age of the Bocaina Formation MDA; [2]: Piedra Amarilla surface; [3]: Age of the Bairro dos Campos tuff-bed (upper Itaiacoca).

	Unit	***Age***	***Tectonic setting***	***Reference***
	Curitiba – Nico Pérez – Angola margin			
Post-collisional	*Neoproterozoic to Cambrian (younger than 565[1] Ma)*			
	Camarinha Formation	~580 Ma (Gaskiers age)	Post-collisional basin	Moro and Brito Neves (2009)
	Neoproterozoic units (older than 565[1] Ma)			
	Bocaina Formation	MDA 565 ± 7	Post-collisional basin	Santos et al. (2021a), this work
Active margin	Turvo-Cajati Complex	MDA 650–630 Ma, Metamorphism 590–585 Ma	Wedge and a back-arc basin – trace the suture zone (Fig. 12)	Faleiros et al. (2011, 2016), Ricardo et al. (2020)
	Morro Grande Formation	MDA 1,110 Ma	Transition - synorogenic basin	This work
Passive margin	Morro Azul Formation	Marinoan correlation (~640 Ma) – Piedra Amarilla-age[2]	Passive continental margin	Santos et al. (2021a)
	Neoproterozoic units (older than 640 Ma)			
	Juruqui Formation	MDA 1,740 Ma Relative – Cryogenian (NIFs* presence)	Passive continental margin	Santos et al. (2021a), Fiori and Gaspar (1993)

	Late Meso- to Neoproterozoic units (older than 889 Ma)			
	Rio Branco Formation	MDA 1,740 Ma	Passive continental margin	Santos et al. (2021a)
	Santana Formation	MDA 1,740 Ma	Passive continental margin	Santos et al. (2021a)
basement	*Mesoproterozoic belts (older than 1,400 Ma)*			
	Parque UTE Group metarhyolites and metagabbros	1,429 ± 21 1,492 ± 4	-	U–Pb ID-TIMS zircon (Oyhantçabal et al. 2005)
	Mina Verdún Group metatuffs	1,433 ± 6	-	U–Pb LA-ICP-MS zircon (Gaucher et al. 2011)
	Paranapanema margin			
	Neoproterozoic units (younger than 613 Ma[3])			
Post-collisional	Volcanism - Fazenda Velha metabasic suite	571 ± 25 Ma	Back-arc magmatism	U–Pb SHRIMP zircon (Forero-Ortega 2018)
	Iporanga Formation	~580 Ma (Gaskiers age)	Wildflysch deposits	Campanha et al. (2008)
Active margin	Apabã Sequence - metavolcanic rocks	645–628 Ma	Flysch-type deposits	U–Pb LA-ICP-MS zircon (Siga Jr. et al. 2009)
	Neoproterozoic units (older than 613 Ma)			
Passive margin	Bairro dos Campos Formation	613 ± 9.6 Ma	Passive continental margin	U-Pb LA-ICP-MS zircon (Forero-Ortega 2018)
	Água Nova Formation	Relative – Cryogenian?	Passive continental margin	-
	Gorotuba Formation	MDA: 875 Ma	Passive continental margin	U–Pb SHRIMP zircon of Apiaí gabbro (Campanha et al. 2016)
	Late Meso- to Neoproterozoic units (older than 875 Ma)			
	Passa Vinte Formation Serra da Boa Vista Formation Mina de Furnas Formation Água Suja Formation Bairro da Serra Formation Betari Formation		Passive continental margin	Campanha et al. (2016)
	Lower Itaiacoca Sequence	1,030–908 Ma	Passive continental margin	Siga Jr et al. (2009)
	Mesoproterozoic belts (older than 1,490 Ma)			
basement	Água Clara Formation	1,590 – 1,470 Ma	Extensional or back-arc basin	U-Pb LA-ICP-MS zircon (Weber et al. 2004)
	Perau Formation	~ 1,470 Ma	Deep-water volcan-sedimentary sequence	Daitx (1996), U-Pb LA-ICP-MS zircon (Siga Jr. et al. 2011a)
	Votuverava Group	~1,490 Ma	Back-arc basin/ magmatism	U–Pb SHRIMP zircon Campanha et al. (2015)
	Basements			
	Statherian granites (*e.g.,* Campanero unit, Illescas rapakivi granite, Tigre, Apiaí, Betara granitoids).	1,754 ± 7 1,760 ± 32 ~1,740 (Tigre, Apiaí, Betara).	A-Type granites - extension	U–Pb SHRIMP zircon (Mallmann et al. 2007), Rb-Sr WR (Bossi et al. 1993), U-Pb LA-ICP-MS (Cury et al. 2002)
	Rhyacian to Orosirian domains (*e.g.,* Setuva Complex and Valentines–Rivera Granulitic complex).	2,058 ± 3 (metamorphic)	-	U–Pb SHRIMP zircon (Santos et al. 2003)
	Rhyacian domains (*e.g.,* Atuba Complex and Valentines–Rivera Granulitic complex).	2,163 ± 22 (magmatic)	-	U–Pb SHRIMP zircon (Santos et al. 2003)
	Archean domains (*e.g.,* La China Complex).	3,404 ± 8 (inherited)	-	U–Pb SHRIMP zircon (Hartmann et al. 2001)

*NIFs: Neoproterozoic iron formations

4.3.7 CONCLUSIONS

In this study, we present eight new detrital zircon samples from the Capiru Group, one detrital zircon sample from the Lajeado Group, and one magmatic zircon sample from the Apiaí Gabbro. These new U-Pb zircon data are incorporated with previous data from the literature within the context of an updated regional-scale, five stage tectonic model for the Ribeira belt during Stenian-Ediacaran times. This revised model is based largely on the provenance of the Capiru and Lajeado groups.

The age spectra are consistent with the evolution of a passive continental margin for the Curitiba microplate (at least for Santana - Rio Branco time), possibly chrono-correlative with the Eastern-Southeastern Paranapanema margin, recorded in lower Itaiacoca and Lajeado groups. No relative paleogeographic positions for these blocks could be suggested.

In the Capiru Group ambit, a younger stage including the Morro Azul and Morro Grande formations are representative of a Neoproterozoic basin-stage. Tectonic perturbation occurred during Morro Grande time, in response to the inversion of the Curitiba microplate margin. After inversion, the Cunhaporanga and Três Córregos arcs were emplaced on the Paranapanema side, which denotes the upper plate aspect for the Paranapanema block. To the Curitiba microplate (lower plate) side, Bocaina formation was deposited. The syn- to post-collisional phase is also represented by the Iporanga and Camarinha formations, with MDAs ~ 580 Ma, under the Gaskiers glaciation (579.63 ± 0,15 e 579.88 ± 0.44) effect.

Through the provenance and geochronological evolution of Lajeado, Itaiacoca and Capiru groups, we suggest that these post-Rodinia crustal fragments shared a linked evolution during Paleoproterozoic (with connected basements), reflecting on the main age-contribution for these basins. The Mesoproterozoic connections were interpreted for Curitiba – Angola - Nico Pérez segment, based on the presence of ages within the 1,508 – 1,110 Ma interval in the Capiru Group spectra. Mesoproterozoic evolution was followed by the extensional processes related to the Rodinia fragmentation (Stenian – Tonian in the region), triggering the passive margins onsetting.

The strata of the upper Capiru (Morro Azul – Morro Grande time) and upper Itaiacoca groups (613 Ma, age of Bairro dos Campos Formation and Abapã Sequence - ~640 Ma) imply this Late Meso- to Neoproterozoic cycle of basins converging at ~ 628 Ma (Stage 5). The ages of the Bocaina Formation (MDA of 565 Ma) and the post-Lajeado units (580 Ma, Iporanga Formation) establishes the end of this Neoproterozoic basin-cycle in Ribeira Belt with syn-orogenic units deposited in a fully collisional setting.

ACKNOWLEDGMENTS

This work was funded by the Diagenesis Project (a partnership between SHELL Brazil and Federal University of Paraná), Project The Río de La Plata Craton and the Western Gondwana Assembly (FAPESP - 15/03737-0, 2017), and Project *Integração de dados e reavaliação do potencial mineral do Vale do Ribeira* of the Geological Survey of Brazil (CPRM - São Paulo). We also thank MSc. A. Spisila that helped with fieldwork in the Capiru Group.

DISCLOSURE STATEMENT

The authors declare that they have no known competing financial interests or personal relationships that could have appeared to influence the work reported in this paper.

5 CONSIDERAÇÕES FINAIS

Dados geocronológicos recentes indicam que a Faixa Ribeira Sul contém sequências de margem passiva meso- e neoproterozóicas que foram justapostas apenas durante o Ciclo Brasiliano-Pan Africano (Campanha e Sadowski 1999, Basei et al. 2003, 2008, Campanha et al. 2016, 2019). Nesse contexto, um dos segmentos menos estudados da Faixa Ribeira Sul é o setor da Microplaca Curitiba.

As unidades supracrustais da Microplaca Curitiba (Grupo Capiru e Complexo Turvo Cajati) se sobrepõem diretamente às rochas do embasamento, e estudos recentes têm mostrado diferentes ciclos de bacias para essas unidades (Ricardo et al. 2020, Santos et al. 2021). Em contrapartida, o terreno Apiaí, adjacente a Microplaca Curitiba apresenta coberturas supracrustais mesoproterozóicas espessas de variadas idades, ambientes tectônicos, além de unidades depositadas em bacias neoproterozóicas.

O Grupo Capiru consiste em sucessões de rochas metassedimentares depositadas em distintos estágios evolutivos de uma bacia que se desenvolveu na margem norte da Microplaca Curitiba. Os estratos do Grupo Capiru fornecem um importante registro de sedimentação que pode representar um *link* entre as bacias do final do Mesoproterozóico e do Neoproterozóico na microplaca Curitiba.

A fim de compreender a geometria e evolução da “bacia” Capiru e suas relações com os blocos cratônicos adjacentes, investigamos, primeiramente, os padrões estruturais e a estratigrafia regional (Seção 4.1).

Apresentamos também uma nova edição do Mapa Geológico do Grupo Capiru (Seção 4.2). Esta contribuição é o mapa regional mais atualizado, que também integra os dados publicados disponíveis. O mapa inclui todas as informações geológicas levantadas pelo projeto de mapeamento do Grupo Capiru, além dos mapas de Fiori (1985) e mapas anteriores das bases de dados dos serviços geológicos estadual e federal (MINEROPAR e CPRM).

Seis formações foram definidas - e os principais tipos de contatos estruturas reavaliados. As seis formações para o agora Grupo Capiru são, portanto: Formações Santana, Juruqui, Rio Branco, Morro Azul, Morro Grande e Bocaina. Para cada formação, realizamos análises geoquímicas de rocha total para complementar nossas interpretações sedimentológicas, além de análises de proveniência por geocronologia U-Pb de zircão detrítico.

No geral, a composição química e mineralógica das rochas do Grupo Capiru sugere que este tenha se depositado em um ambiente tropical, que recebeu sedimentos de fontes continentais ricas em ferro e alumínio, altamente intemperizadas.

Os dados de U-Pb de zircão detrítico de oito amostras coletadas no Grupo Capiru apresentam um forte pico unimodal no intervalo de 2.150-2.175 Ma ao longo de todas as sucessões. Uma das oito amostras - do intervalo inferior da Formação Morro Grande – também contém um pico proeminente em ca. 2.080 Ma. Variações sutis são notadas nas populações subordinadas, com atenção especial para os espectros da Formação Juruqui, onde o pico principal ocorre em 2.150 Ma, e da Formação Bocaina, que contem raros zircões Neoproterozóicos.

O estudo de proveniência sugere, preliminarmente, os seguintes tipos de *composites* de fontes: i) a base do Grupo Capiru, representada pelas formações Santana e Rio Branco, possui assinaturas de proveniência similares com idade máxima de deposição aproximada de 1.740 Ma; ii) o espectro da Formação Juruqui (MDA de 1.740 Ma), que tem como principal característica o pico principal a ca. de 2.150 Ma, levemente diferente dos picos entre 2.160 – 2.175 das outras formações; iii) o intervalo inferior da Formação Morro Grande, apresentando idades máximas de deposição de ~ 1.450 Ma; iv) os intervalos médio e superior da Formação Morro Grande, com MDAs de 1.110 Ma, e por fim, v) o espectro da Formação Bocaina, com as raras contribuições de zircões Neoproterozóicos (~ 690 e 565 Ma).

Os diferentes espectros identificados associados às interpretações com base no modelo estratigráfico sugerem pelo menos três estágios evolutivos para essa(s) bacia(s), em uma história sequencial que engloba o *break-up* do supercontinente Rodinia à formação do Gondwana:

(1) durante o tempo Santana-Juruqui, uma bacia de direção oeste-leste delimitada por planícies costeiras de baixo gradiente recebeu sedimentos siliciclásticos ricos em ferro. É importante mencionar que a interpretação da sequência Santana-Juruqui foi feita com base na característica ferrugionosa dos sedimentos. No entanto, apenas a Formação Juruqui possui registros de formações ferríferas bandadas.

(2) durante o tempo Rio Branco, uma plataforma carbonática se expandiu sob uma tendência transgressiva, com contribuição fosfática nas partes mais profundas da bacia;

(3) no final do tempo Rio Branco, a queda do nível do mar provavelmente causada por uma glaciação global causou o desenvolvimento de *sabkhas* em direção ao continente.

4) após a deposição da Formação Rio Branco, uma planície cárstica foi formada, desenvolvendo a discordância Pré-Morro Azul. Processos de intemperismo e a formação de laterita ocorreram nesse intervalo de tempo indeterminado, tanto nos setores do embasamento quanto na bacia, formando camadas lateríticas e bauxita;

5) após esse *gap* deposicional, foram depositados os pelitos ricos em Al da base da Formação Morro Azul;

(6) um segundo pulso carbonático é registrado no Grupo Capiru, representado pelo intervalo superior da Formação Morro Azul, onde a deposição carbonática ocorreu em ambientes marinhos rasos protegidos ou embaiamentos, onde se desenvolveram estromatólitos e uma série de estruturas microbiais;

(7) após este momento quiescente, outro pulso de sedimentação siliciclástica se inicia com a deposição da Formação Morro Grande. Essa formação é constituída por pelitos ferruginosos na sua base e tem como principal característica a presença de pelitos ricos em alumínio e material carbonoso. Embora depósitos glaciais não tenham sido documentados no Grupo Capiru, os estratos dos intervalos superiores (acima da discordância Pré-Morro Azul) podem ter sido influenciados por efeitos de glaciações neoproterozóicas, resultando no desenvolvimento de discordâncias regionais.

(8) Uma importante discordância também é observada no topo da Formação Morro Grande, definida como Discordância Pré-Bocaina;

(9) a deposição da Formação Bocaina se dá em resposta a um novo pulso de sedimentação. As feições composicionais (como a presença de arenitos feldspáticos e arcóseos) juntamente com zircões neoproterozóicos em sua proveniência, são interpretados como um novo pulso sedimentar em decorrência de processos tectônicos. Dentro do contexto regional, esses depósitos foram interpretados como sin-colisionais.

(10) Os processos colisionais e a colocação de *nappes* seguida por tectônica de escape deformam essas sucessões durante a colisão entre a Microplaca Curitiba e o bloco Paranapanema, que foram envolvidos na assembleia do Gondwana Ocidental.

Algumas semelhanças sedimentológicas e de proveniência do Grupo Capiru e unidades depositadas no cráton Rio de La Prata e na margem leste do Paranapanema foram elencadas. Essas comparações são importantes para as reconstruções paleogeográficas, que devem considerar uma posição tropical ou equatorial semelhante para a Microplaca Curitiba, sul do bloco Paranapanema e partes do cráton Rio de La Plata, durante o intervalo entre 650 - 635 Ma, correlato com a deposição do intervalo Morro Azul – Morro Grande no Grupo Capiru. Esse intervalo pode ser correlacionável ao intervalo superior do Grupo Itaiacoca e de unidades contendo discordâncias regionais relacionadas a este período.

Os dados apresentados neste trabalho discutem a evolução de uma margem continental passiva para a Microplaca Curitiba (pelo menos para o intervalo Santana - Juruqui (?) - Rio Branco), e para a margem leste do Paranapanema, registrada nos grupos Itaiacoca e Lajeado inferiores.

Perturbações tectônicas menores já ocorriam durante o tempo Morro Grande. Neste período, iniciou-se uma inversão tectônica, onde a borda sudeste do Paranapanema provavelmente tornou-se uma margem ativa onde a Seqüência Abapã é um dos registros. Posteriormente, os arcos Cunhaporanga e Três Córregos intrudiram nessas unidades, o que denota o aspecto de placa superior para os blocos a oeste da Microplaca Curitiba. Durante esse período, no âmbito da Microplaca Curitiba (*underplate*), a formação Bocaina foi depositada. Esta fase sin- à pós-colisional também é representada pelas formações Iporanga e Camarinha, com MDAs ~ 580 Ma, sob o efeito da glaciação Gaskiers (579,63 ± 0,15 e 579,88 ± 0,44) no âmbito do terreno Apiaí.

Através da proveniência e evolução geocronológica do Grupo Capiru, sugerimos que esses fragmentos crustais compartilharam uma evolução no Paleoproterozóico (com embasamentos conectados), e retrabalhamentos durante o Meso- e o Neoproterozóico.

REFERÊNCIAS

Adams, E. W., Schröder, S., Grotzinger, J. P., & McCormick, D. S. (2004). Digital reconstruction and stratigraphic evolution of a microbial-dominated, isolated carbonate platform (terminal Proterozoic, Nama Group, Namibia). *Journal of Sedimentary Research*, *74*(4) 479-497.

Affonso, G. M. P. C., Rocha, M. P., Costa, I. S. L., Assumpção, M., Fuck, R. A., Albuquerque, D. F., ... & Beck, S. L. (2021). Lithospheric Architecture of the Paranapanema Block and Adjacent Nuclei Using Multiple Frequency P-Wave Seismic Tomography. *Journal of Geophysical Research: Solid Earth*, *126*(4), e2020JB021183.

Affonso, G. M. P. C., Rocha, M. P., Costa, I. S. L., Assumpção, M., Fuck, R. A., Albuquerque, D. F., ... & Beck, S. L. (2021). Lithospheric Architecture of the Paranapanema Block and Adjacent Nuclei Using Multiple Frequency P-Wave Seismic Tomography. *Journal of Geophysical Research: Solid Earth*, *126*(4), e2020JB021183.

Almeida, F. D. (1967). Origem e evolução da Plataforma Brasileira. Bol. 241, Div. *Geol. Min., Dep. Nac. Prod. Min*.

Almeida, F. F. M., Amaral, G., Cordani, U., & Kawashita, K. (1973). The Precambrian evolution of the South American cratonic margin south of the Amazon River. In *The South Atlantic* (pp. 411-446). Springer, Boston, MA.

Almeida, F. F. M., de Brito Neves, B. B., & Carneiro, C. D. R. (2000). The origin and evolution of the South American Platform. *Earth-Science Reviews*, *50*(1-2), 77-111.

Almeida, F. F., Hasui, Y., & de Brito Neves, B. B. (1976). The upper Precambrian of South America. *Boletim do Instituto de Geociências - USP*, *Série Científica*, (*7*), 45-80.

Almeida, J., Dios, F., Mohriak, W. U., Valeriano, C. D. M., Heilbron, M., Eirado, L. G., & Tomazzoli, E. (2013). Pre-rift tectonic scenario of the Eo-Cretaceous Gondwana break-up along SE Brazil–SW Africa: insights from tholeiitic mafic dyke swarms. *Geological Society, London, Special Publications*, 369(1), 11-40.

Alvarez, P. (1995). Evidence for a Neoproterozoic carbonate ramp on the northern edge of the Central African Craton: relations with Late Proterozoic intracratonic troughs. *Geologische Rundschau*, *84* (3), 636-648.

Alves, A., de Assis Janasi, V., Neto, M. D. C. C., Heaman, L., & Simonetti, A. (2013). U–Pb geochronology of the granite magmatism in the Embu Terrane: Implications for the evolution of the Central Ribeira Belt, SE Brazil. *Precambrian Research*, 230, 1-12.

Alves, L. S. (2006). *O Complexo Granitóide Cunhaporanga, Paraná: a base georreferenciada para os estudos geofísicos, mineralógicos e geoquímicos*. Monograph, Final course assignment, University of São Paulo, São Paulo.

Arrouy, M. J., Poiré, D. G., Gómez Peral, L., & Canalicchio, J. (2015). Sedimentología y estratigrafía del Grupo La Providencia: cubierta superior neoproterozoica, Sistema de Tandilia, Argentina. *Latin American Journal of Sedimentology and Basin Analysis* 22 (2), 1-38.

Arthur, M. A., & Sageman, B. B. (1994). Marine black shales: depositional mechanisms and environments of ancient deposits. *Annual Review of Earth and Planetary Sciences*, *22* (1), 499-551.

Babinski, M., Boggiani, P. C., Fanning, M., Simon, C. M., Sial, A. N. (2008). U-Pb shrimp geochronology and isotope chemostratigraphy (C, O, Sr) of the Tamengo Formation, southern Paraguay belt, Brazil. In: VI South American Symposium on Isotope Geology, 2008, San Carlos de Bariloche. Book of Abstracts.

Babinski, M., Boggiani, P. C., Trindade, R. I. F., & Fanning, C. M. (2013). Detrital zircon ages and geochronological constraints on the Neoproterozoic Puga diamictites and associated BIFs in the southern Paraguay Belt, Brazil. *Gondwana Research*, *23* (3), 988-997.

Babinski, M., Vieira, L. C., & Trindade, R. I. (2007). Direct dating of the Sete Lagoas cap carbonate (Bambuí Group, Brazil) and implications for the Neoproterozoic glacial events. *Terra Nova*, *19* (6), 401-406.

Bahniuk, A. M. (2007). *Controles geológicos da carstificação em metadolomitos da Formação Capiru-Neoproterozóico, região metropolitana de Curitiba/PR*, Masters dissertation, Federal University of Paraná, Curitiba, 180p.

Barao, L. M., Trzaskos, B., Vesely, F. F., de Castro, L. G., Ferreira, F. J., Vasconcellos, E. M., & Barbosa, T. C. (2017). The role of post-collisional strike-slip tectonics in the geological evolution of the late Neoproterozoic volcano-sedimentary Guaratubinha Basin, southern Brazil. *Journal of South American Earth Sciences*, *80*, 29-46.

Basei, M. A. S., Citroni, S. B., & Junior, O. S. (1998a). Estratigrafia e idade das bacias fini-proterozóicas dos Estados do Paraná e Santa Catarina, sul do Brasil. *Boletim IG-USP. Série Científica*, *29*, 195-216.

Basei, M. A. S., Drukas, C. O., Nutman, A. P., Wemmer, K., Dunyi, L., Santos, P. D., ... & Osako, L. (2011). The Itajaí foreland basin: a tectono-sedimentary record of the Ediacaran period, Southern Brazil. *International Journal of Earth Sciences*, *100*(2), 543-569.

Basei, M. A. S., Frimmel, H. E., Neto, M. D. C. C., de Araujo, C. E. G., de Castro, N. A., & Passarelli, C. R. (2018). The tectonic history of the southern Adamastor Ocean based on a correlation of the Kaoko and Dom Feliciano belts. In *Geology of Southwest Gondwana*, 63-85. Springer, Heidelberg.

Basei, M. A. S., Frimmel, H. E., Nutman, A. P., & Preciozzi, F. (2008). West Gondwana amalgamation based on detrital zircon ages from Neoproterozoic Ribeira and Dom Feliciano belts of South America and comparison with coeval sequences from SW Africa. *Geological Society, London, Special Publications*, *294*(1), 239-256.

Basei, M. A. S., Frimmel, H. E., Nutman, A. P., Preciozzi, F., & Jacob, J. (2005). A connection between the Neoproterozoic Dom Feliciano (Brazil/Uruguay) and Gariep (Namibia/South Africa) orogenic belts–evidence from a reconnaissance provenance study. *Precambrian Research*, 139 (3-4), 195-221.

Basei, M. A. S., McReath, I., & Siga Jr, O. (1998b). The Santa Catarina granulite complex of southern Brazil: a review. *Gondwana Research*, *1*(3-4), 383-391.

Basei, M. A. S., Siga Jr, O., Reis Neto, J. D., Passarelli, C. R., Prazeres, H. J., Kaulfuss, G., ... & Lima, P. D. (1999). Paleoproterozoic granulitic belts of the Brazilian

Southern Region (PR-SC). In South American Symposium on Isotope Geology, Cordoba, Argentina. Extended Abstracts (pp. 291-294).

Basei, M. A., Nutman, A., Júnior, O. S., Passarelli, C. R., & Drukas, C. O. (2009). The evolution and tectonic setting of the Luis Alves Microplate of Southeastern Brazil: an exotic terrane during the assembly of Western Gondwana. *Developments in Precambrian Geology*, (16), 273-291.

Basei, M. A., Siga Jr, O., Machiavelli, A., & Mancini, F. (1992). Evolução tectônica dos terrenos entre os Cinturões Ribeira e Dom Feliciano (PR-SC). *Brazilian Journal of Geology*, 22(2), 216-221.

Basei, M., Siga Jr., O., Masquelin, H., Harara, O., Reis Neto, J., & Preciozzi, F. (2000). The Dom Feliciano belt (Brazil-Uruguay) and its foreland (Rio de la Plata Craton): framework, tectonic evolution and correlations with similar terranes of southwestern Africa. Tectonic Evolution of South America, 31st Int. Geol. Congr., Rio de Janeiro, Brazil, 311-334.

Basei, M.A.S. (1985). *O Cinturão Dom Feliciano em Santa Catarina*. São Paulo. Doctoral Thesis, University of São Paulo, 190 p.

Batolla Jr, F., Takahashi, A., Chiodi Filho, C., & Silva, C. (1981). Projeto integração e detalhe geológico no Vale do Ribeira, São Paulo: relatório final, área Ribeirão do Rocha. São Paulo, CPRM/DNPM, 6, 1-101.

Bial, J., Büttner, S. H., & Frei, D. (2015). Formation and emplacement of two contrasting late-Mesoproterozoic magma types in the central Namaqua Metamorphic Complex (South Africa, Namibia): evidence from geochemistry and geochronology. *Lithos*, 224, 272-294.

Bigarella, J. J. (1948). Estudos preliminares na série Açungui. 2. Rochas calcáreas. *Imprensa Paranaense*.

Bigarella, J. J., & Salamuni, R. (1958). Estudos preliminares na Série Açungui: VII–A Formação Votuverava. Curitiba, Instituto de História Natural. *Boletim Geologia*, 2.

Bigarella, J. J., & Salamuni, R. (1967). Sumário das Estruturas Sedimentares Singenéticas no Grupo Açungui. *Boletim Paranaense de Geociências*, 23-25.

Bigarella, J. J., Salamuni, R. (1956). Estudos preliminares na Série Açungui VII: algumas estruturas singenéticas nos dolomitos da Formação Capiru. *Brazilian Archives of Biology and Technology*, 11.

Boggiani, P. C. (1997). *Análise estratigráfica da Bacia Corumbá (Neoproterozoico)-Mato Grosso do Sul*. Doctoral Thesis, University of São Paulo, São Paulo, 181 p.

Boggiani, P. C., Ferreira, V. P., Sial, A. N., Babinski, M., Trindade, R. I. F., Aceñolaza, G., Toselli, A. J., & Parada, M. A. (2003). The cap carbonate of the Puga Hill (Central South America) in the context of the post-Varanger Glaciation. In *IV South American Symposium on Isotope Geology, Salvador, Brazil.* Book of Abstracts.

Boggiani, P. C., Gaucher, C., Sial, A. N., Babinski, M., Simon, C. M., Riccomini, C., Ferreira, V. P., & Fairchild, T. R. (2010). Chemostratigraphy of the Tamengo Formation (Corumbá Group, Brazil): a contribution to the calibration of the Ediacaran carbon-isotope curve. *Precambrian Research*, *182* (4), 382-401.

Bossi, J., & Cingolani, C. (2009). Extension and general evolution of the Río de la Plata Craton. *Developments in Precambrian Geology*, *16*, 73-85.

Bossi, J., Campal, N., Civetta, L., Demarchi, G., Girardi, V. A. V., Mazzucchelli, M., ... & Molesini, M. (1993). Early Proterozoic dike swarms from western Uruguay: geochemistry, Sr, Nd isotopes and petrogenesis. *Chemical Geology*, 106(3-4), 263-277.

Bradley, D. C. (2008). Passive margins through earth history. *Earth-Science Reviews*, *91* (1-4), 1-26.

Brito Neves, B. B. D., Campos Neto, M. D. C., & Fuck, R. A. (1999). From Rodinia to Western Gondwana: an approach to the Brasiliano-Pan African Cycle and orogenic collage. *Episodes-Newsmagazine of the International Union of Geological Sciences*, *22* (3), 155-166.

Brito Neves, B. B. D., Fuck, R. A., & Pimentel, M. M. (2014). The Brasiliano collage in South America: a review. *Brazilian Journal of Geology*, *44*(3), 493-518.

Brito Neves, B. B., & Cordani, U. G. (1991). Tectonic evolution of South America during the late Proterozoic. *Precambrian Research*, *53*(1-2), 23-40.

Brito Neves, B. B., Fuck, R. A., & Cordani, U. G. (1984). Influence of basement structures on the evolution of the major sedimentary basins of Brazil: a case of tectonic heritage. *Journal of Geodynamics*, *1*(3-5), 495-510.

Brito Neves, B., Fuck, R. A., & Pimentel, M. M. (2014). The Brasiliano collage in South America: a review. *Brazilian Journal of Geology*, 44(3), 493-518.

Bruno, H., Almeida, J., Heilbron, M., Salomão, M., & Cury, L. (2018). Architecture of major precambrian tectonic boundaries in the northern part of the Dom Feliciano Orogen, southern Brazil: Implications for the West Gondwana amalgamation. Journal of South American Earth Sciences, (86), 301-317.

Caird, R. A., Pufahl, P. K., Hiatt, E. E., Abram, M. B., Rocha, A. J. D., & Kyser, T. K. (2017). Ediacaran stromatolites and intertidal phosphorite of the Salitre Formation, Brazil: Phosphogenesis during the Neoproterozoic Oxygenation Event. *Sedimentary Geology*, (350), 55-71.

Campal, N., & Schipilov, A. (1999). The eastern edge of the Rio de la Plata Craton: a history of tangential collisions. In *Basement Tectonics 13* (pp. 33-48). Springer, Dordrecht.

Campanha, G. A. C., Basei, M. S., Faleiros, F. M., & Nutman, A. P. (2016). The mesoproterozoic to early neoproterozoic passive margin lajeado group and Apiaí gabbro, southeastern Brazil. *Geoscience Frontiers*, *7* (4), 683-694.

Campanha, G. A. C., Basei, M. S., Tassinari, C. C. G., Nutman, A. P., & Faleiros, F. M. (2008). Constraining the age of the Iporanga Formation with SHRIMP U-Pb zircon: implications for possible Ediacaran glaciation in the Ribeira Belt, SE Brazil. *Gondwana Research*, *13*(1), 117-125.

Campanha, G. A. C., Faleiros, F. M., Basei, M. A. S., Tassinari, C. C. G., Nutman, A. P., & Vasconcelos, P. M. (2015). Geochemistry and age of mafic rocks from the Votuverava Group, southern Ribeira Belt, Brazil: evidence for 1490 Ma oceanic back-arc magmatism. *Precambrian Research*, *266*, 530-550.

Campanha, G. A. C., Faleiros, F. M., Cawood, P. A., Cabrita, D. I. G., Ribeiro, B. V., & Basei, M. A. S. (2019). The tonian Embu Complex in the Ribeira belt (Brazil): revision, depositional age and setting in Rodinia and west Gondwana. *Precambrian Research*, *320*, 31-45.

Campanha, G. A. D. C., & Brito Neves, B. B. D. (2004). Frontal and oblique tectonics in the Brazilian shield. *Episodes-Newsmagazine of the International Union of Geological Sciences*, *27* (4), 255-259.

Campanha, G. D. C., & Sadowski, G. R. (1999). Tectonics of the southern portion of the Ribeira Belt (Apiaı Domain). *Precambrian Research*, *98* (1-2), 31-51.

Campanha, G.A. da C., et al., (1985). Geologia das folhas Iporanga (SG.22-X-B-V-2) e Gruta do Diabo (SG.22-X-B-VI-1), Estado de São Paulo. São Paulo. Contrato IPT/ Pró-Minério (IPT. Relatório, 22 352).

Campanha, G.A. da C., Gimenez Filho, A., Caetano, S.L.V., Pires, F.A., Dantas, A.S.L., Teixeira, A.L., Dehira, L.K., (1986). Geologia e estratigrafia da região das folhas Iporanga e Gruta do Diabo, Vale do Ribeira, São Paulo. In: Congresso Brasileiro de Geologia, 34, Goiânia, 1986. Anais... Goiânia, SBG, vol. 2, pp. 1058e1073.

Campanha, G.A.da C., (1991). *Tectônica Proterozóica no Alto e Médio Vale do Ribeira,* Campo Largo e Rio Branco do Sul/PR, Doctoral Thesis, São Paulo State University, Rio Claro, 215 p.

Campos Neto, M. & Figueiredo, M. C. H. (1995). The Rio Doce Orogeny, southeastern Brazil. *Journal of South American Earth Sciences*, 8(2), 143-162.

Campos Neto, M. C. (2000). Orogenic Systems from Southwestern Gondwana - an approach to Brasiliano-Pan African Cycle and Orogenic Collage in Southeastern Brazil. In: Cordani U.G., Milani E.J., Thomaz Filho A., Campos D.A. (eds.). *Tectonic Evolution of South America*, 31st International Geological Congress, 335-365.

Campos Neto, M. D. C., Basei, M. A. S., de Assis Janasi, V., & Moraes, R. (2011). Orogen migration and tectonic setting of the Andrelândia Nappe system: an Ediacaran western Gondwana collage, south of São Francisco craton. *Journal of South American Earth Sciences*, *32*(4), 393-406.

Campos Neto, M., & Figueiredo, M. C. H. (1995). The Rio Doce Orogeny, southeastern Brazil. *Journal of South American Earth Sciences*, *8* (2), 143-162.

Canfield, D. E., Poulton, S. W., Knoll, A. H., Narbonne, G. M., Ross, G., Goldberg, T., & Strauss, H. (2008). Ferruginous conditions dominated later Neoproterozoic deep-water chemistry. *Science*, 321 (5891), 949-952.

Carvalho, H. D., Crasto, J. P., Silva, Z. C. G., & Vialette, Y. (1987). The Kibaran cycle in Angola—a discussion. *Geological Journal*, 22(S2), 85-102.

Casquet, C., Rapela, C. W., Pankhurst, R. J., Baldo, E. G., Galindo, C., Fanning, C. M., ... & Saavedra, J. (2012). A history of Proterozoic terranes in southern South America: From Rodinia to Gondwana. *Geoscience Frontiers*, *3*(2), 137-145.

Castro -Valente, S., Corval, A., Duarte, B. P., Ellam, R. M., Fallick, A. E., Meighan, I. G., & Dutra, T. (2007). Tectonic boundaries, crustal weakness zones and plume-subcontinental lithospheric mantle interactions in the Serra do Mar dyke swarm, SE Brazil. *Brazilian Journal of Geology*, 37(1), 194-201.

Castro, L. G. D., & Ferreira, F. J. F. (2015). Arcabouço geofísico-estrutural da porção meridional do Cinturão Ribeira. *Brazilian Journal of Geology*, *45* (4), 499-516.

Cava, L. T. (1985a). Technical report of the Phosphorite Project: relatório de etapa. Curitiba, MINEROPAR. 25 p.

Cava, L. T. (1985b). Technical report of the Phosphorite Project: relatório da primeira fase. Curitiba, MINEROPAR. 20 p.

Cava, L. T. (1985c). Technical report of the Phosphorite Project: Prospecção de semi-detalhe área Pacas - Fazenda Primavera. Curitiba, MINEROPAR 61 p.

Cava, L. T. (1985d). Technical report of the Phosphorite Project: mapeamento geológico de detalhe área Pacas - Fazenda Jobar. Curitiba: MINEROPAR. 25 p.

Cava, L. T., Falcade, D. (1986) Projeto Fosforita, Área Campo Magro - Marmeleiro: Technical report. MINEROPAR, internal report. Curitiba, 112 p.

Chiglino, L. (2008). *Quimioestratigrafía de sequências meso e neoproterozóicas do Terreno Nico Pérez: idade, ambiente de sedimentação e correlações*. Master dissertation, Federal University of Pernambuco, Recife, 81 p.

Chiglino, L., Gaucher, C., Sial, A. N., Bossi, J., Ferreira, V. P., & Pimentel, M. M. (2010). Chemostratigraphy of mesoproterozoic and neoproterozoic carbonates of the Nico Pérez terrane, Río de la Plata craton, Uruguay. *Precambrian Research*, *182* (4), 313-336.

Cingolani CA, Hartmann LA, Santos JOS, y McNaughton NJ (2002) U-Pb SHRIMP dating of zircons from the Buenos Aires Complex of the Tandilia Belt, Río de la Plata Craton, Argentina. XV Congreso Geológico Argentino, Actas 1:149–154.

Cingolani, C. A. (2011). The Tandilia System of Argentina as a southern extension of the Río de la Plata craton: an overview. *International Journal of Earth Sciences*, *100*(2), 221-242.

Condon, D. J., Prave, A. R., & Benn, D. I. (2002). Neoproterozoic glacial-rainout intervals: Observations and implications. *Geology*, *30* (1), 35-38.

Condon, D., Zhu, M., Bowring, S., Wang, W., Yang, A., & Jin, Y. (2005). U-Pb ages from the neoproterozoic Doushantuo Formation, China. *Science*, 308 (5718), 95-98.

Cordani, U. G., & Teixeira, W. (2007). Proterozoic accretionary belts in the Amazonian Craton. *Geological Society of America Memoirs*, *200*, 297-320.

Cordani, U. G., Brito Neves, B. B., & Thomaz Filho, A. (2009). Estudo preliminar de integração do Pré-Cambriano com os eventos tectônicos das bacias sedimentares brasileiras (Atualização). *Geociências Petrobras*, *17*(1), 205-219.

Cordani, U. G., D'Agrella Filho, M. S., Brito Neves, B. D., & Trindade, R. I. F. (2003). Tearing up Rodinia: the Neoproterozoic palaeogeography of South American cratonic fragments. *Terra Nova*, 15 (5), 350-359.

Cox, G. M., Halverson, G. P., Minarik, W. G., Le Heron, D. P., Macdonald, F. A., Bellefroid, E. J., & Strauss, J. V. (2013). Neoproterozoic iron formation: An evaluation of its temporal, environmental and tectonic significance. *Chemical Geology*, (362), 232-249.

Cox, G. M., Halverson, G. P., Poirier, A., Le Heron, D., Strauss, J. V., & Stevenson, R. (2016). A model for Cryogenian iron formation. *Earth and Planetary Science Letters*, *433*, 280-292.

Cox, G. M., Halverson, G. P., Stevenson, R. K., Vokaty, M., Poirier, A., Kunzmann, M., Li, Z., Denyszyn, S. W., Strauss, J. V., & Macdonald, F. A. (2016). Continental flood basalt weathering as a trigger for Neoproterozoic Snowball Earth. *Earth and Planetary Science Letters*, (446), 89-99.

Cozzi, A., Grotzinger, J. P., & Allen, P. A. (2004). Evolution of a terminal Neoproterozoic carbonate ramp system (Buah Formation, Sultanate of Oman): Effects of basement paleotopography. *Geological Society of America Bulletin*, 116 (11-12), 1367-1384.

CPRM (2011). Projeto Aerogeofísico Paraná-Santa Catarina. Technical report. Companhia de Prospecção e Recursos Minerais do Brasil (CPRM) and LASA Prospecções S.A.Curitiba, 88 p.

Cury, L. F. (2009). *Geologia do terreno Paranaguá*. Doctoral Thesis, University of São Paulo, São Paulo, 187 p.

Cury, L. F., Kaulfuss, G. A., Siga Jr, O., Basei, M. A. S., Harara, O. M., & Sato, K. (2002). Idades U-Pb (zircões) de 1.75 Ga em granitóides alcalinos deformados dos núcleos Betara e Tigre: Evidências de regimes extensionais do Estateriano na Faixa Apiaí. *Geologia USP. Série Científica*, *2*, 95-108.

Cury, L. F., Santos, L. D. R., Leandro, R., Lange, L., & Bahniuk Rumbelsperger, A. (2017). Stenian Estuarine System and Early Neoproterozoic Microbial Records of Capiru Formation, Southern Ribeira Belt. In AGU Fall Meeting, Book of Abstracts.

Cury, L. F., Siga Jr, O., Harara, O. M. M., dos Prazeres Filho, H. J., & Basei, M. A. S. (2008). Aspectos tectônicos das intrusões dos granitos do cerne, passa três e Rio Abaixo, sudeste do Pré-cambriano Paranaense: estudo baseado em datações. *Geologia USP. Série Científica*, *8* (1), 87-104.

Daitx, E. (1996). *Origem e evolução dos depósitos sulfetados Tipo-Perau (Pb-Zn-Ag), com base nas jazidas Canoas e Perau (Vale do Ribeira, PR).* Doctoral dissertation, São Paulo State University, Rio Claro, 453p.

Dalla Salda, L. (1982). Nama-La Tinta y el inicio de Gondwana. *Acta Geológica Lilloana*, 23-38.

Dalla Salda, L. H., Spalletti, L. A., Poiré, D. G., Barrio, R. E. D., Echeveste, H. J., & Benialgo, A. R. (2006). Tandilia. *Serie correlación geológica*, *21*.

Dalziel, I. W., Lawver, L. A., & Murphy, J. B. (2000). Plumes, orogenesis, and supercontinental fragmentation. *Earth and Planetary Science Letters*, *178*(1-2), 1-11.

De Raaf, J. F. M., Boersma, J. R., & Van Gelder, S. (1977). Wave-generated structures and sequences from a shallow marine succession, Lower Carboniferous, County Cork, Ireland. *Sedimentology*, *24*(4), 451-483.

De Waele, B., Wingate, M. T., Fitzsimons, I. C., & Mapani, B. S. (2003). Untying the Kibaran knot: A reassessment of Mesoproterozoic correlations in southern Africa based on SHRIMP U-Pb data from the Irumide belt. *Geology*, *31*(6), 509-512.

Delpomdor, F. (2007). *Lithostratigraphie et sédimentologie de la chaîne Ouest Congolienne du Néoprotérozoïque supérieur (Formation de la Diamictite supérieure*

et Sous-groupe du Schisto-Calcaire) Bas-Congo, République Démocratique du Congo. Doctoral Thesis, Université Libre de Bruxelles, Belgium, 138 p.

Delpomdor, F., & Préat, A. (2013). Early and late Neoproterozoic C, O and Sr isotope chemostratigraphy in the carbonates of West Congo and Mbuji-Mayi supergroups: a preserved marine signature? *Palaeogeography, Palaeoclimatology, Palaeoecology*, *389*, 35-47.

Dickinson, W. R., & Gehrels, G. E. (2009). Use of U–Pb ages of detrital zircons to infer maximum depositional ages of strata: a test against a Colorado Plateau Mesozoic database. *Earth and Planetary Science Letters*, *288*(1-2), 115-125.

Dott Jr, R. H., & Bourgeois, J. (1982). Hummocky stratification: significance of its variable bedding sequences. *Geological Society of America Bulletin*, *93* (8), 663-680.

Dragone, G. N., Ussami, N., Gimenez, M. E., Klinger, F. G. L., & Chaves, C. A. M. (2017). Western Paraná suture/shear zone and the limits of Rio Apa, Rio Tebicuary and Rio de la Plata cratons from gravity data. *Precambrian Research*, *291*, 162-177.

Drüppel, K., Littmann, S., Romer, R. L., & Okrusch, M. (2007). Petrology and isotope geochemistry of the Mesoproterozoic anorthosite and related rocks of the Kunene Intrusive Complex, NW Namibia. *Precambrian Research*, 156(1-2), 1-31.

Dumas, S., & Arnott, R. W. C. (2006). Origin of hummocky and swaley cross-stratification—The controlling influence of unidirectional current strength and aggradation rate. *Geology*, *34* (12), 1073-1076.

Einsele, G. (2000). *Sedimentary basins. Evolution, facies and sediment budget*. Springer, Berlin, 792 p.

Ernst, R. E., Bleeker, W., Söderlund, U., & Kerr, A. C. (2013). Large Igneous Provinces and supercontinents: Toward completing the plate tectonic revolution. *Lithos*, 174 (2013), pp. 1-14.

Ernst, R. E., Pereira, E., Hamilton, M. A., Pisarevsky, S. A., Rodriques, J., Tassinari, C. C., ... & Van-Dunem, V. (2013). Mesoproterozoic intraplate magmatic 'barcode' record of the Angola portion of the Congo Craton: Newly dated magmatic events at 1505 and 1110 Ma and implications for Nuna (Columbia) supercontinent reconstructions. *Precambrian Research*, 230, 103-118.

Evans, D. A. (2003). A fundamental Precambrian–Phanerozoic shift in earth's glacial style? *Tectonophysics*, 375 (1-4), 353-385.

Evans, D. A., & Mitchell, R. N. (2011). Assembly and breakup of the core of Paleoproterozoic–Mesoproterozoic supercontinent Nuna. *Geology*, *39*(5), 443-446.

Fairchild, T. R. (1977). Conophyton and other columnar stromatolites from the Upper Precambrian Açungui Group near Itapeva, SP, Brazil. *SIMPÓSIO REGIONAL DE GEOLOGIA*, *1*(1977), 179-198.

Fairchild, T. R. (1982). New stromatolites from the Upper Precambrian Açungui Group, eastern Paraná, Brazil, and their potential stratigraphic use. *Boletim IG*, *13*, 43-50.

Faleiros, F. M. (2008). *Evolução de terrenos tectono-metamórficos da Serrania do Ribeira e Planalto Alto Turvo (SP, PR)*. Doctoral Thesis, University of São Paulo, São Paulo, 306 p.

Faleiros, F. M., Campanha, G. A. C., Pavan, M., Almeida, V. V., Rodrigues, S. W. O., & Araújo, B. P. (2016). Short-lived polyphase deformation during crustal thickening and exhumation of a collisional orogen (Ribeira Belt, Brazil). *Journal of Structural Geology*, (93), 106-130.

Faleiros, F. M., da Cruz Campanha, G. A., Martins, L., Vlach, S. R. F., & Vasconcelos, P. M. (2011). Ediacaran high-pressure collision metamorphism and tectonics of the southern Ribeira Belt (SE Brazil): evidence for terrane accretion and dispersion during Gondwana assembly. *Precambrian Research*, *189* (3-4), 263-291.

Faleiros, F. M., Ferrari, V. C., Costa, V. S., & da Cruz Campanha, G. A. (2011). Geoquímica e petrogênese de metabasitos do grupo Votuverava (Terreno Apiaí, Cinturão Ribeira Meridional): evidências de uma bacia retroarco calimiana. *Geologia USP. Série Científica*, *11*(2), 135-155.

Faleiros, F.M., Morais, S.M., Costa, V.S., 2012. Geologia e Recursos Minerais da Folha Apiaí - SG.22-X-B-V - Estados de São Paulo e Paraná, escala 1:100.000,1. ed, vol.1. Programa Geologia do Brasil, CPRM-Serviço Geológico do Brasil, São Paulo, p.107

Fedo, C. M., Wayne Nesbitt, H., & Young, G. M. (1995). Unraveling the effects of potassium metasomatism in sedimentary rocks and paleosols, with implications for paleoweathering conditions and provenance. *Geology*, 23 (10), 921-924.

Ferreira, F. J. F., Fornazzari Neto, L., Szameitat, L. S. A., Guimarães, G. B., Martin, V. M. O., Prazeres Filho, H., & Ulbrich, H. (2014). Gamma-ray spectrometry as a tool for mapping petrographic domains in granitoids: the examples of the Cunhaporanga and Três Córregos granitic complexes, Paraná state, Southern Brazil. *Revista Brasileira de Geofísica*, 32(3), 463-479.

Filpi, T. C. F. C. M. (2021). Estimativas de permeabilidade em aquífero cárstico a partir de métodos de alta resolução. Masters dissertation, Federal University of Paraná, Curitiba.

Fiori (1985) Estudos geológicos integrados do pré-cambriano paranaense Curitiba: MINEROPAR/UFPR, Mapping partnership between Federal University of Paraná and MINEROPAR. 1 map: colored, Scale 1 :250.000.

Fiori, A. P. (1992). Tectônica e estratigrafia do Grupo Açungui, PR. *Boletim do Instituto de Geociências – USP, Série Científica*, (23) 55-74.

Fiori, A. P., & Gaspar, L. A. (1993). Considerações sobre a estratigrafia do Grupo Açungui (Proterozóico Superior), Paraná, sul do Brasil. *Boletim do Instituto de Geociências - USP, Série Científica,* (24) 1-19.

Fiori, A. P., Fassbinder, E., & Salamuni, E. (2003). Evolução geológica do Grupo Açungui. SBG. *Boletim de Resumos, VIII Simpósio de Geologia do Sudeste, São Pedro,* 16 p, Book of Abstracts.

Fiori, A. P., Fassbinder, E., & Salamuni, E. (2003). Evolução geológica do Grupo Açungui. SBG. Boletim de Resumos, VIII Simpósio de Geologia do Sudeste, São Pedro, SP, p 16.

Fiori, A.P. (1991). Tectônica e Estratigrafia do Grupo Açungui a Norte de Curitiba. São Paulo. 261 p. Doctoral Thesis, University of São Paulo, São Paulo, 261p.

Florisbal, L. M., Heaman, L. M., de Assis Janasi, V., & de Fatima Bitencourt, M. (2014). Tectonic significance of the Florianópolis dyke Swarm, Paraná–Etendeka

Magmatic Province: a reappraisal based on precise U–Pb dating. *Journal of Volcanology and Geothermal Research*, 289, 140-150.

Font, E., Nédélec, A., Trindade, R. I. F., Macouin, M., & Charrière, A. (2006). Chemostratigraphy of the Neoproterozoic Mirassol d'Oeste cap dolostones (Mato Grosso, Brazil): an alternative model for Marinoan cap dolostone formation. *Earth and Planetary Science Letters*, *250* (1-2), 89-103.

Fontaneta, G. T. (2012). *Dolomitização e fosfogênese na formação bocaina, grupo Corumbá (ediacarano)*, Master dissertation, University of São Paulo, 148 p.

Forero-Ortega, A. J. (2018). *Tectonic compartimentation of an area in the Ribeira belt, between Itapeva and Ribeirão Branco (SP): Itaiacoca Group and Bairro dos Prestes Formation*, Master dissertation, University of São Paulo, 129 p.

Forero-Ortega, A. J., Campanha, G. A. C., Faleiros, F. M., & Yogi, M. T. A. G. (2020). Pure shear-dominated transpression and vertical extrusion in a strike-slip fault splay from the Itapirapuã Shear Zone, Ribeira Belt, Brazil. *Tectonophysics*, *786*, 228455.

Frascá, M.B.H.O., Campanha, G.A.C., Figueiredo, M.C.H., Sadowski, G.R., (1997). Geoquímica e ambiência tectônica de metabasitos do alto e médio Vale do Ribeira, São Paulo e Paraná. *Revista Brasileira de Geociências* 27, 41e48.

Frimmel, H. E. (2009). Trace element distribution in Neoproterozoic carbonates as palaeoenvironmental indicator. *Chemical Geology*, *258* (3-4), 338-353.

Frimmel, H. E., Basei, M. A., Correa, V. X., & Mbangula, N. (2013). A new lithostratigraphic subdivision and geodynamic model for the Pan-African western Saldania Belt, South Africa. *Precambrian Research*, (*231*) 218-235.

Frimmel, H. E., Basei, M. S., & Gaucher, C. (2011). Neoproterozoic geodynamic evolution of SW-Gondwana: a southern African perspective. *International Journal of Earth Sciences*, *100* (2), 323-354.

Fuck, R. A., Neves, B. B. B., & Schobbenhaus, C. (2008). Rodinia descendants in south America. *Precambrian Research*, *160* (1-2), 108-126.

Gaucher, C., & Poiré, D. (2009). Palaeoclimatic Events. *Developments in Precambrian Geology*, (16), 123-130.

Gaucher, C., & Sprechmann, P. (1999). Upper Vendian skeletal fauna of the Arroyo del Soldado Group, Uruguay. *Beringeria*, *23* (1), 55-91.

Gaucher, C., Blanco, G., Chiglino, L., Poiré, D., & Germs, G. J. (2008). Acritarchs of Las Ventanas Formation (Ediacaran, Uruguay): implications for the timing of coeval rifting and glacial events in western Gondwana. *Gondwana Research*, *13* (4), 488-501.

Gaucher, C., Boggiani, P., Sprechmann, P., Sial, A., & Fairchild, T. (2003). Integrated correlation of the Vendian to Cambrian Arroyo del Soldado and Corumbá Groups (Uruguay and Brazil): palaeogeographic, palaeoclimatic and palaeobiologic implications. *Precambrian Research*, *120* (3-4), 241-278.

Gaucher, C., Chiglino, L., & Peçoits, E. (2004). Southernmost exposures of the Arroyo del Soldado Group (Vendian to Cambrian, Uruguay): palaeogeographic implications for the amalgamation of W-Gondwana. *Gondwana Research*, *7*(3), 701-714.

Gaucher, C., Finney, S. C., Poiré, D. G., Valencia, V. A., Grove, M., Blanco, G., ... & Peral, L. G. (2008). Detrital zircon ages of Neoproterozoic sedimentary successions in Uruguay and Argentina: insights into the geological evolution of the Río de la Plata Craton. *Precambrian Research*, *167*(1-2), 150-170.

Gaucher, C., Frei, R., & Frei, D. (2010). Detrital zircon U–Pb ages of the San Carlos Formation (latest Neoproterozoic, Uruguay) and the allochthonous nature of Arachania. In *VII South American Symposium on Isotope Geology, Extended Abstracts* (pp. 556-559).

Gaucher, C., Frei, R., Chemale, F., Frei, D., Bossi, J., Martínez, G., Chiglino, L., & Cernuschi, F. (2011). Mesoproterozoic evolution of the Río de la Plata Craton in Uruguay: at the heart of Rodinia? *International Journal of Earth Sciences*, *100* (2), 273-288.

Gaucher, C., Frei, R., Samaniego, L., Will, T. M., Chemale, F., Gargiulo, M. F., ... & Li, Q. L. (2021). The Tapes Complex (Nico Pérez Terrane, Uruguay): Constraining the Mesoproterozoic evolution of the Río de la Plata Craton. *Journal of South American Earth Sciences*, *105*, 102906.

Gaucher, C., Frimmel, H. E., & Germs, G. J. (2005a). Organic-walled microfossils and biostratigraphy of the upper Port Nolloth Group (Namibia): implications for latest Neoproterozoic glaciations. *Geological Magazine*, *142* (5), 539-559.

Gaucher, C., Frimmel, H. E., & Germs, G. J. (2009). Tectonic events and palaeogeographic evolution of southwestern Gondwana in the Neoproterozoic and Cambrian. *Developments in Precambrian Geology*, *16*, 295-316.

Gaucher, C., Poiré, D. G., Gómez Peral, L. E., & Chiglino, L. (2005b). Litoestratigrafía, bioestratigrafía y correlaciones de las sucesiones sedimentarias del Neoproterozoico-Cámbrico del Cratón del Rio de la Plata (Uruguay y Argentina). *Latin American Journal of Sedimentology and Basin Analysis*, *12*.

Gehrels, G., 2010a, Age Pick program: University of Arizona Laserchron Center, Tucson, AZ.

GEOSOFT (2001). Magmap – 2-D Frequency DomainProcessing.Application module. Geosoft Technical Note, 34p.

GEOSOFT (2011). Mapping and Processing System - The core software platform for working with large volume spatial data, Quick Start TM Tutorials.

Germs, G. J. B., & Gaucher, C. (2012). Nature and extent of a late Ediacaran (ca. 547 Ma) glacigenic erosion surface in southern Africa. *South African Journal of Geology*, *115* (1), 91-102.

Germs, G.J.B., (1972). New shelly fossils from Nama Group, South West Africa. *American Journal of Science* (272), 752–761.

Gómez-Peral, L. E., Arrouy, M. J., Richiano, S., Cereceda, A., Alé, S. A., & Poiré, D. G. (2021). Unravelling hidden glacial effects in the Cryogenian marine depositional settings of the Tandilia Basin, Argentina. *Precambrian Research*, (361), 106261.

Gómez-Peral, L. E., Kaufman, A. J., & Poiré, D. G. (2014). Paleoenvironmental implications of two phosphogenic events in Neoproterozoic sedimentary successions of the Tandilia System, Argentina. *Precambrian Research*, (252), 88-106.

Gómez-Peral, L. E., Kaufman, A. J., Arrouy, M. J., Richiano, S., Sial, A. N., Poiré, D. G., & Ferreira, V. P. (2018). Preglacial palaeoenvironmental evolution of the ediacaran loma Negra formation, far southwestern gondwana, Argentina. *Precambrian Research*, (315), 120-137.

Gómez-Peral, L. E., Poiré, D. G., Strauss, H., & Zimmermann, U. (2007). Chemostratigraphy and diagenetic constraints on Neoproterozoic carbonate successions from the Sierras Bayas Group, Tandilia System, Argentina. *Chemical Geology*, *237* (1-2), 109-128.

Gómez-Peral, L. E., Raigemborn, M. S., & Poiré, D. G. (2011). Petrología y evolución diagenética de las facies silicoclásticas del Grupo Sierras Bayas, Sistema de Tandilia, Argentina. *Latin American Journal of Sedimentology and Basin Analysis*, *18*.

Gómez-Peral, L. E., Sial, A. N., Arrouy, M. J., Richiano, S., Ferreira, V. P., Kaufman, A. J., & Poiré, D. G. (2017). Paleo-climatic and paleo-environmental evolution of the Neoproterozoic basal sedimentary cover on the Río de La Plata Craton, Argentina: Insights from the δ13C chemostratigraphy. *Sedimentary Geology*, (353), 139-157.

Gray, D. R., Foster, D. A., Meert, J. G., Goscombe, B. D., Armstrong, R., Trouw, R. A. J., & Passchier, C. W. (2008). A Damara orogen perspective on the assembly of southwestern Gondwana. *Geological Society of London, Special Publications*, 294 (1), 257-278.

Grotzinger, J. P., & Knoll, A. H. (1999). Stromatolites in Precambrian carbonates: evolutionary mileposts or environmental dipsticks? *Annual review of earth and planetary sciences*, *27* (1), 313-358.

Grotzinger, J. P., Bowring, S. A., Saylor, B. Z., & Kaufman, A. J. (1995). Biostratigraphic and geochronologic constraints on early animal evolution. *Science*, *270* (5236), 598-604.

Grotzinger, J. P., Watters, W. A., & Knoll, A. H. (2000). Calcified metazoans in thrombolite-stromatolite reefs of the terminal Proterozoic Nama Group, Namibia. *Paleobiology*, *26* (3), 334-359.

Grotzinger, J., & Al-Rawahi, Z. (2014). Depositional facies and platform architecture of microbialite-dominated carbonate reservoirs, Ediacaran–Cambrian Ara Group, Sultanate of Oman Microbialite Reservoirs in Oman. *AAPG bulletin*, *98* (8), 1453-1494.

Guimarães, S. B., dos Reis Neto, J. M., & Siqueira, R. B. (2002). Caracterização dos estromatólitos da Formação Capiru (Proterozóico) nas regiões de Morro Azul e Morro Grande: leste do Paraná. *Boletim Paranaense de Geociências*, *51*.

Haines, P. W. (1988). Storm-dominated mixed carbonate/siliciclastic shelf sequence displaying cycles of hummocky cross-stratification, late Proterozoic Wonoka Formation, South Australia. *Sedimentary Geology*, *58* (2-4), 237-254.

Halverson, G. P. (2006). A Neoproterozoic chronology. In *Neoproterozoic geobiology and paleobiology* (pp. 231-271). Springer, Dordrecht.

Halverson, G. P., Poitrasson, F., Hoffman, P. F., Nédélec, A., Montel, J. M., & Kirby, J. (2011). Fe isotope and trace element geochemistry of the Neoproterozoic syn-glacial Rapitan iron formation. *Earth and Planetary Science Letters*, *309* (1-2), 100-112.

Harara, O. M. M. (2001). *Mapeamento e Investigação Petrológica e Geocronológica dos Litotipos da Região do Alto Rio Negro (PR-SC): um exemplo de sucessivas e distintas atividades magmáticas durante o Neoproterozóico III* . Doctoral Thesis, University of São Paulo, São Paulo, 201 p.

Hartmann, L. A., Campal, N., Santos, J. O. S., McNaughton, N. J., Bossi, J., Schipilov, A., & Lafon, J. M. (2001). Archean crust in the Rio de la Plata Craton, Uruguay—SHRIMP U–Pb zircon reconnaissance geochronology. *Journal of South American Earth Sciences*, 14(6), 557-570.

Hartmann, L. A., Leite, J. A. D., Da Silva, L. C., Remus, M. V. D., McNaughton, N. J., Groves, D. I., ... & Vasconcellos, M. A. Z. (2000). Advances in SHRIMP geochronology and their impact on understanding the tectonic and metallogenic evolution of southern Brazil. *Australian Journal of Earth Sciences*, *47*(5), 829-844.

Hartmann, L. A., Liu, D., Wang, Y., Massonne, H. J., & Santos, J. O. (2008). Protolith age of Santa Maria Chico granulites dated on zircons from an associated amphibolite-facies granodiorite in southernmost Brazil. *Anais da Academia Brasileira de Ciências*, *80*(3), 543-551.

Hartmann, L. A., Piñeyro, D., Bossi, J., Leite, J. A., & McNaughton, N. J. (2000). Zircon U-Pb SHRIMP dating of Palaeoproterozoic Isla Mala granitic magmatism in the Rio de la Plata craton, Uruguay.*Journal of South American Earth Sciences*,13(1-2), 105-113.

Hartmann, L. A., Santos, J. O. S., Bossi, J., Campal, N., Schipilov, A., & McNaughton, N. J. (2002). Zircon and titanite U–Pb SHRIMP geochronology of Neoproterozoic felsic magmatism on the eastern border of the Rio de la Plata Craton, Uruguay. *Journal of South American Earth Sciences*, *15* (2), 229-236.

Hartmann, L. A., Santos, J. O. S., Cingolani, C. A., & McNaughton, N. J. (2002). Two Paleoproterozoic orogenies in the evolution of the Tandilia Belt, Buenos Aires, as evidenced by zircon U-Pb SHRIMP geochronology. *International Geology Review*, *44*(6), 528-543.

Hartmann, L. A., Santos, J. O. S., McNaughton, N. J., Vasconcellos, M. A. Z., & Silva, L. C. (2000). SHRIMP dates recurrent granulite facies metamorphism in the Santa Catarina granulites, southern Brazil. *Anais Academia Brasileira de Ciências*, *72*, 559-572.

Hartmann, L. A., Silva, L. D., & Orlandi Filho, V. (1979). O Complexo Granulítico de Santa Catarina; descrição e implicações genéticas. *Acta Geológica Leopoldensia*, *3*(10), 93-112.

Heilbron, M., & Machado, N. (2003). Timing of terrane accretion in the Neoproterozoic–Eopaleozoic Ribeira orogen (SE Brazil). *Precambrian Research*, 125 (1-2), 87-112.

Heilbron, M., de Morisson Valeriano, C., Peixoto, C., Tupinambá, M., Neubauer, F., Dussin, I., ... & do Eirado Silva, L. G. (2020). Neoproterozoic magmatic arc systems of the central Ribeira belt, SE-Brazil, in the context of the West-Gondwana pre-collisional history: A review. *Journal of South American Earth Sciences*, 102710.

Heilbron, M., Mohriak, W. U., Valeriano, C. M., Milani, E. J., Almeida, J., & Tupinambá, M. (2000). From collision to extension: the roots of the southeastern

continental margin of Brazil. *Geophysical Monograph-American Geophysical Union*, (115), 1-32.

Heilbron, M., Pedrosa-Soares, A. C., Campos Neto, M. D. C., Silva, L. D., Trouw, R. A. J., & Janasi, V. D. A. (2004). Província mantiqueira. In Geologia do continente sul-americano: evolução da obra de Fernando Flávio Marques de Almeida, 203-235.

Heilbron, M., Valeriano, C. M., Tassinari, C. C. G., Almeida, J., Tupinambá, M., Siga, O., & Trouw, R. (2008). Correlation of Neoproterozoic terranes between the Ribeira Belt, SE Brazil and its African counterpart: comparative tectonic evolution and open questions. *Geological Society, London, Special Publications*, *294* (1), 211-237.

Henrique-Pinto, R., Janasi, V. A., Vasconcellos, A. C. B. C., Sawyer, E. W., Barnes, S. J., Basei, M. A., & Tassinari, C. C. (2015). Zircon provenance in meta-sandstones of the São Roque Domain: Implications for the Proterozoic evolution of the Ribeira Belt, SE Brazil. *Precambrian Research*, *256*, 271-288.

Herron, M. M. (1988). Geochemical classification of terrigenous sands and shales from core or log data. *Journal of Sedimentary Research*, *58* (5), 820-829.

Hoffman, P. F. (1999). The break-up of Rodinia, birth of Gondwana, true polar wander and the snowball Earth. *Journal of African Earth Sciences*, *28*(1), 17-33.

Hoffman, P. F., & Schrag, D. P. (2002). The snowball Earth hypothesis: testing the limits of global change. *Terra Nova*, *14* (3), 129-155.

Hoffman, P. F., Abbot, D. S., Ashkenazy, Y., Benn, D. I., Brocks, J. J., Cohen, P. A., Cox, G. M., Creveling, J. R., Donnadieu, Y., Erwin, D. H., Fairchild, I. J., Ferreira, D., Goodman, J. C., Halverson, G. P., Jansen, M. F., Hir, G. L., Love, G. D., Macdonald, F. A., Maloof, A. C., Partin, C. A., Ramstein, G., Rose, B. E. J., Rose, C. V., Sadler, P. M., Tziperman, E., Voigt, A. & Warren, S. G. (2017). Snowball Earth climate dynamics and Cryogenian geology-geobiology. *Science Advances*, *3* (11).

Hoffman, P. F., Hawkins, D. P., Isachsen, C. E., & Bowring, S. A. (1996). Precise U–Pb zircon ages for early Damaran magmatism in the Summas Mountains and Welwitschia Inlier, northern Damara belt, Namibia. *Communications of the Geological Survey of Namibia*, *11*, 47-52.

Hoffman, P. F., Kaufman, A. J., Halverson, G. P., & Schrag, D. P. (1998). A Neoproterozoic snowball earth. *Science*, 281 (5381), 1342-1346.

Hoffmann, K. H., Condon, D. J., Bowring, S. A., & Crowley, J. L. (2004). U-Pb zircon date from the Neoproterozoic Ghaub Formation, Namibia: constraints on Marinoan glaciation. *Geology*, *32* (9), 817-820.

Iñiguez Rodriguez, A. M., del Valle, A., Poiré, D. G., Spalletti, L. A. & Zalba, P. E. (1989). Cuenca precámbrica-paleozoica inferior de Tandilia, Provincia de Buenos Aires. In Chebli, G. & Spalletti, L.A. (Eds.): Cuencas Sedimentarias Argentinas, 245-263, Universidad Nacional de Tucumán.

Jackson, S., N. Pearson, and W. Griffin (2001), In situ isotope ratio determination using laser ablation (LA)-magnetic sector-ICP-MS, in *Laser-Ablation-ICPMS in the Earth Sciences: Principles and Applications*, Short Course Ser., vol. **29**, edited by P. Sylvester, pp. 105– 120, Mineral. Assoc. of Can., St John's, Newfoundland.

Janasi, V. A., Leite, R. J., & Van Schmus, W. R. (2001). U–Pb chronostratigraphy of the granitic magmatism in the Agudos Grandes Batholith (west of Sao Paulo,

Brazil)—implications for the evolution of the Ribeira Belt. *Journal of South American Earth Sciences*, *14* (4), 363-376.

Julià, J., Assumpção, M., & Rocha, M. P. (2008). Deep crustal structure of the Paraná Basin from receiver functions and Rayleigh wave dispersion: Evidence for a fragmented cratonic root. *Journal of Geophysical Research: Solid Earth*, *113*(B8).

Juschaks, L. C. D. S. (2006). *Fácies, estruturas biogênicas e modelos deposicionais dos Metadolomitos da Formação Capiru-Grupo Açungui, Neoproterozoico do Paraná*. Masters dissertation, Federal University of Paraná, 130 p.

Kaulfuss, G. A. (2001). *Geocronologia dos núcleos de embasamento Setuva, Betara e Tigre, norte de Curitiba-Paraná*. Masters dissertation. Universidade de São Paulo, São Paulo, 141p.

Kawashita, K., Gaucher, C., Sprechmann, P., Teixeira, W., Victória, R. (1999). Preliminary chemostratigraphic insights on carbonate rocks from Nico Pérez Terrane (Uruguay). Actas II South American Symposium on Isotope Geology. Córdoba, Argentina, 399–402.

Kellerhals, P., & Matter, A. (2003). Facies analysis of a glaciomarine sequence, the Neoproterozoic Mirbat Sandstone Formation, Sultanate of Oman. *Eclogae Geologicae Helvetiae*, (96), 49-70.

Kirkland, C. L., Smithies, R. H., Taylor, R. J. M., Evans, N., & McDonald, B. (2015). Zircon Th/U ratios in magmatic environs. *Lithos*, *212*, 397-414.

Knoll, A. H. (2000). Learning to tell Neoproterozoic time. *Precambrian Research*, 100 (1-3), 3-20.

Köksal, S. E. R. H. A. T., Göncüoglu, M. C., Toksoy-Köksal, F., Möller, A., & Kemnitz, H. (2008). Zircon typologies and internal structures as petrogenetic indicators in contrasting granitoid types from central Anatolia, Turkey. *Mineralogy and Petrology*, *93*(3), 185-211.

Kröner, A., & Stern, R. J. (2004). Pan-African Orogeny. Encyclopedia of Geology, vol. 1.

Lana, C., Farina, F., Gerdes, A., Alkmim, A., Gonçalves, G. O., & Jardim, A. C. (2017). Characterization of zircon reference materials via high precision U–Pb LA-MC-ICP-MS. *Journal of Analytical Atomic Spectrometry*, *32*(10), 2011-2023.

Leandro, R. (2016). *Caracterização tectonoestratigráfica da sequência terrígena da formação Capiru na Região de Morro Grande, Colombo-PR.* Masters dissertation, Federal University of Paraná, 134 p.

Leite, R. J., Heaman, L. M., de Assis Janasi, V., Martins, L., & Creaser, R. A. (2007). The late-to postorogenic transition in the Neoproterozoic Agudos Grandes Granite Batholith (Apiaí Domain, SE Brazil): constraints from geology, mineralogy, and U–Pb geochronology. *Journal of South American Earth Sciences*, *23* (2-3), 193-212.

Li, Z. X., Bogdanova, S., Collins, A. S., Davidson, A., De Waele, B., Ernst, R. E., ... & Vernikovsky, V. (2008). Assembly, configuration, and break-up history of Rodinia: a synthesis. *Precambrian Research*, *160* (1-2), 179-210.

Li, Z. X., Evans, D. A., & Halverson, G. P. (2013). Neoproterozoic glaciations in a revised global palaeogeography from the breakup of Rodinia to the assembly of Gondwanaland. *Sedimentary Geology*, (294), 219-232.

Lino, L. M., Quiroz-Valle, F. R., Louro, V., Basei, M. Â. S., Vlach, S. R. F., Hueck, M., ... & Citroni, S. B. (2021). Structural architecture and the episodic evolution of the ediacaran Campo Alegre Basin (southern Brazil): Implications for the development of a synorogenic foreland rift and a post-collisional caldera-volcano. *Journal of South American Earth Sciences*, *107*, 103147.

Littmann, S., Romer, R., & Okrusch, M. (2000). Nephelinsyenite der Epembe-Swartbooisdrif-Alkali-Provinz (ESAP)/NW-Namibia. In DMG; Beih. Eur. J. Mineral.

Lopes, A. P., Ribeiro, L. M. D. A. L., Salvador, E. D., Pavan, M., & Silva, A. D. R. D. (2017). Áreas de relevante interesse mineral–Vale do Ribeira: mineralizações polimetálicas (Pb, Ag, Zn, Cu e Au–"tipo panelas") em zonas de cisalhamento rúptil, Cinturão Ribeira Meridional: estados de São Paulo e Paraná.

Lovecchio, J. P., Rohais, S., Joseph, P., Bolatti, N. D., & Ramos, V. A. (2020). Mesozoic rifting evolution of SW Gondwana: a poly-phased, subduction-related, extensional history responsible for basin formation along the Argentinean Atlantic margin. *Earth-Science Reviews*, *203*, 103138.

Ludwig, K. R. (2012). Isoplot 4.15: a geochronological toolkit for Microsoft Excel. *Berkeley Geochronology Center Special Publication*, *5*.

Maack, R. (1947). Breves notícias sobre a geologia dos Estados do Paraná e Santa Catarina. *Brazilian archives of biology and technology*, 169-288.

Machiavelli, A., Basei, M. A. S., & Siga Jr, O. (2011). Suíte Granítica Rio Pien: um arco magmático do Proterozóico Superior na Microplaca Curitiba. *Geochimica Brasiliensis*, *7*(2), 113-129.

Mallmann, G., Chemale Jr, F., Ávila, J. N., Kawashita, K., & Armstrong, R. A. (2007). Isotope geochemistry and geochronology of the Nico Perez terrane, Rio de la Plata craton, Uruguay. *Gondwana Research*, *12*(4), 489-508.

Maniesi, V., 1997. *Petrologia das rochas anfibolíticas das regiões de Adrianópolis, Estados de São Paulo e Paraná*, Doctoral Thesis. University of São Paulo, 296 p.

Maniesi, V., Oliveira, M.A.F., 2000. Petrogênese do metabasitos com afinidades dos toleítos de fundo oceânico das regiões de Adrianópolis e Campo Largo/PR. *Revista Brasileira de Geociências* 30, 607e614.

Maniesi, V., Oliveira, M.A.F., 2002. Metabasitos com afinidades dos basaltos komatiíticos da região de Rio Branco do Sul/PR. *Revista Brasileira de Geociências* 32, 163e168.

Mantovani, M. S. M., & de Brito Neves, B. B. (2005). The Paranapanema lithospheric block: Its importance for Proterozoic (Rodinia, Gondwana) supercontinent theories. *Gondwana Research*, *8* (3), 303-315.

Mantovani, M. S., & de Brito Neves, B. B. (2009). The Paranapanema lithospheric block: its nature and role in the accretion of Gondwana. *Developments in Precambrian Geology*, *16*, 257-272.

Mayer, A., Hofmann, A. W., Sinigoi, S., & Morais, E. (2004). Mesoproterozoic Sm–Nd and U–Pb ages for the Kunene anorthosite complex of SW Angola. *Precambrian Research*, 133(3-4), 187-206.

McCourt, S., Armstrong, R. A., Grantham, G. H., & Thomas, R. J. (2006). Geology and evolution of the Natal belt, South Africa. *Journal of African Earth Sciences*, 46(1-2), 71-92.

McCourt, S., Armstrong, R. A., Jelsma, H., & Mapeo, R. B. M. (2013). New U–Pb SHRIMP ages from the Lubango region, SW Angola: insights into the Palaeoproterozoic evolution of the Angolan Shield, southern Congo Craton, Africa. *Journal of the Geological Society*, *170*(2), 353-363.

McLennan, S. M. (1993). Weathering and global denudation. *The Journal of Geology*, 101 (2), 295-303.

McMechan, M. E. (2000). Vreeland diamictites–Neoproterozoic glaciogenic slope deposits, Rocky Mountains, northeast British Columbia. *Bulletin of Canadian Petroleum Geology*, *48* (3), 246-261.

McMenamin, M. A., & McMenamin, D. L. S. (1990). *The Emergence of Animals the Cambrian Breakthrough*. Columbia University Press.

McReath, I., & Kaulfuss, G. (2003). The Atuba complex, Southern South American platform: archean components and paleoproterozoic to neoproterozoic tectonothermal events. *Gondwana Research*, 6(2), 251-263.

Meert, J. G., & Powell, C. M. (2001). Assembly and break-up of Rodinia: introduction to the special volume. *Precambrian Research*, *110*, 1-8.

Meert, J. G., & Torsvik, T. H. (2003). The making and unmaking of a supercontinent: Rodinia revisited. *Tectonophysics*, *375*(1-4), 261-288.

Menge, G. F. (1998). *The antiformal structure and general aspects of the Kunene Complex, Namibia*. Zeitschrift der Deutschen Geologischen Gesellschaft, 431-448.

Mineropar (1989). Mapa Geológico do Estado do Paraná. Curitiba : DNPM-MINEROPAR, 1989. 1 map: colored.; 1,97 x 97 cm. Scale 1 :650.000.

Möller, A., Hensen, B. J., Armstrong, R. A., Mezger, K., & Ballevre, M. (2003). U–Pb zircon and monazite age constraints on granulite-facies metamorphism and deformation in the Strangways Metamorphic Complex (central Australia). *Contributions to Mineralogy and Petrology*, *145*(4), 406-423.

Morgan, W. J. (1981). 13. Hotspot tracks and the opening of the Atlantic and Indian Oceans. *The oceanic lithosphere*, *7*, 443.

Moro, R. D. P. X., & de Brito Neves, B. B. (2009). Análise Estrutural e de Deformação de Clastos das Unidades Sedimentares da Formação Camarinha-PR. *Geologia USP. Série Científica*, *9* (1), 15-31.

Nascimento, D. B., Schmitt, R. S., Ribeiro, A., Trouw, R. A., Passchier, C. W., & Basei, M. A. (2017). Depositional ages and provenance of the Neoproterozoic Damara Supergroup (northwest Namibia): Implications for the Angola-Congo and Kalahari cratons connection. *Gondwana Research*, (52) 153-171.

Nesbitt, H., & Young, G. M. (1982). Early Proterozoic climates and plate motions inferred from major element chemistry of lutites. *Nature*, 299 (5885), 715-717.

O'Connor, J. M., & Duncan, R. A. (1990). Evolution of the Walvis Ridge - Rio Grande Rise hotspot system: Implications for African and South American plate motions over plumes. J*ournal of Geophysical Research: Solid Earth*, 95(B11), 17475-17502.

Okubo, J. (2019). *Evolução sedimentar e paleoambiental da Formação Sete Lagoas (Grupo Bambuí, norte de Minas Gerais) no contexto das bacias sedimentares do período Ediacarano terminal.* Doctoral Thesis. São Paulo State University, Rio Claro, 190 p.

Okubo, J., Muscente, A. D., Luvizotto, G. L., Uhlein, G. J., & Warren, L. V. (2018). Phosphogenesis, aragonite fan formation and seafloor environments following the Marinoan glaciation. *Precambrian Research*, (311), 24-36.

Oliveira, A.I., Leonardos, O. H. (1943), *Geologia do Brasil*. 2. ed. Rio de Janeiro.

Oliveira, E. P. (1918), Regiões carboníferas dos Estados do Sul. Bol. do Serviço Geológico e Mineralógico do Brasil, Rio de Janeiro. 125p. and one map.

Oliveira, E. P. (1927), Geologia e recursos minerais do Estado do Paraná. Serviço Geológico e Mineralógico do Brasil, Rio de Janeiro, Monografia VI. 172p., photos and maps.

Oliveira, M. A. F., Maniesi, V., Teixeira, W., & Daitx, E. C. (2002). Caracterização isotópica de metabasitos e anfibolitos dos grupos Açungui e Setuva na porção sul da Faixa Ribeira. *Geologia USP. Série Científica*, 2, 161-170.

Oliveira, M. A. F., Maniesi, V., Teixeira, W., & Daitx, E. C. (2002). Caracterização isotópica de metabasitos e anfibolitos dos grupos Açungui e Setuva na porção sul da Faixa Ribeira. *Geologia USP. Série Científica*, 2, 161-170.

Oliveira, M.A.F. de, Maniesi, V., Nardy, A.J.R., (2012). Litogeoquímica, química mineral e termobarometria do Metagabro de Apiaí, SP. *Geociências UNESP* 31 (4), 665e680.

Oliveira, R. S., Nogueira, A. C. R., Romero, G. R., Truckenbrodt, W., & da Silva Bandeira, J. C. (2019). Ediacaran ramp depositional model of the Tamengo Formation, Brazil. *Journal of South American Earth Sciences*, *96*, 102348.

Oriolo, S., Oyhantçabal, P., Basei, M. A., Wemmer, K., & Siegesmund, S. (2016). The Nico Pérez Terrane (Uruguay): From Archean crustal growth and connections with the Congo Craton to late Neoproterozoic accretion to the Río de la Plata Craton. *Precambrian Research*, 280, 147-160.

Oriolo, S., Oyhantçabal, P., Konopásek, J., Basei, M. A., Frei, R., Sláma, J., ... & Siegesmund, S. (2019). Late Paleoproterozoic and Mesoproterozoic magmatism of the Nico Pérez Terrane (Uruguay): tightening up correlations in southwestern Gondwana. *Precambrian Research*, 327, 296-313.

Oriolo, S., Oyhantçabal, P., Wemmer, K., & Siegesmund, S. (2017). Contemporaneous assembly of Western Gondwana and final Rodinia break-up: implications for the supercontinent cycle. *Geoscience Frontiers*, *8* (6), 1431-1445.

Owen-Smith, T. M., Ashwal, L. D., Sudo, M., & Trumbull, R. B. (2017). Age and petrogenesis of the Doros Complex, Namibia, and implications for early plume-derived melts in the Paraná–Etendeka LIP. *Journal of Petrology*, 58(3), 423-442.

Oyhantçabal, P., Oriolo, S., Philipp, R. P., Wemmer, K., & Siegesmund, S. (2018). The Nico Pérez Terrane of Uruguay and Southeastern Brazil. In *Geology of Southwest Gondwana* (pp. 161-188). Springer, Cham.

Oyhantçabal, P., Oriolo, S., Wemmer, K., Basei, M. A. S., Frei, D., & Siegesmund, S. (2021). Provenance of metasedimentary rocks of the western Dom Feliciano Belt in

Uruguay: Insights from U–Pb detrital zircon geochronology, Hf and Nd model ages, and geochemical data. *Journal of South American Earth Sciences*, 108, 103139.

Oyhantçabal, P., Sánchez Bettucci, L., Peçoits, E., Aubet, N., Peel, E., Preciozzi, F., & Basei, M. A. (2005). Nueva propuesta estratigráfica para las supracorticales del Cinturón Dom Feliciano (Proterozoico, Uruguay). In *XII Congreso Latinoamericano de Geologıa, Quito (CD-ROM*.

Oyhantçabal, P., Siegesmund, S., & Wemmer, K. (2011). The Río de la Plata Craton: a review of units, boundaries, ages and isotopic signature. *International Journal of Earth Sciences*, *100*(2), 201-220.

Oyhantçabal, P., Siegesmund, S., Wemmer, K., & Layer, P. (2010). The sierra ballena shear zone in the southernmost dom feliciano belt (Uruguay): evolution, kinematics, and deformation conditions. *International Journal of Earth Sciences*, 99(6), 1227-1246.

Oyhantçabal, P., Siegesmund, S., Wemmer, K., Presnyakov, S., & Layer, P. (2009). Geochronological constraints on the evolution of the southern Dom Feliciano Belt (Uruguay). *Journal of the Geological Society*, 166(6), 1075-1084.

Panahi, A., Young, G. M., & Rainbird, R. H. (2000). Behavior of major and trace elements (including REE) during Paleoproterozoic pedogenesis and diagenetic alteration of an Archean granite near Ville Marie, Quebec, Canada. *Geochimica et Cosmochimica Acta*, 64 (13), 2199-2220.

Parry, L. A., Boggiani, P. C., Condon, D. J., Garwood, R. J., Leme, J. D. M., McIlroy, D., ... & Liu, A. G. (2017). Ichnological evidence for meiofaunal bilaterians from the terminal Ediacaran and earliest Cambrian of Brazil. *Nature Ecology & Evolution*, *1* (10), 1455-1464.

Passarelli C.R, Basei MAS, Siga Jr. O, Harara MM (2018) The Luis Alves and Curitiba Terranes: Continental Fragments in the Adamastor Ocean. In: S. Siegesmund et al. (eds) Geology of Southwest Gondwana, *Regional Geology Reviews*, Springer, Heidelberg, 189–215.

Passarelli, C. R. (2001). Caracterização estrutural e geocronológica dos domínios tectônicos da porção sul-oriental do Estado de São Paulo. Doctoral dissertation, Universidade de São Paulo, São Paulo, 281p.

Passarelli, C. R., Basei, M. A. S., Neto, M. D. C. C., Júnior, O. S., & dos Prazeres Filho, H. J. (2004). Geocronologia e geologia isotópica dos terrenos Pré-Cambrianos da porção sul-oriental do Estado de São Paulo. *Geologia USP. Série Científica*, *4*(1), 55-74.

Passarelli, C. R., Basei, M. A. S., Siga, O., & Harara, O. M. M. (2018). The Luis Alves and Curitiba terranes: continental fragments in the Adamastor Ocean. In *Geology of Southwest Gondwana* (pp. 189-215). Springer, Cham.

Passarelli, C. R., Basei, M. A. S., Wemmer, K., Siga, O., & Oyhantçabal, P. (2011). Major shear zones of southern Brazil and Uruguay: escape tectonics in the eastern border of Rio de La plata and Paranapanema cratons during the Western Gondwana amalgamation. *International Journal of Earth Sciences*, *100*(2), 391-414.

Passarelli, C. R., Basei, M. A., Prazeres-Filho, H. J., Szabó, G. A., & Marco-Neto, J. (2007). Structural and geochronological constraints on the evolution of the Juréia

Massif, Registro Domain, State of São Paulo, Brazil. *Anais da Academia Brasileira de Ciências*, *79*(3), 441-455.

Passarelli, C. R., Verma, S. K., McReath, I., Basei, M. A., & Siga Jr., O. (2019). Tracing the history from Rodinia break-up to the Gondwana amalgamation in the Embu Terrane, southern Ribeira Belt, Brazil. *Lithos*, (342) 1-17.

Patias, D., Cury, L. F., & Siga Jr, O. (2019). Transpressional deformation during Ediacaran accretion of the Paranaguá Terrane, southernmost Ribeira Belt, western Gondwana. *Journal of South American Earth Sciences*, *96*, 102374.

Patias, D., Cury, L. F., Faleiros, F. M., Calderón, M., Siga Jr, O., & Theye, T. (2020). Late Neoproterozoic PTt paths of syn-and post-collisional metamorphism in the Paranaguá Terrane, Ribeira Belt (Brazil): implications for West Gondwana assembly. *International Geology Review*, 1-24.

Paula-Santos, G. M., da Cruz Campanha, G. A., Faleiros, F. M., Hollanda, M. H. B. M., & de Oliveira Rodrigues, S. W. (2021). Carbon isotope variations of high magnitude recorded in carbonate rocks from the Stenian-Tonian Lajeado Group, Southeast Brazil. *Journal of South American Earth Sciences*, (109) 103268.

Pedrosa-Soares, C. A., Vidal, P., Leonardos, O. H., & de Brito Neves, B. B. (1998). Neoproterozoic oceanic remnants in eastern Brazil: further evidence and refutation of an exclusively ensialic evolution for the Araçuaí–West Congo Orogen. *Geology*, *26* (6), 519-522.

Peel E, Preciozzi F (2006) Geochronologic synthesis of the Piedra Alta Terrane, Uruguay. V South American Symposium on Isotope Geology. Punta del Este, Uruguay, pp 234–237.

Pettijohn, F. J., Potter, P. E., & Siever, R. (2012). *Sand and sandstone*. Springer, Heiderberg.

Philipp, R. P., Pimentel, M. M., & Basei, M. A. S. (2018). The tectonic evolution of the São Gabriel terrane, Dom Feliciano belt, southern Brazil: the closure of the Charrua ocean. In *Geology of Southwest Gondwana* (pp. 243-265). Springer, Cham.

Pinto, R., & de Assis Janasi, V. (2014). Histórico do Conhecimento Geológico sobre o Pré-Cambriano Paulista até o ano de 1955. *Terrae Didática*, 10(1), 52-66. Raposo, M. I. B., & Ernesto, M. (1991). Paleomagnetism of the dykes of the Ponta Grossa arch. *Boletim IG-USP* (10), 85-89.

Piper, J. D. (2000). The Neoproterozoic supercontinent: Rodinia or Palaeopangaea? *Earth and Planetary Science Letters*, *176*(1), 131-146.

Piper, J. D. (2000). The Neoproterozoic supercontinent: Rodinia or Palaeopangaea? *Earth and Planetary Science Letters*, *176*(1), 131-146.

Pires, F. A. (1989). *Análise paleoambiental e estratigráfica de sequências metassedimentares (Grupo Açungui) na região de Iporanga e Apiaí – São Paulo*. Master dissertation, University of São Paulo, São Paulo, 151 p.

Pires, F. A. (2017). Faciologia e análise paleoambiental da Seqüência Deposicional Furnas-Lajeado (Gr. Açungui), de idade proterozóica. Revista Brasileira de Geociências, 21(4), 355-362.

Pisarevsky, S. A., Wingate, M. T., Powell, C. M., Johnson, S., & Evans, D. A. (2003). Models of Rodinia assembly and fragmentation. *Geological Society, London, Special Publications*, *206*(1), 35-55.

Poidevin, J. L. (2007). Stratigraphie isotopique du strontium et datation des formations carbonatées et glaciogéniques Néoprotérozoiques du Nord et de l'Ouest du craton du Congo. *Comptes Rendus Geoscience*, 339(3-4), 259-273.

Poiré, D. G. (1987). *Mineralogía y sedimentología de la Formación Sierras Bayas en el Núcleo Septentrional de las sierras homónimas, partido de Olavarría, provincia de Buenos Aires*. Doctoral Thesis, University of La Plata, La Plata, 271 p.

Poiré, D. G. (2004). Sedimentary history of the Neoproterozoic of Olavarría, Tandilia System, Argentina: new evidence from their sedimentary sequences and unconformities-A "snowball Earth" or a "phantom" glacial. In *1 Symposium on Neoproterozoic-Early Paleozoic Events in SW-Gondwana, Extended Abstracts*, 46-48.

Poiré, D. G. (2008). Marcadores geologicos regionales del Neoproterozoico de Olavarria, Sistema de Tandilia. In *XVII Congreso Geológico Argentino* 7 (10.10), 2008.

Poiré, D. G., & Gaucher, C. (2009). Lithostratigraphy. *Developments in Precambrian Geology*, (16), 87-101.

Poiré, D. G., & Spalletti, L. A. (2005). La cubierta sedimentaria precámbrica/paleozoica inferior del Sistema de Tandilia. In *Geología y Recursos Minerales de la provincial de Buenos Aires. Relatorio del XVI Congreso Geológico Argentino*, 51-68.

Poiré, D. G., Peral, L. E. G., & Arrouy, M. J. (2018). The Glaciations in South America. In *Geology of Southwest Gondwana*, 527-541. Springer, Heidelberg.

Praekelt, H. E., Germs, G. J. B., & Kennedy, J. H. (2008). A distinct unconformity in the Cango Caves Group of the Neoproterozoic to early Paleozoic Saldania Belt in South Africa: its regional significance. *South African Journal of Geology*, *111* (4), 357-368.

Prazeres Filho, H. J., Harara, O. M., Basei, M. A. S., Passarelli, C. R., & Siga Jr., O. (2003). Litoquímica, geocronologia U-Pb e geologia isotópica (Sr-Nd-Pb) das rochas graníticas dos batólitos Cunhaporanga e Três Córregos na porção sul do Cinturão Ribeira, Estado do Paraná. *Geologia USP. Série Científica*, (3), 51-70.

Preciozzi, F., & Peel, E. (2006). Geochronologic synthesis of the Piedra Alta Terrane, Uruguay.

Pruss, S. B., Bosak, T., Macdonald, F. A., McLane, M., & Hoffman, P. F. (2010). Microbial facies in a Sturtian cap carbonate, the Rasthof Formation, Otavi Group, northern Namibia. *Precambrian Research*, *181* (1-4), 187-198.

Ramos, V. A., Vujovich, G., Martino, R., & Otamendi, J. (2010). Pampia: a large cratonic block missing in the Rodinia supercontinent. *Journal of Geodynamics*, *50*(3-4), 243-255.

Rapalini, A. E., & Vilas, J. F. (1991a). Preliminary paleomagnetic data from the Sierra Grande Formation: Tectonic consequences of the first mid-Paleozoic paleopoles from Patagonia. *Journal of South American Earth Sciences*, *4*(1-2), 25-41.

Rapalini, A. E., & Vilas, J. F. (1991b). Tectonic rotations in the Late Palaeozoic continental margin of southern South America determined and dated by palaeomagnetism. *Geophysical Journal International*, *107*(2), 333-351.

Rapela, C. W., Fanning, C. M., Casquet, C., Pankhurst, R. J., Spalletti, L., Poiré, D., & Baldo, E. G. (2011). The Rio de la Plata craton and the adjoining Pan-African/brasiliano terranes: their origins and incorporation into south-west Gondwana. *Gondwana research*, *20*(4), 673-690.

Rapela, C. W., Pankhurst, R. J., Casquet, C., Fanning, C. M., Baldo, E. G., González-Casado, J. M., ... & Dahlquist, J. (2007). The Río de la Plata craton and the assembly of SW Gondwana. *Earth-Science Reviews*, *83*(1-2), 49-82.

Redivo, H. V., Mizusaki, A. M., & Santana, A. V. (2019). REE patterns and trustworthiness of stable carbon isotopes of Salitre Formation, Irecê Basin (Neoproterozoic), São Francisco Craton. *Journal of South American Earth Sciences*, (90), 255-264.

Reis Neto, J. M. D. (1994). *Faixa Itaiacoca: registro de uma colisão entre dois blocos continentais no Neoproterozóico*, Doctoral Thesis, University of São Paulo, São Paulo, 253 p.

Remus, M. V. D., Souza, R. S., Cupertino, J. A., De Ros, L. F., Dani, N., & Vignol-Lelarge, M. L. (2008). Proveniência sedimentar: métodos e técnicas analíticas aplicadas. *Revista Brasileira de Geociências*, 38(2 suppl), 166-185.

Renne, P. R., Deckart, K., Ernesto, M., Fe, G., & Piccirillo, E. M. (1996). Age of the Ponta Grossa dike swarm (Brazil), and implications to Paraná flood volcanism. *Earth and Planetary Science Letters*, 144(1-2), 199-211.

Ricardo, B. S., Faleiros, F. M., de Moraes, R., Júnior, O. S., & Campanha, G. A. (2020). Tectonic implications of juxtaposed high-and low-pressure metamorphic field gradient rocks in the Turvo-Cajati Formation, Curitiba Terrane, Ribeira Belt, Brazil. *Precambrian Research*, 345, 105766.

Riccomini, C. (1989). *O rift continental do sudeste do Brasil*, Doctoral Thesis, University of São Paulo, São Paulo, 256p.

Riccomini, C., & Assumpção, M. (1999). Quaternary tectonics in Brazil. *Episodes*, 22, 221-225.

Riccomini, C., Sant'Anna, L. G., & Ferrari, A. L. (2004). Evolução geológica do rift continental do sudeste do Brasil. Geologia do continente Sul-Americano: evolução da obra de Fernando Flávio Marques de Almeida, 383-405.

Rigoti, F.H. (*in prep*) *Caracterização hidrogeofísica de aquíferos no estado do Paraná*, Doctoral Thesis, Federal University of Paraná, Curitiba.

Rossetti, L., Lima, E. F., Waichel, B. L., Hole, M. J., Simões, M. S., & Scherer, C. M. (2018). Lithostratigraphy and volcanology of the Serra Geral Group, Paraná-Etendeka Igneous Province in southern Brazil: Towards a formal stratigraphical framework. *Journal of Volcanology and Geothermal Research*, 355, 98-114.

Rostirolla, S. P., Ahrendt, A., Soares, P. C., & Carmignani, L. (1999). Basin analysis and mineral endowment of the Proterozoic Itajaı Basin, south-east Brazil. *Basin Res*, *11*, 127-142.

Ruiz, R., Goguitchaichvili, A., Morales, J., Trindade, R. I. F., Alva Valdivia, L. M., & Urrutia-Fucugauchi, J. (2009). Absolute Thellier paleointensities from Ponta Grossa dikes (southern Brazil) and the early Cretaceous geomagnetic field strength. *Geofísica internacional*, 48(2), 243-251.Salamuni, E., Ebert, H. D., & Hasui, Y. (2016). Morfotectônica da bacia sedimentar de Curitiba. *Brazilian Journal of Geology*, 34(4), 469-478.

Salamuni, R., & Bigarella, J. J. (1967). Sumário das Estruturas Sedimentares Singenéticas no Grupo Açungui. *Boletim Paranaense de Geociências*, 23-25.

Sallun Filho, W., & Fairchild, T. R. (2005). Estudo comparativo entre estromatólitos do tipo Conophyton das Faixas Ribeira e Brasília. *Revista do Instituto Geológico*, *26*(1-2), 1-18.

Sánchez Bettucci L, Peel E, Oyhantçabal, P. (2010) Precambrian geotectonic units of the Río de La Plata craton. *Int Geol Rev*, 52:32–50.

Sanchez, E. A. M. (2014). *Microbialitos e microfósseis da Formação Sete Lagoas, Neoproterozoico, Brasil: implicações geomicrobiológicas em um contexto de mudanças climáticas e evolutivas*. Doctoral Thesis, University of São Paulo, São Paulo, 298 p.

Sánchez-Bettucci, L., Oyhantçabal, P., Loureiro, J., Ramos, V. A., Preciozzi, F., & Basei, M. A. S. (2004). Mineralizations of the Lavalleja Group (Uruguay), a probable Neoproterozoic volcano-sedimentary sequence. *Gondwana Research*, *7*(3), 745-751.

Sanders, C., & Grotzinger, J. (2021). Sedimentological and stratigraphic constraints on depositional environment for Ediacaran carbonate rocks of the São Francisco Craton: Implications for phosphogenesis and paleoecology. *Precambrian Research*, 363, 106328.

Santana, A. V. (2016). *Análise estratigráfica em alta resolução em rampa carbonática dominada por microbiolitos, Formação Salitre, Bacia de Irecê, Bahia*. Doctoral Thesis, University of Brasília, Brasília, 183 p.

Santos, J. O. S., Hartmann, L. A., Bossi, J., Campal, N., Schipilov, A., Piñeyro, D., & McNaughton, N. J. (2003). Duration of the Trans-Amazonian Cycle and its correlation within South America based on U-Pb SHRIMP geochronology of the La Plata Craton, Uruguay. *International Geology Review*, *45*(1), 27-48.

Santos, J. O. S., Hartmann, L. A., Gaudette, H. E., Groves, D. I., Mcnaughton, N. J., & Fletcher, I. R. (2000). A new understanding of the provinces of the Amazon Craton based on integration of field mapping and U-Pb and Sm-Nd geochronology. *Gondwana Research*, *3*(4), 453-488.

Santos, J. O. S., Potter, P. E., Reis, N. J., Hartmann, L. A., Fletcher, I. R., & McNaughton, N. J. (2003). Age, source, and regional stratigraphy of the Roraima Supergroup and Roraima-like outliers in northern South America based on U-Pb geochronology. *Geological Society of America Bulletin*, *115*(3), 331-348.

Santos, J. O. S., Rizzotto, G. J., Potter, P. E., McNaughton, N. J., Matos, R. S., Hartmann, L. A., ... & Quadros, M. E. S. (2008). Age and autochthonous evolution of the Sunsás Orogen in West Amazon Craton based on mapping and U–Pb geochronology. *Precambrian Research*, *165*(3-4), 120-152.

Santos, J. O., Chernicoff, C. J., Zappettini, E. O., McNaughton, N. J., & Hartmann, L. A. (2017). Large geographic and temporal extensions of the Río de la Plata Craton,

South America, and its metacratonic eastern margin. *International Geology Review*, *61*(1), 56-85.

Santos, L. D. R., Leandro, R., Bahniuk, A., & Cury, L. F. (2018). Low-temperature metamorphism in the Capiru Formation, Morro Grande Synform, Southern Ribeira Belt. *Brazilian Journal of Geology*, *48* (1), 95-113.

Santos, L.D.R., Leandro, R., Fedalto, G., Spisila, A., Bahniuk, A. M., Siga, O., & Cury, L. F. (2021). The Capiru Group: From passive margin to syn-orogenic units, implications for the evolution of the northern margin of the Curitiba microplate, Western Gondwana. *Journal of South American Earth Sciences*, 103555.

Santos, L.D.R., Spisila, A.L., Patias, D., Bongiolo, A.B.S., Szameizat, L. Cury, L.F. (2021). The Geology of the Capiru Group, Curitiba Terrane, Southern Ribeira Belt, Brazil. *Journal of Maps, in press.*

Sato, K., Basei, M. A. S., Júnior, O. S., Sproesser, W. M., & Passarelli, C. R. (2008). Novas técnicas aplicadas ao método U-Pb no CPGeo-IGc/USP: avanços na digestão química, espectrometria de massa (TIMS) e exemplos de aplicação integrada com SHRIMP. *Geologia USP. Série Científica*, *8*(2), 76-99.

Sato, K., Siga Jr, O., da Silva, J. A., McReath, I., Dunyi, L., Iizuka, T., ... & Basei, M. A. S. (2009). Análises in situ de U e Pb em zircão por SHRIMP II por controle remoto e de Hf por LA-ICP-MS: um exemplo de datação e da evolução genética de zircão através da razão 176Hf/177Hf em amostra da pedreira Ita no Complexo Atuba, SE Brasil. *Geologia USP. Série Científica*, *9*(3), 61-69.

Sato, K., Siga Jr, O., Nutman, A. P., Basei, M. A., McReath, I., & Kaulfuss, G. (2003). The Atuba complex, Southern South American platform: archean components and paleoproterozoic to neoproterozoic tectonothermal events. *Gondwana Research*, *6* (2), 251-263.

Saylor, B. Z., Kaufman, A. J., Grotzinger, J. P., & Urban, F. (1998). A composite reference section for terminal Proterozoic strata of southern Namibia. *Journal of Sedimentary Research*, *68*(6), 1223-1235.

Schmitt, R.S., de Araújo Fragoso, R., & Collins, A. S. (2018). Suturing Gondwana in the Cambrian: the orogenic events of the final amalgamation. In Geology of Southwest Gondwana, 411-432. Springer, Heidelberg.

Seth, B., Armstrong, R. A., Brandt, S., Villa, I. M., & Kramers, J. D. (2003). Mesoproterozoic U–Pb and Pb–Pb ages of granulites in NW Namibia: reconstructing a complete orogenic cycle. *Precambrian Research*, 126(1-2), 147-168.

Shanmugam, G. (2017). Global case studies of soft-sediment deformation structures (SSDS): Definitions, classifications, advances, origins, and problems. *Journal of Palaeogeography*, *6* (4), 251-320.

Shukowsky, W., Mantovani, M. S. M., Ferreira, F., Guimarães, G. B., Alves, L. S., & Ulbrich, H. (2006). Estudos gravimétricos na região do Arco de Ponta Grossa, Paraná, Brasil meridional. In Anais. Geociências e as sociedades do futuro (p. 255). Aracaju: SBG Núcleo Bahia-Sergipe. Book of Abstracts.

Sial, A. N., Gaucher, C., Misi, A., Boggiani, P. C., Alvarenga, C. J. S. D., Ferreira, V. P., ... & Cezario, W. D. S. (2016). Correlations of some Neoproterozoic carbonate-dominated successions in South America based on high-resolution chemostratigraphy. *Brazilian Journal of Geology*, *46* (3), 439-488.

Siga Jr O, Faleiros FM, Campanha GAC, Basei MAS, Sato K, Passarelli CR (2014) Neoproterozoic records in metasedimentary sequenceof Turvo-Cajati Complex (S-SE Brazil): U-Pb detrital zircon geochronology. In: 9th South American Symposium on Isotope Geology, São Paulo, vol 219. Book of Abstracts.

Siga Jr, O. (1995). Domínios tectônicos do sudeste do Paraná e nordeste de Santa Catarina: geocronologia e evolução crustal. Doctoral Thesis, University of São Paulo, São Paulo, 212p.

Siga Jr, O., Basei, M. Â. S., Passarelli, C. R., Harara, O. M., Sato, K., Cury, L. F., & dos Prazeres Filho, H. J. (2007). Geocronologia de rochas gnáissico-migmatíticas e sienograníticas do Núcleo Setuva (Pr): implicações tectônicas. *Brazilian Journal of Geology*, 37 (1), 114-128.

Siga Jr, O., Basei, M. Â. S., Passarelli, C. R., Harara, O. M., Sato, K., Cury, L. F., & dos Prazeres Filho, H. J. (2016). Geocronologia de rochas gnáissico-migmatíticas e sienograníticas do Núcleo Setuva (Pr): implicações tectônicas. *Revista Brasileira de Geociências*, 37 (1), 114-128.

Siga Jr, O., Basei, M. A. S., Passarelli, C. R., Sato, K., Cury, L. F., & McReath, I. (2009). Lower and Upper Neoproterozoic magmatic records in Itaiacoca Belt (Paraná-Brazil): Zircon ages and lithostratigraphy studies. *Gondwana Research*, *15* (2), 197-208.

Siga Jr, O., Basei, M. A. S., Sato, K., dos Prazeres Filho, H. J., Cury, L. F., Weber, W., Passareli, C. R., Harara, O. M., & dos Reis Neto, J. M. (2003). U-Pb (Zircon) ages of metavolcanic rocks from the Itaiacoca Group: tectonic implications. *Geologia USP. Série Científica*, (3), 39-49.

Siga Jr, O., Basei, M. A. S., Sato, K., Passarelli, C. R., Nutman, A., McReath, I., & dos Prazeres Filho, H. J. (2011a). Calymmian (1.50–1.45 Ga) magmatic records in Votuverava and Perau sequences, south-southeastern Brazil: Zircon ages and Nd–Sr isotopic geochemistry. *Journal of South American Earth Sciences*, *32* (4), 301-308.

Siga Jr, O., Basei, M. A., & Machiavell, A. (1993). Evolução geotectônica da porção NE de Santa Catarina e SE do Paraná, com base em interpretações geocronológicas. *Brazilian Journal of Geology*, *23*(3), 215-223.

Siga Jr, O., Basei, M. S., Neto, J. R., Machiavelli, A., & Harara, O. M. (1995). O Complexo Atuba: um cinturão Paleoproterozóico intensamente retrabalhado no Neoproterozóico. *Boletim do Instituto de Geociências - USP, Série Científica*, (26) 69-98.

Siga Jr, O., Basei, M. S., Neto, J. R., Machiavelli, A., & Harara, O. M. (1995). O Complexo Atuba: um cinturão Paleoproterozóico intensamente retrabalhado no Neoproterozóico. *Boletim IG-USP. Série Científica*, *26*, 69-98.

Siga Jr, O., Campanha, G. D. C., Faleiros, F. M., Basei, M. A. S., Sato, K., Dantas, E., & McReath, I. (2012). Detrital Zircon U-Pb and Hafnio Geochronology from the Capiru and Turvo-Cajati Formations (S-SE Brazil): Tectonic Implications. In *VIII South American Symposium on Isotope Geology—SSAGI*. 302.

Siga Jr, O., Cury, L. F., McReath, I., Ribeiro, L. M. D. A. L., Sato, K., Basei, M. Â. S., & Passarelli, C. R. (2011b). Geology and geochronology of the Betara region in

south-southeastern Brazil: evidence for possible Statherian (1.80–1.75 Ga) and Calymmian (1.50–1.45 Ga) extension events. *Gondwana Research*, *19* (1), 260-274.

Siga Jr., O., Basei, M. Â. S., Passarelli, C. R., Harara, O. M., Sato, K., Cury, L. F., & dos Prazeres Filho, H. J. (2007). Geocronologia de rochas gnáissico-migmatíticas e sienograníticas do Núcleo Setuva (Pr): implicações tectônicas. *Brazilian Journal of Geology*, 37(1), 114-128.

Silva, I. E. da. (2010). *Estromatólitos Neoproterozoicos registrados no conjunto litológico Rio Branco (Formação Capiru, Grupo Açungui)*. Master dessertation, Federal University of Paraná, Curitiba.

Silva, L.C. (1987). Geologia do pré-cambriano/eo-paleozóico de Santa Catarina. In: Silva, L.C. & Bortoluzzi, C.A. eds. Texto explicativo para o Mapa Geológico do Estado de Santa Catarina. Florianópolis, CPRM. p. 12-90.

Siqueira, R.; Hollanda, M. H. B. M.; Basei, M. A. S. A novel approach to (LA-ICP-MS acquired) U-Th-Pb data processing. In: SOUTH AMERICAN SYMPOSIUM ON ISOTOPE GEOLOGY, 9, 2014, São Paulo. Program and Abstracts... São Paulo: Centro de Pesquisas Geocronológicas, 2014. v. 1, p. 306.

Strugale, M., Rostirolla, S. P., Mancini, F., Portela Filho, C. V., Ferreira, F. J. F., & de Freitas, R. C. (2007). Structural framework and Mesozoic–Cenozoic evolution of Ponta Grossa Arch, Paraná Basin, southern Brazil. *Journal of South American Earth Sciences*, 24(2-4), 203-227.Sato, K., Siga Jr, O., Nutman, A. P., Basei, M. A.,

Sundell, K. E., Gehrels, G. E., & Pecha, M. E. (2021). Rapid U-Pb Geochronology by Laser Ablation Multi-collector ICP-MS. *Geostandards and Geoanalytical Research*, *45*(1), 37-57.

Taylor, S. R., & McLennan, S. M. (1985). The continental crust: its composition and evolution. Blackwell, Oxford (1985), 312 p.

Teixeira, W., Geraldes, M. C., Matos, R., Ruiz, A. S., Saes, G., & Vargas-Mattos, G. (2010). A review of the tectonic evolution of the Sunsás belt, SW Amazonian Craton. *Journal of South American Earth Sciences*, *29*(1), 47-60.

Theodorovicz, A., Câmara, M. M., Morais, S. M., Godoy, H. K., & Takahashi, A. T. (1986). Projeto Engenheiro Maia-Ribeirão Branco–Relatório Final. *CPRM/PRÓ MINÉRIO, unpublished report*.

Tupinambá, M., Heilbron, M., Duarte, B. P., Nogueira, J. R., Valladares, C., Almeida, J., Silva, L. G. E., Medeiros, S. R. de, Almeida, C. G. de, Miranda, A., Ragatky, C. D., Mendes, J., & Ludka, I. (2007). Geologia da Faixa Ribeira Setentrional: estado da arte e conexões com a Faixa Araçuaí. *Geonomos*, 15 (1), 67-79

Van Schijndel, V., Cornell, D. H., Frei, D., Simonsen, S. L., & Whitehouse, M. J. (2014). Crustal evolution of the Rehoboth Province from Archaean to Mesoproterozoic times: insights from the Rehoboth Basement Inlier. *Precambrian Research*, *240*, 22-36.

Vieira, L. C., Almeida, R. P., Trindade, R. I., Nogueira, A. C., & Janikian, L. (2016). A Formação Sete Lagoas em sua área-tipo: fácies, estratigrafia e sistemas deposicionais. *Revista Brasileira de Geociências*, 37 (4), 168-181.

Vieira, T. A. T., da Silva Schmitt, R., Mendes, J. C., Moraes, R., Luvizotto, G. L., de Andrade Silva, R. L., ... & de Medeiros, S. R. (2022). Contrasting PTt paths of

basement and cover within the Búzios Orogen, SE Brazil–Tracking Ediacaran-Cambrian subduction zones. *Precambrian Research*, 368, 106479.

Warren, L. V., Fairchild, T. R., Gaucher, C., Boggiani, P. C., Poire, D. G., Anelli, L. E., & Inchausti, J. C. (2011). Corumbella and in situ Cloudina in association with thrombolites in the Ediacaran Itapucumi Group, Paraguay. *Terra Nova*, 23 (6), 382-389.

Watters, W. A., & Grotzinger, J. P. (2001). Digital reconstruction of calcified early metazoans, terminal Proterozoic Nama Group, Namibia. *Paleobiology*, *27* (1), 159-171.

Weber, W., Júnior, O. S., Sato, K., dos Reis Neto, J. M., Basei, M. A. S., & Nutman, A. P. (2004). A Formação Água Clara na Região de Araçaíba-SP: registro U-Pb de uma bacia mesoproterozóica. *Geologia USP. Série Científica*, 4(1), 101-110.

Williams, I. S., & Claesson, S. (1987). Isotopic evidence for the Precambrian provenance and Caledonian metamorphism of high grade paragneisses from the Seve Nappes, Scandinavian Caledonides. *Contributions to Mineralogy and Petrology*, 97(2), 205-217.

Yamato, A. A. (1999). *Mapeamento geológico de parte da Folha Bocaiúva do Sul (SG. 22-XDI-2), escala 1: 50.000*, Masters dissertation, University of São Paulo, 108 p.

Yonkee, W. A., Dehler, C. D., Link, P. K., Balgord, E. A., Keeley, J. A., Hayes, D. S., ... & Johnston, S. M. (2014). Tectono-stratigraphic framework of Neoproterozoic to Cambrian strata, west-central US: Protracted rifting, glaciation, and evolution of the North American Cordilleran margin. *Earth-Science Reviews*, *136*, 59-95.

Young, G. M., & Nesbitt, H. W. (1998). Processes controlling the distribution of Ti and Al in weathering profiles, siliciclastic sediments and sedimentary rocks. Journal of Sedimentary research, 68 (3), 448-455.

Zalán, P. V., and Oliveira, J. A. (2005). Origem e evolução estrutural do Sistema de Riftes Cenozóicos do Sudeste do Brasil. *Boletim de Geociências da PETROBRAS*, 13(2), 269-300.

Zanella, R. R., Trzaskos, B., de Castro, L. G., & Ferreira, F. J. F. (2020). Geophysical-structural framework of the Campo Alegre basin (Santa Catarina State, southern Brazil). *Journal of Applied Geophysics*, *183*, 104189.

Zanella, R. R., Trzaskos, B., de Castro, L. G., & Ferreira, F. J. F. (2020). Geophysical-structural framework of the Campo Alegre basin (Santa Catarina State, southern Brazil). *Journal of Applied Geophysics*, *183*, 104189.

Zou, J., Rezaee, R., Xie, Q., & You, L. (2019). Characterization of the combined effect of high temperature and moisture on methane adsorption in shale gas reservoirs. *Journal of Petroleum Science and Engineering*, *182*, 106353.

ANEXO 1 – MAPA GEOLÓGICO DO GRUPO CAPIRU

THE GEOLOGY OF THE CAPIRU GROUP, CURITIBA TERRANE, SOUTHERN RIBEIRA BELT (BRAZIL)

Santos, L.D.R.[1,2], Spisila, A.L.[3], Patias, D.[4], Bongiolo, A.B.S.[1,5], Szameitat, L.[1,5], Cury, L.F.[1,2]

1: Department of Geology, Federal University of Paraná (Brazil); 2: LAMIR Institute; 3: CPRM: Geological Survey of Brazil;
4: School of Earth and Environmental Sciences, University of Queensland (Australia); 5: LPGA - Laboratory of Research in Applied Geophysics.

© Journal of Maps, 2021

Funded by the Capiru Project (*Projeto Capiru*), CNPq 481429/2013 - UFPR; Diagenesis Project, UPFR - Shell - FUNPAR; Microbial Project, UFPR - PETROBRAS - FUNPAR.

CAPIRU GROUP - LITHOSTRATIGRAPHIC UNITS

BOCAINA FORMATION

- meta-heteroliths, including arkosic sandstone/silt and quartz sandstone/silt couplets
- m-thick interbeds of arkose and quartz-sandstones

MORRO GRANDE FORMATION

- upper Morro Grande interval, composed of tabular beds of meta quartz sandstones
- middle and lower intervals, including metacarbonaceous claystones, heteroliths and tabular beds of sandstones, finely laminated iron-rich mudstones and claystones

MORRO AZUL FORMATION

- carbonaceous meta-mudstones, finely laminated
- discontinuous metacarbonaceous mudstones and wedge--shaped lenses of very coarse-grained and pebbly conglomeratic sandstones, laminated dolostone, and metric beds of columnar stromatolites, teepee structures, contraction cracks, and laminated dolostones

RIO BRANCO FORMATION

- metabauxites, metalaterites and metacarbonaceous mudstones, graphite-schists and discontinuous lenses of paragneisses
- metadolostones (grainstones, wackstones and packstones), marbles and breccias
- quartz-sandstones and orthoquartzites
- finely laminated metamudstones and dolostones, calk-silicate rocks, and para-derivated amphibolites

JURUQUI FORMATION

- finely laminated ferruginous metamudstones and banded iron formations
- ferruginous metasandstones, orthoquartzites and arkose metasandstones

SANTANA FORMATION

- ferruginous metamudstones, phyllites and schists
- meta- sandstones and arkose sandstones, quartzites and muscovite-schists
- quartz metasandstones and othoquartzites.

BASEMENT

SETUVA COMPLEX

- quartz-muscovite schists
- quartz-muscovite-biotite schists and biotite-schists
- mylonitic syenogranites, deformed syenogranites and quartz-syenogranites
- syenogranitic gneisses
- syenogranites

- Cities
- Road (BR-476)
- Contour (100m)
- A-D Structural sections
- Bedding plane trend
- Fe Banded Fe-formations
- Stromatolite

STRUCTURES

- Transcurrent fault
- Approximated transcurrent fault
- Thrust fault
- Approximated thrust fault
- Inferred thrust fault
- Dykes with thicknesses representative on the scale
- Dyke-traces

CONTACTS

- Defined
- Approximated
- Inferred

Projection: Transverse Mercator
Datum SIRGAS 2000 UTM Zone 22S
Geographic Coordinate System: GCS SIRGAS 2000

Mapped at 1:5000 to 1:25000. Additional information from the interpretation of airborne magnetometric and gammaspectrometric survey by the Geologic Survey of Brazil (CPRM, 2010), see text for details, and the synthetic aperture radar (SAR-RTC) of the PALSAR - one of the three instruments on the Advanced Land Observing Satellite-1 (ALOS), a mission of the Japan Aerospace Exploration Agency (JAXA,2021). Base map compiled from DSG (Brazil), 1:25.000 topographic base, (MI-2841 and MI-2842 squares, 2004), through the BDGEX. Geological bases are from the files of the MINEROPAR (Geological Survey of Paraná State, Brazil, http://www.iat.pr.gov.br/Pagina/Mapeamento-Geologico, in Portuguese), and CPRM (Geological Survey of Brazil) records.

Figure A. Structural map of study area on a Digital Elevation Model. See main map for detail of local geology. MASZ: Morro Agudo Shear Zone; LSZ: Lancinha Shear Zone. MGSZ: Morro Grande Shear Zone.

Figure B. Regional geological and tectonic framework of the Southern Ribeira Belt (after Basei et al. 2008): 1: Alkaline complexes, (2-6) APIAÍ TERRANE - 2: Molasse basins of Castro Group and Camarinha Formation, 3: Granites, 4: Neoproterozoic successions, 5: Neoproterozoic granites (CP: Cunhaporanga and TC: Três Córregos Complexes); 6: Statherian units, (7-10) CURITIBA AND LUÍS ALVES TERRANE - 7: Extensional basins and granites, 8: Neoproterozoic successions (including Capiru Group and Turvo-Cajati Complex), 9: Reworked Rhyacian orthogneisses, migmatites (Atuba Complex) and Rhyacian gneisses, 10: Orthogneisses and granulites; (11-12) PARANAGUÁ TERRANE - 11: Neoproterozoic granites, 12: Meso- to Neoproterozoic successions, LSZ: Lancinha Shear Zone, SAS: Setuva Antiform Structure, PSZ: Piên Suture Zone.

Figure C. Location of the Ribeira Belt within the framework of the Western Gondwana around 550 Ma (after Gray et al. 2007, Brito Neves et al. 2014, Oriolo et al. 2017).

Figure D. Structural section A-A' across the Setuva Antiform Structure (SAS), showing the structural relationships between the basement rocks (Setuva Complex) and the Capiru Group metasedimentary cover.

Geology of the Capiru Group. June, 2021.

ANEXO 2 – FORMALIZAÇÃO DAS UNIDADES SEGUNDO O CÓDIGO ESTRATIGRÁFICO

Formalization of the Capiru Group formations following the stratigraphic code

Name	*Santana Formation*
Name derivation	Type area located near the Santana Hill
Category & rank	Lithostratigraphic Formation, formerly included in the Setuva Fm (Bigarella & Salamuni 1956, 1958).
Type area	Head of Santana Hill (Yamato 1999; this work), Santana River region. UTM 22S 683867/7221076, elev. 1096 m.
Unit and boundary reference section	SE of Lança district, city of Rio Branco do Sul. UTM 22S 680753/7218940 (Lorena Hill), 683420/7221932, 686852/7221002. Lower boundary (UTM 22S 687531/7221381): structural, by Bocaina thrust fault, poorly exposed; imbricated towards Bocaina Fm. schists and phyllites. Upper boundary (UTM 684848/7223692): depositional contact with Rio Branco Fm. Marbles. Sharp, parallel to the S0 bedding. W. boundary: same as the upper boundary (between Santana/ Rio Branco Fm). E. boundary (UTM 22S 690128/7211696) : transitional with the Juruqui Fm.
Lower boundary reference location	UTM 22S 687531/7221381, W of Campo Novo district, city of Rio Branco do Sul.
Unit description (preserved sedimentary features)	Divide into 2 informal intervals: **Lower interval**: includes a lower succession of medium- to fine-grained tabular quartz-sandstone beds, 1 to 3 m-thick, laterally continuous for up to 20 m. The sandstone Santana lithofacies display, from bottom to top: horizontal lamination/ low-angle cross-stratification, symmetrical ripple cross-lamination, and wavy bedding. Swalley and hummocky cross-stratification commonly occur in the upper parts of succession. This facies association transitions upwards to the Santanta ferruginous mudstone beds. The contact between the lower and upper intervals is sharp. **Upper interval:** consists of laminated ferruginous mudstones, laterally persistent and flat.
Unit description, metamorphic features	The Santana Fm. is a quartzite-rich unit (basal interval), white to yellow, almost totally recrystallized. The quartzite composition is mainly quartz, white mica and chlorite. The purple phyllites, and muscovite-schist (upper interval) are ferruginous (~15% of magnetite). The upper interval shows extensive development of metamorphic foliation, where the composite S1//S2 foliation is the main metamorphic surface. Quartz veins (up to 3 m) and iron-rich venules are common throughout the unit.
Dimensions	~750 m-thick at the reference section, > than 1300 m in unrestored length (outcropping thickness).
Geologic age	Unknown
Correlations	The Santana Fm. may pass into the Juruqui Fm (towards W).

Name	*Juruqui Formation*
Name derivation	Type-area formerly suggested nearby the Juruqui River (city of Campo Magro), in Fiori (1992).
Category & rank	Lithostratigraphic Formation, formerly referenced as 'Juruqui Assemblage', that originally included all the ferruginous metapelites of the Capiru area.
Type area	We suggest two different type-sections, aiming to include the previous type-area (Fiori, 1992) and a new one, standardizing the name throughout the region: i) Juruqui River type-section (exemplifying the formerly 'Juruqui Assemblage' of Fiori (1992). UTM 22S 665959/7195224, elev. 1010 m.

	ii) Passa Vinte River type-section (exemplifying the rocks now encompassed into this unit). UTM 22S 701139/7224306, elev. 968 m.
Unit and boundary reference section	BR-476, north of Rio Branco do Sul, displaying the transition between Santana and Juruqui formations, UTM 22S 690128/7211696; Juruqui reforestation area, Bocaiúva do Sul, contact between basement and Juruqui Form. given by the Setuva thrust/ transcurrent fault, UTM 22S 698134/7223418; Cachoeirinha River region, depositional contact between Juruqui and Rio Branco formations, UTM 22S 659984/7193518. Lower boundary (UTM 22S 690128/7211696): structural, by Setuva thrust fault, poorly exposed; imbricated towards Atuba Complex basement rocks. Upper boundary (UTM 659984/7193518): contact with Rio Branco Fm. marbles. The upper contact is sharp, parallel to the S0 bedding. Often structurally controlled (by transcurrent faults parallel to the S0 bedding). E. boundary: interpreted through Setuva thrust fault; W. boundary (UTM 22S 690128/7211696): transitional with the Santana Fm.
Lower boundary reference location	UTM 22S 690128/7211696, W of São Pedro district, city of Bocaiúva do Sul.
Unit description (preserved sedimentary features)	Divide into 3 informal intervals: **Lower interva**l: it is mainly constituted of tabular beds of coarse- to medium-grained arkose sandstones with lenses of conglomeratic feldspathic and quartz sandstones. The coarse-grained sandstones are poorly sorted, and frequently trough cross-stratified. The immature coarse-grained deposits finally pass into moderately well sorted, medium-grained sandstones with asymmetric wave ripples on the bed tops. **Middle interva**l: consists of m- coarsening-upward cycles of laminated medium-grained sandstones to ferruginous mudstones in dm-scale beds. The only recognized sedimentary structures are the planar lamination, and normal-graded beds in the sandstone beds. Towards the top, the occurrence of dm ferriferous laminated beds interbedded with variable amounts of clastic Fe-coated quartz sand grains (GIFs?) becomes common. **Upper interval**: consists of monotonous ferruginous muddy siltstones interbedded with finely laminated mudstones. Up to 0.5-m-thick beds of continuous interbedded chert and hematite layers are also common.
Unit description, metamorphic features	The Juruqui Fm. is mainly a metapelitic ferruginous unit. Quartzites are impure and restricted to lens bodies. The red sericite-phyllites are ferruginous (~15% of magnetite). The upper interval shows extensive development of metamorphic foliation, where the composite S1 foliation is the main metamorphic surface. Quartz veins (up to 3 m) and iron-rich venules are common throughout the unit.
Dimensions	~700 m-thick at the reference section, > than 3,000 m in unrestored length.
Geologic age	Unknown
Correlations	The Santana Fm. may pass into the Juruqui Fm (towards W).

Name	*Rio Branco Formation*
Name derivation	Type-area formerly suggested in the Rio Branco do Sul region (Bigarella and Salamuni, 1956).
Category & rank	Lithostratigraphic Formation, formerly referenced as 'Rio Branco Assemblage' of Fiori (1992), a term that used to include all the carbonate units of the Capiru area.
Type area	Quarries of Rio Branco do Sul region. Rio Branco type-section, Pedreira do Bom Jardim quarry, UTM 22S 669754/7206394, elev. 1045 m.
Unit and boundary reference section	Sharp depositional contact between Juruqui and Rio Branco formations (UTM 22S 659984/7193518), north to the PR-90 Road, access in 16832 m of PR-90, city of

	Campo Magro. Rio Branco oolitic dolostones occurrences (UTM 22S 679573/7209262), PR-417 quarries. Rio Branco dolostone/ metasandstone interbeds (UTM 22S 671500/ 7206625), city of Rio Branco do Sul. Areias district. Lower boundary (UTM 22S 693267.24/7215671.73): unconformity Santana-Rio Branco formations, poorly exposed. Cabeça da Anta locality, city of Bocaiúva do Sul. Lower boundary (UTM 22S 659984/7193518): unconformity between Juruqui and Rio Branco formations, access in 16832 m of PR-90, city of Campo Magro. Upper boundary (UTM 675766.77/7207081): contact with Morro Azul Fm. marbles. The upper contact is structurally controlled, sub-parallel to the S0 bedding, given by the Morro Grande Shear Zone. E. boundary: sharp contact, with Juruqui Formation. W. boundary (UTM 675766.77/7207081): structural with Morro Azul Formation, through Morro Grande Shear Zone.
Lower boundary reference location	UTM 22S 693267.24/7215671.73, W of Cabeça da Anta locality, city of Bocaiúva do Sul.
Unit description (preserved sedimentary features)	Divide into 2 informal intervals: **Lower interval:** the lower interval of Rio Branco Fm. is mainly constituted by ooid and intraclast grainstone beds, with horizontal lamination, symmetric ripples, planar, trough, and hummocky cross-stratification upsection. **Upper interval:** is predominantly composed of finely laminated dolograinstone/ packstone-shale and wackestone-siltstone interbedded with cm- massive to nodular mudstone beds. The uppermost part comprises a ~10-m-thick succession of cm-thick stacked beds of muddy dolostone interbedded with dolostone shale and siltstone, which becomes increasingly shale-rich towards the top.
Unit description, metamorphic features	The Rio Branco Fm. is a dolomitic marble unit interbedded with orthoquartzites lenses. Mineral recrystallization is extensively developed. Calcite and quartz venulation is a common feature. Meta-marls and calk-silicate rocks are common at the top.
Dimensions	~700 m-thick, > than 3500 m in unrestored length.
Geologic age	MDAs of 2,100 My (Basei et al., 2008).
Correlations	None

Name	*Morro Azul Formation*
Name derivation	Type-area formerly suggested in the Morro Azul region, city of Almirante Tamandaré.
Category & rank	Lithostratigraphic Formation, formerly referenced as 'Rio Branco Assemblage' of Fiori (1992), a term used to include all the carbonate units of the Capiru area.
Type area	Quarries of Morro Azul region. Morro Azul type-section, Polical quarry, UTM 22S 680851/7207379, elev. 966 m. Includes the metadolomites of the Bacaetava karstic domain, an important geosite of the region.
Unit and boundary reference section	Structural contact between Rio Branco and Morro Azul formations (UTM 22S 675766/7207081), PR-417 Road, Morro Grande region, city of Colombo. Carbonaceous metapelites of the basal Morro Azul interval (UTM 22 S 672784/7214000); Morro Azul conglomeratic sandstone lags (basal interval, key-bed overlying the Morro Grande disconformity), UTM 22S 688437/7209893. Morro Azul microbial mats (formerly described as a Rio Branco Assemblage - Guimarães et al. 2002), UTM 22 S 676272/7207144. Morro azul stromatolitic dolostones (formerly described in the Rio Branco Assemblage), UTM 22 S 679447/ 7207797, later included in the Morro Grande Assemblage (Fiori and Gaspar, 1993).

	Lower boundary (UTM 22S 671549/7200511): Morro Azul disconformity and damage zone of Morro Grande Shear Zone (UTM 22S 676150.41/7207455.28). Morro Grande locality, city of Colombo. Lower boundary (UTM 22S 693603.277/7228601.270): Morro Grande Shear Zone damage zone, access through BR-476 road. Campestre locality, city of Bocaiúva do Sul. Upper boundary (UTM 22S 680050.00/7207139): contact with Morro Grande Fm. metapelites. The upper contact is depositional, sharp, and parallel to the S0 bedding. E. boundary: structurally controlled, given by Morro Grande Shear Zone, with the Rio Branco Formation. W. boundary: sharp, with Morro Grande Formation.
Lower boundary reference location	UTM 22S UTM 22S 671549/7200511, south of PR-417 road, Morro Grande locality, city of Colombo.
Unit description (preserved sedimentary features)	Divide into 3 informal intervals: **Lower interval**: is constituted by a basal and discontinuous interval of poorly laminated carbonaceous mudstones and wedge-shaped bodies of very coarse-grained and pebbly conglomeratic sandstones. **Middel interval:** it is the most representative interval, composed of intensely laminated dolostone and metric beds of columnar stromatolites, often bifurcated, scattered in isolated m-biohermes. Structures such as contraction cracks, teepees, intraformational breccias and laminated mudstones with fenestral porosity are seen upsection. **Upper interval**: is constituted of mm- to cm-laminated dolostone defined by alternation of darker/lighter couplets and carbon-rich mudstones.
Unit description, metamorphic features	The Morro Azul Fm. is mainly a dolomitic marble unit. The basal interval includes quartzites and carbonaceous phyllites and schists.
Dimensions	~550 m-thick, > than 3200 m in unrestored length.
Geologic age	Unknown
Correlations	None

Name	*Morro Grande Formation*
Name derivation	Type-area formerly suggested in the Morro Grande region, city of Colombo.
Category & rank	Lithostratigraphic Formation, formerly referenced as 'Morro Grande Assemblage' of Fiori (1992), a term used to describe the rhythmic units of the Capiru area plus the stromatolitic metadolostone bodies (Fiori and Gaspar, 1993), the lasts, now included into the Morro Azul Formation.
Type area	Morro Grande Synform region Morro Grande type-section, Morro Grande quarry, UTM 22S 680446.00/7206383.00, elev. 987 m.
Unit and boundary reference section	Sharp, depositional contact between Morro Azul and Morro Grande formations (UTM 22S UTM 22S 680050.00/7207139), PR-417 Road, Morro Grande region, city of Colombo. Morro Grande meta-rhythmites (UTM 22 S 681859/7202020 and 661726/7196030). Morro Grande metasandstones (UTM 22 S 678177/7207274). Lower boundary (UTM 22S 680050.00/7207139): sharp, depositional contact between Morro Azul and Morro Grande formations. Morro Grande locality, city of Colombo. Upper boundary: consists of the uppermost unit of the Capiru Group in the Morro Grande Synform Structure region. Upper boundaries include angular unconformities with Cambrian (Camarinha Fm.), Tertiary (Guabirotuba Fm) and Quaternary deposits. E. boundary: sharp contact with Morro Azul Formation. W. boundary: May include structural contact (given by Morro Grande Shear Zone structure) with Rio Branco Formation marls, where Morro Azul Formation is not present.

Lower boundary reference location	UTM 22S UTM 22S 680050.00/7207139, Morro Grande quarry, Morro Grande locality, city of Colombo.
Unit description (preserved sedimentary features)	Divide into 3 informal intervals: **Lower interval:** consists of carbonaceous claystone, heterolithic facies and sandstones. The laminated, organic carbon-rich claystone is interbedded with mudstone (C/M heterolith) or fine-grained sandstone layers (C/S). The sandstone facies show horizontal lamination, ripple cross-lamination and rare cross-stratification in concave-up base sets with conglomeratic sandstone lags. **Middle interval:** is characterized by monotonous finely laminated iron-rich mudstones, showing cm- scattered clay rounded clasts. **Upper interval:** constituted of fine-grained tabular quartz-sandstone beds The sandstones are constituted of sub-rounded to rounded grains, planar laminated and continuous for more than 25 m.
Unit description, metamorphic features	The Morro Grande formation is composed of metapelites and metasandstones with extensive development of S1 foliation, developed under low-grade conditions.
Dimensions	~500 m-thick, > than 2100 m in unrestored length.
Geologic age	MDAs of 1,100 My (Cury et al., 2017).
Correlations	None

Name	*Bocaina Formation*
Name derivation	Type area located near the Bocaina Hill
Category & rank	Lithostratigraphic Formation, formerly included in the Setuva Fm (Bigarella & Salamuni 1956, 1958).
Type area	Head of Bocaina Hill (Fiori et al. 1992, Yamamato 1999, this work), Passa Vinte River region. UTM 22S 700115/7226670, elev. 1394 m.
Unit and boundary reference section	W of São Pedro district, city of Bocaiúva do Sul. UTM 22S 700297.82/7227529.92; 704385.67/7229093.45; 702138.32/7230082.82 Lower boundary (UTM 22S 700574/7225121): structural, by Setuva thrust fault, poorly exposed; imbricated towards Setuva Core schists and deformed granitoids; Upper boundary: consists of the uppermost unit of the Capiru Group in the Northern Setuva Antiform Structure region. Upper boundaries include angular unconformities with Quaternary deposits. W. boundary (UTM 22S 693928/7224647): structural, given by Bocaina thrust fault; E. boundary: same as lower boundary (Setuva thrust fault).
Lower boundary reference location	UTM 22S 700574/7225121, no geographic reference
Unit description (preserved sedimentary features)	Divide into 3 informal intervals: **Lower interval:** m-thick interbeds of arkose and quartz-sandstones. Arkose is white to yellow, texturally and compositionally immature, organized in dm-thick lenticular amalgamated stacks with erosive, concave bases and sharp upper surfaces, often capped with cm- to dm-thick, planar laminated, sandy mudstones. Trough cross-strata are often seen. Quartz-sandstone is either (a) white medium to coarse-grained, well to sub-rounded organized in lenticular to sigmoidal beds; or (b) yellow fine-grained sandstones, that fines upward into siltstone. The lower interval base is structurally controlled. The upper contact is sharp into the Middle interval. **Middle interval:** arkose and quartz-sandstones, laterally continuous, tabular, upward-fining, texture and compositionally immature to mature transitioned, organized in 5 to 50 cm tabular beds, with abrupt top and bases. Occurrence of detrital euhedral feldspar grains along the bed bases. Planar lamination is the most common sedimentary

	structure, followed by planar cross-stratification, and asymmetric ripples at the top sets. The upper contact is transitional into the Upper interval. **Upper interval:** White and red to purple arkose/gray silt and quartz-sandstone/gray silt couplets with sharp basal and upper contact. Fine-grained interbeds are laterally continuous, wavy laminated sets are common at the upper sets.
Unit description, metamorphic features	The lower Bocaina Fm. boundary is marked by a phyllonitic unit of highly deformed muscovite-biotite schists derived from Setuva Domains ortho-derivate basement rocks. The lower interval is constituted of white impure quartzites, with feldspar grains and granitic granules. The middle interval is represented by yellow tabular beds of impure quartzites with euhedral K-feldspar grains and ortho-quartzites. Towards the top, the schistosity overprints most of the sedimentary features. The upper interval includes rhythmic phyllites and slates, greenish, with extensive development of metamorphic foliation, where the composite S1//S2 foliation is the main metamorphic surface. Quartz veins and iron-rich venules are common throughout the unit.
Dimensions	~650 m-thick at the reference section, > than 2500 m in unrestored length.
Geologic age	Unknown
Correlations	None.

ANEXO 3 – DADOS ISOTÓPICOS

9/24/2019	SPOT	SITE	RATIOS																AGES						
117X-16A - QUARTZITO IM			207/235	1sigma	206/238	1 sigma	coef. corr	238/206	1 sigma	207/206	1 sigma	208/206	1 sigma	Pb total	Pb rad	Th	U	Th/U	$T_{206/238}$	1 sigma	$T_{207/235}$	1 sigma	$T_{207/206}$	1 sigma	Conc.
J-61 - MARCELA														comum	ppm	ppm	ppm								206/238
SPL2784 , Analyte Excite 193nm Excimer Laser Ablation System, 6Hz, 6mJ, 20µm, 100% Energia, Hélio: MFC1=0.300L/min, MFC2=0.300L/min.														%											207/235
SPL 2967	54.1		4.5974	0.0565	0.2832	0.0043	0.99	3.5306	0.0532	0.1177	0.0026	0.2219	0.0093	2.51	23	81	89	0.91	1608	22	1749	11	1922	40	91
SPL 2967	10.1		5.1466	0.0852	0.3003	0.0019	0.99	3.3298	0.0206	0.1243	0.0021	0.1916	0.0089	0.00	40	94	125	0.75	1693	9	1844	13	2019	30	91
SPL 2967	90.1		5.1677	0.1154	0.3121	0.0039	0.99	3.2037	0.0397	0.1201	0.0034	0.1875	0.0067	0.00	40	132	111	1.19	1751	19	1847	20	1957	50	94
SPL 2967	92.1		5.5527	0.1172	0.3191	0.0044	0.99	3.1338	0.0431	0.1262	0.0038	0.2770	0.0143	1.97	36	249	120	2.08	1785	22	1909	20	2046	53	93
SPL 2967	43.1		5.4258	0.0858	0.3311	0.0030	0.99	3.0199	0.0270	0.1188	0.0022	0.1874	0.0115	1.29	50	184	161	1.15	1844	14	1889	14	1939	33	97
SPL 2967	80.1		6.3947	0.1152	0.3448	0.0039	0.96	2.9004	0.0326	0.1345	0.0026	0.1466	0.0170	3.96	12	37	29	1.28	1910	19	2032	16	2158	34	93
SPL 2967	97.1		6.2710	0.1071	0.3467	0.0016	0.99	2.8845	0.0132	0.1312	0.0020	0.1558	0.0033	0.83	83	206	198	1.04	1919	8	2014	14	2114	27	95
SPL 2967	87.1		6.5069	0.1113	0.3542	0.0038	0.98	2.8235	0.0301	0.1332	0.0022	0.2119	0.0088	0.00	17	44	41	1.08	1955	18	2047	15	2141	28	95
SPL 2967	100.1		6.0195	0.1257	0.3562	0.0025	0.86	2.8077	0.0200	0.1226	0.0026	0.1738	0.0057	0.10	25	35	61	0.58	1964	12	1979	18	1994	38	99
SPL 2967	35.1		6.5343	0.1505	0.3573	0.0023	0.97	2.7985	0.0180	0.1326	0.0029	0.1996	0.0070	0.90	18	35	49	0.71	1970	11	2051	20	2133	38	96
SPL 2967	5.1		6.6849	0.1397	0.3665	0.0024	0.99	2.7282	0.0176	0.1323	0.0028	0.0866	0.0033	0.50	56	50	159	0.32	2013	11	2071	18	2128	36	97
SPL 2967	98.1		6.3461	0.1630	0.3721	0.0024	0.47	2.6874	0.0170	0.1237	0.0032	0.2179	0.0083	0.66	17	44	41	1.08	2039	11	2025	22	2010	45	100
SPL 2967	29.1		6.4855	0.1818	0.3736	0.0036	0.41	2.6769	0.0261	0.1259	0.0035	0.2233	0.0142	3.00	12	28	27	1.01	2046	17	2044	25	2042	51	100
SPL 2967	13.1		7.0173	0.1088	0.3744	0.0024	0.99	2.6713	0.0172	0.1360	0.0022	0.1117	0.0119	2.12	18	10	62	0.15	2050	11	2114	13	2176	29	96
SPL 2967	38.1		6.3935	0.0976	0.3764	0.0028	0.89	2.6564	0.0199	0.1232	0.0020	0.1648	0.0026	0.67	66	176	165	1.07	2060	13	2031	13	2003	29	101
SPL 2967	42.1		6.9583	0.1048	0.3766	0.0029	0.98	2.6557	0.0205	0.1340	0.0023	0.1759	0.0123	1.50	25	43		0.72	2060	14	2106	13	2151	30	97
SPL 2967	67.1		6.3938	0.1431	0.3772	0.0037	0.22	2.6509	0.0257	0.1229	0.0024	0.1859	0.0049	1.69	21	39	50	0.77	2063	17	2031	20	1999	35	101
SPL 2967	40.1		7.0981	0.1157	0.3786	0.0034	0.99	2.6414	0.0236	0.1360	0.0024	0.3998	0.0699	0.00	57	335	374	0.90	2070	16	2124	15	2177	31	97
SPL 2967	63.1		6.9986	0.1426	0.3798	0.0041	0.99	2.6329	0.0287	0.1336	0.0021	0.2040	0.0086	1.05	31	118	118	1.00	2075	19	2111	18	2146	28	98
SPL 2967	62.1		6.4773	0.1222	0.3850	0.0037	0.99	2.5977	0.0248	0.1220	0.0020	0.2280	0.0096	2.25	29	106	132	0.80	2099	17	2043	17	1986	30	102
SPL 2967	73.1		7.3063	0.1576	0.3863	0.0031	0.76	2.5886	0.0205	0.1372	0.0026	0.2389	0.0428	7.28	35	66	60	1.09	2106	14	2150	19	2192	33	97
SPL 2967	**45.1**		**7.1512**	**0.0993**	**0.3873**	**0.0029**	**0.99**	**2.5823**	**0.0194**	**0.1339**	**0.0022**	**0.1839**	**0.0067**	**0.40**	**78**	**154**	**169**	**0.91**	**2110**	**14**	**2130**	**13**	**2150**	**29**	**99**
SPL 2967	24.1		7.3066	0.0895	0.3931	0.0024	0.99	2.5440	0.0157	0.1348	0.0019	0.1037	0.0100	1.32	52	69	138	0.50	2137	11	2150	11	2162	24	99
SPL 2967	69.1		7.0622	0.1146	0.3933	0.0027	0.88	2.5427	0.0173	0.1302	0.0025	0.1705	0.0654	0.00	28	33	47	0.69	2138	12	2119	16	2101	34	100
SPL 2967	12.1		7.4206	0.1105	0.3938	0.0030	0.97	2.5395	0.0192	0.1367	0.0025	0.1523	0.0116	0.71	53	131	135	0.97	2140	14	2163	14	2185	32	98
SPL 2967	9.1		7.4541	0.1395	0.3955	0.0039	0.86	2.5287	0.0252	0.1367	0.0030	0.2541	0.0082	0.39	14	34	30	1.15	2148	18	2167	17	2186	38	99
SPL 2967	33.1		7.3676	0.1711	0.3971	0.0027	0.54	2.5180	0.0171	0.1345	0.0029	0.1753	0.0101	0.87	18	26	41	0.63	2156	12	2157	21	2158	37	99
SPL 2967	15.1		7.5005	0.1413	0.3985	0.0030	0.45	2.5096	0.0189	0.1365	0.0027	0.1920	0.0053	0.28	22	43	47	0.90	2162	14	2173	17	2184	34	99
SPL 2967	3.1		7.5061	0.1802	0.3988	0.0035	0.93	2.5078	0.0223	0.1365	0.0033	0.1694	0.0118	0.74	13	22	28	0.77	2163	16	2174	22	2184	42	99
SPL 2967	81.1		7.6145	0.1462	0.3999	0.0034	0.95	2.5007	0.0215	0.1381	0.0026	0.1248	0.0085	3.51	12	18	32	0.56	2169	16	2187	18	2204	33	99
SPL 2967	17.1		7.4730	0.1227	0.3999	0.0043	0.81	2.5004	0.0266	0.1355	0.0023	0.1808	0.0172	0.00	21	40	46	0.87	2169	20	2170	15	2171	29	99
SPL 2967	23.1		7.5210	0.1074	0.4007	0.0028	0.47	2.4957	0.0174	0.1361	0.0021	0.1401	0.0027	0.00	26	34	60	0.57	2172	13	2175	13	2179	26	99
SPL 2967	41.1		7.5896	0.1257	0.4009	0.0039	0.61	2.4946	0.0243	0.1373	0.0025	0.2014	0.0076	2.94	18	28	41	0.70	2173	18	2184	15	2194	33	99
SPL 2967	72.1		8.3926	0.1760	0.4016	0.0037	0.85	2.4898	0.0229	0.1516	0.0031	0.7838	0.2740	0.00	0	1	24	0.05	2177	17	2274	19	2364	35	95
SPL 2967	7.1		7.4753	0.1557	0.4021	0.0028	0.99	2.4870	0.0174	0.1348	0.0030	0.1895	0.0152	1.00	27	60	63	0.96	2179	13	2170	20	2162	39	100
SPL 2967	26.1		7.5292	0.1142	0.4028	0.0030	0.68	2.4826	0.0182	0.1356	0.0023	0.2783	0.0064	0.37	27	67	55	1.22	2182	14	2176	14	2171	29	100
SPL 2967	22.1		7.5269	0.1189	0.4032	0.0030	0.50	2.4802	0.0186	0.1354	0.0020	0.2614	0.0057	0.20	27	61	55	1.11	2184	14	2176	14	2169	25	100
SPL 2967	48.1		7.4838	0.1061	0.4036	0.0033	0.98	2.4777	0.0201	0.1345	0.0022	0.1966	0.0078	1.55	31	65	69	0.95	2186	15	2171	13	2157	29	100
SPL 2967	89.1		7.6088	0.1770	0.4046	0.0062	0.65	2.4716	0.0377	0.1364	0.0039	0.1839	0.0069	0.65	20	36	44	0.82	2190	28	2186	21	2182	49	100
SPL 2967	60.1		7.4989	0.1206	0.4067	0.0046	0.99	2.4588	0.0280	0.1337	0.0024	0.2179	0.0282	0.29	52	185	115	1.60	2200	22	2173	16	2147	32	101
SPL 2967	56.1		7.5711	0.0973	0.4071	0.0040	0.99	2.4563	0.0240	0.1349	0.0019	0.1308	0.0048	0.58	62	106	209	0.51	2202	19	2181	12	2162	25	100
SPL 2967	95.1		7.7063	0.1458	0.4072	0.0024	0.95	2.4560	0.0144	0.1373	0.0026	0.1389	0.0087	0.81	18	22	43	0.50	2202	11	2197	17	2193	32	100
SPL 2967	21.1		8.9850	0.1510	0.4121	0.0037	0.82	2.4266	0.0219	0.1581	0.0025	0.1702	0.0181	0.19	29	64	56	1.13	2224	17	2336	16	2436	27	95
SPL 2967	32.1		7.7120	0.1616	0.4131	0.0030	0.42	2.4209	0.0176	0.1354	0.0026	0.1922	0.0044	0.99	18	29	39	0.74	2229	14	2198	19	2169	34	101
SPL 2967	61.1		7.7021	0.1381	0.4141	0.0048	0.92	2.4147	0.0282	0.1349	0.0026	0.1567	0.0058	0.57	23	42	55	0.76	2234	22	2197	16	2163	33	101
SPL 2967	19.1		7.7867	0.1273	0.4142	0.0032	0.69	2.4140	0.0185	0.1363	0.0019	0.2005	0.0035	0.86	38	71	82	0.87	2234	14	2207	15	2181	25	101
SPL 2967	58.1		7.7372	0.1258	0.4146	0.0046	0.94	2.4122	0.0265	0.1354	0.0022	0.1807	0.0060	1.45	45	99	106	0.94	2236	21	2201	15	2169	28	101
SPL 2967	75.1		7.9704	0.1496	0.4199	0.0027	0.92	2.3814	0.0155	0.1377	0.0024	0.1733	0.0027	0.53	40	67	90	0.75	2260	12	2228	17	2198	31	101
SPL 2967	30.1		7.9416	0.1622	0.4210	0.0027	0.97	2.3754	0.0154	0.1368	0.0026	0.1393	0.0071	0.46	33	61	81	0.75	2265	12	2224	19	2187	34	101
SPL 2967	53.1		8.4303	0.1924	0.4363	0.0082	0.72	2.2918	0.0431	0.1401	0.0048	0.0593	0.0670	0.00	15	29	29	0.99	2334	37	2278	21	2229	58	102
SPL 2967	93.1		8.2671	0.2145	0.4434	0.0069	0.93	2.2552	0.0349	0.1352	0.0042	0.1615	0.0081	0.78	16	27	36	0.73	2366	31	2261	24	2167	54	104
SPL 2967	6.1		9.8601	0.3455	0.4570	0.0055	0.14	2.1883	0.0264	0.1565	0.0055	0.1773	0.0196	1.39	10	20	20	1.05	2426	24	2422	32	2418	59	100
SPL 2967	18.1		10.1670	0.2257	0.4605	0.0044	0.87	2.1716	0.0209	0.1601	0.0033	0.1273	0.0153	0.43	10	10	19	0.54	2442	20	2450	21	2457	35	99
SPL 2967	20.1		10.5850	0.1800	0.4707	0.0039	0.98	2.1246	0.0176	0.1631	0.0024	0.1509	0.0231	1.15	26	58	56	1.04	2486	17	2487	16	2488	25	99
SPL 2967	44.1		10.6677	0.1811	0.4779	0.0047	0.83	2.0925	0.0205	0.1619	0.0029	0.1400	0.0175	0.94	19	28	35	0.80	2518	20	2495	16	2476	30	100

SPL 2967	85.1	10.8732	0.1966	0.4784	0.0060	0.81	2.0904	0.0262	0.1648	0.0028	0.1424	0.0092	0.03	13	14	24	0.57	2520	26	2512	16	2506	29	100
SPL 2967	88.1	16.5130	0.2301	0.5388	0.0040	0.99	1.8561	0.0136	0.2223	0.0027	0.1074	0.0051	0.67	30	36	62	0.57	2778	17	2907	13	2997	20	95
SPL 2967	66.1	18.4880	0.3430	0.5970	0.0065	0.97	1.6750	0.0183	0.2246	0.0035	0.1188	0.0288	0.44	35	43	52	0.83	3018	26	3015	18	3014	25	100
SPL 2967	96.1	18.4598	0.3147	0.5978	0.0032	0.86	1.6729	0.0088	0.2240	0.0037	0.1137	0.0085	0.70	40	42	60	0.71	3021	13	3014	16	3009	26	100
SPL 2967	14.1	18.7116	0.2872	0.6005	0.0047	0.33	1.6653	0.0131	0.2260	0.0038	0.1160	0.0101	0.26	32	28	48	0.58	3032	19	3027	15	3024	27	100
SPL 2967	28.1	22.4311	0.2975	0.6476	0.0051	0.92	1.5442	0.0123	0.2512	0.0036	0.1651	0.0080	0.98	26	23	35	0.64	3219	20	3203	13	3193	23	100
SPL 2967	31.1	24.6005	0.4679	0.6833	0.0036	0.69	1.4635	0.0078	0.2611	0.0043	0.1037	0.0028	0.00	63	43	83	0.52	3357	14	3292	19	3254	25	101
SPL 2967	34.1	1.3407	0.0334	0.1046	0.0009	0.94	9.5567	0.0782	0.0929	0.0019	0.1196	0.0359	0.21	21	-2	79	-0.03	642	5	864	13	1486	39	74
SPL 2967	91.1	1.5099	0.0503	0.1190	0.0019	0.99	8.3999	0.1374	0.0920	0.0029	0.1344	0.0658	0.00	37	63	44	1.43	725	11	934	17	1467	53	77
SPL 2967	59.1	1.6912	0.0382	0.1255	0.0017	0.99	7.9657	0.1105	0.0977	0.0017	0.1084	0.0153	4.04	73	306	793	0.39	762	10	1005	11	1581	29	75
SPL 2967	74.1	1.8508	0.0487	0.1365	0.0010	0.99	7.3241	0.0528	0.0983	0.0019	0.0947	0.0081	1.84	34	81	92	0.88	825	5	1064	14	1592	34	77
SPL 2967	37.1	2.2115	0.0386	0.1432	0.0010	0.99	6.9832	0.0495	0.1120	0.0021	0.1939	0.0284	13.06	52	43	289	0.15	863	6	1185	12	1832	31	72
SPL 2967	8.1	2.2034	0.0475	0.1478	0.0011	0.99	6.7666	0.0493	0.1081	0.0023	0.0908	0.0233	1.85	52	110	165	0.67	889	6	1182	15	1768	39	75
SPL 2967	2.1	2.8167	0.0570	0.1783	0.0012	0.99	5.6076	0.0386	0.1146	0.0024	0.1835	0.0093	27.62	29	246	306	0.81	1058	7	1360	16	1873	40	77
SPL 2967	51.1	3.1147	0.0544	0.1901	0.0016	0.94	5.2609	0.0429	0.1188	0.0021	0.1785	0.0113	6.02	44	178	206	0.86	1122	8	1436	13	1939	32	78
SPL 2967	71.1	3.1512	0.0957	0.1942	0.0022	0.99	5.1499	0.0597	0.1177	0.0022	0.1548	0.0229	4.55	33	93	125	0.74	1144	11	1445	15	1922	29	79
SPL 2967	76.1	3.3533	0.0644	0.1995	0.0015	0.98	5.0116	0.0377	0.1219	0.0024	0.1265	0.0211	5.07	40	132	192	0.69	1173	8	1494	16	1984	36	78
SPL 2967	16.1	3.8121	0.0899	0.2058	0.0021	0.99	4.8590	0.0500	0.1343	0.0022	0.0947	0.0290	6.30	31	198	193	1.03	1206	11	1595	15	2155	27	75
SPL 2967	27.1	3.4115	0.0448	0.2107	0.0014	0.98	4.7462	0.0305	0.1174	0.0017	0.2120	0.0109	7.90	52	261	260	1.00	1233	7	1507	11	1918	26	81
SPL 2967	99.1	3.6448	0.0600	0.2160	0.0009	0.99	4.6302	0.0202	0.1224	0.0020	0.3239	0.0960	16.96	45	42	152	0.28	1261	5	1559	13	1991	30	80
SPL 2967	57.1	3.4665	0.0634	0.2179	0.0024	0.99	4.5892	0.0506	0.1154	0.0020	0.1248	0.0329	0.31	57	9	80	0.11	1271	13	1520	13	1886	29	83
SPL 2967	82.1	4.6717	0.1470	0.2233	0.0039	0.96	4.4786	0.0784	0.1517	0.0042	0.1098	0.0272	0.00	6	-27	4	-7.87	1299	19	1762	20	2366	46	73
SPL 2967	49.1	3.2196	0.0575	0.2340	0.0018	0.99	4.2727	0.0336	0.0998	0.0022	0.2228	0.0403	0.00	33	24	-52	-0.46	1356	10	1462	12	1620	32	92
SPL 2967	52.1	3.1343	0.0644	0.2349	0.0029	0.99	4.2579	0.0530	0.0968	0.0023	0.1771	0.0468	0.00	23	-47	-5	8.69	1360	15	1441	13	1563	32	94
SPL 2967	94.1	4.2560	0.1171	0.2412	0.0041	0.99	4.1465	0.0712	0.1280	0.0045	0.2075	0.0307	0.00	9	3	14	0.21	1393	22	1685	23	2071	60	82
SPL 2967	11.1	4.1090	0.0684	0.2418	0.0015	0.99	4.1362	0.0258	0.1233	0.0023	0.1961	0.0248	4.96	28	100	227	0.44	1396	8	1656	14	2004	34	84
SPL 2967	55.1	4.2608	0.0811	0.2457	0.0040	0.99	4.0696	0.0655	0.1258	0.0033	0.2013	0.0124	3.17	19	89	76	1.18	1416	20	1686	15	2040	46	84
SPL 2967	65.1	4.5040	0.1033	0.2524	0.0031	0.93	3.9627	0.0483	0.1294	0.0024	0.1941	0.0410	1.87	29	128	100	1.28	1451	15	1732	17	2090	33	83
SPL 2967	86.1	5.8663	0.1006	0.2562	0.0026	0.99	3.9038	0.0394	0.1661	0.0021	0.1495	0.0106	0.00	34	5	-15	-0.32	1470	13	1956	13	2519	21	75
SPL 2967	36.1	4.3730	0.0927	0.2567	0.0016	0.99	3.8954	0.0235	0.1235	0.0022	0.1692	0.0146	1.49	21	15	43	0.34	1473	8	1707	16	2008	31	86
SPL 2967	79.1	4.2535	0.0893	0.2571	0.0021	0.98	3.8892	0.0315	0.1200	0.0027	0.1453	0.1403	2.58	40	84	133	0.63	1475	11	1684	19	1956	40	87
SPL 2967	39.1	4.8519	0.0814	0.2783	0.0022	0.99	3.5933	0.0283	0.1264	0.0022	0.1655	0.0062	0.07	29	24	33	0.73	1583	11	1794	14	2049	30	88
SPL 2967	70.1	4.8633	0.1115	0.2799	0.0020	0.97	3.5726	0.0258	0.1260	0.0030	0.1545	0.0318	2.47	21	59	66	0.90	1591	10	1796	22	2043	44	88
SPL 2967	25.1	4.8289	0.0721	0.2836	0.0020	0.99	3.5257	0.0247	0.1235	0.0018	0.2388	0.0104	0.00	30	35	51	0.68	1610	10	1790	12	2007	25	89
SPL 2967	46.1	7.7882	0.1046	0.2887	0.0022	0.98	3.4637	0.0263	0.1956	0.0030	0.1183	0.0155	0.49	89	87	281	0.31	1635	11	2207	12	2790	25	74
SPL 2967	1.1	5.3866	0.1293	0.2924	0.0026	0.99	3.4198	0.0306	0.1336	0.0032	0.2091	0.0180	7.54	21	89	99	0.90	1654	13	1883	20	2146	42	87
SPL 2967	4.1	5.3586	0.1237	0.2976	0.0029	0.99	3.3600	0.0329	0.1306	0.0033	0.2416	0.0092	3.76	13	32	37	0.87	1680	14	1878	20	2106	44	89
SPL 2967	77.1	5.5644	0.1092	0.3097	0.0019	0.99	3.2288	0.0203	0.1303	0.0023	0.1729	0.0268	0.00	75	-184	148	-1.24	1739	10	1911	17	2102	30	91
SPL 2967	50.1	6.9891	0.0997	0.3393	0.0028	0.99	2.9473	0.0241	0.1494	0.0024	0.1441	0.0197	0.00	46	47	103	0.46	1883	13	2110	12	2339	28	89
SPL 2967	84.1	7.0541	0.1048	0.3436	0.0028	0.99	2.9106	0.0241	0.1489	0.0021	0.1100	0.0139	1.18	32	32	99	0.33	1904	14	2118	13	2333	24	89
SPL 2967	47.1	6.3731	0.0962	0.3492	0.0026	0.88	2.8639	0.0215	0.1324	0.0022	0.2146	0.2504	55.03	81	59	118	0.50	1931	13	2029	13	2130	29	95
SPL 2967	78.1	6.4793	0.1558	0.3606	0.0041	0.07	2.7735	0.0316	0.1303	0.0033	0.1557	0.0569	19.35	8	0	10	0.03	1985	20	2043	21	2102	45	97
SPL 2967	64.1	7.0069	0.1322	0.3636	0.0040	0.91	2.7503	0.0303	0.1398	0.0022	0.4471	0.1621	35.02	48	81	84	0.96	1999	19	2112	17	2224	28	94
SPL 2967	83.1	8.0724	0.1106	0.3872	0.0031	0.98	2.5827	0.0208	0.1512	0.0021	0.1524	0.0179	3.31	28	-3	63	-0.04	2110	15	2239	13	2360	23	94
SPL 2967	68.1	4.6987	0.0914	0.2821	0.0025	0.99	3.5442	0.0316	0.1208	0.0022	0.1998	0.0210	4.01	13	-2	20	-0.09	1602	13	1767	15	1968	33	90

9/24/2019	SPOT	SITE						RATIOS											AGES						
177-X-18A1 - QUARTZITO I		207/235	1sigma	206/238	1 sigma	coef. corr	238/206	1 sigma	207/206	1 sigma	208/206	1 sigma	Pb total comum %	Pb rad ppm	Th ppm	U ppm	Th/U	$T_{206/238}$	1 sigma	$T_{207/235}$	1 sigma	$T_{207/206}$	1 sigma	Conc. 206/238	
J-61 - MARCELA MENDES																								207/235	
SPL2966 , Analyte Excite 193nm Excimer Laser Ablation System, 6Hz, 6mJ, 20µm, 100% Energia, Hélio: MFC1=0.300L/min, MFC2=0.300L/min.																									
SPL 2966	40.1	5.5752	0.0997	0.3070	0.0041	0.97	3.2576	0.0434	0.1317	0.0022	0.1608	0.0651	3.39	71	247	217	1.14	1726	19	1912	13	2121	29	90	
SPL 2966	62.1	4.7620	0.0962	0.3241	0.0027	0.67	3.0858	0.0253	0.1066	0.0018	0.1686	0.0067	1.58	21	46	63	0.74	1810	13	1778	17	1742	31	101	
SPL 2966	5.1	5.9488	0.1366	0.3250	0.0035	0.94	3.0772	0.0335	0.1328	0.0031	0.2154	0.0157	2.45	20	84	52	1.62	1814	17	1968	20	2135	41	92	
SPL 2966	11.1	5.5729	0.1446	0.3297	0.0056	0.96	3.0330	0.0511	0.1226	0.0031	0.2229	0.0715	0.00	8	16	21	0.78	1837	26	1912	21	1994	44	96	
SPL 2966	73.1	6.2791	0.1177	0.3481	0.0027	0.99	2.8728	0.0221	0.1308	0.0021	0.2349	0.0166	1.99	42	89	78	1.15	1925	13	2016	17	2109	28	95	
SPL 2966	37.1	7.1839	0.1306	0.3482	0.0030	0.99	2.8721	0.0248	0.1496	0.0026	0.1777	0.0409	0.25	27	90	66	1.36	1926	14	2135	16	2342	29	90	
SPL 2966	63.1	5.8778	0.1462	0.3497	0.0029	0.85	2.8595	0.0241	0.1219	0.0026	0.2358	0.0109	2.57	22	63	52	1.22	1933	14	1958	22	1984	38	98	
SPL 2966	58.1	6.1823	0.1757	0.3533	0.0037	0.01	2.8306	0.0295	0.1269	0.0035	0.2399	0.0216	0.00	11	28	26	1.09	1950	18	2002	25	2056	48	97	
SPL 2966	59.1	6.2229	0.1182	0.3568	0.0026	0.98	2.8026	0.0203	0.1265	0.0025	0.3014	0.0770	0.00	20	72	61	1.19	1967	12	2008	18	2050	35	97	
SPL 2966	60.1	6.7174	0.1261	0.3574	0.0025	0.99	2.7982	0.0198	0.1363	0.0026	0.1693	0.0151	1.20	42	204	160	1.27	1970	12	2075	17	2181	33	94	
SPL 2966	95.1	6.6125	0.1232	0.3580	0.0033	0.84	2.7930	0.0254	0.1339	0.0021	0.1841	0.0080	1.56	25	65	58	1.13	1973	15	2061	16	2150	27	95	
SPL 2966	50.1	6.2391	0.1141	0.3594	0.0030	0.01	2.7827	0.0235	0.1259	0.0024	0.1749	0.0062	0.00	26	57	66	0.87	1979	14	2010	16	2042	35	98	
SPL 2966	3.1	6.2664	0.1537	0.3612	0.0036	0.01	2.7688	0.0277	0.1258	0.0026	0.1965	0.0122	2.21	14	32	33	0.98	1988	17	2014	21	2041	37	98	
SPL 2966	23.1	6.2539	0.1666	0.3617	0.0041	0.33	2.7651	0.0315	0.1254	0.0035	0.2446	0.0147	0.44	16	35	40	0.88	1990	19	2012	23	2035	51	98	
SPL 2966	46.1	6.2554	0.1905	0.3622	0.0046	0.65	2.7612	0.0354	0.1253	0.0041	0.3254	0.0177	0.88	8	28	18	1.59	1992	22	2012	27	2033	59	99	
SPL 2966	31.1	6.2943	0.1367	0.3637	0.0027	0.74	2.7493	0.0208	0.1255	0.0025	0.1964	0.0063	0.51	41	92	100	0.92	2000	13	2018	19	2036	35	99	
SPL 2966	30.1	6.6051	0.1547	0.3645	0.0027	0.82	2.7436	0.0202	0.1314	0.0030	0.1640	0.0141	0.87	27	36	69	0.52	2003	13	2060	21	2117	40	97	
SPL 2966	97.1	6.2177	0.1192	0.3660	0.0038	0.80	2.7326	0.0282	0.1232	0.0022	0.1891	0.0041	0.58	22	51	53	0.97	2010	18	2007	17	2003	31	100	
SPL 2966	70.1	6.3555	0.1078	0.3664	0.0029	0.78	2.7292	0.0216	0.1258	0.0020	0.1052	0.0178	2.25	25	30	69	0.44	2012	14	2026	15	2040	29	99	
SPL 2966	80.1	6.6363	0.0934	0.3676	0.0022	0.95	2.7206	0.0166	0.1309	0.0020	0.1047	0.0168	3.20	45	126	85	1.48	2018	11	2064	13	2111	27	97	
SPL 2966	55.1	6.7596	0.1378	0.3776	0.0029	0.81	2.6483	0.0200	0.1298	0.0026	0.0903	0.0039	0.97	27	28	70	0.39	2065	13	2080	18	2096	35	99	
SPL 2966	17.1	7.0135	0.1231	0.3784	0.0037	0.99	2.6425	0.0260	0.1344	0.0020	0.1050	0.0062	3.94	48	98	205	0.48	2069	17	2113	16	2156	26	97	
SPL 2966	74.1	6.4497	0.1539	0.3808	0.0037	0.94	2.6260	0.0255	0.1228	0.0024	0.3157	0.0170	1.08	19	96	47	2.03	2080	17	2039	21	1998	36	102	
SPL 2966	32.1	7.2971	0.1696	0.3843	0.0040	0.74	2.6022	0.0270	0.1377	0.0034	0.2467	0.0088	0.02	15	35	33	1.07	2096	19	2148	21	2199	43	97	
SPL 2966	35.1	7.2583	0.1436	0.3867	0.0029	0.94	2.5857	0.0191	0.1361	0.0025	0.1898	0.0202	4.95	39	75	86	0.86	2108	13	2144	18	2178	32	98	
SPL 2966	69.1	7.3450	0.1488	0.3868	0.0042	0.92	2.5853	0.0281	0.1377	0.0029	0.1898	0.0112	3.34	23	79	54	1.47	2108	20	2154	18	2199	36	97	
SPL 2966	10.1	7.2965	0.1387	0.3882	0.0032	0.99	2.5763	0.0210	0.1363	0.0024	0.1261	0.0142	0.72	34	57	91	0.63	2114	15	2148	18	2181	31	98	
SPL 2966	44.1	7.3068	0.1798	0.3896	0.0030	0.57	2.5666	0.0195	0.1360	0.0031	0.1188	0.0047	0.58	29	31	70	0.44	2121	14	2150	22	2177	40	98	
SPL 2966	53.1	7.4581	0.1362	0.3909	0.0043	0.66	2.5581	0.0281	0.1384	0.0030	0.1741	0.0060	0.15	17	31	39	0.80	2127	20	2168	16	2207	37	98	
SPL 2966	2.1	7.4777	0.1484	0.3929	0.0040	0.56	2.5453	0.0260	0.1380	0.0025	0.1631	0.0052	0.50	24	42	53	0.80	2136	19	2170	18	2203	32	98	
SPL 2966	49.1	7.3543	0.1419	0.3930	0.0035	0.01	2.5446	0.0226	0.1357	0.0027	0.1935	0.0098	0.54	20	43	45	0.95	2137	16	2155	18	2173	34	99	
SPL 2966	67.1	7.3568	0.1174	0.3933	0.0021	0.99	2.5428	0.0139	0.1357	0.0028	0.2047	0.0596	0.85	11	30	8	3.92	2138	11	2156	20	2173	38	99	
SPL 2966	52.1	7.5948	0.1574	0.3933	0.0037	0.34	2.5423	0.0237	0.1400	0.0029	0.1934	0.0102	0.79	15	30	34	0.89	2138	17	2184	19	2228	37	97	
SPL 2966	7.1	7.5487	0.1522	0.3949	0.0039	0.17	2.5324	0.0247	0.1386	0.0027	0.1770	0.0051	0.00	32	57	72	0.80	2145	18	2179	18	2210	34	98	
SPL 2966	90.1	7.5484	0.1521	0.3949	0.0038	0.99	2.5321	0.0241	0.1386	0.0028	0.1975	0.0103	0.31	19	14	35	0.39	2146	17	2179	19	2210	35	98	
SPL 2966	21.1	7.3979	0.1888	0.3952	0.0041	0.95	2.5305	0.0264	0.1358	0.0038	0.2879	0.0146	0.02	22	87	49	1.77	2147	19	2161	24	2174	49	99	
SPL 2966	29.1	7.5361	0.1641	0.3967	0.0040	0.99	2.5205	0.0254	0.1378	0.0032	0.2063	0.0704	9.01	19	39	67	0.58	2154	19	2177	19	2199	40	98	
SPL 2966	47.1	7.5829	0.1721	0.3973	0.0035	0.99	2.5172	0.0224	0.1384	0.0031	0.1829	0.0307	1.62	15	18	49	0.37	2156	16	2183	21	2208	40	98	
SPL 2966	38.1	7.4356	0.1101	0.3980	0.0036	0.43	2.5123	0.0225	0.1355	0.0020	0.1695	0.0038	0.37	48	87	108	0.81	2160	16	2165	13	2170	25	99	
SPL 2966	89.1	7.7340	0.1798	0.3990	0.0058	0.78	2.5062	0.0363	0.1406	0.0035	0.1958	0.0186	1.04	10	22	22	1.02	2164	27	2201	21	2234	43	98	
SPL 2966	42.1	7.4987	0.1114	0.3991	0.0039	0.45	2.5058	0.0246	0.1363	0.0020	0.1341	0.0125	0.66	33	70	74	0.95	2165	18	2173	13	2180	26	99	
SPL 2966	83.1	7.4101	0.1140	0.3995	0.0027	0.91	2.5029	0.0169	0.1345	0.0021	0.2104	0.0050	1.43	36	71	72	0.99	2167	12	2162	14	2158	27	100	
SPL 2966	41.1	7.4852	0.1189	0.4000	0.0042	0.59	2.5001	0.0264	0.1357	0.0023	0.1914	0.0062	0.21	26	57	55	1.03	2169	19	2171	14	2173	30	99	
SPL 2966	93.1	7.6303	0.1526	0.4001	0.0036	0.88	2.4995	0.0226	0.1383	0.0024	0.1666	0.0085	1.69	26	37	58	0.65	2169	17	2188	18	2206	31	99	
SPL 2966	4.1	7.7376	0.1591	0.4002	0.0037	0.68	2.4989	0.0233	0.1402	0.0027	0.1445	0.0080	0.33	29	51	67	0.76	2170	17	2201	18	2230	33	98	
SPL 2966	33.1	7.5581	0.1727	0.4015	0.0031	0.59	2.4906	0.0191	0.1365	0.0028	0.1417	0.0113	0.67	23	33	55	0.60	2176	14	2180	20	2184	36	99	
SPL 2966	76.1	8.5896	0.1777	0.4017	0.0036	0.99	2.4892	0.0224	0.1551	0.0027	0.1561	0.0179	3.16	31	93	83	1.12	2177	16	2295	19	2403	30	94	
SPL 2966	51.1	7.6830	0.1557	0.4022	0.0030	0.98	2.4861	0.0186	0.1385	0.0028	0.1720	0.0153	1.48	18	46	41	1.12	2179	14	2195	18	2209	36	99	
SPL 2966	100.1	7.4642	0.1407	0.4029	0.0038	0.49	2.4820	0.0234	0.1344	0.0022	0.1761	0.0044	0.51	23	43	50	0.86	2182	17	2169	16	2156	28	100	
SPL 2966	81.1	7.4204	0.1250	0.4031	0.0033	0.83	2.4808	0.0201	0.1335	0.0023	0.1605	0.0106	0.51	35	68	77	0.88	2183	15	2163	15	2145	30	100	
SPL 2966	92.1	7.6002	0.1702	0.4034	0.0040	0.53	2.4787	0.0245	0.1366	0.0029	0.3372	0.0143	3.24	13	36	24	1.50	2185	18	2185	20	2185	37	99	
SPL 2966	12.1	7.3524	0.1999	0.4042	0.0064	0.74	2.4742	0.0391	0.1319	0.0040	0.1945	0.0142	4.63	10	17	23	0.73	2188	29	2155	25	2124	54	101	
SPL 2966	71.1	7.7005	0.1896	0.4042	0.0063	0.82	2.4741	0.0388	0.1382	0.0034	0.2295	0.0111	0.00	14	33	28	1.19	2188	29	2197	22	2204	43	99	
SPL 2966	77.1	7.5676	0.2201	0.4047	0.0048	0.76	2.4709	0.0294	0.1356	0.0037	0.1666	0.0073	0.83	13	23	28	0.81	2191	22	2181	26	2172	47	100	
SPL 2966	34.1	7.5801	0.1899	0.4055	0.0041	0.99	2.4663	0.0249	0.1356	0.0034	0.2029	0.0128	0.64	20	81	52	1.57	2194	19	2183	23	2172	44	100	

SPL 2966	84.1	7.4417	0.1191	0.4055	0.0032	0.98	2.4662	0.0194	0.1331	0.0022	0.1571	0.0047	0.33	39	92	104	0.89	2194	15	2166	14	2139	29	101
SPL 2966	96.1	7.4390	0.1203	0.4055	0.0031	0.98	2.4662	0.0186	0.1331	0.0019	0.1897	0.0141	1.34	46	89	106	0.84	2194	14	2166	15	2139	25	101
SPL 2966	99.1	7.5083	0.1524	0.4057	0.0035	0.21	2.4647	0.0211	0.1342	0.0025	0.1823	0.0064	0.44	17	32	36	0.88	2195	16	2174	18	2154	32	100
SPL 2966	65.1	7.7692	0.1755	0.4060	0.0040	0.70	2.4629	0.0245	0.1388	0.0030	0.1926	0.0081	2.31	12	31	26	1.18	2197	19	2205	20	2212	38	99
SPL 2966	94.1	7.6585	0.1330	0.4084	0.0038	0.32	2.4484	0.0230	0.1360	0.0021	0.1702	0.0068	0.54	27	44	57	0.78	2208	18	2192	15	2177	27	100
SPL 2966	54.1	7.8455	0.1218	0.4096	0.0027	0.85	2.4412	0.0163	0.1389	0.0021	0.1199	0.0174	0.91	25	41	58	0.70	2213	12	2213	14	2214	27	99
SPL 2966	87.1	7.8771	0.1944	0.4182	0.0027	0.42	2.3914	0.0153	0.1366	0.0032	0.1486	0.0051	0.66	21	36	47	0.77	2252	12	2217	22	2185	41	101
SPL 2966	1.1	9.7208	0.1948	0.4438	0.0042	0.57	2.2533	0.0215	0.1589	0.0028	0.1029	0.0037	0.66	36	38	75	0.50	2368	19	2409	18	2444	30	98
SPL 2966	57.1	10.3479	0.2490	0.4478	0.0049	0.65	2.2333	0.0243	0.1676	0.0043	0.2345	0.0114	1.30	10	22	19	1.19	2385	22	2466	22	2534	43	96
SPL 2966	13.1	9.7700	0.2079	0.4548	0.0056	0.75	2.1986	0.0272	0.1558	0.0031	0.0827	0.0048	0.61	23	22	47	0.46	2417	25	2413	20	2410	33	100
SPL 2966	88.1	10.2957	0.2066	0.4624	0.0050	0.96	2.1624	0.0232	0.1615	0.0030	0.2551	0.0120	0.60	18	26	34	0.75	2450	22	2462	19	2471	32	99
SPL 2966	43.1	10.4275	0.2627	0.4705	0.0042	0.69	2.1254	0.0189	0.1607	0.0039	0.0980	0.0079	0.65	20	18	39	0.46	2486	18	2473	23	2463	40	100
SPL 2966	18.1	11.5831	0.2553	0.4717	0.0038	0.89	2.1199	0.0170	0.1781	0.0040	0.1432	0.0037	0.42	49	64	90	0.71	2491	17	2571	20	2635	37	96
SPL 2966	91.1	10.7035	0.2397	0.4745	0.0059	0.92	2.1074	0.0264	0.1636	0.0035	0.1385	0.0061	0.92	15	18	27	0.68	2503	26	2498	21	2493	36	100
SPL 2966	85.1	10.3103	0.2133	0.4749	0.0036	0.69	2.1056	0.0159	0.1575	0.0029	0.1494	0.0046	0.63	31	62	58	1.07	2505	16	2463	19	2428	30	101
SPL 2966	75.1	10.9043	0.2113	0.4785	0.0039	0.99	2.0900	0.0172	0.1653	0.0030	0.1677	0.0119	0.63	33	52	66	0.79	2521	17	2515	20	2511	31	100
SPL 2966	66.1	14.9845	0.2432	0.5025	0.0045	0.99	1.9901	0.0177	0.2163	0.0035	0.1223	0.0250	0.50	90	147	139	1.06	2624	19	2814	16	2953	26	93
SPL 2966	6.1	15.1584	0.2850	0.5102	0.0045	0.99	1.9600	0.0173	0.2155	0.0036	0.1345	0.0070	5.29	67	53	90	0.59	2657	19	2825	18	2947	27	94
SPL 2966	72.1	17.1447	0.3232	0.5541	0.0047	0.99	1.8048	0.0152	0.2244	0.0036	0.1362	0.0066	1.89	43	53	130	0.41	2842	19	2943	18	3013	26	96
SPL 2966	16.1	18.4303	0.3163	0.6120	0.0060	0.01	1.6341	0.0159	0.2184	0.0030	0.0624	0.0029	1.02	30	28	62	0.45	3078	24	3012	17	2969	22	102
SPL 2966	24.1	1.1441	0.0680	0.0770	0.0011	0.90	12.9851	0.1885	0.1077	0.0032	0.1317	0.0825	3.70	30	120	390	0.31	478	6	774	19	1762	57	61
SPL 2966	14.1	1.8856	0.0903	0.1290	0.0023	0.99	7.7512	0.1405	0.1060	0.0025	0.1035	0.0351	0.00	27	44	30	1.47	782	12	1076	17	1732	30	72
SPL 2966	25.1	2.2923	0.0567	0.1409	0.0012	0.97	7.0972	0.0611	0.1180	0.0030	0.1507	0.0456	2.38	15	74	92	0.80	850	7	1210	17	1926	47	70
SPL 2966	82.1	2.5743	0.0400	0.1487	0.0010	0.99	6.7262	0.0463	0.1256	0.0019	0.1040	0.0406	0.00	18	28	83	0.34	894	6	1293	11	2037	27	69
SPL 2966	20.1	2.3519	0.0507	0.1538	0.0012	0.99	6.5024	0.0511	0.1109	0.0026	0.1010	0.0059	7.60	45	187	342	0.55	922	7	1228	15	1814	42	75
SPL 2966	19.1	2.3664	0.0515	0.1544	0.0012	0.98	6.4777	0.0504	0.1112	0.0027	0.1044	0.0104	3.37	44	118	253	0.46	925	7	1233	16	1819	44	75
SPL 2966	28.1	2.8622	0.0797	0.1877	0.0021	0.99	5.3267	0.0592	0.1106	0.0027	0.1057	0.0161	0.00	11	32	-32	-1.02	1109	11	1372	18	1809	39	80
SPL 2966	68.1	3.0360	0.0699	0.1935	0.0022	0.93	5.1693	0.0581	0.1138	0.0023	0.8229	0.1501	0.00	-25	113	418	0.27	1140	12	1417	16	1861	35	80
SPL 2966	78.1	3.3303	0.0484	0.2035	0.0013	0.99	4.9139	0.0307	0.1187	0.0018	0.0981	0.0100	9.19	52	123	360	0.34	1194	7	1488	11	1937	27	80
SPL 2966	15.1	4.1162	0.0737	0.2230	0.0020	0.99	4.4846	0.0409	0.1339	0.0020	0.1178	0.0083	4.77	77	165	390	0.42	1298	11	1658	14	2150	26	78
SPL 2966	39.1	3.8897	0.0629	0.2251	0.0023	0.99	4.4426	0.0450	0.1253	0.0019	0.2418	0.0220	0.00	23	34	23	1.47	1309	12	1612	12	2033	27	81
SPL 2966	27.1	3.9815	0.0947	0.2329	0.0020	0.99	4.2936	0.0362	0.1240	0.0025	0.1962	0.0571	0.00	53	136	98	1.40	1350	10	1630	16	2014	34	82
SPL 2966	45.1	4.2317	0.1034	0.2332	0.0019	0.99	4.2874	0.0346	0.1316	0.0031	0.1410	0.0064	6.61	37	110	199	0.55	1351	10	1680	21	2119	41	80
SPL 2966	48.1	4.3845	0.1473	0.2458	0.0031	0.98	4.0676	0.0521	0.1293	0.0038	0.1655	0.2450	0.41	46	76	101	0.75	1417	15	1709	23	2089	51	82
SPL 2966	79.1	6.6605	0.1905	0.2630	0.0028	0.85	3.8029	0.0401	0.1837	0.0032	0.0858	0.0451	0.00	47	39	20	1.98	1505	12	2067	14	2687	25	72
SPL 2966	61.1	4.6238	0.1032	0.2651	0.0023	0.31	3.7725	0.0331	0.1265	0.0025	0.5142	0.2350	82.14	147	38	55	0.70	1516	12	1754	19	2050	35	86
SPL 2966	86.1	5.3145	0.1208	0.2934	0.0021	0.99	3.4086	0.0243	0.1314	0.0024	0.1101	0.0182	0.36	32	60	62	0.97	1658	10	1871	17	2117	31	88
SPL 2966	9.1	5.7105	0.1257	0.3062	0.0027	0.99	3.2655	0.0293	0.1352	0.0025	0.1535	0.0092	3.08	31	70	98	0.71	1722	13	1933	18	2167	32	89
SPL 2966	26.1	6.3617	0.1297	0.3248	0.0021	0.89	3.0792	0.0198	0.1421	0.0027	0.3025	0.0587	2.97	51	382	117	3.27	1813	10	2027	18	2253	32	89
SPL 2966	36.1	10.8357	0.3012	0.3371	0.0043	0.99	2.9662	0.0379	0.2331	0.0050	0.1450	0.0339	10.92	27	51	73	0.70	1873	20	2509	21	3074	33	74
SPL 2966	98.1	6.9926	0.1257	0.3733	0.0030	0.99	2.6790	0.0218	0.1359	0.0021	0.2894	0.0889	36.36	54	96	109	0.89	2045	14	2110	16	2175	27	96
SPL 2966	56.1	7.9637	0.1547	0.3898	0.0036	0.80	2.5654	0.0237	0.1482	0.0035	0.5628	0.3231	77.38	45	28	48	0.57	2122	17	2227	19	2325	42	95
SPL 2966	8.1	7.4341	0.1554	0.3935	0.0036	0.45	2.5413	0.0230	0.1370	0.0025	0.2955	0.0163	5.87	8	-11	25	-0.46	2139	16	2165	19	2190	32	98
SPL 2966	64.1	7.7052	0.1439	0.4052	0.0039	0.87	2.4679	0.0237	0.1379	0.0024	0.2458	0.1586	21.02	33	45	52	0.88	2193	18	2197	17	2201	30	99
SPL 2966	22.1	10.0508	0.2084	0.4571	0.0040	0.97	2.1875	0.0190	0.1595	0.0037	0.0303	0.0097	0.83	38	-1	86	-0.01	2427	17	2439	19	2450	39	99

8/18/2020	SPOT	SITE	RATIOS															AGES						
ICM-8A - M 756			207/235	1sigma	206/238	1 sigma	coef. corr	238/206	1 sigma	207/206	1 sigma	208/206	1 sigma	Pb total comum %	Pb rad ppm	Th ppm	U ppm	Th/U	$T_{206/238}$	1 sigma	$T_{207/235}$	1 sigma	$T_{207/206}$	1 sigma	Conc. 206/238
J-61 - MARCELA																								207/235
SPL3256 , Analyte Excite 193nm Excimer Laser Ablation System, 6Hz, 6mJ, 20µm, 100%(0.89J/cm²) Energia, Hélio: MFC1=0.300L/min, MFC2=0.300L/min.																								
SPL 3256	67.1		5.4634	0.0911	0.3055	0.0019	0.99	3.2733	0.0206	0.1297	0.0021	0.2060	0.0062	1.5	80	380	351	1	1719	10	1895	15	2094	29	90
SPL 3256	45.1		5.3611	0.0806	0.3058	0.0020	0.99	3.2706	0.0209	0.1272	0.0020	0.1712	0.0224	3.6	43	137	248	1	1720	10	1879	14	2059	28	91
SPL 3256	34.1		4.5599	0.0881	0.3071	0.0021	0.87	3.2560	0.0222	0.1077	0.0021	0.1663	0.0070	2.4	26	80	69	1	1727	10	1742	16	1761	37	99
SPL 3256	15.1		4.5556	0.1331	0.3100	0.0027	0.93	3.2260	0.0282	0.1066	0.0031	0.3719	0.0066	1.0	41	220	114	2	1741	13	1741	24	1742	52	99
SPL 3256	31.1		5.4660	0.1055	0.3106	0.0016	0.98	3.2196	0.0170	0.1276	0.0023	0.1542	0.0063	2.3	64	238	232	1	1744	8	1895	16	2066	32	91
SPL 3256	59.1		5.0593	0.1001	0.3139	0.0021	0.99	3.1856	0.0215	0.1169	0.0020	0.1595	0.0044	2.5	145	598	609	1	1760	10	1829	17	1909	31	96
SPL 3256	16.1		4.7937	0.1174	0.3263	0.0030	0.94	3.0646	0.0277	0.1065	0.0025	0.1849	0.0033	0.3	70	203	181	1	1820	14	1784	20	1741	43	102
SPL 3256	62.1		5.4849	0.0875	0.3298	0.0021	0.98	3.0317	0.0192	0.1206	0.0023	0.0994	0.0073	4.3	21	33	60	1	1838	10	1898	14	1965	34	96
SPL 3256	20.1		6.2327	0.1547	0.3352	0.0033	0.99	2.9837	0.0296	0.1349	0.0039	0.0399	0.0188	7.7	29	33	171	0	1863	16	2009	23	2162	50	92
SPL 3256	82.1		6.0810	0.1102	0.3441	0.0029	0.99	2.9060	0.0249	0.1282	0.0024	0.1803	0.0094	2.2	26	89	84	1	1906	14	1988	16	2073	33	95
SPL 3256	80.1		6.4079	0.0931	0.3508	0.0023	0.99	2.8508	0.0189	0.1325	0.0021	0.3620	0.0103	1.2	82	653	273	2	1938	11	2033	13	2131	28	95
SPL 3256	98.1		6.4816	0.1223	0.3550	0.0027	0.96	2.8171	0.0216	0.1324	0.0025	0.1719	0.0355	2.6	21	62	47	1	1958	13	2043	18	2130	33	95
SPL 3256	30.1		6.2184	0.0972	0.3552	0.0021	0.98	2.8154	0.0166	0.1270	0.0024	0.1903	0.0188	4.9	19	56	42	1	1959	10	2007	14	2056	34	97
SPL 3256	38.1		6.2492	0.0810	0.3579	0.0017	0.97	2.7941	0.0134	0.1266	0.0018	0.1740	0.0015	0.9	60	148	138	1	1972	8	2011	11	2052	25	98
SPL 3256	19.1		6.2894	0.2205	0.3624	0.0044	0.44	2.7592	0.0338	0.1259	0.0045	0.7428	0.0160	5.0	27	201	41	5	1994	21	2017	31	2041	64	98
SPL 3256	61.1		6.5679	0.1392	0.3627	0.0033	0.83	2.7572	0.0251	0.1313	0.0026	0.2830	0.0051	0.1	19	66	41	2	1995	16	2055	19	2116	34	97
SPL 3256	35.1		6.4024	0.1069	0.3636	0.0019	0.99	2.7502	0.0146	0.1277	0.0021	0.0741	0.0130	1.2	37	74	85	1	1999	9	2033	15	2067	29	98
SPL 3256	73.1		5.4131	0.0755	0.3657	0.0020	0.35	2.7342	0.0147	0.1073	0.0016	0.7575	0.2379	0.0	52	101	133	1	2009	9	1887	12	1755	27	106
SPL 3256	90.1		6.7970	0.0853	0.3662	0.0022	0.98	2.7311	0.0161	0.1346	0.0019	0.1095	0.0188	2.0	37	44	97	0	2011	10	2085	12	2159	25	96
SPL 3256	1.1		6.7748	0.1254	0.3677	0.0035	0.99	2.7199	0.0257	0.1336	0.0027	0.0921	0.0072	3.6	41	67	136	0	2018	16	2082	17	2146	35	96
SPL 3256	32.1		6.8535	0.1676	0.3684	0.0029	0.99	2.7144	0.0215	0.1349	0.0034	0.1821	0.0092	1.5	18	51	61	1	2022	14	2093	22	2163	44	96
SPL 3256	96.1		6.6475	0.1540	0.3725	0.0032	0.93	2.6848	0.0227	0.1294	0.0027	0.1275	0.0196	0.4	35	50	88	1	2041	15	2066	20	2090	37	98
SPL 3256	78.1		6.8856	0.0823	0.3730	0.0021	0.99	2.6812	0.0148	0.1339	0.0017	0.2052	0.0236	0.7	66	189	279	1	2043	10	2097	11	2150	22	97
SPL 3256	89.1		6.9238	0.0905	0.3737	0.0027	0.90	2.6763	0.0195	0.1344	0.0019	0.1643	0.0865	0.2	16	81	27	3	2047	13	2102	11	2156	24	97
SPL 3256	99.1		6.7829	0.0932	0.3742	0.0025	0.99	2.6724	0.0180	0.1315	0.0017	0.1432	0.0038	0.2	80	187	187	1	2049	12	2083	13	2118	23	98
SPL 3256	**94.1**		**6.7372**	**0.1402**	**0.3744**	**0.0033**	**0.90**	**2.6711**	**0.0235**	**0.1305**	**0.0025**	**0.1699**	**0.0151**	**2.9**	**26**	**30**	**59**	**1**	**2050**	**15**	**2078**	**18**	**2105**	**33**	**98**
SPL 3256	36.1		6.6571	0.1434	0.3780	0.0027	0.85	2.6452	0.0190	0.1277	0.0028	0.3545	0.0060	0.8	20	88	40	2	2067	13	2067	19	2067	39	100
SPL 3256	26.1		6.9551	0.1026	0.3794	0.0032	0.95	2.6360	0.0220	0.1330	0.0025	0.1936	0.0037	0.4	25	56	53	1	2073	15	2106	13	2138	33	98
SPL 3256	41.1		7.0781	0.1020	0.3800	0.0018	0.63	2.6314	0.0121	0.1351	0.0021	0.1889	0.0075	1.4	35	74	75	1	2076	8	2121	13	2165	27	97
SPL 3256	54.1		6.8332	0.0895	0.3805	0.0025	0.88	2.6283	0.0173	0.1303	0.0021	0.2363	0.0037	0.3	68	210	142	1	2078	12	2090	12	2101	28	99
SPL 3256	55.1		6.9248	0.2874	0.3810	0.0052	0.30	2.6248	0.0360	0.1318	0.0061	0.1885	0.0258	4.4	4	11	9	1	2081	25	2102	36	2122	81	99
SPL 3256	46.1		6.9137	0.0954	0.3814	0.0022	0.97	2.6222	0.0151	0.1315	0.0017	0.1834	0.0055	1.7	35	81	75	1	2083	10	2100	12	2118	22	99
SPL 3256	77.1		6.9541	0.0838	0.3815	0.0020	0.84	2.6213	0.0138	0.1322	0.0017	0.0773	0.0021	1.1	69	89	177	1	2083	9	2106	11	2128	22	98
SPL 3256	44.1		6.9520	0.1573	0.3826	0.0036	0.96	2.6134	0.0243	0.1318	0.0029	0.1874	0.0206	1.7	14	34	32	1	2089	17	2105	21	2122	38	99
SPL 3256	71.1		7.2306	0.1464	0.3837	0.0030	0.55	2.6060	0.0201	0.1367	0.0026	0.3337	0.0051	2.4	28	103	54	2	2094	14	2140	18	2185	33	97
SPL 3256	58.1		7.1248	0.1652	0.3842	0.0036	0.80	2.6026	0.0245	0.1345	0.0029	0.3022	0.0060	0.3	26	101	51	2	2096	17	2127	21	2157	39	98
SPL 3256	25.1		6.9899	0.1687	0.3849	0.0046	0.74	2.5982	0.0313	0.1317	0.0041	0.4146	0.0318	0.6	9	38	18	2	2099	21	2110	22	2121	54	99
SPL 3256	66.1		7.3224	0.1342	0.3856	0.0024	0.84	2.5935	0.0165	0.1377	0.0024	0.2063	0.0104	0.8	28	69	56	1	2102	11	2152	17	2199	31	97
SPL 3256	68.1		7.3613	0.1353	0.3860	0.0028	0.82	2.5908	0.0188	0.1383	0.0024	0.3123	0.0177	0.6	43	151	88	2	2104	13	2156	17	2206	31	97
SPL 3256	27.1		7.0944	0.0959	0.3871	0.0023	0.99	2.5831	0.0151	0.1329	0.0021	0.2153	0.0091	1.6	39	122	102	1	2109	11	2123	12	2137	28	99
SPL 3256	64.1		7.0780	0.0812	0.3876	0.0017	0.90	2.5798	0.0116	0.1324	0.0016	0.1467	0.0019	0.3	103	194	222	1	2112	8	2121	10	2130	22	99
SPL 3256	40.1		7.1007	0.0933	0.3878	0.0018	0.99	2.5789	0.0117	0.1328	0.0019	0.0851	0.0140	0.4	59	63	159	0	2112	8	2124	12	2135	26	99
SPL 3256	4.1		7.4467	0.2160	0.3880	0.0093	0.21	2.5776	0.0620	0.1392	0.0049	0.1381	0.0176	2.8	10	20	21	1	2113	43	2167	28	2217	67	97
SPL 3256	29.1		7.2977	0.0900	0.3893	0.0022	0.94	2.5690	0.0144	0.1360	0.0020	0.1154	0.0026	0.6	50	76	110	1	2119	10	2149	11	2176	25	98
SPL 3256	49.1		7.2825	0.1059	0.3899	0.0034	0.86	2.5646	0.0225	0.1355	0.0026	0.4632	0.0225	0.0	22	89	40	2	2122	16	2147	13	2170	33	98
SPL 3256	81.1		7.2538	0.1018	0.3900	0.0027	0.97	2.5640	0.0174	0.1349	0.0020	0.0936	0.0022	0.6	79	113	178	1	2123	12	2143	12	2163	26	99
SPL 3256	43.1		7.4383	0.1147	0.3901	0.0028	0.42	2.5637	0.0184	0.1383	0.0020	0.1305	0.0110	1.3	24	46	52	1	2123	13	2166	14	2206	25	98
SPL 3256	37.1		7.3227	0.1152	0.3904	0.0023	0.92	2.5612	0.0153	0.1360	0.0024	0.1015	0.0072	2.6	27	36	69	1	2125	11	2152	14	2177	30	98
SPL 3256	11.1		7.2978	0.3121	0.3905	0.0052	0.74	2.5611	0.0344	0.1356	0.0068	0.2768	0.0138	1.9	18	65	33	2	2125	24	2149	38	2171	87	98
SPL 3256	53.1		7.2032	0.1501	0.3918	0.0038	0.62	2.5523	0.0248	0.1333	0.0034	0.3102	0.0104	0.7	10	34	19	2	2131	18	2137	19	2142	45	99
SPL 3256	7.1		7.2422	0.1645	0.3923	0.0035	0.32	2.5491	0.0230	0.1339	0.0030	0.2653	0.0104	0.8	34	131	71	2	2133	16	2142	20	2150	39	99
SPL 3256	97.1		7.1453	0.1457	0.3923	0.0032	0.96	2.5490	0.0207	0.1321	0.0025	0.1433	0.0055	1.9	32	73	70	1	2134	15	2130	18	2126	33	100
SPL 3256	75.1		7.2850	0.0849	0.3928	0.0023	0.99	2.5460	0.0146	0.1345	0.0022	0.2480	0.0289	2.4	31	129	54	2	2136	11	2147	13	2158	29	99
SPL 3256	87.1		7.8194	0.1493	0.3931	0.0033	0.92	2.5436	0.0215	0.1443	0.0027	0.1504	0.0110	2.2	8	15	15	1	2137	15	2210	17	2279	32	96
SPL 3256	57.1		7.2398	0.1439	0.3936	0.0029	0.99	2.5406	0.0187	0.1334	0.0026	0.2590	0.0064	0.8	62	263	143	2	2140	14	2141	19	2143	34	99
SPL 3256	6.1		7.3583	0.2352	0.3953	0.0051	0.60	2.5300	0.0329	0.1350	0.0044	0.2465	0.0125	0.2	15	48	30	2	2147	24	2156	28	2164	55	99
SPL 3256	23.1		7.5515	0.2003	0.3959	0.0031	0.92	2.5258	0.0199	0.1383	0.0034	0.0260	0.0149	1.2	25	8	52	0	2150	14	2179	23	2206	43	98
SPL 3256	100.1		7.2633	0.1367	0.3961	0.0037	0.83	2.5247	0.0238	0.1330	0.0023	0.4948	0.0130	0.6	46	234	79	3	2151	17	2144	17	2138	30	100
SPL 3256	76.1		7.2891	0.0944	0.3962	0.0020	0.94	2.5240	0.0126	0.1334	0.0018	0.1672	0.0344	0.5	37	143	71	2	2151	9	2147	11	2144	23	100
SPL 3256	14.1		7.7132	0.3417	0.3962	0.0064	0.54	2.5237	0.0405	0.1412	0.0072	0.2693	0.0187	1.8	12	41	23	2	2152	29	2198	40	2242	90	97
SPL 3256	74.1		7.3879	0.1126	0.3966	0.0030	0.99	2.5214	0.0188	0.1351	0.0022	0.2658	0.0353	1.6	22	59	49	1	2153	14	2160	14	2165	28	99
SPL 3256	83.1		7.4943	0.1139	0.3968	0.0035	0.82	2.5199	0.0224	0.1370	0.0025	0.2658	0.0086	0.9	32	121	62	2	2154	16	2172	14	2189	31	99
SPL 3256	95.1		7.4830	0.1517	0.3972	0.0034	0.56	2.5175	0.0216	0.1366	0.0026	0.1253	0.0048	0.3	35	61	77	1	2156	16	2171	18	2185	33	99
SPL 3256	3.1		7.1827	0.1849	0.3977	0.0044	0.87	2.5144	0.0276	0.1310	0.0036	0.1864	0.0125	0.1	22	58	44	1	2159	20	2134	23	2111	48	101

SPL 3256	10.1	7.7219	0.2098	0.4002	0.0030	0.99	2.4986	0.0188	0.1399	0.0044	0.2052	0.0159	0.8	56	153	149	1	2170	14	2199	25	2226	54	98
SPL 3256	56.1	7.4748	0.1861	0.4016	0.0034	0.75	2.4900	0.0214	0.1350	0.0030	0.2432	0.0067	0.6	35	112	70	2	2176	16	2170	22	2164	39	100
SPL 3256	9.1	7.6348	0.2205	0.4051	0.0032	0.74	2.4686	0.0193	0.1367	0.0045	0.3760	0.0059	0.3	70	330	131	3	2192	15	2189	26	2186	58	100
SPL 3256	51.1	7.6726	0.1390	0.4055	0.0034	0.78	2.4659	0.0205	0.1372	0.0031	0.1782	0.0157	2.1	14	31	28	1	2194	16	2193	16	2192	39	100
SPL 3256	93.1	7.6003	0.1539	0.4072	0.0030	0.30	2.4558	0.0180	0.1354	0.0024	0.2210	0.0025	0.6	64	204	132	2	2202	14	2185	18	2169	30	100
SPL 3256	21.1	7.6628	0.1886	0.4077	0.0030	0.65	2.4528	0.0183	0.1363	0.0033	0.1894	0.0042	1.1	59	130	115	1	2204	14	2192	22	2181	41	100
SPL 3256	69.1	7.7051	0.1670	0.4078	0.0031	0.67	2.4524	0.0188	0.1370	0.0027	0.1518	0.0520	0.0	20	30	42	1	2205	14	2197	20	2190	33	100
SPL 3256	24.1	7.5910	0.2126	0.4078	0.0035	0.73	2.4524	0.0208	0.1350	0.0038	0.1901	0.0076	0.7	30	74	61	1	2205	16	2184	25	2164	48	100
SPL 3256	92.1	7.6107	0.2119	0.4087	0.0044	0.70	2.4467	0.0261	0.1351	0.0039	0.3071	0.0133	2.6	13	45	23	2	2209	20	2186	25	2165	50	101
SPL 3256	22.1	7.7768	0.2141	0.4100	0.0031	0.83	2.4390	0.0185	0.1376	0.0038	0.1243	0.0073	1.0	28	44	58	1	2215	14	2206	25	2197	48	100
SPL 3256	91.1	7.8422	0.2553	0.4115	0.0057	0.78	2.4299	0.0334	0.1382	0.0047	0.2996	0.0281	4.6	7	19	12	1	2222	26	2213	31	2205	60	100
SPL 3256	52.1	8.4643	0.1035	0.4143	0.0029	0.94	2.4134	0.0168	0.1482	0.0023	0.1184	0.0312	0.5	48	41	129	0	2235	13	2282	12	2325	29	97
SPL 3256	8.1	8.0438	0.2118	0.4144	0.0047	0.68	2.4131	0.0274	0.1408	0.0041	0.1758	0.0122	1.2	14	33	28	1	2235	22	2236	24	2237	51	99
SPL 3256	86.1	8.2071	0.1401	0.4172	0.0032	0.89	2.3969	0.0181	0.1427	0.0028	0.0703	0.0223	0.0	24	27	56	0	2248	14	2254	16	2260	33	99
SPL 3256	13.1	8.1089	0.2277	0.4232	0.0031	0.60	2.3627	0.0174	0.1390	0.0044	0.1542	0.0192	1.0	34	59	72	1	2275	14	2243	27	2214	56	101
SPL 3256	5.1	7.8896	0.1385	0.4245	0.0039	0.88	2.3556	0.0214	0.1348	0.0025	0.1370	0.0093	1.7	57	70	124	1	2281	17	2218	16	2161	32	102
SPL 3256	12.1	8.3807	0.3979	0.4391	0.0128	0.83	2.2775	0.0664	0.1384	0.0093	0.2022	0.0331	6.8	11	24	20	1	2347	57	2273	42	2208	118	103
SPL 3256	84.1	10.7998	0.1754	0.4694	0.0033	0.99	2.1302	0.0149	0.1669	0.0033	0.1055	0.0165	1.4	23	38	42	1	2481	15	2506	17	2526	33	99
SPL 3256	85.1	10.9422	0.1824	0.4768	0.0044	0.93	2.0975	0.0192	0.1665	0.0031	0.0794	0.0045	0.1	23	23	43	1	2513	19	2518	16	2522	32	99
SPL 3256	47.1	13.9568	0.1750	0.5248	0.0030	0.93	1.9056	0.0108	0.1929	0.0022	0.1228	0.0057	0.4	49	65	76	1	2719	12	2747	12	2767	18	99
SPL 3256	48.1	14.3955	0.1789	0.5318	0.0030	0.82	1.8806	0.0105	0.1963	0.0022	0.0903	0.0045	0.2	49	51	79	1	2749	13	2776	12	2796	18	99
SPL 3256	2.1	20.5467	0.4407	0.6186	0.0061	0.90	1.6167	0.0159	0.2409	0.0048	0.2212	0.0093	1.3	25	47	30	2	3104	24	3117	21	3126	32	99
SPL 3256	50.1	0.8829	0.0147	0.0659	0.0005	0.90	15.1672	0.1195	0.0971	0.0018	0.0895	0.0138	13.6	25	392	398	1	412	3	643	7	1570	34	64
SPL 3256	39.1	0.9538	0.0146	0.0798	0.0004	1.00	12.5354	0.0569	0.0867	0.0014	0.1261	0.0565	0.0	1	-347	-438	1	495	2	680	7	1354	28	72
SPL 3256	60.1	1.6183	0.0473	0.1136	0.0011	1.00	8.8055	0.0829	0.1034	0.0018	0.1882	0.0109	1.0	103	311	323	1	693	6	977	14	1685	31	70
SPL 3256	79.1	1.6203	0.0215	0.1285	0.0006	1.00	7.7806	0.0385	0.0914	0.0012	0.3934	0.0160	1.1	79	461	315	1	779	4	978	8	1456	25	79
SPL 3256	65.1	2.3252	0.0355	0.1529	0.0009	0.99	6.5400	0.0364	0.1103	0.0018	0.1496	0.0124	5.0	99	235	584	0	917	5	1220	11	1804	29	75
SPL 3256	33.1	2.1650	0.0401	0.1545	0.0006	1.00	6.4718	0.0269	0.1016	0.0018	0.1698	0.0076	11.0	52	483	511	1	926	4	1170	13	1654	32	79
SPL 3256	63.1	2.1413	0.0307	0.1640	0.0009	1.00	6.0971	0.0337	0.0947	0.0013	0.1809	0.0203	2.6	142	755	869	1	979	5	1162	9	1522	24	84
SPL 3256	18.1	2.7303	0.0570	0.1689	0.0011	1.00	5.9205	0.0400	0.1172	0.0026	0.1308	0.0077	1.9	198	746	1101	1	1006	6	1337	17	1915	43	75
SPL 3256	17.1	3.6716	0.0938	0.2217	0.0020	1.00	4.5100	0.0406	0.1201	0.0029	0.1831	0.0235	1.5	75	331	366	1	1291	10	1565	20	1958	44	82
SPL 3256	42.1	4.1412	0.0527	0.2530	0.0011	0.92	3.9527	0.0173	0.1187	0.0017	0.1301	0.0152	0.8	52	232	193	1	1454	6	1662	11	1937	26	87
SPL 3256	70.1	4.8993	0.0750	0.2737	0.0016	1.00	3.6537	0.0216	0.1298	0.0021	0.0493	0.0046	3.9	53	128	365	0	1560	8	1802	14	2096	29	86
SPL 3256	88.1	5.0551	0.0672	0.2805	0.0018	1.00	3.5647	0.0226	0.1307	0.0018	0.1965	0.0098	2.2	53	193	134	1	1594	9	1829	11	2107	24	87
SPL 3256	28.1	5.2878	0.0617	0.2966	0.0015	1.00	3.3712	0.0169	0.1293	0.0018	0.1435	0.0182	6.3	46	355	298	1	1675	7	1867	10	2088	25	89
SPL 3256	72.1	5.4943	0.0954	0.3009	0.0018	1.00	3.3232	0.0203	0.1324	0.0023	0.1208	0.0619	4.2	52	341	219	2	1696	9	1900	15	2130	31	89

9/20/2019	SPOT	SITE						RATIOS												AGES					
ICM-11 - METARENITO		207/235	1sigma	206/238	1 sigma	coef. corr	238/206	1 sigma	207/206	1 sigma	208/206	1 sigma	Pb total	Pb rad	Th	U	Th/U	$T_{206/238}$	1 sigma	$T_{207/235}$	1 sigma	$T_{207/206}$	1 sigma	Conc.
J-61 - MARCELA TRINDADE													comum	ppm	ppm	ppm									206/238
SPL2965 , Analyte Excite 193nm Excimer Laser Ablation System, 6Hz, 6mJ, 20µm, 100% Energia, Hélio: MFC1=0.300L/min, MFC2=0.300L/min.													%												207/235
SPL 2965	26.1	4.6526	0.0982	0.2849	0.0028	0.97	3.5104	0.0347	0.1185	0.0026	0.2352	0.0406	8.10	17	62	37	1.706	1616	14	1759	16	1933	38	91
SPL 2965	36.1	4.8979	0.0901	0.2963	0.0023	0.95	3.3754	0.0262	0.1199	0.0018	0.0628	0.0086	3.29	75	438	276	1.589	1673	11	1802	16	1955	27	92
SPL 2965	63.1	4.9450	0.0823	0.2976	0.0033	0.99	3.3600	0.0374	0.1205	0.0018	0.0548	0.0268	0.05	50	71	128	0.552	1679	16	1810	14	1964	26	92
SPL 2965	53.1	5.0049	0.1033	0.2988	0.0022	0.98	3.3469	0.0243	0.1215	0.0029	0.3522	0.0924	1.76	32	205	80	2.566	1685	11	1820	19	1978	42	92
SPL 2965	46.1	5.3155	0.0833	0.2992	0.0020	0.96	3.3428	0.0228	0.1289	0.0020	0.1460	0.0143	2.50	53	315	168	1.872	1687	10	1871	14	2083	26	90
SPL 2965	54.1	5.2025	0.1045	0.3044	0.0028	0.96	3.2856	0.0299	0.1240	0.0025	0.2500	0.0124	2.35	59	378	176	2.142	1713	14	1853	17	2014	37	92
SPL 2965	48.1	5.4589	0.0826	0.3105	0.0020	0.98	3.2208	0.0210	0.1275	0.0019	0.2134	0.0070	1.50	92	382	275	1.388	1743	10	1894	13	2064	26	92
SPL 2965	24.1	5.7721	0.1153	0.3154	0.0029	0.92	3.1705	0.0293	0.1327	0.0026	0.1377	0.0118	1.88	56	111	162	0.683	1767	14	1942	16	2134	34	90
SPL 2965	60.1	4.6835	0.0758	0.3191	0.0021	0.92	3.1342	0.0207	0.1065	0.0016	0.1169	0.0059	0.88	106	239	314	0.762	1785	10	1764	14	1740	28	101
SPL 2965	28.1	5.7625	0.0787	0.3234	0.0017	0.98	3.0918	0.0165	0.1292	0.0018	0.2599	0.0204	2.41	82	366	174	2.107	1807	8	1941	13	2087	25	93
SPL 2965	78.1	6.1625	0.1161	0.3274	0.0028	0.99	3.0540	0.0265	0.1365	0.0021	0.1642	0.0074	0.00	71	274	166	1.645	1826	14	1999	16	2183	26	91
SPL 2965	75.1	6.1537	0.1269	0.3362	0.0031	0.78	2.9748	0.0276	0.1328	0.0022	0.1004	0.0186	2.10	11	31	37	0.841	1868	15	1998	18	2135	30	93
SPL 2965	50.1	6.2679	0.1355	0.3455	0.0027	0.99	2.8942	0.0225	0.1316	0.0027	0.2162	0.0295	1.49	75	434	185	2.354	1913	13	2014	18	2119	35	94
SPL 2965	44.1	5.7951	0.1332	0.3467	0.0035	0.95	2.8842	0.0290	0.1212	0.0028	0.2420	0.0399	0.92	14	57	27	2.109	1919	16	1946	19	1974	41	98
SPL 2965	98.1	5.8589	0.0840	0.3473	0.0031	0.99	2.8798	0.0255	0.1224	0.0016	0.3915	0.0435	0.87	63	278	184	1.512	1921	15	1955	13	1991	23	98
SPL 2965	55.1	6.1935	0.1194	0.3536	0.0025	0.61	2.8283	0.0202	0.1270	0.0023	0.1378	0.0105	0.36	95	254	236	1.075	1952	12	2004	17	2057	32	97
SPL 2965	12.1	6.4144	0.1045	0.3536	0.0024	0.99	2.8282	0.0195	0.1316	0.0019	0.2106	0.0504	1.24	60	53	139	0.385	1952	12	2034	15	2119	25	95
SPL 2965	71.1	6.6185	0.1101	0.3573	0.0030	0.98	2.7985	0.0236	0.1343	0.0020	0.1568	0.0053	1.52	47	271	126	2.157	1970	15	2062	15	2155	26	95
SPL 2965	72.1	6.0738	0.1190	0.3583	0.0033	0.99	2.7913	0.0261	0.1230	0.0021	0.1896	0.0167	1.75	65	131	216	0.605	1974	16	1986	16	2000	30	99
SPL 2965	58.1	6.1041	0.1070	0.3589	0.0026	0.99	2.7859	0.0205	0.1233	0.0024	0.2634	0.0631	1.71	20	100	44	2.268	1977	13	1991	16	2005	34	99
SPL 2965	25.1	6.1766	0.2179	0.3599	0.0039	0.09	2.7786	0.0298	0.1245	0.0043	0.5009	0.0293	2.86	10	65	18	3.593	1982	18	2001	32	2021	64	99
SPL 2965	82.1	6.6297	0.1161	0.3636	0.0031	0.49	2.7502	0.0236	0.1322	0.0019	0.0950	0.0029	0.11	30	44	79	0.552	1999	15	2063	15	2128	26	96
SPL 2965	65.1	6.4157	0.1051	0.3638	0.0038	0.31	2.7486	0.0285	0.1279	0.0019	0.1189	0.0025	0.27	40	72	101	0.712	2000	18	2034	14	2069	27	98
SPL 2965	9.1	6.3088	0.1419	0.3650	0.0030	0.80	2.7398	0.0228	0.1254	0.0026	0.2212	0.0089	0.72	18	53	44	1.193	2006	14	2020	20	2034	36	99
SPL 2965	30.1	6.9352	0.1171	0.3740	0.0023	0.64	2.6742	0.0167	0.1345	0.0022	0.1520	0.0075	4.14	26	65	64	1.028	2048	11	2103	15	2158	28	97
SPL 2965	20.1	6.8398	0.1168	0.3775	0.0034	0.99	2.6490	0.0238	0.1314	0.0026	0.2737	0.0240	1.91	18	100	50	1.987	2065	16	2091	16	2117	34	98
SPL 2965	19.1	6.9072	0.1291	0.3808	0.0027	0.95	2.6261	0.0185	0.1316	0.0028	0.1883	0.0208	0.15	26	82	56	1.456	2080	12	2100	17	2119	36	99
SPL 2965	57.1	7.1815	0.1572	0.3819	0.0041	0.93	2.6187	0.0281	0.1364	0.0031	0.1702	0.0144	2.53	33	74	65	1.132	2085	19	2134	19	2182	40	97
SPL 2965	49.1	7.0958	0.1099	0.3835	0.0029	0.93	2.6078	0.0200	0.1342	0.0021	0.1168	0.0067	1.01	40	51	86	0.593	2092	14	2124	14	2154	27	98
SPL 2965	95.1	7.6804	0.1573	0.3877	0.0043	0.96	2.5790	0.0286	0.1437	0.0029	0.2057	0.0321	0.00	38	118	83	1.424	2112	20	2194	17	2272	34	96
SPL 2965	99.1	7.2525	0.0981	0.3896	0.0034	0.99	2.5668	0.0224	0.1350	0.0019	0.0754	0.0437	1.70	32	74	57	1.284	2121	16	2143	13	2164	24	98
SPL 2965	88.1	7.3047	0.0812	0.3901	0.0036	0.99	2.5636	0.0234	0.1358	0.0016	0.1526	0.0199	0.15	32	174	100	1.738	2123	17	2149	12	2175	22	98
SPL 2965	6.1	7.3533	0.1029	0.3903	0.0032	0.99	2.5622	0.0210	0.1366	0.0021	0.1476	0.0102	2.26	33	166	90	1.842	2124	15	2155	13	2185	27	98
SPL 2965	76.1	7.3040	0.1533	0.3910	0.0041	0.85	2.5573	0.0271	0.1355	0.0024	0.1773	0.0107	0.33	51	107	103	1.031	2128	19	2149	19	2170	30	98
SPL 2965	8.1	7.1078	0.1402	0.3922	0.0029	0.84	2.5497	0.0189	0.1314	0.0024	0.1614	0.0105	1.89	13	26	30	0.878	2133	14	2125	18	2117	32	100
SPL 2965	84.1	7.4106	0.1161	0.3931	0.0047	0.91	2.5438	0.0302	0.1367	0.0021	0.1702	0.0212	0.49	45	104	100	1.037	2137	22	2162	14	2186	27	98
SPL 2965	89.1	7.4133	0.1149	0.3932	0.0054	0.73	2.5433	0.0352	0.1367	0.0021	0.1193	0.0047	0.77	23	35	56	0.635	2138	25	2163	14	2186	27	98
SPL 2965	93.1	7.3437	0.1137	0.3940	0.0028	0.95	2.5381	0.0178	0.1352	0.0021	0.0053	0.0029	0.67	67	22	176	0.126	2141	13	2154	14	2166	27	99
SPL 2965	33.1	7.3677	0.1556	0.3943	0.0038	0.62	2.5364	0.0244	0.1355	0.0027	0.1782	0.0138	2.05	16	27	37	0.72	2143	18	2157	19	2171	34	99
SPL 2965	96.1	7.5024	0.1078	0.3945	0.0030	0.95	2.5347	0.0193	0.1379	0.0022	0.3646	0.0184	0.58	68	229	135	1.703	2144	14	2173	13	2201	28	98
SPL 2965	51.1	7.3863	0.1440	0.3956	0.0036	0.85	2.5281	0.0232	0.1354	0.0027	0.2231	0.0059	0.56	43	115	91	1.273	2149	17	2159	18	2170	34	99
SPL 2965	35.1	7.3652	0.1570	0.3962	0.0035	0.85	2.5239	0.0224	0.1348	0.0025	0.1446	0.0084	1.41	35	68	76	0.897	2152	16	2157	19	2162	32	99
SPL 2965	67.1	7.4754	0.1252	0.3969	0.0042	0.67	2.5197	0.0264	0.1366	0.0022	0.2018	0.0058	1.10	30	78	63	1.239	2155	19	2170	15	2185	28	99
SPL 2965	21.1	7.6001	0.1306	0.3969	0.0034	0.86	2.5192	0.0218	0.1389	0.0025	0.1497	0.0164	2.32	35	67	74	0.898	2155	16	2185	15	2213	32	98
SPL 2965	90.1	7.6159	0.1269	0.3990	0.0031	0.87	2.5062	0.0192	0.1384	0.0024	0.1548	0.0063	0.24	42	84	92	0.907	2164	14	2187	15	2208	31	98
SPL 2965	83.1	7.6377	0.1175	0.3992	0.0038	0.98	2.5051	0.0238	0.1388	0.0019	0.1877	0.0301	0.87	47	129	102	1.27	2165	18	2189	15	2212	25	98
SPL 2965	5.1	7.5370	0.1252	0.4004	0.0032	0.56	2.4973	0.0197	0.1365	0.0022	0.1573	0.0125	1.41	17	31	39	0.784	2171	15	2177	15	2183	29	99
SPL 2965	13.1	7.5562	0.1132	0.4011	0.0027	0.74	2.4931	0.0165	0.1366	0.0017	0.1783	0.0131	0.65	68	143	155	0.918	2174	12	2180	13	2185	22	99
SPL 2965	74.1	7.4706	0.1206	0.4013	0.0034	0.87	2.4917	0.0211	0.1350	0.0019	0.1442	0.0141	0.42	65	146	142	1.027	2175	16	2169	15	2164	24	100
SPL 2965	7.1	7.4929	0.1114	0.4023	0.0036	0.72	2.4854	0.0224	0.1351	0.0020	0.1491	0.0063	0.71	36	61	82	0.745	2180	17	2172	13	2165	26	100
SPL 2965	14.1	7.6475	0.1282	0.4054	0.0027	0.65	2.4668	0.0162	0.1368	0.0025	0.1403	0.0051	0.40	24	42	51	0.814	2194	12	2190	15	2187	32	100
SPL 2965	10.1	8.1063	0.1799	0.4131	0.0040	0.27	2.4205	0.0236	0.1423	0.0026	0.2629	0.0171	4.02	12	37	24	1.557	2229	18	2243	20	2255	32	99
SPL 2965	16.1	10.3144	0.1662	0.4470	0.0033	0.98	2.2371	0.0163	0.1674	0.0033	0.4151	0.0168	0.93	26	77	45	1.704	2382	14	2463	15	2531	33	96
SPL 2965	73.1	11.3301	0.1961	0.4625	0.0041	0.99	2.1622	0.0191	0.1777	0.0023	0.3086	0.0057	0.46	95	352	160	2.205	2451	18	2551	16	2631	22	96
SPL 2965	32.1	10.4310	0.1954	0.4713	0.0042	0.58	2.1217	0.0189	0.1605	0.0025	0.2281	0.0103	0.67	57	142	99	1.438	2489	18	2474	17	2461	27	100

SPL 2965	97.1	10.4391	0.1558	0.4729	0.0042	0.84	2.1146	0.0188	0.1601	0.0023	0.1840	0.0080	0.54	50	89	88	1.009	2496	19	2475	14	2457	24	100
SPL 2965	15.1	14.3998	0.2096	0.4902	0.0032	0.77	2.0401	0.0133	0.2131	0.0035	0.1180	0.0077	1.33	54	188	104	1.8	2571	14	2776	14	2929	27	92
SPL 2965	81.1	15.2329	0.2139	0.5080	0.0041	0.99	1.9687	0.0158	0.2175	0.0025	0.1642	0.0513	3.43	108	1046	362	2.893	2648	18	2830	14	2962	19	93
SPL 2965	66.1	15.4545	0.2359	0.5196	0.0052	0.99	1.9246	0.0193	0.2157	0.0029	0.0907	0.0338	2.12	116	681	393	1.734	2697	22	2844	14	2949	22	94
SPL 2965	3.1	15.0323	0.1827	0.5431	0.0046	0.99	1.8411	0.0156	0.2007	0.0026	0.1051	0.0217	0.36	42	91	71	1.281	2797	20	2817	14	2832	22	99
SPL 2965	41.1	18.4990	0.3247	0.5627	0.0044	0.98	1.7771	0.0138	0.2384	0.0038	0.1090	0.0109	0.67	77	116	133	0.872	2878	18	3016	16	3109	25	95
SPL 2965	92.1	18.2325	0.2849	0.5755	0.0042	0.74	1.7375	0.0125	0.2298	0.0035	0.1287	0.0143	0.20	72	95	100	0.953	2931	17	3002	15	3050	25	97
SPL 2965	69.1	17.5541	0.2662	0.5830	0.0062	0.81	1.7152	0.0183	0.2184	0.0030	0.1242	0.0117	0.16	114	133	170	0.784	2961	25	2966	14	2969	22	99
SPL 2965	4.1	17.5054	0.2309	0.5835	0.0055	0.99	1.7139	0.0162	0.2176	0.0029	0.0901	0.0252	1.48	71	413	164	2.51	2963	22	2963	13	2963	22	99
SPL 2965	56.1	19.2468	0.3454	0.5862	0.0044	0.90	1.7060	0.0128	0.2381	0.0041	0.2856	0.0172	0.82	50	90	65	1.383	2974	18	3054	18	3108	28	97
SPL 2965	40.1	19.7454	0.3247	0.5899	0.0044	0.99	1.6951	0.0128	0.2427	0.0040	0.0854	0.0053	1.14	43	44	62	0.71	2989	19	3079	17	3138	26	97
SPL 2965	17.1	18.8728	0.2981	0.5920	0.0046	0.95	1.6891	0.0131	0.2312	0.0043	0.1423	0.0081	0.39	39	46	53	0.879	2998	19	3035	15	3060	30	98
SPL 2965	2.1	19.4743	0.2962	0.6029	0.0057	0.94	1.6585	0.0158	0.2343	0.0030	0.1501	0.0104	1.30	27	44	40	1.103	3042	23	3066	15	3081	21	99
SPL 2965	18.1	20.2995	0.2996	0.6286	0.0042	0.97	1.5907	0.0106	0.2342	0.0043	0.1499	0.0184	0.64	32	39	49	0.811	3144	17	3106	14	3081	30	101
SPL 2965	11.1	26.5952	0.3978	0.6809	0.0052	0.90	1.4686	0.0111	0.2833	0.0038	0.3067	0.0184	1.94	30	59	33	1.8	3348	20	3369	15	3381	21	99
SPL 2965	87.1	27.2300	0.3278	0.6877	0.0069	0.99	1.4542	0.0146	0.2872	0.0031	0.0665	0.0227	0.43	108	175	135	1.291	3374	27	3392	13	3402	17	99
SPL 2965	77.1	1.7750	0.0726	0.1085	0.0023	0.99	9.2149	0.1954	0.1186	0.0020	0.2258	0.0954	1.64	34	50	86	0.584	664	12	1036	14	1936	26	64
SPL 2965	80.1	2.0818	0.0298	0.1311	0.0009	0.98	7.6297	0.0537	0.1152	0.0015	0.3904	0.1117	7.37	225	3889	1162	3.346	794	5	1143	10	1883	29	69
SPL 2965	43.1	2.0914	0.0411	0.1455	0.0013	0.99	6.8721	0.0627	0.1042	0.0019	0.1460	0.0116	2.81	30	36	46	0.79	876	7	1146	12	1701	30	76
SPL 2965	38.1	2.5564	0.0967	0.1508	0.0024	0.99	6.6314	0.1063	0.1230	0.0032	0.2843	0.0355	2.29	28	-15	40	-0.39	905	13	1288	19	2000	43	70
SPL 2965	39.1	2.8990	0.0812	0.1673	0.0020	0.87	5.9767	0.0706	0.1257	0.0035	0.2267	0.0502	12.72	6	106	59	1.78	997	11	1382	20	2038	49	72
SPL 2965	45.1	2.7923	0.0428	0.1807	0.0012	0.98	5.5327	0.0362	0.1120	0.0016	0.3049	0.0304	7.54	52	1134	266	4.268	1071	7	1353	11	1833	26	79
SPL 2965	31.1	2.6855	0.0516	0.1818	0.0015	0.99	5.5001	0.0439	0.1071	0.0017	0.2951	0.0626	3.48	171	1404	617	2.276	1077	8	1324	14	1751	29	81
SPL 2965	85.1	3.0174	0.0731	0.1842	0.0031	0.99	5.4278	0.0910	0.1188	0.0015	0.1210	0.0352	0.00	57	-475	24	-19.7	1090	15	1412	12	1938	22	77
SPL 2965	64.1	3.0717	0.0507	0.1882	0.0020	0.96	5.3148	0.0561	0.1184	0.0017	0.2292	0.0268	5.01	57	939	251	3.736	1111	11	1426	12	1932	25	77
SPL 2965	61.1	4.1925	0.0901	0.1903	0.0016	0.98	5.2555	0.0445	0.1598	0.0025	0.2080	0.0206	1.28	99	-64	128	-0.5	1123	8	1673	13	2454	26	67
SPL 2965	34.1	3.6844	0.0625	0.2187	0.0016	0.99	4.5734	0.0340	0.1222	0.0018	0.2485	0.0154	5.63	99	1882	416	4.523	1275	9	1568	15	1989	26	81
SPL 2965	1.1	3.6467	0.0471	0.2196	0.0016	0.99	4.5530	0.0336	0.1204	0.0015	0.1809	0.0484	2.81	66	-17	239	-0.07	1280	8	1560	10	1962	22	82
SPL 2965	22.1	3.8017	0.0721	0.2210	0.0021	0.94	4.5255	0.0436	0.1248	0.0025	0.2684	0.1095	4.26	65	959	312	3.078	1287	11	1593	15	2026	34	80
SPL 2965	52.1	3.9481	0.0994	0.2214	0.0022	0.99	4.5167	0.0440	0.1293	0.0028	0.1556	0.0141	4.37	27	100	55	1.817	1289	11	1624	18	2089	38	79
SPL 2965	100.1	4.0449	0.0451	0.2448	0.0018	0.99	4.0851	0.0300	0.1198	0.0015	0.2773	0.1224	11.35	169	11850	1376	8.609	1412	10	1643	11	1954	24	85
SPL 2965	59.1	4.3530	0.0788	0.2448	0.0016	0.99	4.0847	0.0264	0.1290	0.0024	0.1413	0.0381	1.37	64	271	203	1.332	1412	8	1703	16	2084	33	82
SPL 2965	70.1	4.1422	0.0907	0.2578	0.0031	0.99	3.8794	0.0468	0.1165	0.0019	0.1745	0.0835	-205.90	0	27	-7	-3.7	1478	15	1663	16	1904	29	88
SPL 2965	27.1	4.4253	0.0723	0.2610	0.0016	0.99	3.8320	0.0232	0.1230	0.0018	0.2053	0.0466	3.71	117	1154	405	2.849	1495	8	1717	13	2000	26	87
SPL 2965	79.1	4.8039	0.0836	0.2682	0.0024	0.98	3.7284	0.0333	0.1299	0.0018	0.1302	0.0186	0.00	69	-175	120	-1.45	1532	12	1786	14	2097	24	85
SPL 2965	94.1	5.0331	0.0881	0.2733	0.0022	0.98	3.6587	0.0289	0.1336	0.0023	0.1929	0.0180	3.04	33	232	82	2.843	1558	11	1825	14	2145	30	85
SPL 2965	37.1	5.6510	0.1188	0.3063	0.0028	0.91	3.2649	0.0299	0.1338	0.0030	0.1879	0.0385	9.05	10	77	32	2.445	1722	14	1924	19	2149	39	89
SPL 2965	29.1	6.4169	0.0885	0.3234	0.0018	0.99	3.0921	0.0170	0.1439	0.0020	0.2423	0.0733	0.00	55	-516	102	-5.04	1806	9	2035	14	2275	28	88
SPL 2965	47.1	5.9011	0.0973	0.3315	0.0022	0.01	3.0163	0.0201	0.1291	0.0019	0.2102	0.0519	27.66	39	1377	150	9.166	1846	11	1961	15	2086	26	94
SPL 2965	23.1	10.4005	0.2033	0.3594	0.0035	0.99	2.7823	0.0268	0.2099	0.0037	0.2040	0.0363	1.47	73	1148	185	6.209	1979	16	2471	15	2905	28	80
SPL 2965	42.1	7.4249	0.1408	0.3930	0.0026	0.96	2.5448	0.0169	0.1370	0.0024	0.1839	0.0143	-5.18	-9	-17	-12	1.407	2136	12	2164	17	2190	32	98
SPL 2965	62.1	7.4624	0.1185	0.4001	0.0027	0.98	2.4997	0.0166	0.1353	0.0022	0.1448	0.0357	0.00	22	-31	52	-0.59	2169	13	2168	16	2168	28	100
SPL 2965	91.1	11.9341	0.1804	0.4036	0.0032	0.98	2.4779	0.0196	0.2145	0.0033	0.1286	0.0213	1.66	74	459	152	3.024	2185	15	2599	14	2940	25	84
SPL 2965	68.1	11.1060	0.2216	0.4438	0.0050	0.94	2.2531	0.0254	0.1815	0.0033	0.1001	0.0297	-3.84	-5	-64	-15	4.286	2368	22	2532	19	2666	31	93
SPL 2965	86.1	18.4027	0.2363	0.5941	0.0064	0.96	1.6833	0.0181	0.2247	0.0027	0.0427	0.0377	0.00	-98	-822	-334	2.461	3006	26	3011	14	3014	21	99

13/06/02014 SPOT SITE E-87 - OSWALDO MG-01-Q QUARTZITO SPL 1180,6Hz, 6mJ, 32um		RATIOS											Pb total comum %	Pb rad ppm	Th ppm	U ppm	Th/U	AGES				conc. 206/238 207/206 %
		207/235	1sigma	206/238	1 sigma	coef. corr	238/206	1 sigma	207/206	1 sigma	208/206	1 sigma						T206/238	1 sigma	T207/206	1 sigma	
MG-01-Q	75.1	29.9452	0.4647	0.6988	0.0080	0.81	1.4311	0.0164	0.3108	0.0039	0.1648	0.0043	0.11	96.4	40.9	100.3	0.408	3.416	0.030	3.525	0.019	96
MG-01-Q	80.1	18.5747	0.3103	0.5821	0.0073	0.88	1.7178	0.0215	0.2314	0.0033	0.0551	0.0032	0.22	57.7	11.4	82.3	0.139	2.957	0.030	3.062	0.023	96
MG-01-Q	7.1	18.5533	0.4389	0.5887	0.0084	0.39	1.6986	0.0241	0.2286	0.0053	0.1740	0.0089	0.33	51.1	28.9	69.2	0.418	2.984	0.034	3.042	0.037	98
MG-01-Q	56.1	17.4410	0.3918	0.5664	0.0070	0.69	1.7655	0.0219	0.2233	0.0046	0.1689	0.0050	0.11	89.3	47.8	120.3	0.397	2.893	0.029	3.005	0.033	96
MG-01-Q	8.1	16.6845	0.3679	0.5635	0.0066	0.56	1.7746	0.0209	0.2147	0.0045	0.2514	0.0071	0.14	80.0	67.4	106.5	0.633	2.881	0.027	2.942	0.034	97
MG-01-Q	27.1	14.9331	0.2794	0.5344	0.0054	0.62	1.8714	0.0188	0.2027	0.0035	0.1882	0.0054	0.08	129.5	102.9	185.7	0.554	2.760	0.023	2.848	0.028	96
MG-01-Q	59.1	14.8344	0.3019	0.5334	0.0058	0.76	1.8748	0.0205	0.2017	0.0038	0.2746	0.0051	0.10	165.4	155.6	225.1	0.691	2.756	0.025	2.840	0.031	97
MG-01-Q	3.1	14.1508	0.2961	0.5287	0.0053	0.21	1.8913	0.0190	0.1941	0.0037	0.2477	0.0092	0.06	120.0	95.9	172.9	0.555	2.736	0.022	2.777	0.031	98
MG-01-Q	30.1	13.7119	0.2550	0.5161	0.0051	0.64	1.9375	0.0192	0.1927	0.0033	0.1154	0.0027	0.06	152.4	74.7	246.7	0.303	2.683	0.022	2.765	0.028	97
MG-01-Q	17.1	13.0745	0.2718	0.5080	0.0072	0.57	1.9685	0.0278	0.1867	0.0040	0.2090	0.0054	0.13	79.1	71.4	122.0	0.585	2.648	0.031	2.713	0.036	97
MG-01-Q	1.1	11.7900	0.2571	0.4890	0.0054	0.21	2.0451	0.0225	0.1749	0.0036	0.1583	0.0044	0.18	75.8	47.9	129.6	0.3690	2.566	0.023	2.605	0.034	98
MG-01-Q	54.1	10.7668	0.2791	0.4622	0.0063	0.80	2.1636	0.0293	0.1690	0.0042	0.1712	0.0054	0.14	62.6	43.0	107.1	0.4010	2.449	0.027	2.547	0.041	96
MG-01-Q	67.1	10.0427	0.1720	0.4499	0.0052	0.81	2.2229	0.0255	0.1619	0.0022	0.0925	0.0046	0.23	146.2	60.2	279.5	0.215	2.395	0.023	2.476	0.023	96
MG-01-Q	36.1	9.8592	0.2242	0.4445	0.0060	0.53	2.2495	0.0302	0.1609	0.0033	0.1088	0.0036	0.19	84.4	44.4	157.5	0.282	2.371	0.027	2.465	0.035	96
MG-01-Q	63.1	9.1212	0.1524	0.4201	0.0047	0.94	2.3807	0.0265	0.1575	0.0020	0.0891	0.0021	0.04	171.2	79.1	344.1	0.230	2.261	0.021	2.429	0.021	93
MG-01-Q	37.1	9.3035	0.2211	0.4313	0.0061	0.93	2.3184	0.0328	0.1564	0.0035	0.0970	0.0039	0.32	68.9	30.4	133.0	0.229	2.312	0.028	2.417	0.038	95
MG-01-Q	20.1	8.0600	0.2965	0.4035	0.0090	0.37	2.4784	0.0551	0.1449	0.0061	0.2209	0.0143	1.14	22.2	26.3	44.3	0.594	2.185	0.041	2.286	0.074	95
MG-01-Q	73.1	7.8155	0.3689	0.4019	0.0118	0.15	2.4880	0.0728	0.1410	0.0073	0.1538	0.0278	0.50	11.8	9.5	23.0	0.412	2.178	0.054	2.240	0.089	97
MG-01-Q	81.2	7.2997	0.1643	0.3838	0.0062	0.84	2.6055	0.0419	0.1379	0.0031	0.1082	0.0077	0.23	28.1	15.3	61.1	0.250	2.094	0.029	2.202	0.039	95
MG-01-Q	81.1	7.3520	0.1412	0.3892	0.0051	0.01	2.5695	0.0339	0.1370	0.0025	0.1350	0.0050	0.27	37.7	22.6	79.2	0.285	2.119	0.024	2.190	0.031	96
MG-01-Q	57.1	7.1898	0.2542	0.3837	0.0063	0.08	2.6062	0.0429	0.1359	0.0049	0.0878	0.0099	0.32	33.1	14.7	74.8	0.196	2.094	0.029	2.176	0.063	96
MG-01-Q	25.1	7.6079	0.2257	0.4080	0.0056	0.33	2.4512	0.0335	0.1353	0.0041	0.1404	0.0081	0.79	36.5	38.0	76.0	0.500	2.206	0.026	2.167	0.054	101
MG-01-Q	41.1	7.1627	0.2084	0.3846	0.0064	0.36	2.6004	0.0436	0.1351	0.0038	0.1327	0.0133	0.23	75.2	43.4	166.4	0.261	2.098	0.030	2.165	0.049	96
MG-01-Q	24.1	6.9316	0.1724	0.3723	0.0044	0.92	2.6861	0.0318	0.1350	0.0034	0.2214	0.0080	0.77	56.3	85.0	125.0	0.680	2.040	0.021	2.164	0.043	94
MG-01-Q	2.1	7.3076	0.1549	0.3927	0.0039	0.88	2.5463	0.0254	0.1350	0.0027	0.1836	0.0054	0.13	120.6	122.6	255.9	0.479	2.135	0.018	2.163	0.035	98
MG-01-Q	22.1	7.0209	0.2091	0.3783	0.0052	0.01	2.6433	0.0360	0.1346	0.0040	0.2226	0.0111	0.42	41.3	52.2	84.1	0.620	2.068	0.024	2.159	0.053	95
MG-01-Q	82.1	6.9209	0.1363	0.3733	0.0051	0.67	2.6789	0.0365	0.1345	0.0024	0.1004	0.0048	0.30	39.3	20.6	89.4	0.231	2.045	0.024	2.157	0.032	94
MG-01-Q	35.1	6.9748	0.1932	0.3775	0.0059	0.99	2.6489	0.0415	0.1340	0.0036	0.1324	0.0063	0.80	54.4	52.9	165.0	0.321	2.065	0.028	2.151	0.046	95
MG-01-Q	19.1	6.9603	0.1938	0.3781	0.0063	0.52	2.6446	0.0439	0.1335	0.0041	0.1400	0.0061	0.30	42.6	39.2	98.5	0.397	2.068	0.029	2.145	0.053	96
MG-01-Q	52.1	6.8662	0.1555	0.3750	0.0042	0.34	2.6667	0.0301	0.1328	0.0029	0.2146	0.0082	0.15	135.5	163.5	279.8	0.584	2.053	0.020	2.135	0.038	96
MG-01-Q	78.1	6.3888	0.1029	0.3535	0.0037	0.99	2.8285	0.0299	0.1311	0.0018	0.1259	0.0032	0.06	85.2	65.2	197.0	0.331	1.952	0.018	2.112	0.025	92
MG-01-Q	61.1	6.6280	0.1880	0.3674	0.0063	0.68	2.7221	0.0464	0.1309	0.0038	0.0895	0.0074	0.49	27.8	15.7	66.6	0.236	2.017	0.030	2.109	0.049	95
MG-01-Q	64.1	6.6963	0.1348	0.3716	0.0048	0.77	2.6914	0.0345	0.1307	0.0023	0.0870	0.0055	0.20	80.7	34.6	193.2	0.179	2.037	0.022	2.108	0.030	96
MG-01-Q	69.1	6.7366	0.1155	0.3753	0.0042	0.92	2.6644	0.0296	0.1302	0.0017	0.3404	0.0053	0.07	173.5	300.0	343.1	0.874	2.054	0.020	2.100	0.023	97
MG-01-Q	5.1	6.5374	0.2042	0.3648	0.0067	0.01	2.7415	0.0500	0.1300	0.0045	0.2997	0.0172	0.67	27.8	42.2	59.5	0.710	2.005	0.031	2.098	0.061	95
MG-01-Q	46.1	6.4960	0.1864	0.3635	0.0059	0.60	2.7509	0.0449	0.1296	0.0036	0.1706	0.0128	0.33	65.4	79.4	143.8	0.552	1.999	0.028	2.093	0.050	95
MG-01-Q	15.1	6.5454	0.1822	0.3664	0.0060	0.73	2.7291	0.0449	0.1296	0.0040	0.2366	0.0073	0.30	43.4	56.6	94.0	0.602	2.013	0.028	2.092	0.053	96
MG-01-Q	44.1	6.3809	0.2308	0.3586	0.0073	0.46	2.7889	0.0568	0.1291	0.0049	0.2128	0.0143	0.27	31.2	34.6	66.6	0.519	1.975	0.035	2.085	0.067	94
MG-01-Q	76.1	6.6375	0.1124	0.3732	0.0042	0.79	2.6793	0.0301	0.1290	0.0019	0.3011	0.0053	0.08	97.5	134.8	193.5	0.697	2.045	0.020	2.084	0.026	98
MG-01-Q	34.1	6.4927	0.1599	0.3651	0.0042	0.43	2.7391	0.0318	0.1290	0.0031	0.1130	0.0046	0.13	58.5	37.7	139.0	0.272	2.006	0.020	2.084	0.042	96
MG-01-Q	84.1	6.5536	0.1251	0.3689	0.0047	0.66	2.7110	0.0347	0.1289	0.0023	0.1172	0.0049	0.27	65.3	45.6	148.4	0.307	2.024	0.022	2.082	0.031	97
MG-01-Q	79.1	6.1497	0.1208	0.3470	0.0046	0.90	2.8815	0.0384	0.1285	0.0024	0.0913	0.0055	1.11	40.8	21.1	115.0	0.184	1.920	0.022	2.078	0.033	92
MG-01-Q	83.1	6.8905	0.1555	0.3890	0.0061	0.59	2.5705	0.0403	0.1285	0.0029	0.1815	0.0081	0.13	35.4	32.1	75.4	0.4260	2.118	0.028	2.077	0.040	101
MG-01-Q	66.1	6.3967	0.1390	0.3612	0.0049	0.81	2.7688	0.0375	0.1285	0.0024	0.0996	0.0037	0.28	56.7	31.7	135.5	0.2340	1.988	0.023	2.077	0.033	95
MG-01-Q	74.1	6.5806	0.1294	0.3721	0.0050	0.48	2.6875	0.0359	0.1283	0.0024	0.5395	0.0554	0.24	56.9	118.8	100.1	1.187	2.039	0.023	2.074	0.033	98
MG-01-Q	48.1	6.2725	0.2919	0.3549	0.0071	0.52	2.8174	0.0567	0.1282	0.0062	0.1884	0.0166	1.71	20.6	20.9	45.7	0.457	1.958	0.034	2.073	0.085	94
MG-01-Q	68.1	6.4864	0.1332	0.3672	0.0048	0.88	2.7235	0.0353	0.1281	0.0023	0.1644	0.0045	0.14	63.7	56.1	143.0	0.392	2.016	0.022	2.072	0.032	97
MG-01-Q	45.1	6.3126	0.1384	0.3573	0.0044	0.75	2.7986	0.0345	0.1281	0.0025	0.1499	0.0035	0.33	114.0	105.1	267.2	0.393	1.969	0.021	2.072	0.034	95
MG-01-Q	4.1	6.1897	0.1718	0.3558	0.0055	0.32	2.8106	0.0438	0.1262	0.0039	0.1378	0.0160	1.79	29.1	24.1	74.6	0.324	1.962	0.026	2.045	0.055	95
MG-01-Q	77.1	6.3736	0.1182	0.3666	0.0046	0.81	2.7275	0.0340	0.1261	0.0021	0.1333	0.0073	0.19	64.3	47.8	151.3	0.316	2.014	0.022	2.044	0.030	98
MG-01-Q	28.1	6.2798	0.1236	0.3613	0.0036	0.66	2.7675	0.0274	0.1260	0.0023	0.0884	0.0021	0.07	158.8	90.6	390.1	0.232	1.988	0.017	2.044	0.032	97
MG-01-Q	23.1	6.2171	0.1321	0.3583	0.0037	0.89	2.7907	0.0291	0.1258	0.0025	0.1988	0.0021	0.29	98.7	123.5	227.9	0.542	1.974	0.018	2.041	0.036	96
MG-01-Q	60.1	6.3034	0.1597	0.3634	0.0044	0.01	2.7516	0.0335	0.1258	0.0031	0.1786	0.0049	0.20	76.4	72.9	172.1	0.424	1.998	0.021	2.040	0.043	97
MG-01-Q	13.1	6.1265	0.1156	0.3532	0.0043	0.97	2.8310	0.0345	0.1258	0.0023	0.0862	0.0070	0.16	169.5	134.6	414.6	0.325	1.950	0.020	2.040	0.032	95
MG-01-Q	18.1	6.6346	0.1367	0.3828	0.0049	0.90	2.6123	0.0337	0.1257	0.0026	0.1695	0.0031	2.65	93.1	137.0	204.3	0.671	2.089	0.023	2.039	0.037	102

MG-01-Q	32.1	6.1272	0.1429	0.3540	0.0039	0.78	2.8248	0.0313	0.1255	0.0029	0.1501	0.0060	0.18	76.6	75.8	182.4	0.415	1.954	0.019	2.036	0.040	95
MG-01-Q	42.1	6.1968	0.2183	0.3587	0.0070	0.21	2.7878	0.0546	0.1253	0.0046	0.0615	0.0096	0.34	29.5	11.3	71.8	0.158	1.976	0.033	2.033	0.066	97
MG-01-Q	38.1	6.0653	0.1300	0.3530	0.0043	0.95	2.8329	0.0342	0.1246	0.0025	0.1332	0.0040	0.25	98.1	87.5	236.5	0.3700	1.949	0.020	2.023	0.035	96
MG-01-Q	39.1	6.0155	0.1323	0.3505	0.0043	0.14	2.8530	0.0352	0.1245	0.0025	0.2842	0.0267	0.14	129.3	180.3	274.6	0.657	1.937	0.021	2.021	0.035	95
MG-01-Q	47.1	6.0028	0.1707	0.3514	0.0056	0.57	2.8459	0.0450	0.1239	0.0034	0.2089	0.0065	0.35	56.9	63.9	126.2	0.506	1.941	0.026	2.013	0.049	96
MG-01-Q	55.1	5.8368	0.1482	0.3425	0.0041	0.01	2.9199	0.0353	0.1236	0.0030	0.1555	0.0046	0.16	68.6	61.6	166.0	0.371	1.899	0.020	2.009	0.044	94
MG-01-Q	70.1	5.9363	0.1135	0.3505	0.0042	0.46	2.8527	0.0345	0.1228	0.0020	0.1603	0.0030	0.48	85.5	100.9	211.3	0.478	1.937	0.020	1.998	0.029	96
MG-01-Q	16.1	5.6663	0.1091	0.3384	0.0041	0.28	2.9551	0.0357	0.1214	0.0023	0.0632	0.0298	0.18	123.9	41.8	340.5	0.123	1.879	0.020	1.978	0.033	95
MG-01-Q	62.1	5.6869	0.1324	0.3417	0.0049	0.55	2.9264	0.0419	0.1207	0.0026	0.1315	0.0036	0.19	42.6	32.8	106.6	0.308	1.895	0.023	1.967	0.038	96
MG-01-Q	65.1	5.6944	0.1123	0.3428	0.0043	0.77	2.9169	0.0362	0.1205	0.0020	0.1015	0.0047	0.17	68.8	42.2	174.7	0.242	1.900	0.020	1.963	0.030	96
MG-01-Q	26.1	5.6491	0.1202	0.3429	0.0035	0.56	2.9159	0.0301	0.1195	0.0024	0.1165	0.0034	0.14	121.4	91.2	308.0	0.296	1.901	0.017	1.948	0.036	97
MG-01-Q	40.1	5.5941	0.1140	0.3413	0.0039	0.98	2.9298	0.0335	0.1189	0.0021	0.1414	0.0212	0.35	187.6	144.8	517.1	0.280	1.893	0.019	1.939	0.032	97
MG-01-Q	49.1	4.9457	0.1581	0.3105	0.0044	0.67	3.2210	0.0454	0.1155	0.0037	0.2448	0.0082	0.52	41.7	55.8	103.4	0.540	1.743	0.022	1.888	0.058	92
MG-01-Q	72.1	4.9010	0.0915	0.3171	0.0037	0.12	3.1534	0.0367	0.1121	0.0017	0.1958	0.0079	0.10	112.1	126.9	286.7	0.443	1.776	0.018	1.834	0.028	96
MG-01-Q	43.1	4.8542	0.1167	0.3161	0.0041	0.79	3.1636	0.0412	0.1114	0.0025	0.1761	0.0067	0.13	95.1	105.1	250.0	0.420	1.771	0.020	1.822	0.040	97
MG-01-Q	9.1	4.8527	0.1061	0.3166	0.0042	0.01	3.1586	0.0420	0.1112	0.0025	0.1772	0.0108	0.11	134.4	180.0	349.9	0.514	1.773	0.021	1.819	0.041	97
MG-01-Q	71.1	4.7612	0.0828	0.3132	0.0035	0.87	3.1930	0.0354	0.1103	0.0015	0.1650	0.0017	0.04	157.0	179.8	420.9	0.427	1.756	0.017	1.804	0.025	97
MG-01-Q	12.1	4.5783	0.2150	0.3066	0.0071	0.62	3.2621	0.0754	0.1083	0.0059	0.1512	0.0105	0.50	17.0	17.0	47.8	0.3560	1.724	0.035	1.771	0.096	97
MG-01-Q	11.1	3.2961	0.1329	0.2519	0.0049	0.01	3.9696	0.0768	0.0949	0.0043	0.3569	0.0178	0.27	28.9	79.4	84.0	0.944	1.448	0.025	1.526	0.087	94
MG-01-Q	53.1	3.2199	0.0837	0.2490	0.0029	0.01	4.0165	0.0463	0.0938	0.0024	0.1709	0.0040	0.12	90.1	123.0	300.2	0.410	1.433	0.015	1.504	0.048	95
MG-01-Q	10.1	3.2695	0.0897	0.2534	0.0037	0.65	3.9467	0.0582	0.0936	0.0027	0.3044	0.0053	0.28	65.4	167.5	198.4	0.844	1.456	0.019	1.500	0.055	97
MG-01-Q	6.1	3.2098	0.0831	0.2520	0.0030	0.23	3.9685	0.0478	0.0924	0.0024	0.3934	0.0115	0.15	66.9	158.8	195.7	0.811	1.449	0.016	1.475	0.049	98
MG-01-Q	21.1	3.2092	0.1142	0.2522	0.0044	0.56	3.9653	0.0690	0.0923	0.0037	0.4285	0.0092	0.63	39.0	111.5	110.6	1.0080	1.450	0.023	1.473	0.074	98
MG-01-Q	50.1	15.1105	0.2871	0.5065	0.0052	0.99	1.9744	0.0202	0.2164	0.0038	0.1095	0.0017	0.11	220.0	87.9	371.8	0.236	2.642	0.022	2.954	0.029	89
MG-01-Q	33.1	4.8081	0.0808	0.2986	0.0026	0.91	3.3489	0.0294	0.1168	0.0021	0.1063	0.0110	17.02	74.8	48.1	166.4	0.289	1.684	0.013	1.908	0.033	88
MG-01-Q	14.1	12.9146	0.2493	0.4695	0.0062	0.96	2.1301	0.0281	0.1995	0.0039	0.7226	0.0090	0.08	133.4	284.5	157.9	1.802	2.481	0.027	2.822	0.032	87
MG-01-Q	58.1	16.1861	0.3111	0.5038	0.0053	0.98	1.9851	0.0207	0.2330	0.0043	0.1987	0.0098	0.20	146.5	82.4	227.3	0.362	2.630	0.023	3.073	0.029	85
MG-01-Q	51.1	4.9663	0.1285	0.2851	0.0034	0.96	3.5077	0.0424	0.1263	0.0034	0.1819	0.0141	0.38	98.6	70.7	280.5	0.252	1.617	0.017	2.048	0.047	78
MG-01-Q	31.1	19.4903	0.3546	0.4535	0.0046	0.99	2.2052	0.0225	0.3117	0.0052	0.0935	0.0044	0.75	195.0	93.1	532.4	0.175	2.411	0.021	3.529	0.026	68
MG-01-Q	85.1	7.8436	0.1128	0.2810	0.0027	0.94	3.5591	0.0344	0.2025	0.0023	0.0247	0.0026	-6.16	-5.9	-8.5	-22.9	0.372	1.596	0.014	2.846	0.019	56
MG-01-Q	29.1	2.8395	0.0742	0.1767	0.0021	0.99	5.6595	0.0665	0.1166	0.0028	0.2567	0.0098	0.40	84.3	120.6	274.5	0.439	1.049	0.011	1.904	0.043	55

29/05/02014	SPOT	SITE	RATIOS															AGES				
E-87 - OSWALDO			207/235	1sigma	206/238	1 sigma	coef. corr	238/206	1 sigma	207/206	1 sigma	208/206	1 sigma	Pb total comum %	Pb rad ppm	Th ppm	U ppm	Th/U	$T_{206/238}$	1 sigma	$T_{207/206}$	1 sigma	Conc. 206/238 207/206
MG - 01F	40.1		7.24740	0.19390	0.38770	0.00420	0.250	2.57930	0.02770	0.13560	0.00380	0.15840	0.00480	0.1	117.0	147.6	263.1	0.6	2.112	0.019	2.171	0.049	97
MG - 01F	43.1		7.25580	0.21190	0.39310	0.00470	0.340	2.54370	0.03010	0.13390	0.00420	0.10070	0.01640	0.1	119.6	72.5	282.4	0.3	2.137	0.022	2.149	0.054	99
MG - 01F	48.1		7.34530	0.22060	0.39400	0.00480	0.350	2.53790	0.03110	0.13520	0.00430	0.38270	0.00890	0.3	102.3	232.2	187.5	1.2	2.141	0.022	2.167	0.055	98
MG - 01F	46.1		7.42140	0.20950	0.39590	0.00460	0.010	2.52610	0.02910	0.13600	0.00400	0.09260	0.00610	0.2	85.2	54.8	195.5	0.3	2.150	0.021	2.176	0.052	98
MG - 01F	56.1		7.45450	0.22140	0.39590	0.00480	0.810	2.52600	0.03060	0.13660	0.00420	0.20410	0.01810	0.5	134.1	194.4	272.8	0.7	2.150	0.022	2.184	0.053	98
MG - 01F	3.2		7.38300	0.14460	0.39680	0.00350	0.860	2.51990	0.02200	0.13490	0.00260	0.15180	0.00580	0.3	268.5	198.5	621.5	0.3	2.154	0.016	2.163	0.033	99
MG - 01F	63.1		7.47230	0.26150	0.39770	0.00570	0.010	2.51450	0.03630	0.13630	0.00500	0.24140	0.00950	0.9	52.0	73.7	107.6	0.7	2.158	0.026	2.180	0.063	98
MG - 01F	58.1		7.52600	0.17270	0.39890	0.00360	0.900	2.50660	0.02250	0.13680	0.00300	0.39470	0.00320	0.2	283.2	618.0	544.4	1.1	2.164	0.016	2.187	0.038	98
MG - 01F	4.1		7.60880	0.18000	0.40200	0.00420	0.520	2.48770	0.02580	0.13730	0.00330	0.13790	0.00720	0.2	133.4	107.7	263.0	0.4	2.178	0.019	2.193	0.041	99
MG - 01F	37.1		7.32740	0.17130	0.40220	0.00400	0.940	2.48630	0.02450	0.13210	0.00330	0.16490	0.00620	0.5	211.3	387.1	461.9	0.8	2.179	0.018	2.126	0.043	102
MG - 01F	18.1		7.56840	0.31800	0.40230	0.00810	0.060	2.48570	0.05020	0.13640	0.00640	0.57610	0.01840	1.3	44.4	126.5	70.3	1.8	2.180	0.037	2.183	0.082	99
MG - 01F	5.1		7.58680	0.16210	0.40290	0.00380	0.520	2.48220	0.02360	0.13660	0.00290	0.11790	0.00310	0.0	181.7	125.9	377.6	0.3	2.182	0.018	2.184	0.038	99
MG - 01F	30.1		7.46740	0.24140	0.40350	0.00570	0.600	2.47810	0.03530	0.13420	0.00510	0.34320	0.06990	0.4	79.2	178.4	138.9	1.3	2.185	0.026	2.154	0.065	101
MG - 01F	64.1		7.63790	0.17770	0.40360	0.00380	0.990	2.47750	0.02320	0.13720	0.00340	0.22130	0.01750	0.3	137.9	216.9	318.6	0.7	2.186	0.018	2.193	0.045	99
MG - 01F	3.1		7.51340	0.17590	0.40510	0.00410	0.350	2.46870	0.02510	0.13450	0.00310	0.17850	0.00320	0.1	171.4	156.9	331.8	0.5	2.192	0.019	2.158	0.040	101
MG - 01F	34.1		7.68500	0.16290	0.40550	0.00360	0.740	2.46640	0.02200	0.13750	0.00300	0.16030	0.00330	0.1	236.0	220.8	495.0	0.4	2.194	0.017	2.196	0.038	99
MG - 01F	44.1		7.78100	0.19370	0.40570	0.00410	0.290	2.46460	0.02480	0.13910	0.00350	0.14920	0.00530	0.2	157.8	161.3	333.5	0.5	2.195	0.019	2.216	0.045	99
MG - 01F	14.1		7.75530	0.21960	0.40610	0.00580	0.720	2.46240	0.03530	0.13850	0.00390	0.24980	0.00860	0.3	99.0	142.0	191.4	0.7	2.197	0.027	2.209	0.050	99
MG - 01F	13.1		7.55520	0.15070	0.40660	0.00430	0.830	2.45940	0.02620	0.13480	0.00250	0.06450	0.00200	0.2	257.8	97.7	574.2	0.2	2.199	0.020	2.161	0.033	101
MG - 01F	15.1		7.60480	0.20920	0.40750	0.00570	0.770	2.45420	0.03410	0.13540	0.00390	0.08020	0.00500	0.1	116.9	58.0	256.0	0.2	2.203	0.026	2.169	0.051	101
MG - 01F	7.1		7.77470	0.20990	0.41110	0.00480	0.910	2.43270	0.02860	0.13720	0.00380	0.28900	0.00520	0.9	105.6	152.8	192.9	0.8	2.220	0.022	2.192	0.049	101
MG - 01F	54.1		7.10760	0.33280	0.37910	0.00750	0.790	2.63810	0.05230	0.13600	0.00690	0.29300	0.02250	2.1	35.6	58.2	76.7	0.8	2.072	0.035	2.177	0.088	95
MG - 01F	55.1		7.15850	0.16830	0.38270	0.00350	0.980	2.61310	0.02400	0.13570	0.00300	0.05590	0.00860	2.0	187.9	93.4	515.8	0.2	2.089	0.016	2.173	0.039	96
MG - 01F	26.1		7.18480	0.16870	0.38550	0.00390	0.980	2.59410	0.02600	0.13520	0.00380	0.24860	0.00630	1.1	117.3	203.3	273.9	0.7	2.102	0.018	2.166	0.048	97
MG - 01F	49.1		7.25060	0.24470	0.38600	0.00550	0.990	2.59060	0.03690	0.13620	0.00530	0.85470	0.03160	0.3	93.3	346.6	143.7	2.4	2.104	0.026	2.180	0.070	96
MG - 01F	22.1		7.89100	0.18390	0.41990	0.00500	0.999	2.38140	0.02820	0.13630	0.00310	0.16420	0.00620	2.0	197.1	428.4	583.5	0.7	2.260	0.023	2.181	0.039	103
MG - 01F	8.1		8.08750	0.17810	0.41630	0.00410	0.860	2.40200	0.02360	0.14090	0.00310	0.27350	0.00450	1.1	179.4	233.6	315.4	0.7	2.244	0.019	2.238	0.038	100
MG - 01F	57.1		7.55340	0.18110	0.40510	0.00380	0.999	2.46850	0.02340	0.13520	0.00330	0.07540	0.00480	0.6	136.3	128.4	308.9	0.4	2.192	0.018	2.167	0.043	101
MG - 01F	53.1		7.90130	0.20160	0.41570	0.00420	0.930	2.40540	0.02440	0.13780	0.00340	0.38520	0.01220	0.3	176.1	352.7	325.8	1.1	2.241	0.019	2.200	0.043	101
MG - 01F	31.1		3.35170	0.12100	0.25860	0.00350	0.170	3.86640	0.05160	0.09400	0.00380	0.33040	0.00900	0.3	71.2	214.8	213.9	1.0	1.483	0.018	1.508	0.078	98
MG - 01F	23.1		3.52670	0.09750	0.26930	0.00330	0.550	3.71360	0.04590	0.09500	0.00270	0.24640	0.00920	0.1	139.8	272.2	418.6	0.7	1.537	0.017	1.528	0.054	100
MG - 01F	11.1		4.19820	0.10480	0.29030	0.00290	0.920	3.44440	0.03440	0.10490	0.00260	0.11530	0.00970	0.6	124.7	90.1	363.6	0.2	1.643	0.014	1.712	0.045	95
MG - 01F	6.1		4.71780	0.09680	0.30930	0.00270	0.950	3.23340	0.02810	0.11060	0.00220	0.16370	0.00430	0.3	278.8	453.0	777.8	0.6	1.737	0.013	1.810	0.036	95
MG - 01F	35.1		4.88400	0.09750	0.31840	0.00250	0.010	3.14090	0.02510	0.11130	0.00220	0.03450	0.00250	0.2	302.8	84.5	912.8	0.1	1.782	0.012	1.820	0.037	97
MG - 01F	47.1		4.83540	0.11510	0.32160	0.00280	0.970	3.10950	0.02690	0.10910	0.00260	0.14940	0.00500	1.2	308.2	386.9	964.0	0.4	1.797	0.014	1.784	0.043	100
MG - 01F	42.1		5.61620	0.14560	0.33300	0.00330	0.890	3.00340	0.02990	0.12230	0.00330	0.20300	0.01720	0.6	161.7	271.0	422.1	0.6	1.853	0.016	1.991	0.048	93
MG - 01F	41.1		5.77710	0.12130	0.34300	0.00270	0.980	2.91570	0.02310	0.12220	0.00260	0.23820	0.00460	0.1	357.0	750.3	833.7	0.9	1.901	0.013	1.988	0.038	95
MG - 01F	59.1		6.27750	0.20250	0.34820	0.00440	0.970	2.87180	0.03640	0.13070	0.00410	0.32240	0.05790	0.5	87.9	177.7	210.2	0.8	1.926	0.021	2.108	0.054	91
MG - 01F	50.1		5.98050	0.13280	0.34940	0.00300	0.990	2.86200	0.02420	0.12410	0.00290	0.01800	0.00230	0.8	246.1	155.9	733.5	0.2	1.932	0.014	2.017	0.041	95
MG - 01F	32.1		6.50570	0.13470	0.35970	0.00310	0.990	2.78010	0.02410	0.13120	0.00290	0.13070	0.00320	0.3	206.1	190.7	500.6	0.4	1.981	0.015	2.114	0.039	93
MG - 01F	51.1		6.37320	0.19650	0.36020	0.00440	0.880	2.77630	0.03420	0.12830	0.00410	0.20090	0.00580	0.1	86.1	116.3	202.0	0.6	1.983	0.021	2.075	0.057	95
MG - 01F	16.1		6.48450	0.14820	0.36140	0.00420	0.980	2.76700	0.03180	0.13010	0.00290	0.10680	0.00980	0.0	169.6	108.1	401.2	0.3	1.989	0.020	2.100	0.039	94
MG - 01F	27.1		6.30410	0.28680	0.36400	0.00730	0.940	2.74730	0.05500	0.12560	0.00690	0.49700	0.02010	1.4	40.3	113.7	74.3	1.5	2.001	0.035	2.037	0.096	98
MG - 01F	60.1		6.62820	0.16850	0.37130	0.00370	0.760	2.69350	0.02650	0.12950	0.00320	0.12180	0.00870	0.1	125.2	109.4	294.6	0.4	2.035	0.017	2.091	0.043	97
MG - 01F	20.1		6.87020	0.16200	0.37350	0.00450	0.990	2.67720	0.03230	0.13340	0.00300	0.16390	0.01600	0.3	144.3	182.4	290.4	0.6	2.046	0.021	2.143	0.039	95
MG - 01F	61.1		6.73490	0.19180	0.37430	0.00420	0.460	2.67140	0.03020	0.13050	0.00370	0.18140	0.02160	0.1	108.7	101.2	259.4	0.4	2.050	0.020	2.105	0.050	97
MG - 01F	10.1		6.94460	0.26320	0.37620	0.00600	0.990	2.65830	0.04270	0.13390	0.00650	0.33740	0.01480	1.5	50.4	78.1	127.3	0.6	2.058	0.029	2.150	0.086	95
MG - 01F	36.1		2.98490	0.08230	0.23300	0.00240	0.930	4.29150	0.04490	0.09290	0.00270	0.31690	0.00540	0.2	136.0	391.0	421.9	0.9	1.350	0.013	1.486	0.055	90
MG - 01F	25.1		2.02720	0.04710	0.18790	0.00200	0.730	5.32290	0.05670	0.07830	0.00170	0.08310	0.01390	0.6	203.9	283.8	980.8	0.3	1.110	0.011	1.153	0.044	96
MG - 01F	38.1		2.36780	0.07340	0.20900	0.00230	0.470	4.78570	0.05320	0.08220	0.00280	0.13720	0.00550	0.4	89.5	144.7	387.2	0.4	1.223	0.012	1.250	0.067	97
MG - 01F	24.1		16.55720	0.47930	0.57290	0.00980	0.520	1.74550	0.02990	0.20960	0.00630	0.29770	0.00670	0.2	66.1	77.3	83.5	0.9	2.920	0.040	2.903	0.048	100
MG - 01F	2.1		18.35860	0.40880	0.59450	0.00680	0.890	1.68200	0.01930	0.22400	0.00490	0.23120	0.00700	0.3	123.1	86.3	154.4	0.6	3.008	0.028	3.009	0.036	99
MG - 01F	33.1		18.80640	0.43720	0.59920	0.00710	0.610	1.66900	0.01980	0.22760	0.00590	0.08300	0.00580	0.2	95.5	32.8	133.3	0.2	3.026	0.029	3.036	0.042	99
MG - 01F	21.1		24.09600	0.45300	0.66610	0.00720	0.110	1.50130	0.01620	0.26240	0.00460	0.21430	0.00180	0.3	299.1	231.3	336.1	0.7	3.291	0.028	3.261	0.027	100
MG - 01F	62.1		7.51950	0.21860	0.39680	0.00490	0.480	2.52010	0.03100	0.13740	0.00410	0.14450	0.04480	18.8	78.0	74.9	174.3	0.4	2.154	0.023	2.195	0.053	98
MG - 01F	28.1		1.63920	0.05360	0.15650	0.00180	0.980	6.38880	0.07260	0.07600	0.00240	0.11650	0.01530	3.6	127.5	466.5	790.2	0.6	0.937	0.010	1.094	0.061	85
MG - 01F	45.1		2.69460	0.05860	0.21270	0.00170	0.990	4.70040	0.03680	0.09190	0.00210	0.27030	0.00580	0.8	364.8	994.7	1432.0	0.7	1.243	0.009	1.464	0.043	84

SPL 1177,6Hz, 6mJ, 32um

MG - 01F - FILITO - M 311

MG - 01F	12.1	4.96120	0.14880	0.27910	0.00350	0.980	3.58290	0.04550	0.12890	0.00340	0.14080	0.00770	2.1	94.5	144.9	199.6	0.7	1.587	0.017	2.083	0.047	76
MG - 01F	1.1	5.34810	0.24220	0.29680	0.00550	0.960	3.36960	0.06190	0.13070	0.00690	0.15320	0.01860	2.9	42.9	39.2	94.7	0.4	1.675	0.027	2.107	0.093	79
MG - 01F	29.1	5.41550	0.13460	0.29840	0.00310	0.990	3.35140	0.03510	0.13160	0.00350	0.31560	0.01890	2.9	179.3	419.5	606.5	0.7	1.683	0.016	2.120	0.046	79
MG - 01F	9.1	5.14340	0.12290	0.30310	0.00300	0.990	3.29950	0.03310	0.12310	0.00310	0.26110	0.00790	1.3	145.5	192.7	398.2	0.5	1.707	0.015	2.001	0.046	85
MG - 01F	52.1	5.99230	0.16390	0.30800	0.00340	0.990	3.24690	0.03570	0.14110	0.00380	0.09930	0.01030	1.2	92.7	95.2	236.4	0.4	1.731	0.017	2.241	0.048	77
MG - 01F	19.1	6.03860	0.14040	0.33030	0.00390	0.950	3.02790	0.03550	0.13260	0.00310	0.17850	0.00660	0.5	121.8	138.4	301.3	0.5	1.840	0.019	2.133	0.041	86
MG - 01F	17.1	6.21220	0.15060	0.33220	0.00400	0.960	3.01030	0.03660	0.13560	0.00340	0.18240	0.00560	1.5	121.6	240.0	290.9	0.8	1.849	0.020	2.172	0.043	85
MG - 01F	39.1	6.44150	0.24050	0.34630	0.00560	0.630	2.88800	0.04660	0.13490	0.00570	0.19130	0.01060	0.1	46.4	63.7	116.6	0.5	1.917	0.027	2.163	0.077	88

9/18/2019	SPOT	SITE					RATIOS											AGES							
ICM-08B - METARENITO G		207/235	1sigma	206/238	1 sigma	coef. corr	238/206	1 sigma	207/206	1 sigma	208/206	1 sigma	Pb total	Pb rad	Th	U	Th/U	$T_{206/238}$	1 sigma	$T_{207/235}$	1 sigma	$T_{207/206}$	1 sigma	Conc.	Conc.
J-61 - MARCELA TRINDADE													comum	ppm	ppm	ppm									206/238
SPL2964 , Analyte Excite 193nm Excimer Laser Ablation System, 6Hz, 6mJ, 20µm, 100% Energia, Hélio: MFC1=0.300L/min, MFC2=0.300L/min.													%											207/235	207/206
SPL 2964	45.1	2.3377	0.0519	0.2095	0.0015	0.80	4.7731	0.0341	0.0809	0.0017	0.1663	0.0069	0.00	30	123	139	0.89	1226	8	1224	16	1220	42	100	100
SPL 2964	37.1	2.3382	0.0471	0.2121	0.0018	0.69	4.7157	0.0389	0.0800	0.0017	0.1542	0.0035	0.41	52	199	229	0.87	1240	9	1224	14	1196	43	101	103
SPL 2964	87.1	2.3161	0.0318	0.2131	0.0013	0.97	4.6917	0.0285	0.0788	0.0010	0.0909	0.0015	0.44	89	212	452	0.47	1246	7	1217	10	1167	25	102	106
SPL 2964	68.1	2.4296	0.0390	0.2141	0.0014	0.82	4.6709	0.0315	0.0823	0.0013	0.1775	0.0035	0.09	45	195	206	0.95	1251	8	1251	11	1253	32	99	99
SPL 2964	83.1	3.3492	0.0833	0.2584	0.0023	0.69	3.8695	0.0348	0.0940	0.0025	0.4817	0.0130	1.96	14	108	41	2.66	1482	12	1493	19	1508	50	99	98
SPL 2964	35.1	3.4132	0.0686	0.2692	0.0020	0.86	3.7147	0.0279	0.0920	0.0018	0.3483	0.0121	0.93	21	105	69	1.52	1537	10	1507	16	1466	37	101	104
SPL 2964	20.1	5.0403	0.1020	0.3276	0.0026	0.84	3.0521	0.0243	0.1116	0.0020	0.1008	0.0055	1.75	22	35	67	0.53	1827	13	1826	17	1825	33	100	100
SPL 2964	64.1	4.9394	0.1011	0.3317	0.0023	0.91	3.0152	0.0212	0.1080	0.0022	0.2955	0.0092	0.33	64	294	172	1.71	1846	11	1809	17	1766	37	102	104
SPL 2964	92.1	5.2065	0.0984	0.3356	0.0031	0.84	2.9795	0.0272	0.1125	0.0019	0.1916	0.0067	0.34	74	227	196	1.16	1866	15	1854	16	1840	31	100	101
SPL 2964	3.1	5.5693	0.0856	0.3474	0.0020	0.82	2.8784	0.0168	0.1163	0.0019	0.2780	0.0071	1.24	45	168	109	1.54	1922	10	1911	13	1900	29	100	101
SPL 2964	57.1	6.0039	0.0866	0.3612	0.0023	0.39	2.7682	0.0180	0.1205	0.0017	0.2090	0.0076	0.66	25	72	59	1.22	1988	11	1976	13	1964	25	100	101
SPL 2964	39.1	6.4592	0.1236	0.3622	0.0027	0.99	2.7612	0.0208	0.1294	0.0026	0.2083	0.0059	0.89	86	233	225	1.04	1992	13	2040	17	2089	35	97	95
SPL 2964	18.1	6.5538	0.1140	0.3630	0.0030	0.92	2.7545	0.0227	0.1309	0.0023	0.0906	0.0063	1.67	26	37	69	0.54	1997	14	2053	15	2110	30	97	94
SPL 2964	75.1	6.2472	0.1556	0.3685	0.0035	0.84	2.7137	0.0254	0.1230	0.0028	0.1397	0.0078	0.61	19	48	50	0.95	2022	16	2011	21	2000	41	100	101
SPL 2964	71.1	6.4102	0.1045	0.3700	0.0028	0.54	2.7027	0.0202	0.1257	0.0021	0.2609	0.0507	0.31	65	273	146	1.88	2029	13	2034	14	2038	30	99	99
SPL 2964	24.1	6.4079	0.0831	0.3716	0.0021	0.99	2.6913	0.0150	0.1251	0.0019	0.1624	0.0026	0.52	61	162	185	0.87	2037	10	2033	12	2030	27	100	100
SPL 2964	1.1	6.4300	0.0959	0.3730	0.0024	0.94	2.6807	0.0175	0.1250	0.0020	0.1189	0.0066	0.86	69	128	178	0.72	2044	11	2036	13	2029	29	100	100
SPL 2964	66.1	6.4977	0.1005	0.3734	0.0025	0.65	2.6778	0.0179	0.1262	0.0019	0.1853	0.0031	0.14	50	126	124	1.01	2046	12	2046	14	2046	27	99	99
SPL 2964	70.1	6.4586	0.0976	0.3746	0.0027	0.98	2.6695	0.0191	0.1250	0.0020	0.1858	0.0069	1.72	56	161	135	1.19	2051	12	2040	13	2029	28	100	101
SPL 2964	98.1	6.6361	0.1260	0.3776	0.0039	0.87	2.6485	0.0271	0.1275	0.0023	0.2413	0.0095	2.27	16	46	32	1.41	2065	18	2064	17	2063	32	100	100
SPL 2964	5.1	6.6601	0.1962	0.3780	0.0041	0.66	2.6455	0.0287	0.1278	0.0040	0.0994	0.0218	3.84	5	7	12	0.55	2067	19	2067	26	2068	54	99	99
SPL 2964	73.1	6.4533	0.1191	0.3783	0.0029	0.92	2.6433	0.0199	0.1237	0.0021	0.1252	0.0081	1.16	25	53	64	0.83	2068	13	2040	16	2011	31	101	102
SPL 2964	21.1	6.6537	0.0923	0.3791	0.0020	0.22	2.6381	0.0142	0.1273	0.0020	0.1492	0.0036	0.37	53	93	134	0.70	2072	10	2066	12	2061	28	100	100
SPL 2964	60.1	7.0409	0.1254	0.3811	0.0028	0.95	2.6243	0.0195	0.1340	0.0026	0.5202	0.0599	0.88	17	49	37	1.31	2081	13	2117	16	2151	34	98	96
SPL 2964	26.1	6.8915	0.1545	0.3840	0.0049	0.22	2.6040	0.0329	0.1302	0.0037	0.0922	0.0188	5.11	6	8	15	0.52	2095	23	2098	20	2100	50	99	99
SPL 2964	29.1	6.9681	0.0887	0.3853	0.0025	0.95	2.5951	0.0171	0.1311	0.0019	0.2236	0.0105	2.35	25	71	60	1.19	2101	12	2107	12	2113	25	99	99
SPL 2964	77.1	7.3105	0.1146	0.3884	0.0030	0.99	2.5747	0.0200	0.1365	0.0024	0.1256	0.0143	0.35	63	140	151	0.92	2115	15	2150	16	2183	31	98	96
SPL 2964	44.1	7.2488	0.1322	0.3904	0.0022	0.99	2.5616	0.0144	0.1347	0.0021	0.1315	0.0394	0.90	54	107	184	0.58	2125	10	2143	17	2160	29	99	98
SPL 2964	48.1	7.3492	0.2104	0.3907	0.0053	0.34	2.5595	0.0345	0.1364	0.0041	0.5152	0.0356	1.43	10	61	17	3.52	2126	25	2155	26	2182	52	98	97
SPL 2964	34.1	7.2906	0.1116	0.3907	0.0030	0.98	2.5595	0.0199	0.1353	0.0019	0.5030	0.0119	1.83	39	193	82	2.35	2126	14	2148	14	2168	25	98	98
SPL 2964	23.1	6.9658	0.1260	0.3912	0.0024	0.79	2.5559	0.0158	0.1291	0.0024	0.1291	0.0125	0.85	32	66	76	0.88	2129	11	2107	16	2086	33	101	102
SPL 2964	42.1	7.1957	0.1327	0.3915	0.0030	0.99	2.5544	0.0197	0.1333	0.0026	0.4408	0.0408	2.13	34	145	68	2.14	2130	14	2136	17	2142	34	99	99
SPL 2964	85.1	7.1846	0.1062	0.3923	0.0027	0.99	2.5489	0.0176	0.1328	0.0017	0.2033	0.0173	1.23	52	153	142	1.08	2134	12	2135	13	2136	23	99	99
SPL 2964	4.1	7.3117	0.1480	0.3931	0.0035	0.78	2.5436	0.0227	0.1349	0.0030	0.1862	0.0126	0.71	14	32	33	0.95	2137	16	2150	18	2163	38	99	98
SPL 2964	40.1	6.9872	0.1512	0.3933	0.0037	0.64	2.5424	0.0239	0.1288	0.0030	0.1634	0.0067	3.56	21	43	48	0.90	2138	17	2110	19	2082	41	101	102
SPL 2964	15.1	7.8284	0.1970	0.3935	0.0056	0.71	2.5410	0.0364	0.1443	0.0035	0.1974	0.0212	0.00	6	13	12	1.11	2139	26	2211	23	2279	42	96	93
SPL 2964	99.1	7.1781	0.1100	0.3947	0.0037	0.62	2.5337	0.0236	0.1319	0.0021	0.5346	0.0260	1.07	28	155	48	3.25	2145	17	2134	14	2123	28	100	100
SPL 2964	55.1	7.2464	0.0969	0.3965	0.0025	0.99	2.5219	0.0156	0.1325	0.0017	0.1282	0.0039	1.47	71	122	185	0.66	2153	11	2142	12	2132	22	100	100
SPL 2964	53.1	7.4127	0.0993	0.3980	0.0027	0.54	2.5124	0.0173	0.1351	0.0017	0.2823	0.0101	0.34	43	145	88	1.64	2160	13	2163	12	2165	22	99	99
SPL 2964	2.1	7.3702	0.1144	0.3985	0.0024	0.87	2.5096	0.0151	0.1341	0.0021	0.1881	0.0037	0.23	65	165	143	1.16	2162	11	2157	14	2153	28	100	100
SPL 2964	63.1	7.3709	0.1409	0.3995	0.0033	0.83	2.5031	0.0206	0.1338	0.0027	0.4778	0.0092	0.86	49	266	92	2.90	2167	15	2157	17	2149	36	100	100
SPL 2964	96.1	7.4142	0.1061	0.4002	0.0028	0.78	2.4988	0.0174	0.1344	0.0018	0.1584	0.0086	0.91	29	54	66	0.82	2170	13	2163	13	2156	24	100	100
SPL 2964	86.1	7.3103	0.1059	0.4004	0.0029	0.94	2.4974	0.0180	0.1324	0.0018	0.1986	0.0587	4.70	49	125	142	0.88	2171	13	2150	13	2130	23	100	101
SPL 2964	79.1	7.6571	0.1606	0.4023	0.0027	0.76	2.4858	0.0170	0.1380	0.0028	0.3876	0.0179	1.22	12	51	22	2.31	2180	13	2192	19	2203	35	99	98
SPL 2964	25.1	7.6657	0.1160	0.4041	0.0033	0.74	2.4748	0.0199	0.1376	0.0024	0.2862	0.0114	1.09	21	70	45	1.57	2188	15	2193	14	2197	31	99	99
SPL 2964	50.1	7.5367	0.1928	0.4048	0.0034	0.70	2.4704	0.0207	0.1350	0.0029	0.1552	0.0087	1.30	16	33	36	0.92	2191	16	2177	23	2164	37	100	101
SPL 2964	58.1	7.5374	0.1473	0.4048	0.0027	0.99	2.4704	0.0167	0.1350	0.0028	0.5001	0.0185	0.18	30	136	58	2.36	2191	13	2177	18	2165	37	100	101
SPL 2964	93.1	7.6332	0.2444	0.4060	0.0061	0.01	2.4633	0.0370	0.1364	0.0044	0.4615	0.0657	0.18	15	77	26	2.94	2196	28	2189	28	2182	54	100	100
SPL 2964	82.1	7.6309	0.1385	0.4061	0.0029	0.71	2.4627	0.0176	0.1363	0.0022	0.3984	0.0476	1.75	18	81	37	2.19	2197	13	2189	16	2181	28	100	100
SPL 2964	33.1	7.4681	0.1121	0.4066	0.0033	0.97	2.4597	0.0198	0.1332	0.0020	0.2303	0.0124	0.44	42	120	90	1.34	2199	15	2169	13	2141	27	101	102
SPL 2964	27.1	7.6933	0.2532	0.4068	0.0048	0.31	2.4580	0.0289	0.1371	0.0045	0.1772	0.0215	5.16	5	11	11	1.05	2200	22	2196	30	2191	56	100	100
SPL 2964	67.1	7.6796	0.1337	0.4069	0.0035	0.93	2.4578	0.0210	0.1369	0.0024	0.0880	0.0075	1.38	23	30	58	0.52	2201	16	2194	16	2188	32	100	100
SPL 2964	16.1	7.8953	0.1770	0.4070	0.0036	0.70	2.4569	0.0220	0.1407	0.0028	0.2887	0.0215	0.00	15	52	30	1.73	2201	17	2219	20	2236	36	99	98
SPL 2964	13.1	7.8681	0.2135	0.4071	0.0061	0.01	2.4566	0.0368	0.1402	0.0039	0.2428	0.0115	4.60	7	19	14	1.34	2202	28	2216	24	2229	48	99	98
SPL 2964	38.1	7.7127	0.1986	0.4075	0.0049	0.68	2.4539	0.0293	0.1373	0.0038	0.1880	0.0090	1.35	13	29	27	1.09	2204	22	2198	23	2193	48	100	100
SPL 2964	78.1	7.8971	0.1363	0.4078	0.0028	0.85	2.4523	0.0168	0.1405	0.0022	0.1110	0.0021	0.36	51	84	122	0.69	2205	13	2219	16	2233	27	99	98
SPL 2964	59.1	7.6729	0.1582	0.4090	0.0031	0.79	2.4448	0.0182	0.1361	0.0029	0.3685	0.0114	0.43	28	118	54	2.21	2210	14	2193	19	2178	38	100	101
SPL 2964	6.1	7.8842	0.1357	0.4097	0.0030	0.64	2.4410	0.0179	0.1396	0.0026	0.1654	0.0104	1.25	27	43	57	0.75	2213	14	2218	15	2222	33	99	99
SPL 2964	89.1	7.7270	0.1389	0.4099	0.0035	0.66	2.4396	0.0207	0.1367	0.0022	0.1749	0.0028	0.41	79	168	177	0.95	2214	16	2200	16	2186	27	100	101
SPL 2964	100.1	7.5271	0.1516	0.4111	0.0036	0.99	2.4323	0.0212	0.1328	0.0024	0.2214	0.0322	3.15	19	68	44	1.52	2220	17	2176	18	2135	32	102	103
SPL 2964	17.1	7.8289	0.1325	0.4114	0.0033	0.27	2.4305	0.0194	0.1380	0.0020	0.1752	0.0034	0.05	30	59	63	0.93	2222	15	2212	15	2202	25	100	100

SPL 2964	74.1	7.0151	0.1516	0.4123	0.0037	0.98	2.4255	0.0217	0.1234	0.0027	0.1632	0.0522	0.78	39	173	101	1.71	2225	17	2113	19	2006	37	105	110
SPL 2964	80.1	7.6881	0.1115	0.4124	0.0022	0.99	2.4248	0.0128	0.1352	0.0020	0.1918	0.0068	0.19	75	231	153	1.51	2226	10	2195	14	2167	26	101	102
SPL 2964	81.1	7.8176	0.1393	0.4134	0.0027	0.56	2.4187	0.0160	0.1371	0.0025	0.3505	0.0212	0.33	32	121	63	1.92	2231	13	2210	16	2191	32	100	101
SPL 2964	32.1	7.7060	0.1492	0.4165	0.0039	0.98	2.4010	0.0224	0.1342	0.0024	0.3497	0.0067	1.08	28	119	61	1.95	2245	18	2197	17	2153	31	102	104
SPL 2964	28.1	7.8980	0.1091	0.4170	0.0027	0.87	2.3978	0.0155	0.1374	0.0020	0.3537	0.0080	0.00	27	111	53	2.08	2247	12	2219	12	2194	26	101	102
SPL 2964	31.1	7.9426	0.1288	0.4204	0.0028	0.95	2.3786	0.0156	0.1370	0.0024	0.2111	0.0398	0.03	17	44	38	1.16	2262	13	2225	15	2190	30	101	103
SPL 2964	12.1	8.3210	0.1379	0.4220	0.0033	0.63	2.3697	0.0183	0.1430	0.0024	0.1415	0.0048	0.33	27	50	56	0.89	2269	15	2267	15	2264	30	100	100
SPL 2964	54.1	7.9029	0.1270	0.4246	0.0032	0.57	2.3552	0.0178	0.1350	0.0021	0.1685	0.0161	0.32	56	144	115	1.25	2281	15	2220	15	2164	27	102	105
SPL 2964	10.1	8.3790	0.1325	0.4269	0.0036	0.69	2.3422	0.0196	0.1423	0.0024	0.1891	0.0106	1.98	18	39	36	1.08	2292	16	2273	15	2256	29	100	101
SPL 2964	19.1	8.4828	0.1312	0.4288	0.0035	0.97	2.3320	0.0190	0.1435	0.0020	0.2511	0.0368	0.62	47	167	97	1.72	2300	16	2284	14	2269	24	100	101
SPL 2964	62.1	8.1231	0.1670	0.4326	0.0031	0.95	2.3118	0.0164	0.1362	0.0030	0.4412	0.0363	0.37	36	191	65	2.96	2317	14	2245	19	2179	38	103	106
SPL 2964	8.1	10.3360	0.1301	0.4734	0.0034	0.67	2.1125	0.0151	0.1584	0.0023	0.1063	0.0034	0.59	39	47	77	0.61	2498	15	2465	12	2438	24	101	102
SPL 2964	11.1	15.1715	0.1911	0.5561	0.0038	0.80	1.7982	0.0122	0.1979	0.0027	0.2267	0.0050	0.48	76	151	116	1.31	2851	16	2826	12	2809	22	100	101
SPL 2964	65.1	15.9381	0.2155	0.5694	0.0040	0.97	1.7563	0.0124	0.2030	0.0029	0.1921	0.0037	0.31	37	66	58	1.13	2905	17	2873	13	2851	24	101	101
SPL 2964	94.1	18.6601	0.2686	0.5816	0.0051	0.98	1.7193	0.0152	0.2327	0.0030	0.1226	0.0057	0.30	57	70	89	0.78	2955	21	3024	14	3071	21	97	96
SPL 2964	88.1	19.3676	0.3698	0.5996	0.0055	0.58	1.6677	0.0152	0.2343	0.0038	0.1598	0.0044	0.18	33	43	45	0.97	3028	22	3060	18	3081	26	98	98
SPL 2964	41.1	19.6009	0.3593	0.6206	0.0048	0.99	1.6113	0.0123	0.2291	0.0044	0.1085	0.0232	0.29	21	27	32	0.84	3112	19	3072	18	3045	31	101	102
SPL 2964	9.1	19.9352	0.2701	0.6249	0.0047	0.99	1.6003	0.0120	0.2314	0.0033	0.2247	0.0086	4.93	37	78	88	0.89	3129	19	3088	14	3062	23	101	102
SPL 2964	30.1	1.6180	0.0232	0.1006	0.0005	0.99	9.9405	0.0531	0.1167	0.0017	0.1692	0.0205	13.86	38	150	269	0.56	618	3	977	9	1906	26	63	32
SPL 2964	76.1	1.8736	0.0636	0.1358	0.0017	0.99	7.3627	0.0901	0.1000	0.0020	0.0729	0.0139	0.40	50	192	137	1.41	821	9	1072	14	1625	31	76	50
SPL 2964	14.1	2.9658	0.0431	0.1679	0.0012	0.99	5.9551	0.0438	0.1281	0.0020	0.1982	0.0063	6.14	26	145	187	0.78	1001	7	1399	11	2072	28	71	48
SPL 2964	7.1	2.9442	0.0513	0.1805	0.0012	0.99	5.5405	0.0375	0.1183	0.0022	0.0945	0.0266	9.75	7	77	45	1.72	1070	7	1393	13	1931	33	76	55
SPL 2964	52.1	2.6179	0.0495	0.1890	0.0014	0.97	5.2904	0.0403	0.1004	0.0016	0.3162	0.0111	1.60	29	177	113	1.56	1116	8	1306	13	1632	30	85	68
SPL 2964	22.1	2.1589	0.0338	0.1897	0.0013	0.88	5.2725	0.0352	0.0826	0.0015	0.2727	0.0091	17.80	34	104	133	0.78	1120	7	1168	11	1259	35	95	88
SPL 2964	51.1	3.6461	0.0444	0.2089	0.0013	0.99	4.7861	0.0287	0.1266	0.0014	0.1517	0.0415	0.44	56	18	166	0.11	1223	7	1560	9	2051	20	78	59
SPL 2964	49.1	4.1903	0.0769	0.2120	0.0013	0.99	4.7180	0.0292	0.1434	0.0024	0.0531	0.0118	1.88	43	101	158	0.64	1239	7	1672	15	2268	29	74	54
SPL 2964	84.1	2.6954	0.0474	0.2389	0.0014	0.98	4.1859	0.0250	0.0818	0.0014	0.0383	0.0041	0.39	36	36	176	0.20	1381	7	1327	13	1241	33	104	111
SPL 2964	91.1	4.3174	0.1220	0.2424	0.0032	0.99	4.1257	0.0542	0.1292	0.0023	0.1016	0.0357	0.73	97	130	464	0.28	1399	15	1697	17	2087	30	82	67
SPL 2964	46.1	4.1105	0.0763	0.2737	0.0020	0.98	3.6540	0.0267	0.1089	0.0021	0.2003	0.0065	3.11	37	132	134	0.99	1559	10	1656	16	1782	35	94	87
SPL 2964	36.1	4.9768	0.0792	0.2876	0.0019	0.96	3.4766	0.0235	0.1255	0.0019	0.1758	0.0048	1.97	33	81	95	0.85	1630	10	1815	14	2036	26	89	80
SPL 2964	47.1	5.3682	0.1089	0.2881	0.0017	0.97	3.4711	0.0211	0.1351	0.0024	0.0472	0.0144	4.94	51	31	199	0.15	1632	9	1880	17	2166	31	86	75
SPL 2964	61.1	4.9962	0.0886	0.2940	0.0026	0.99	3.4019	0.0296	0.1233	0.0026	0.1903	0.0354	2.23	21	101	56	1.82	1661	13	1819	16	2004	38	91	82
SPL 2964	90.1	5.2360	0.1171	0.2950	0.0032	0.99	3.3897	0.0367	0.1287	0.0022	0.0821	0.0044	0.65	69	98	252	0.39	1667	15	1858	16	2081	30	89	80
SPL 2964	72.1	5.4028	0.0869	0.3150	0.0020	0.99	3.1749	0.0200	0.1244	0.0020	0.2012	0.0533	0.94	107	1233	533	2.32	1765	10	1885	14	2020	29	93	87
SPL 2964	69.1	5.8430	0.0828	0.3187	0.0022	0.99	3.1376	0.0220	0.1330	0.0020	0.0805	0.0035	0.72	54	108	146	0.74	1783	11	1953	12	2137	26	91	83
SPL 2964	97.1	6.0218	0.0824	0.3215	0.0023	0.99	3.1100	0.0224	0.1358	0.0018	0.1849	0.0230	0.15	28	42	74	0.57	1797	11	1979	12	2175	23	90	82
SPL 2964	43.1	6.0028	0.1508	0.3346	0.0033	0.94	2.9885	0.0294	0.1301	0.0034	0.0518	0.0550	-3.93	-13	12	-26	-0.47	1861	16	1976	22	2099	45	94	88
SPL 2964	95.1	14.6180	0.1894	0.4681	0.0034	0.99	2.1364	0.0155	0.2265	0.0028	0.1485	0.0063	2.37	90	229	262	0.88	2475	15	2791	12	3027	20	88	81
SPL 2964	56.1	5.7004	0.0706	0.3383	0.0023	0.99	2.9561	0.0200	0.1222	0.0017	0.0118	0.0072	0.44	22	-4	53	-0.07	1878	11	1931	12	1989	25	97	94

8/17/2020	SPOT	SITE	RATIOS																AGES						
117-X-18B - M 756			207/235	1sigma	206/238	1 sigma	coef. corr	238/206	1 sigma	207/206	1 sigma	208/206	1 sigma	Pb total comum %	Pb rad ppm	Th ppm	U ppm	Th/U	$T_{206/238}$	1 sigma	$T_{207/235}$	1 sigma	$T_{207/206}$	1 sigma	Conc. 206/238
J-61 - MARCELA																									207/235
SPL3255 , Analyte Excite 193nm Excimer Laser Ablation System, 6Hz, 6mJ, 20µm, 100%(0.89J/cm²) Energia, Hélio: MFC1=0.300L/min, MFC2=0.300L/min.																									
SPL 3255	78.1		0.7929	0.0205	0.0917	0.0012	0.97	10.9085	0.1434	0.0627	0.0017	0.0826	0.0417	5.7	166	272	1462	0.2	565	7	593	12	699	56	95
SPL 3255	57.1		0.9617	0.0360	0.1136	0.0010	0.97	8.8054	0.0770	0.0614	0.0023	0.0455	0.0047	6.1	100	94	886	0.1	693	6	684	19	654	80	101
SPL 3255	62.1		4.4785	0.1129	0.2736	0.0027	0.98	3.6546	0.0358	0.1187	0.0034	0.1535	0.0152	2.9	79	241	257	0.9	1559	14	1727	21	1937	53	90
SPL 3255	89.1		4.3156	0.1237	0.2886	0.0034	0.58	3.4654	0.0403	0.1085	0.0035	0.1028	0.0058	1.3	49	140	152	0.9	1634	17	1696	24	1774	59	96
SPL 3255	100.1		5.8153	0.1657	0.3271	0.0033	0.99	3.0568	0.0310	0.1289	0.0041	0.1756	0.0156	0.5	28	95	48	2.0	1824	16	1949	26	2083	59	93
SPL 3255	38.1		6.3685	0.1655	0.3460	0.0035	0.99	2.8898	0.0289	0.1335	0.0036	0.1060	0.0086	3.3	68	120	236	0.5	1916	17	2028	22	2144	46	94
SPL 3255	28.1		6.3728	0.2556	0.3463	0.0045	0.75	2.8873	0.0375	0.1335	0.0054	0.1426	0.0084	1.7	25	70	66	1.1	1917	22	2029	35	2144	72	94
SPL 3255	5.1		6.2417	0.2539	0.3585	0.0044	0.86	2.7893	0.0345	0.1263	0.0051	0.2275	0.0102	2.7	17	53	35	1.5	1975	21	2010	35	2047	72	98
SPL 3255	18.1		6.1931	0.1430	0.3624	0.0033	0.88	2.7596	0.0251	0.1240	0.0031	0.1929	0.0053	2.7	55	150	134	1.1	1993	16	2003	20	2014	44	99
SPL 3255	60.1		6.7162	0.2253	0.3628	0.0040	0.97	2.7566	0.0302	0.1343	0.0043	0.1698	0.0130	3.0	47	123	138	0.9	1995	19	2075	30	2155	58	96
SPL 3255	61.1		6.0846	0.2337	0.3632	0.0061	0.92	2.7537	0.0459	0.1215	0.0049	0.2253	0.0099	4.0	23	59	61	1.0	1997	28	1988	33	1979	73	100
SPL 3255	63.1		6.3186	0.2255	0.3644	0.0042	0.68	2.7441	0.0319	0.1258	0.0048	0.1909	0.0078	0.9	16	45	36	1.3	2003	20	2021	32	2039	69	99
SPL 3255	55.1		6.4747	0.3000	0.3689	0.0075	0.77	2.7108	0.0548	0.1273	0.0065	0.1739	0.0161	1.7	25	60	61	1.0	2024	35	2042	40	2061	83	99
SPL 3255	67.1		6.7698	0.1910	0.3695	0.0040	0.99	2.7062	0.0296	0.1329	0.0043	0.2090	0.0099	2.0	31	88	105	0.8	2027	19	2082	26	2136	57	97
SPL 3255	91.1		6.4348	0.2222	0.3702	0.0051	0.51	2.7015	0.0374	0.1261	0.0052	0.2363	0.0276	9.9	36	104	69	1.5	2030	24	2037	31	2044	73	99
SPL 3255	85.1		6.9528	0.1904	0.3708	0.0039	0.99	2.6968	0.0280	0.1360	0.0040	0.1549	0.0059	4.3	46	112	190	0.6	2033	18	2105	25	2177	51	96
SPL 3255	25.1		6.4147	0.2393	0.3716	0.0046	0.88	2.6909	0.0334	0.1252	0.0047	0.2114	0.0095	1.3	23	63	50	1.3	2037	22	2034	33	2032	67	100
SPL 3255	51.1		6.7174	0.1900	0.3722	0.0059	0.29	2.6870	0.0424	0.1309	0.0043	0.1627	0.0122	1.5	17	40	38	1.0	2040	28	2075	25	2110	56	98
SPL 3255	37.1		6.8523	0.1723	0.3744	0.0034	0.99	2.6707	0.0243	0.1327	0.0035	0.1544	0.0162	6.7	65	152	228	0.7	2050	16	2093	23	2134	46	97
SPL 3255	1.1		6.9105	0.2482	0.3761	0.0046	0.99	2.6587	0.0327	0.1333	0.0049	0.1903	0.0107	8.5	39	98	130	0.8	2058	22	2100	32	2141	64	98
SPL 3255	14.1		6.9797	0.1591	0.3795	0.0042	0.90	2.6353	0.0293	0.1334	0.0028	0.1975	0.0083	1.3	45	168	100	1.7	2074	20	2109	21	2143	37	98
SPL 3255	73.1		6.7294	0.1618	0.3809	0.0050	0.65	2.6254	0.0345	0.1281	0.0031	0.2145	0.0051	0.8	54	231	120	1.9	2080	23	2076	21	2073	43	100
SPL 3255	43.1		7.1647	0.2177	0.3827	0.0055	0.99	2.6127	0.0374	0.1358	0.0042	0.1782	0.0117	6.6	24	39	90	0.4	2089	26	2132	27	2174	54	97
SPL 3255	7.1		7.0486	0.2047	0.3837	0.0041	0.74	2.6061	0.0278	0.1332	0.0039	0.1732	0.0042	0.6	58	141	131	1.1	2094	19	2118	26	2141	52	98
SPL 3255	31.1		6.6018	0.2167	0.3857	0.0029	0.90	2.5924	0.0192	0.1241	0.0041	0.1337	0.0047	2.6	50	107	128	0.8	2103	13	2060	29	2016	59	102
SPL 3255	**93.1**		**7.2330**	**0.2293**	**0.3865**	**0.0050**	**0.71**	**2.5872**	**0.0333**	**0.1357**	**0.0046**	**0.1665**	**0.0139**	**2.8**	**14**	**38**	**31**	**1.2**	**2107**	**23**	**2141**	**28**	**2173**	**60**	**98**
SPL 3255	21.1		7.0871	0.1575	0.3872	0.0031	0.92	2.5825	0.0210	0.1327	0.0032	0.1859	0.0032	1.5	71	183	174	1.1	2110	15	2122	20	2135	41	99
SPL 3255	47.1		7.1993	0.1768	0.3886	0.0034	0.99	2.5736	0.0226	0.1344	0.0034	0.1543	0.0156	5.7	90	132	213	0.6	2116	16	2136	23	2156	44	99
SPL 3255	96.1		7.2727	0.1998	0.3890	0.0043	0.92	2.5708	0.0281	0.1356	0.0042	0.1862	0.0113	5.8	25	54	49	1.1	2118	20	2145	25	2172	53	98
SPL 3255	79.1		7.4168	0.1880	0.3914	0.0035	0.99	2.5550	0.0228	0.1374	0.0038	0.1695	0.0079	3.3	52	133	149	0.9	2129	16	2163	23	2195	48	98
SPL 3255	49.1		7.4994	0.1965	0.3919	0.0064	0.81	2.5515	0.0414	0.1388	0.0041	0.1855	0.0075	0.5	18	41	37	1.1	2132	29	2173	24	2212	52	98
SPL 3255	52.1		7.3817	0.1545	0.3922	0.0046	0.86	2.5498	0.0299	0.1365	0.0030	0.1446	0.0069	1.7	36	71	74	1.0	2133	21	2159	19	2183	38	98
SPL 3255	68.1		7.2164	0.3732	0.3922	0.0084	0.81	2.5497	0.0548	0.1334	0.0084	0.2172	0.0272	3.8	14	43	35	1.2	2133	39	2139	46	2144	106	99
SPL 3255	81.1		7.2069	0.1856	0.3924	0.0035	0.98	2.5483	0.0228	0.1332	0.0035	0.1870	0.0062	0.2	69	174	142	1.2	2134	16	2137	22	2141	45	99
SPL 3255	66.1		7.4709	0.2286	0.3941	0.0045	0.99	2.5374	0.0292	0.1375	0.0048	0.1798	0.0089	4.4	36	85	107	0.8	2142	21	2170	28	2196	61	98
SPL 3255	74.1		7.2267	0.1572	0.3945	0.0045	0.03	2.5352	0.0288	0.1329	0.0027	0.2301	0.0052	1.2	46	144	95	1.5	2143	21	2140	19	2136	35	100
SPL 3255	76.1		7.4086	0.2160	0.3951	0.0068	0.38	2.5313	0.0438	0.1360	0.0045	0.2274	0.0117	0.8	16	49	32	1.5	2146	32	2162	26	2177	58	99
SPL 3255	94.1		7.3895	0.2088	0.3965	0.0037	0.80	2.5223	0.0237	0.1352	0.0036	0.3151	0.0138	0.1	40	171	74	2.3	2153	17	2160	25	2166	46	99
SPL 3255	3.1		7.3728	0.2486	0.3973	0.0042	0.50	2.5168	0.0268	0.1346	0.0047	0.1754	0.0085	2.0	25	56	53	1.1	2157	20	2158	31	2159	60	99
SPL 3255	2.1		7.3940	0.2315	0.3977	0.0049	0.96	2.5142	0.0308	0.1348	0.0043	0.1820	0.0144	0.6	59	180	119	1.5	2159	22	2160	28	2162	55	99
SPL 3255	53.1		7.4724	0.1699	0.3980	0.0038	0.83	2.5125	0.0239	0.1362	0.0029	0.2347	0.0051	1.2	33	83	61	1.4	2160	17	2170	20	2179	37	99
SPL 3255	35.1		7.5277	0.2565	0.3990	0.0030	0.55	2.5064	0.0186	0.1368	0.0047	0.0645	0.0051	0.4	40	29	103	0.3	2164	14	2176	30	2188	59	99
SPL 3255	22.1		7.4873	0.1801	0.3994	0.0039	0.82	2.5040	0.0244	0.1360	0.0036	0.1526	0.0078	0.6	60	104	130	0.8	2166	18	2171	22	2177	46	99
SPL 3255	75.1		7.2774	0.1386	0.4000	0.0045	0.99	2.5002	0.0284	0.1320	0.0026	0.2019	0.0195	0.5	78	198	160	1.2	2169	21	2146	19	2124	36	101
SPL 3255	65.1		7.5938	0.2326	0.4003	0.0045	0.33	2.4982	0.0280	0.1376	0.0044	0.1628	0.0060	0.4	27	64	59	1.1	2170	21	2184	27	2197	56	99
SPL 3255	56.1		7.4174	0.2903	0.4004	0.0047	0.53	2.4974	0.0292	0.1343	0.0050	0.1792	0.0062	1.6	25	59	56	1.1	2171	22	2163	35	2156	65	100
SPL 3255	86.1		7.5074	0.2176	0.4009	0.0037	0.29	2.4947	0.0233	0.1358	0.0043	0.2367	0.0091	0.4	31	116	63	1.8	2173	17	2174	26	2175	54	99
SPL 3255	23.1		7.5052	0.1866	0.4014	0.0043	0.99	2.4910	0.0267	0.1356	0.0037	0.1643	0.0042	1.3	67	167	229	0.7	2176	20	2174	23	2172	49	100
SPL 3255	54.1		7.4284	0.2545	0.4015	0.0046	0.96	2.4906	0.0285	0.1342	0.0045	0.2649	0.0158	1.1	37	95	79	1.2	2176	21	2164	31	2153	59	100
SPL 3255	10.1		7.5095	0.2710	0.4017	0.0076	0.82	2.4894	0.0472	0.1356	0.0051	0.1951	0.0246	0.4	13	29	24	1.2	2177	35	2174	32	2172	65	100
SPL 3255	20.1		7.4687	0.2519	0.4021	0.0099	0.71	2.4867	0.0615	0.1347	0.0059	0.1804	0.0284	7.1	11	21	20	1.1	2179	46	2169	30	2160	76	100
SPL 3255	9.1		7.1638	0.2433	0.4023	0.0056	0.68	2.4856	0.0348	0.1291	0.0046	0.1409	0.0080	1.1	18	35	36	1.0	2180	26	2132	30	2086	61	102
SPL 3255	45.1		7.5825	0.2602	0.4045	0.0052	0.80	2.4723	0.0315	0.1360	0.0046	0.1491	0.0122	3.6	22	44	42	1.0	2190	23	2183	31	2176	60	100
SPL 3255	11.1		7.5966	0.1612	0.4054	0.0042	0.93	2.4664	0.0258	0.1359	0.0027	0.1754	0.0035	1.8	71	153	171	0.9	2194	19	2184	19	2175	35	100
SPL 3255	88.1		7.6488	0.2126	0.4058	0.0047	0.64	2.4643	0.0284	0.1367	0.0044	0.1409	0.0027	0.6	64	123	134	0.9	2196	21	2191	25	2186	56	100
SPL 3255	39.1		7.3936	0.1982	0.4066	0.0042	0.64	2.4595	0.0253	0.1319	0.0036	0.1904	0.0053	1.4	46	108	96	1.1	2199	19	2160	24	2123	48	101
SPL 3255	72.1		7.3112	0.1756	0.4074	0.0055	0.01	2.4546	0.0330	0.1302	0.0030	0.2418	0.0170	1.2	23	50	46	1.1	2203	25	2150	21	2100	39	102
SPL 3255	26.1		7.7260	0.2685	0.4084	0.0053	0.73	2.4488	0.0317	0.1372	0.0049	0.1985	0.0169	3.0	18	32	36	0.9	2207	24	2200	31	2192	62	100
SPL 3255	33.1		7.6605	0.3128	0.4085	0.0039	0.65	2.4478	0.0236	0.1360	0.0055	0.1620	0.0142	0.1	12	23	24	1.0	2208	18	2192	37	2177	70	100
SPL 3255	83.1		7.7100	0.2074	0.4097	0.0043	0.46	2.4408	0.0258	0.1365	0.0040	0.2144	0.0100	0.4	26	86	53	1.6	2214	20	2198	24	2183	50	100
SPL 3255	24.1		7.9587	0.2927	0.4097	0.0057	0.57	2.4408	0.0338	0.1409	0.0054	0.1737	0.0108	1.6	16	32	32	1.0	2214	26	2226	34	2238	67	99
SPL 3255	82.1		7.6294	0.2984	0.4111	0.0069	0.01	2.4325	0.0408	0.1346	0.0065	0.1736	0.0127	1.1	14	37	28	1.3	2220	32	2188	36	2159	82	101
SPL 3255	8.1		9.0075	0.3301	0.4141	0.0063	0.84	2.4147	0.0365	0.1577	0.0061	0.1774	0.0189	3.9	11	-9	22	-0.4	2234	29	2339	33	2432	66	95
SPL 3255	17.1		7.8867	0.2083	0.4143	0.0053	0.80	2.4139	0.0312	0.1381	0.0034	0.2767	0.0106	3.5	24	65	42	1.5	2234	24	2218	24	2203	44	100

SPL 3255	36.1	7.6372	0.2464	0.4182	0.0041	0.35	2.3914	0.0236	0.1325	0.0042	0.2089	0.0089	0.4	28	71	58	1.2	2252	19	2189	30	2131	57	102
SPL 3255	16.1	7.9354	0.1801	0.4206	0.0052	0.76	2.3773	0.0294	0.1368	0.0030	0.0859	0.0060	2.2	36	39	78	0.5	2263	24	2224	20	2187	37	101
SPL 3255	46.1	8.0123	0.2442	0.4265	0.0058	0.60	2.3449	0.0320	0.1363	0.0044	0.2368	0.0087	0.7	27	85	58	1.5	2290	26	2232	28	2180	56	102
SPL 3255	15.1	8.3806	0.2159	0.4419	0.0066	0.86	2.2632	0.0341	0.1376	0.0034	0.1710	0.0149	2.2	25	50	50	1.0	2359	30	2273	24	2197	44	103
SPL 3255	71.1	9.6524	0.2044	0.4553	0.0062	0.10	2.1963	0.0297	0.1538	0.0033	0.1087	0.0066	0.1	55	64	108	0.6	2419	27	2402	20	2388	36	100
SPL 3255	92.1	9.8710	0.2656	0.4615	0.0043	0.17	2.1668	0.0201	0.1551	0.0041	0.1927	0.0097	1.7	22	54	40	1.4	2446	19	2423	25	2403	45	100
SPL 3255	64.1	10.5569	0.3373	0.4732	0.0093	0.08	2.1135	0.0414	0.1618	0.0064	0.1670	0.0109	2.0	17	30	31	1.0	2497	41	2485	30	2475	65	100
SPL 3255	42.1	10.2523	0.3611	0.4806	0.0049	0.76	2.0807	0.0213	0.1547	0.0053	0.0909	0.0125	2.7	18	18	31	0.6	2530	21	2458	34	2399	58	102
SPL 3255	12.1	11.2532	0.3192	0.4993	0.0060	0.84	2.0028	0.0242	0.1635	0.0043	0.1206	0.0141	4.8	22	23	40	0.6	2611	26	2544	26	2492	44	102
SPL 3255	70.1	18.6864	0.3743	0.6057	0.0088	0.43	1.6510	0.0241	0.2238	0.0046	0.1307	0.0039	0.1	83	93	110	0.8	3053	36	3026	20	3008	33	100
SPL 3255	69.1	18.7516	0.3701	0.6102	0.0083	0.01	1.6387	0.0222	0.2229	0.0044	0.1130	0.0021	0.1	115	122	158	0.8	3071	33	3029	19	3002	32	101
SPL 3255	87.1	21.4012	0.6051	0.6417	0.0093	0.91	1.5583	0.0225	0.2419	0.0081	0.0717	0.0081	1.8	26	20	38	0.5	3196	37	3157	27	3132	53	101
SPL 3255	44.1	0.5491	0.0235	0.0627	0.0008	0.98	15.9582	0.1929	0.0636	0.0027	0.1419	0.0258	22.5	123	178	1019	0.2	392	5	444	15	727	90	88
SPL 3255	77.1	0.6752	0.0210	0.0783	0.0011	0.99	12.7680	0.1735	0.0625	0.0016	0.0744	0.0180	12.1	182	316	1594	0.2	486	6	524	12	692	55	92
SPL 3255	58.1	0.7439	0.0297	0.0817	0.0009	0.98	12.2448	0.1292	0.0661	0.0023	0.0781	0.0103	10.6	105	120	1043	0.1	506	5	565	17	809	73	89
SPL 3255	13.1	1.1522	0.0464	0.0881	0.0015	0.96	11.3558	0.1925	0.0949	0.0034	0.2200	0.0940	29.9	133	493	633	0.8	544	9	778	21	1526	73	69
SPL 3255	41.1	1.6560	0.0490	0.1103	0.0009	0.93	9.0622	0.0733	0.1088	0.0039	0.1517	0.0224	9.5	119	816	878	0.9	675	5	992	20	1780	59	68
SPL 3255	48.1	1.9115	0.0394	0.1334	0.0011	0.98	7.4982	0.0594	0.1039	0.0024	0.1581	0.0227	7.5	109	374	710	0.5	807	6	1085	15	1696	41	74
SPL 3255	27.1	2.4128	0.0879	0.1444	0.0018	0.98	6.9253	0.0877	0.1212	0.0046	0.1693	0.0106	17.1	60	162	570	0.3	869	10	1246	27	1974	72	69
SPL 3255	59.1	1.8591	0.0649	0.1444	0.0016	0.99	6.9231	0.0749	0.0933	0.0032	0.1448	0.0154	3.2	56	225	264	0.9	870	9	1067	23	1495	62	81
SPL 3255	97.1	2.1306	0.0477	0.1521	0.0012	1.00	6.5753	0.0530	0.1016	0.0025	0.0850	0.0063	5.5	108	181	658	0.3	913	7	1159	16	1654	46	78
SPL 3255	34.1	2.9467	0.1219	0.1755	0.0025	0.98	5.6965	0.0821	0.1217	0.0045	0.1087	0.0058	4.2	91	227	433	0.5	1043	14	1394	28	1982	70	74
SPL 3255	19.1	3.4795	0.0749	0.2105	0.0022	0.99	4.7503	0.0493	0.1199	0.0031	0.1535	0.0556	5.6	55	176	270	0.7	1232	12	1523	19	1954	55	80
SPL 3255	90.1	2.9315	0.0716	0.2141	0.0022	0.98	4.6717	0.0487	0.0993	0.0031	0.0925	0.0050	5.9	97	302	687	0.4	1250	12	1390	21	1611	61	89
SPL 3255	98.1	4.0446	0.0877	0.2419	0.0021	0.99	4.1335	0.0365	0.1213	0.0030	0.1462	0.0058	5.0	92	248	442	0.6	1397	11	1643	20	1975	46	84
SPL 3255	50.1	3.9840	0.0858	0.2475	0.0023	0.96	4.0397	0.0376	0.1167	0.0024	0.3180	0.2747	0.0	60	160	376	0.4	1426	12	1631	17	1907	37	87
SPL 3255	4.1	4.3032	0.1247	0.2510	0.0022	0.99	3.9845	0.0357	0.1244	0.0037	0.1373	0.0154	8.2	94	219	462	0.5	1444	12	1694	25	2020	54	85
SPL 3255	84.1	4.5328	0.1235	0.2529	0.0023	0.99	3.9544	0.0352	0.1300	0.0036	0.2092	0.0063	1.0	45	166	131	1.3	1453	12	1737	22	2098	48	83
SPL 3255	6.1	4.3341	0.1433	0.2553	0.0028	1.00	3.9166	0.0423	0.1231	0.0046	0.2351	0.0354	2.7	14	26	38	0.7	1466	14	1700	29	2002	66	86
SPL 3255	32.1	5.1805	0.1989	0.2822	0.0026	0.92	3.5440	0.0330	0.1332	0.0050	0.2469	0.0123	2.7	24	72	62	1.2	1602	13	1849	31	2140	67	86
SPL 3255	**99.1**	**4.8819**	**0.1113**	**0.2824**	**0.0024**	**0.98**	**3.5408**	**0.0295**	**0.1254**	**0.0029**	**0.1185**	**0.0048**	**3.8**	**102**	**236**	**401**	**0.6**	**1604**	**12**	**1799**	**19**	**2034**	**41**	**89**
SPL 3255	40.1	6.4398	0.1552	0.3209	0.0032	0.99	3.1162	0.0313	0.1455	0.0038	0.1451	0.0095	5.2	85	207	490	0.4	1794	16	2038	23	2294	46	88
SPL 3255	29.1	6.5202	0.2156	0.3461	0.0037	0.97	2.8891	0.0305	0.1366	0.0044	0.1675	0.0147	10.9	56	103	196	0.5	1916	17	2049	28	2185	56	93
SPL 3255	30.1	7.0258	0.2667	0.3755	0.0040	0.93	2.6634	0.0287	0.1357	0.0054	0.2013	0.0502	17.3	23	49	56	0.9	2055	19	2115	34	2173	72	97
SPL 3255	95.1	11.6596	0.2548	0.3942	0.0033	0.99	2.5369	0.0212	0.2145	0.0045	0.1481	0.0110	3.0	100	270	313	0.9	2142	15	2577	21	2940	35	83
SPL 3255	80.1	7.4356	0.1801	0.4068	0.0035	0.99	2.4583	0.0211	0.1326	0.0037	0.1533	0.0361	16.6	80	128	211	0.6	2200	16	2165	24	2132	48	101

							Ratios *							Ages* (Ma)					
AL-75	f(206%)	^{204}Pb cps	^{206}Pb mV[1]	Th/U	^{206}Pb/^{204}Pb	1σ%	^{207}Pb/^{206}Pb	1σ %	^{207}Pb/^{235}U	1σ %	^{206}Pb/^{238}U	1σ %	Rho	^{207}Pb/^{206}Pb	2σ abs	^{206}Pb/^{238}U	2σ abs	^{207}Pb/^{235}U	2σ abs
003-ZR01	0.11	11	0.0005	0.20	20942	16.53	0.14764	0.68	7.033	1.76	0.3847	1.47	0.83	2132	31	2098	52	2116	31
004-ZR02	0.06	15	0.0007	0.52	17383	27.48	0.13151	0.66	7.346	1.30	0.3864	1.04	0.80	2201	24	2106	37	2154	23
005-ZR03	0.04	14	0.0007	0.35	19180	22.17	0.12876	0.60	8.371	1.35	0.4245	1.11	0.82	2264	23	2281	43	2272	24
006-ZR04	0.03	13	0.0008	0.27	19124	21.93	0.16216	0.56	6.472	1.47	0.3652	1.30	0.89	2078	20	2007	45	2042	26
007-ZR05	0.08	16	0.0015	0.32	47590	23.42	0.12852	0.57	10.524	1.14	0.4707	0.92	0.81	2478	19	2486	38	2482	21
008-ZR06	0.08	18	0.0013	0.25	33628	28.67	0.14301	0.67	6.928	1.12	0.3902	0.87	0.78	2081	21	2124	31	2102	20
009-ZR07	0.09	16	0.0011	0.12	26567	30.21	0.13788	0.69	7.082	1.23	0.3906	0.98	0.79	2118	23	2125	35	2122	22
010-ZR08	0.07	17	0.0007	0.16	14024	27.54	0.13257	0.90	8.652	1.31	0.4250	1.06	0.81	2319	23	2283	41	2302	24
013-ZR09	0.19	13	0.0003	0.34	7850	20.52	0.14094	0.72	7.843	1.91	0.4036	1.73	0.91	2239	25	2185	64	2213	34
014-ZR10	0.09	11	0.0005	0.18	16058	26.99	0.13659	0.74	7.563	1.83	0.4015	1.63	0.89	2184	26	2176	60	2180	33
015-ZR11	0.02	10	0.0019	0.81	67996	16.21	0.14047	0.55	8.297	1.07	0.4284	0.83	0.78	2233	19	2298	32	2264	19
016-ZR12	0.04	13	0.0014	0.57	37254	19.64	0.13482	0.46	7.133	1.19	0.3837	1.03	0.87	2162	16	2094	37	2128	21
017-ZR13	0.03	15	0.0021	0.15	56961	23.43	0.13625	0.49	7.801	1.19	0.4152	1.02	0.86	2180	17	2239	39	2208	21
018-ZR14	0.03	15	0.0018	0.24	56356	26.35	0.13308	0.56	7.375	1.54	0.4019	1.38	0.90	2139	20	2178	51	2158	27
019-ZR15	0.05	11	0.0009	0.24	32545	16.99	0.13788	0.61	7.616	1.25	0.4006	1.03	0.82	2201	21	2172	38	2187	22
020-ZR16	0.07	19	0.0009	0.24	21995	22.83	0.13358	0.69	7.223	1.22	0.3921	0.94	0.77	2146	24	2133	34	2139	22
024-ZR18	0.10	28	0.0017	0.37	15681	30.80	0.13314	0.61	6.415	1.22	0.3494	1.00	0.81	2140	21	1932	33	2034	21
025-ZR19	0.07	21	0.0013	0.28	21218	31.91	0.13701	0.48	7.677	1.02	0.4064	0.83	0.81	2190	16	2198	31	2194	18
026-ZR20	0.04	21	0.0016	0.24	33838	37.00	0.12259	0.52	6.121	0.98	0.3621	0.75	0.76	1994	18	1992	26	1993	17
027-ZR21	0.08	16	0.0008	0.32	19676	36.45	0.14336	0.44	8.217	1.19	0.4157	1.05	0.88	2268	15	2241	40	2255	21
028-ZR22	0.10	20	0.0007	0.17	14462	30.15	0.13567	0.61	7.489	1.42	0.4003	1.23	0.86	2173	21	2170	45	2172	25
029-ZR23	0.18	13	0.0004	0.17	8515	22.91	0.13533	0.59	7.595	1.77	0.4070	1.63	0.92	2168	20	2201	61	2184	31
030-ZR24	0.05	16	0.0019	0.32	28738	24.32	0.13658	0.73	7.288	1.34	0.3870	1.07	0.80	2184	25	2109	38	2147	24
033-ZR25	0.04	16	0.0022	0.17	42370	25.41	0.13852	0.52	8.055	0.93	0.4217	0.67	0.73	2209	18	2268	26	2237	17
034-ZR26	0.01	15	0.0020	0.44	277559	84.48	0.13755	0.47	7.544	1.19	0.3978	1.03	0.86	2197	16	2159	38	2178	21
036-ZR28	0.03	18	0.0020	0.26	47557	24.92	0.13780	0.42	7.929	1.12	0.4173	0.97	0.87	2200	14	2248	37	2223	20
037-ZR29	0.08	26	0.0014	0.22	19293	30.20	0.13446	0.60	6.911	1.23	0.3728	1.01	0.82	2157	21	2042	35	2100	22
038-ZR30	0.02	16	0.0016	0.45	62123	35.48	0.12512	0.56	6.500	1.19	0.3768	0.99	0.83	2031	20	2061	35	2046	21
039-ZR31	0.04	17	0.0006	0.95	42434	49.78	0.13682	0.79	7.815	1.77	0.4142	1.54	0.87	2187	27	2234	58	2210	32
040-ZR32	0.01	16	0.0013	0.62	131962	79.76	0.13634	0.65	7.554	1.42	0.4018	1.21	0.85	2181	22	2177	45	2179	25
043-ZR33	0.16	28	0.0013	0.09	9141	38.79	0.15719	0.84	10.675	2.31	0.4925	2.12	0.92	2426	28	2581	90	2495	43
044-ZR34	0.04	10	0.0009	0.29	37186	23.31	0.13733	0.59	7.734	1.52	0.4084	1.35	0.89	2194	20	2208	51	2201	27
045-ZR35	0.21	12	0.0003	0.35	7198	18.97	0.13807	0.71	7.711	2.41	0.4050	2.27	0.94	2203	25	2192	84	2198	43
046-ZR36	0.03	16	0.0024	0.37	44557	23.81	0.12725	0.53	6.951	1.15	0.3962	0.95	0.82	2060	19	2151	35	2105	20
047-ZR37	0.04	10	0.0011	0.45	37384	15.74	0.16024	0.61	10.446	1.29	0.4728	1.08	0.84	2458	21	2496	45	2475	24
048-ZR38	0.05	16	0.0012	0.30	29234	21.33	0.12850	0.76	6.612	1.45	0.3732	1.18	0.81	2078	26	2044	41	2061	25
049-ZR39	0.04	16	0.0014	0.39	33736	34.58	0.13096	0.90	6.786	1.34	0.3758	0.92	0.69	2111	31	2057	32	2084	24
053-ZR41	0.03	11	0.0017	0.31	46003	18.46	0.12535	0.76	6.019	1.58	0.3482	1.33	0.84	2034	27	1926	44	1979	27
055-ZR43	0.03	15	0.0023	0.56	56442	22.97	0.15246	0.65	8.635	1.22	0.4107	0.96	0.79	2374	22	2218	36	2300	22
056-ZR44	0.03	17	0.0019	0.44	51041	19.85	0.13692	0.59	7.668	1.09	0.4061	0.83	0.77	2189	20	2197	31	2193	19
057-ZR45	0.05	19	0.0014	0.26	28976	22.73	0.12716	0.65	6.649	1.52	0.3792	1.32	0.87	2059	23	2073	47	2066	27
058-ZR46	0.03	13	0.0021	0.48	59135	27.86	0.13686	0.67	7.748	1.23	0.4106	0.97	0.79	2188	23	2218	36	2202	22
059-ZR47	0.03	13	0.0016	0.36	43632	17.53	0.12771	0.68	6.776	1.27	0.3848	1.00	0.79	2067	24	2099	36	2083	22
060-ZR48	0.13	27	0.0008	0.50	11385	33.95	0.13711	0.93	7.553	1.55	0.3995	1.19	0.76	2191	32	2167	44	2179	28
063-ZR49	0.04	14	0.0012	0.44	39364	20.25	0.13616	0.67	7.750	1.26	0.4128	1.00	0.79	2179	23	2228	38	2202	23
064-ZR50	0.05	17	0.0006	0.41	31552	52.03	0.12909	0.74	6.896	1.71	0.3874	1.49	0.87	2086	26	2111	54	2098	30
065-ZR51	0.03	30	0.0025	0.49	51473	34.72	0.13054	0.72	7.022	1.16	0.3901	0.83	0.71	2105	25	2123	30	2114	20
066-ZR52	0.06	16	0.0010	0.37	24068	30.74	0.12783	0.62	6.665	1.23	0.3781	0.99	0.81	2068	22	2067	35	2068	22
068-ZR54	0.04	16	0.0017	0.31	38932	23.86	0.13790	0.67	7.858	1.34	0.4133	1.10	0.82	2201	23	2230	41	2215	24
069-ZR55	0.25	28	0.0008	0.26	6154	60.11	0.12673	0.88	6.407	1.53	0.3666	1.20	0.78	2053	31	2013	42	2033	27

070-ZR56	0.05	12	0.0015	0.40	33565	19.70	0.12814	0.82	6.661	1.61	0.3770	1.34	0.83	2073	29	2062	47	2067	28
073-ZR57	0.03	12	0.0015	0.37	47986	16.13	0.13565	0.74	7.427	1.57	0.3970	1.34	0.85	2172	26	2155	49	2164	28
074-ZR58	0.05	21	0.0018	0.24	32086	25.64	0.13636	0.61	7.328	1.26	0.3897	1.04	0.82	2181	21	2122	38	2152	22
075-ZR59	0.04	15	0.0009	0.21	37797	49.60	0.12620	0.66	6.555	1.62	0.3767	1.44	0.89	2046	23	2061	51	2053	28
076-ZR60	0.02	15	0.0023	0.36	76441	44.81	0.12484	0.55	6.589	1.47	0.3828	1.31	0.89	2027	19	2089	47	2058	26
077-ZR61	0.07	19	0.0009	0.29	22527	23.26	0.12775	0.63	6.587	1.48	0.3740	1.28	0.87	2067	22	2048	45	2058	26
078-ZR62	0.25	14	0.0003	0.45	6026	21.27	0.14140	0.82	7.732	2.41	0.3966	2.24	0.93	2244	28	2153	82	2200	43
080-ZR64	0.07	14	0.0008	0.59	22383	20.16	0.16363	0.82	10.649	1.45	0.4720	1.14	0.78	2494	28	2492	47	2493	27
083-ZR65	0.03	11	0.0012	0.43	49072	20.13	0.12625	0.79	6.390	1.48	0.3671	1.20	0.81	2046	28	2016	41	2031	26
084-ZR66	0.04	13	0.0013	0.33	34516	19.95	0.13548	0.60	7.460	1.17	0.3993	0.93	0.80	2170	21	2166	34	2168	21
085-ZR67	0.07	26	0.0014	0.26	21430	27.11	0.14926	0.68	8.952	1.38	0.4350	1.15	0.83	2337	23	2328	45	2333	25
086-ZR68	0.09	17	0.0008	0.32	17732	17.80	0.13422	0.62	7.353	1.56	0.3973	1.38	0.89	2154	22	2157	51	2155	28
087-ZR69	0.03	9	0.0012	0.19	44177	15.61	0.12997	0.54	6.875	1.25	0.3836	1.07	0.85	2097	19	2093	38	2095	22
088-ZR70	0.02	11	0.0018	0.06	60825	19.02	0.12293	0.54	6.324	1.03	0.3731	0.79	0.77	1999	19	2044	28	2022	18
089-ZR71	0.10	17	0.0006	0.24	15143	26.68	0.13172	0.64	7.140	1.48	0.3931	1.29	0.87	2121	22	2137	47	2129	26
089-ZR72	0.06	15	0.0009	0.29	25054	25.66	0.12672	0.73	6.825	1.27	0.3906	0.98	0.77	2053	26	2125	35	2089	22
090-ZR73	0.09	19	0.0008	0.39	16419	23.26	0.12277	0.88	6.082	2.07	0.3593	1.84	0.89	1997	31	1979	63	1988	36
094-ZR75	0.03	15	0.0018	0.25	52265	19.71	0.13433	0.62	7.143	1.49	0.3856	1.31	0.88	2155	21	2102	47	2129	26
095-ZR76	0.08	12	0.0007	0.14	19207	25.01	0.13011	0.64	6.994	1.46	0.3898	1.26	0.86	2099	22	2122	46	2111	26
096-ZR77	0.05	10	0.0009	0.28	29630	15.32	0.13191	0.69	7.106	1.57	0.3907	1.37	0.87	2124	24	2126	49	2125	28
098-ZR79	0.08	16	0.0006	0.30	19430	24.11	0.13132	0.67	7.241	1.73	0.3999	1.56	0.90	2116	23	2168	57	2142	31
099-ZR80	0.10	9	0.0005	0.34	15593	17.89	0.10555	0.82	4.507	1.49	0.3097	1.19	0.80	1724	30	1739	36	1732	25
100-ZR81	0.05	13	0.0009	0.27	29540	17.60	0.13764	0.71	7.600	1.73	0.4004	1.53	0.89	2198	25	2171	56	2185	31
103-ZR82	0.05	11	0.0011	0.17	30315	18.19	0.13432	0.57	7.511	1.22	0.4055	1.01	0.83	2155	20	2194	37	2174	22
104-ZR83	0.06	16	0.0008	0.34	24407	23.21	0.16706	0.58	11.245	1.45	0.4882	1.28	0.88	2528	19	2563	54	2544	27
106-ZR85	0.05	16	0.0010	0.51	31527	24.48	0.14715	0.59	9.029	1.52	0.4450	1.36	0.89	2313	20	2373	54	2341	28
107-ZR86	0.05	14	0.0015	0.33	29189	24.20	0.14092	0.54	7.342	1.12	0.3779	0.91	0.81	2239	19	2066	32	2154	20
Dados descartados do diagrama de frequencia devido ao elevado grau de discordância																			
035-ZR27	0.01	16	0.0017	0.36	296302	88.05	0.14944	0.57	7.916	1.09	0.3842	0.85	0.78	2340	19	2096	30	2222	20
093-ZR74	0.21	75	0.0024	0.76	7203	54.12	0.13835	1.48	6.845	2.33	0.3588	1.76	0.75	2207	51	1976	60	2092	41
079-ZR63	0.11	27	0.0012	0.18	14342	31.51	0.13710	0.71	6.706	1.24	0.3547	0.95	0.76	2191	24	1957	32	2073	22
050-ZR40	0.04	11	0.0012	0.45	40063	36.13	0.12091	1.03	5.147	1.60	0.3087	1.16	0.73	1970	37	1734	35	1844	27
054-ZR42	0.06	15	0.0013	0.31	25449	23.56	0.13315	0.71	6.168	1.51	0.3359	1.28	0.85	2140	25	1867	41	2000	26
023-ZR17	0.05	24	0.0018	0.24	28183	25.04	0.12875	0.54	5.763	1.19	0.3246	0.99	0.84	2081	19	1812	31	1941	20
Dados descartados pelo elevado erro analítico ou Pb comum																			
097-ZR78	0.14	32	0.0014	0.56	10797	35.05	0.11751	0.74	3.732	3.38	0.2303	3.27	0.97	1919	27	1336	79	1578	53
067-ZR53	0.46	17	0.0002	1.05	3292	23.99	0.10679	1.21	4.621	4.17	0.3138	3.97	0.95	1745	44	1759	122	1753	68
105-ZR84	0.45	16	0.0002	0.91	3355	22.58	0.14435	0.97	8.330	5.79	0.4185	5.70	0.98	2280	33	2254	215	2268	102
108-ZR87	11.50	331	0.0006	0.54	129	7.50	0.24522	7.28	16.009	8.00	0.4734	3.31	0.41	3154	222	2499	136	2877	147

Data report template (with modifications) from http://www.plasmage.org/recommendations

[1] Convertion factor from mV to CPS is 62500000

[*] data not corrected for common-Pb

[**] Discordance calculated as (1-(^{206}Pb/^{238}U age/^{207}Pb/^{206}Pb age))*100

Decay constants of Jaffey et al 1971 used

AL-79 METABASITO																		
			RAZÕES							IDADES								
Spot#	Th/U	f(206%)[1]	$^{207}Pb/^{206}Pb$	1σ (%)	$^{207}Pb/^{235}U$	1σ (%)	$^{206}Pb/^{238}U$	1σ (%)	Rho[2]	$^{207}Pb/^{206}Pb$	1σ (abs)	$^{207}Pb/^{235}U$	1σ (abs)	$^{206}Pb/^{238}U$	1σ (abs)	Disc. (%)[3]	Comentário
Concordia Age																		
24-ZR08	0.57	0.03	0.06822	0.82	1.400	1.54	0.1488	1.25	0.81	875	34	889	18	894	21	-2.17	Concordia Age 889 Ma
56-ZR22	0.51	0.06	0.06876	0.61	1.433	1.11	0.1512	0.84	0.76	891	25	903	13	908	14	-1.81	Concordia Age 889 Ma
05-ZR03	0.62	0.08	0.06882	1.42	1.434	2.21	0.1511	1.66	0.75	893	58	903	26	907	28	-1.51	Concordia Age 889 Ma
30-ZR14	0.44	0.12	0.06878	1.99	1.421	2.83	0.1498	1.98	0.70	892	81	898	33	900	33	-0.89	Concordia Age 889 Ma
53-ZR19	0.51	0.07	0.06882	0.79	1.418	1.37	0.1495	1.05	0.77	893	33	897	16	898	18	-0.54	Concordia Age 889 Ma
25-ZR09	0.55	0.04	0.06846	1.21	1.387	1.83	0.1470	1.32	0.72	883	50	884	21	884	22	-0.15	Concordia Age 889 Ma
08-ZR06	0.59	0.09	0.06894	1.91	1.419	2.76	0.1493	1.96	0.71	897	78	897	33	897	33	0.01	Concordia Age 889 Ma
64-ZR27	0.33	0.04	0.06890	0.80	1.416	1.30	0.1490	0.95	0.73	896	33	895	15	895	16	0.03	Concordia Age 889 Ma
29-ZR13	0.61	0.03	0.06890	1.25	1.411	1.89	0.1485	1.36	0.72	896	51	893	22	892	23	0.36	Concordia Age 889 Ma
66-ZR29	0.34	0.13	0.06850	0.81	1.382	1.36	0.1463	1.03	0.76	884	33	881	16	880	17	0.44	Concordia Age 889 Ma
58-ZR24	0.44	0.08	0.06895	0.95	1.399	1.45	0.1472	1.03	0.71	897	39	889	17	885	17	1.34	Concordia Age 889 Ma
68-ZR31	0.33	0.02	0.06921	0.79	1.417	1.27	0.1485	0.92	0.72	905	33	896	15	893	15	1.37	Concordia Age 889 Ma
55-ZR21	0.44	0.06	0.06891	0.98	1.387	1.55	0.1459	1.14	0.74	896	40	883	18	878	19	2.01	Concordia Age 889 Ma
65-ZR28	0.50	0.08	0.06906	0.74	1.392	1.24	0.1462	0.93	0.75	900	30	886	15	880	15	2.31	Concordia Age 889 Ma
69-ZR32	0.49	0.06	0.06904	1.11	1.389	1.58	0.1459	1.07	0.67	900	45	884	19	878	17	2.43	Concordia Age 889 Ma
03-ZR01	0.54	0.09	0.06913	1.48	1.386	2.20	0.1454	1.58	0.72	903	61	883	26	875	26	3.04	Concordia Age 889 Ma
63-ZR26	0.45	0.12	0.06910	0.90	1.383	1.41	0.1452	1.01	0.72	902	37	882	17	874	17	3.10	Concordia Age 889 Ma
*Discordantes**																		
34-ZR16	0.54	0.09	0.06975	1.24	1.424	1.89	0.1481	1.38	0.73	921	51	899	22	890	23	3.37	Não utilizado no cálculo de idade
33-ZR15	0.49	0.06	0.07028	1.54	1.439	2.31	0.1485	1.68	0.73	936	62	905	27	893	28	4.67	Não utilizado no cálculo de idade
67-ZR30	0.48	0.09	0.06946	0.81	1.382	1.30	0.1443	0.95	0.73	912	33	881	15	869	15	4.79	Não utilizado no cálculo de idade
35-ZR17	0.50	0.21	0.06993	2.09	1.408	2.94	0.1460	2.02	0.69	926	85	892	35	878	33	5.16	Não utilizado no cálculo de idade
57-ZR23	0.46	0.28	0.07046	1.08	1.427	1.56	0.1468	1.07	0.68	942	44	900	19	883	18	6.21	Não utilizado no cálculo de idade
59-ZR25	0.27	0.08	0.07004	0.97	1.389	1.45	0.1438	1.01	0.70	929	40	884	17	866	16	6.80	Não utilizado no cálculo de idade
06-ZR04	0.30	0.23	0.07006	1.64	1.378	2.34	0.1426	1.62	0.69	930	67	880	27	860	26	7.58	Não utilizado no cálculo de idade
54-ZR20	0.44	0.21	0.07060	1.13	1.414	1.81	0.1452	1.36	0.75	946	46	895	21	874	22	7.59	Não utilizado no cálculo de idade
26-ZR10	0.48	0.09	0.07157	1.37	1.450	1.96	0.1469	1.35	0.69	974	56	910	23	884	22	9.26	Não utilizado no cálculo de idade
28-ZR12	0.54	0.10	0.06697	1.24	1.475	1.93	0.1597	1.43	0.74	837	51	920	23	955	25	-14.12	Não utilizado no cálculo de idade
04-ZR02	0.49	0.09	0.06450	2.43	1.274	2.70	0.1432	1.11	0.41	758	101	834	30	863	18	-13.83	Não utilizado no cálculo de idade
*Descartados**																		
27-ZR11	0.52	0.10	0.06920	5.01	1.388	5.20	0.1454	1.36	0.26	905	200	884	61	875	22	3.24	Alto erro analítico
36-ZR18	0.49	0.25	0.06857	3.57	1.396	5.22	0.1477	3.80	0.73	886	144	887	61	888	63	-0.23	Alto erro analítico
09-ZR07	0.29	0.38	0.07604	7.21	1.343	9.31	0.1281	5.88	0.63	1096	276	865	106	777	86	29.13	Alto erro analítico
07-ZR05	0.44	0.54	0.06348	11.35	1.320	13.18	0.1507	6.70	0.51	724	448	854	147	905	113	-24.94	Alto erro analítico

[1]Porcentagem de Pb comum; [2]Coeficiente de correlação; [3]Discordância calculada por (idade $^{206}Pb/^{238}U$ / idade $^{207}Pb/^{206}Pb$)x100

* Pontos não utilizados nos cálculos das idades.